Mind the gap: characterization of periplasmic cytochromes from *Shewanella oneidensis* involved in extracellular electron transfer

Bruno Miguel Oliveira Maia da Fonseca

Dissertation presented to obtain the Ph.D degree in Biochemistry

Instituto de Tecnologia Química e Biológica | Universidade Nova de Lisboa

Oeiras, May, 2013

INSTITUTO
DE TECNOLOGIA
QUÍMICA E BIOLÓGICA
/UNL

Knowledge Creation

From left to right: Ricardo O. Louro, Ilídio J. Correia, Irene Díaz-Moreno, Bruno M. Fonseca, Kylie A. Vincent, Teresa Catarino, Hermínia de Lencastre

President of the Jury

- Doctor Hermínia Maria Francisco Roncon Garcez de Lencastre (Instituto de Tecnologia Química e Biológica da Universidade Nova de Lisboa)

Members of the Jury

- Doctor Irene Díaz-Moreno (Instituto de Bioquímica Vegetal y Fotosíntesis, Universidad Sevilla)
- Doctor Kylie A. Vincent (Department of Chemistry, University of Oxford)
- Doctor Ilídio Joaquim Sobreira Correia (Faculdade de Ciências da Saúde da Universidade da Beira Interior)
- Doctor Maria Teresa Nunes Mangas Catarino (Faculdade de Ciências e Tecnologia da Universidade Nova de Lisboa)

Supervisor

- Doctor Ricardo Saraiva Loureiro Oliveira Louro (Instituto de Tecnologia Química e Biológica da Universidade Nova de Lisboa)

"If we knew what it was we were doing, it would not be called research, would it?"

Albert Einstein

Aos meus pais e irmão.

Agradecimentos

O trabalho obtido durante este longo percurso foi apenas possível graças a um grupo de pessoas que me apoiaram e que eu quero aqui reconhecer.

Ao meu orientador, Doutor Ricardo O. Louro, por me ter dado a oportunidade de poder trabalhar no seu laboratório. Estou lhe grato por todos os momentos bons que tive mas também pelos momentos maus, que de certa forma me moldaram e me fizeram crescer como pessoa e como cientista. Pelos inúmeros conselhos de amigo e diversas discussões científicas. Foi realmente um privilégio e uma honra ter sido um dos seus pupilos.

À minha comissão de tese, Doutora Teresa Catarino e Doutor Carlos A. Salgueiro, pela supervisão do trabalho e encorajamento.

Ao Doutor Cláudio Soares por toda a ajuda nos cálculos teóricos realizados nesta tese. Sem si muitas das conclusões teriam ficado mais pobres.

À Doutora Patrícia Pereira, pela sua paciência e ajuda nos meus primeiros passos no laboratório.

Ao Doutor Liang Shi e à Doutora Sara Belchik por me terem recebido de braços abertos no seu laboratório, e pela paciência e empenho em me ensinarem técnicas de biologia molecular. Obrigado por terem tornado a minha estadia nos EUA tão agradável.

Ao Doutor Alfred M. Spormann por me ter recebido no seu laboratório e me ter deixado participar no seu tão prestigiado curso de Microbiologia em Stanford.

A todos os meus colegas de laboratório por terem feito a minha vida no ITQB menos dura com as suas conversas, brincadeiras, partidas e cantorias. Ao nosso ex-colega Eduardo Calçada, que foi também uma fonte de enorme

alegria no laboratório, apesar da sua curta estadia. Um obrigado especial à Doutora Catarina Paquete, ao Doutor Ivo Saraiva e à Sónia Neto pela sua amizade e por me terem ajudado directamente no trabalho realizado.

À Engª. Isabel Pacheco pela sua amizade e apoio constante na purificação das proteínas.

Ao Engº. João Carita pela disponibilidade que sempre demonstrou para me ensinar e ajudar nos crescimentos, especialmente quando iniciei a minha caminhada no ITQB.

A todos os colegas e funcionários do ITQB, pela amizade e pela ajuda nas mais variadas situações.

Aos meus amigos do 5º piso, em especial ao Pedro Matos, pela companhia nas centenas de noites passadas no ITQB. Quero agradecer também pelas inúmeras vezes que me cederam sem hesitação os seus aparelhos e reagentes tão necessários.

À Fundação para a Ciência e Tecnologia (FCT) por ter financiado o meu doutoramento e ao ITQB por ter proporcionado um excelente ambiente para a realização do meu trabalho científico.

À minha querida família, Pai, Mãe, Hugo e Avós, pelo carinho e apoio incondicional, e por me terem aturado nos dias mais complicados. Muito obrigado e desculpem por todos os momentos em que tive que pôr o meu trabalho à vossa frente.

Finalmente, à Helena por ter estado comigo nesta viagem desde o dia um. Obrigado por me complementares, por me ajudares a manter a sanidade, e me mostres que o mundo pode ser feito a dois.

Um muito obrigado a todos, sem vocês não teria chegado ao fim!

Thesis Publications

Fonseca, B.M., Paquete, C.M., Neto, S.E., Pacheco, I., Soares, C.M., Louro, R.O. (2013) "Mind the gap: cytochrome interactions reveal electron pathways across the periplasm of *Shewanella oneidensis* MR-1" *Biochem. J.* vol. 449, pp. 101–108

Fonseca, B.M., Tien, M., Rivera, R., Shi, L., Louro, R.O. (2012) "Efficient and selective isotopic labeling of hemes to facilitate the study of multiheme proteins" *BioTechniques Rapid Dispatches* doi: 10.2144/000113859

Fonseca, B.M., Paquete, C.M., Salgueiro, C.A., Louro, R.O. (2012) "The role of intramolecular interactions in the functional control of multiheme cytochromes *c*" *FEBS Lett.* vol. 586, pp. 504-509

Fonseca B.M., Saraiva I.H., Paquete C.M., Soares C.M., Pacheco I., Salgueiro C.A., Louro R.O. (2009) "The tetraheme cytochrome from *Shewanella oneidensis* MR-1 shows thermodynamic bias for functional specificity of the hemes" *J. Biol. Inorg. Chem.* vol. 14, pp. 375-385

Other Publications

Alves, A.S., Paquete, C.M., **Fonseca, B.M.**, Louro, R.O. (2011) "Exploration of the 'cytochromome' of *Desulfuromonas acetoxidans*, a marine bacterium capable of powering Microbial Fuel Cells" *Metallomics* vol. 3, pp. 349-353 (Cover issue)

Alves, A.S., **Fonseca, B.M.**, Louro, R.O. (2010) "Sludge oomph: harnessing the power of sediment microbiota" Microbiology Book Series - Current Research, Technology and Education Topics in Applied Microbiology and Microbial Biotechnology, A. Méndez-Villas (Ed), pp. 64-73

Abbreviations

dALA	*δ*-aminolevulinic acid
Amp	Ampicillin
Chl	Chloramphenicol
COSY	Correlation spectroscopy
Ccm	Cytochrome *c* maturation
CcpA	Diheme cytochrome *c* peroxidase
CM	Cytoplasmic membrane
CymA	Cytoplasmic membrane cytochrome A
DEAE	Diethylaminoethanol
DIR	Dissimilatory iron reduction
DDM	*n*-dodecyl-*β*-D-maltoside
ET	Electron transfer
FccA	Flavocytochrome *c*
FAD	Flavin adenine dinucleotide
FMN	Flavin mononucleotide
FRT	Flp recombination target
FTIR	Fourier transform infrared spectroscopy
HMQC	Heteronuclear multiple quantum correlation
HTP	Hydroxyapatite
IPTG	Isopropyl *β*-D-1-thiogalactopyranoside
IUPAC-IUB	International union of pure and applied chemistry - International union of biochemistry
Kan	Kanamycin
K_d	Dissociation constant
LB	Luria-Bertani

MFC	Microbial fuel cell
MtrA	Metal terminal reductase subunit A
MtrB	Metal terminal reductase subunit B
MtrC	Metal terminal reductase subunit C
MC	Monte Carlo
NMR	Nuclear magnetic resonance
NOESY	Nuclear overhauser effect spectroscopy
OM	Outer-membrame
OmcA	Outer-membrane cytochrome subunit A
PCR	Polymerase chain reaction
PAGE	Polyacrylamide gel electrophoresis
PDB	Protein data base
RDC	Residual dipolar coupling
ScyA	Monoheme cytochrome c_5
SAXS	Small-angle X-ray scattering
STC	Small tetraheme cytochrome *c*
SoSTC	STC from *Shewanella frigidimarina* NCIMB400
SfSTC	STC from *Shewanella oneidensis* MR-1
SDS	Sodium dodecyl sulfate
TB	Terrific broth
TPPI	Time proportional phase incrementation
Tris	Tris(hydroxymethyl)aminomethane
TpIc$_3$	Type I tetraheme cytochrome c_3

Resumo

A redução dissimilatória de ferro é um importante processo biogeoquímico com um grande impacto no ciclo do ferro, bem como no de outros elementos químicos, que causa uma alteração drástica da composição dos sedimentos e solos terrestres.

As bactérias capazes de reduzir ferro obtêm energia através da oxidação de substratos orgânicos, associada à redução de metais. Como muitos destes metais, nas condições de crescimento das bactérias redutoras de ferro são insolúveis ou pouco solúveis, estes organismos desenvolveram vários mecanismos para uma eficiente transferência de electrões para compostos extracelulares.

Um dos organismos-modelo usado no estudo deste fenómeno é a γ-proteobacteria Gram-negativa *Shewanella oneidensis* MR-1, principalmente devido ao seu fácil cultivo e manipulação genética em laboratório. Esta bactéria também ganhou relevância por ter sido o primeiro organismo que se demostrou ser capaz de produzir electricidade numa bateria microbiana sem a adição de mediadores redox.

A transferência directa de electrões entre células de *Shewanella* e substratos extracelulares, tais como metais ou eléctrodos de baterias microbianas, requer citocromos multi-hémicos do tipo *c*. Estes citocromos permitem a transferência de electrões da membrana citoplasmática, através do espaço periplasmático e da membrana externa, para o aceitador terminal de electrões extracelular. Vários, de entre os 41 citocromos tipo *c* previamente identificados no genoma de *S. oneidensis* MR-1 foram implicados neste processo de transferência electrónica. No entanto, a cadeia de transferência

não está ainda totalmente identificada e compreendida. Este trabalho focou-se no estudo da função biológica dos citocromos periplasmáticos envolvidos na transferência electrónica entre as duas membranas celulares e sua subsequente caracterização.

Usando espectroscopia de ressonância magnética nuclear (RMN), medições cinéticas da transferência de electrões e cálculos electrostáticos foi possível identificar interacções proteína-proteína e os seus respectivos locais de ligação, bem como determinar as constantes de dissociação destes complexos. Os resultados mostram que tanto o STC (small tetraheme cytochrome *c*) como o FccA (flavocytochrome *c*), dois citocromos tetra-hémicos solúveis muito abundantes no periplasma, interagem com os seus parceiros redox membranares, o citocromo tetra-hémico cymA localizado na membrana citoplasmática e o citocromo deca-hémico MtrA situado na membrana externa. Estas interacções ocorrem sempre através de um único hemo, o que impede o estabelecimento de complexos redox estáveis capazes de cobrir a distância entre a membrana citoplasmática e a membrana externa. Os dados recolhidos mostram assim a coexistência de duas vias independentes de transferência electrónica extracelular em *S. oneidensis* MR-1, estabelecidas por interacções proteicas transientes.

Para um melhor entendimento de como se processa o fluxo de electrões na cadeia de transferência electrónica extracelular de *S. oneidensis* MR-1 é necessário caracterizar termodinâmicamente os citocromos envolvidos neste processo. Com esse objectivo, foi feita a caracterização do citocromo STC na gama de pH fisiológico, analisando experiências de RMN de amostras parcialmente oxidadas e titulações redox seguidas por espectroscopia visível no intervalo de pH entre 5.5 e 9.0. Os dados recolhidos revelaram a existência

de interacções redox e redox-Bohr que ocorrem durante a titulação dos hemos. Esta caracterização detalhada das propriedades termodinâmicas do STC mostrou ainda que as interacções electrostáticas intramoleculares entre cofactores redox têm um papel importante no estabelecimento da função biológica da proteína, controlando a forma como os electrões fluem e são distribuídos pelos cofactores a pH fisiológico.

A caracterização de citocromos de elevada complexidade, como multi-hemicos com grande número de hemos (e. g. MtrA), citocromos membranares (e. g. CymA) ou apresentando ambas as características (e.g. MtrC e OmcA) requer o desenvolvimento de novas estratégias. Assim, para o estudo destas proteínas, foi aqui desenvolvido um novo método que permite a produção, em *Escherichia coli*, de citocromos multi-hemicos do tipo *c* isotopicamente marcados de forma específica nos hemos. Este método permite, num único passo, expressar e incorporar eficientemente hemos marcados em átomos específicos, permitindo uma adequada caracterização espectroscópica das proteínas.

A caracterização destes citocromos multi-hemicos permitirá compreender melhor a função destas proteínas, determinar como elas interagem entre si e como os electrões chegam até aos aceitadores extracelulares insolúveis.

Futuramente, esta caracterização permitirá também uma mais informada e eficiente construção de aparelhos e sistemas bioelectroquímicos para a produção de bioenergia e biorremediação envolvendo espécies do género *Shewanella*.

Abstract

Dissimilatory iron reduction (DIR) is an important biogeochemical process with a strong impact not only on the iron cycle but also on the biogeochemical cycles of other elements, changing dramatically the composition of the planet's sediments and soils.

Bacteria capable of DIR obtain energy for growth by coupling the oxidation of organic substrates to the reduction of metal oxides. Due to their chemical and physical properties many metal oxides are effectively insoluble or poorly soluble under the growth conditions of these bacteria. In order to overcome this obstacle, these organisms have developed various mechanisms to efficiently transfer electrons to extracellular compounds.

One of the model organisms used to study this phenomenon, is the Gram-negative ɣ-proteobacterium *Shewanella oneidensis* MR-1 mainly due to its easy laboratory cultivation and genetic tractability. It also gained prominence by being the first organism shown to be capable of powering a microbial fuel cell (MFC) without the need of redox mediators.

Direct electron transfer between *Shewanella* cells and extracellular substrates, such as metal oxides and electrodes from MFCs, involves *c*-type multiheme cytochromes. These cytochromes allow the electron transfer from the cytoplasmic membrane through the periplasmic space and the outer-membrane to the extracellular terminal electron acceptor. Several of the 41 putative *c*-type cytochromes encoded in the genome of *S. oneidensis* MR-1 have been implicated in this process although the electron transfer chain organization still remains to be fully identified and understood. This work focuses on unraveling the biological function of periplasmic cytochromes

involved in bridging electron transfer between the two cellular membranes and their subsequent characterization.

Using NMR to probe protein-protein interactions, kinetic measurements of electron transfer and electrostatic calculations, it was possible to identify protein partners and their docking sites, and determine the dissociation constants. The results showed that both the small tetraheme cytochrome *c* (STC) and the tetraheme flavocytochrome *c* (FccA), two highly abundant soluble periplasmic cytochromes, interact with their membrane associated redox partners, the cytoplasmic membrane tetraheme cytochrome CymA and the outer-membrane decaheme cytochrome MtrA, through a single heme avoiding the establishment of stable redox complexes capable of spanning the periplasmic space. This revealed the co-existence of two non-mixing redox pathways that can lead to extracellular electron transfer in *S. oneidensis* MR-1 established through transient protein interactions.

To better understand how this electron flow occurs, a detailed thermodynamic characterization of the cytochromes involved in the pathway is needed.

Characterization of STC in the physiological pH range was performed, with data collected in the pH range 5.5-9.0 from NMR experiments using partially oxidized samples and from redox titrations followed by visible spectroscopy. These data allowed "parsing" of the redox and redox-protonation interactions that occur during the titration of hemes. This detailed characterization of the thermodynamic properties of the cytochrome showed that electrostatic intramolecular interactions between redox co-factors play an important role in establishing the biological function of the protein by controlling how the electrons flow through and are distributed between the co-factors at physiological pH.

However, the complexity associated with the characterization of multiheme cytochromes with higher numbers of hemes (*e.g.* MtrA), membrane bound (*e.g.* CymA) or displaying both circumstances concurrently (*e.g.* MtrC and OmcA), requires the development of novel strategies to analyze these proteins.

Here, a novel method for production of recombinant multiheme cytochromes *c* in *Escherichia coli* with specific isotopic labeled hemes is reported. Specific isotopic labeling of hemes provides a unique opportunity for a detailed functional and structural characterization of more complex multiheme cytochromes. This method achieves, in a single step, efficient expression and incorporation of hemes isotopically labeled in specific atom positions adequate for spectroscopic characterization of these proteins.

The full characterization of these multiheme cytochromes will allow a better understanding of how these proteins function and interact with each other in the bacterial cell and how the electrons reach their extracellular insoluble acceptors.

Ultimately, this will also allow for a more rational design of bioelectrochemical devices and bioengineered systems for bioenergy production and bioremediation that involve *Shewanella* species.

Table of Contents

Index of Figures

Chapter I – General introduction

Chapter II – The tetraheme cytochrome from *Shewanella oneidensis* MR-1 shows thermodynamic bias for functional specificity of the hemes

Chapter V – Efficient and selective isotopic labeling of hemes to facilitate the study of multiheme proteins

Chapter VI – Concluding remarks and future perspectives

Appendices

Index of Tables

Chapter I – General Introduction

Chapter II – The tetraheme cytochrome from *Shewanella oneidensis* MR-1 shows thermodynamic bias for functional specificity of the hemes

Chapter IV – Mind the gap: cytochrome interactions reveal electron pathways across the periplasm of *Shewanella oneidensis* MR-1

Chapter VI – Concluding remarks and future perspectives

CHAPTER I

General Introduction

INTRODUCTION

Earth as we presently know it owes its existence to Life, just as much as Life owes its existence to Earth. This symbiotic relationship started approximately 4 billion years ago and has been evolving and changing the biogeochemistry of the planet ever since [1,2]. Though higher organisms have played a key role in recent geochemistry, it is within the microbes that we find the most important biogeochemical agents. Microorganisms have changed the Earth in numerous ways, affecting the chemistry, distribution and the bioavailability of nearly all elements in the periodic table [2]. And most remarkably, they have performed these changes in every possible niche known to Man, even the most extreme ones [2,3].

GEOMICROBIOLOGY AND METAL CYCLING

The ability of microorganisms to transfer electrons to and from metals was one of the recent major discoveries made by the Geomicrobiology field [4,5]. The importance of this finding is evident, having changed the way scientists nowadays apprehend metal cycles.

Metals are highly abundant on our planet. Hence, under certain environmental conditions, they play a key role in microbial metabolism as the dominant electron donor or terminal electron acceptor [1,2,4,5]. These metabolisms are thought to be among the most ancient, having probably driven the carbon cycle in the early Life stage and catalyzed the deposition of massive sedimentary ore deposits known as banded iron formations [6,7]. Today, these microbial metabolisms still remain widespread and ecologically influential, controlling the mobilization, distribution and speciation of many

metals (*e.g.* Fe, Mn, Cr, Hg, Au, Mo, Co, Pd, As, Se, U, Te and V) [1,2,4,5,8,9]. Furthermore, the establishment of these metal redox cycles in specific environmental niches contribute greatly to other biotic redox cycles and geochemically relevant abiotic redox conversions.

Because of the importance of microorganisms to both ancient and modern biogeochemical cycles and their potential usefulness in several biotechnologies (*e.g.* microbial fuel cells and bioremediation of environments contaminated by toxic heavy metals), an increase in scientific interest to study these organisms and their metabolisms arose.

Microbial influence on the iron redox cycle. Iron is the most "ironic" of the elements. It is the fourth most abundant element in the Earth's crust, and after oxygen, the most abundant redox-active element capable of sustaining Life *via* iron-coupled redox reactions. On the other hand, at circumneutral pH, oxygen promotes the rapid oxidation of soluble ferrous iron to insoluble ferric iron oxides, leaving the vast majority of the planet's environment with vanishingly low iron concentrations that limits the existence of Life. As a result, only in oxygen-limited environments, such as oxic/anoxic interfaces of sediments, is iron abundant enough that microorganisms can use it as an electron donor or acceptor to sustain growth [10-13].

The elemental cycle of iron comprises complex abiotic and microbiological interactions (Figure 1.1). First thought to be only an abiotic phenomenon, the discovery of microorganisms capable of oxidizing iron raised the hypothesis of biotic involvement in the iron redox cycle [10-13].

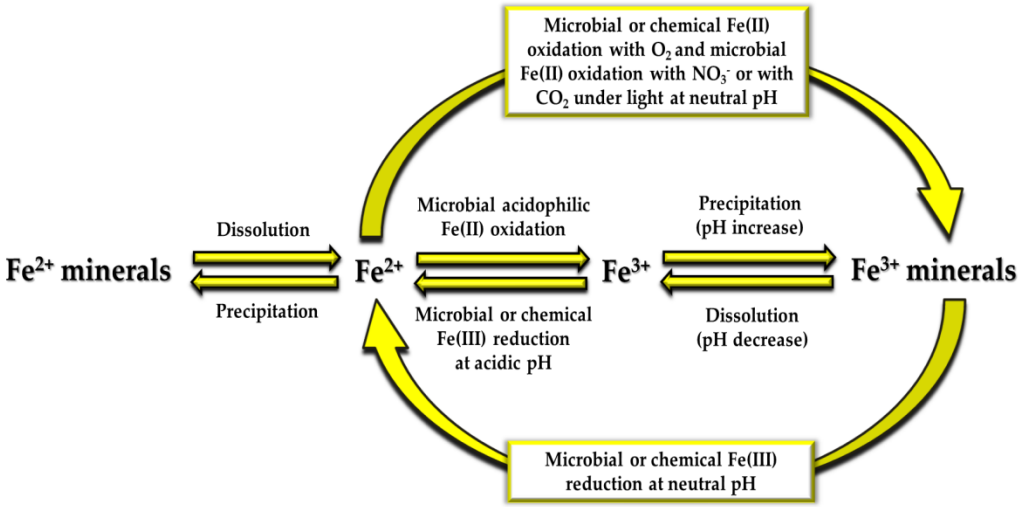

Figure 1.1. Iron biogeochemical redox cycle. Adapted from [11].

Under circumneutral pH conditions the biogeochemical cycling of iron comprises oxic and anoxic habitats where iron is either occurring in its oxidized Fe(III) or reduced Fe(II) redox state, as precipitated or dissolved species. In oxic environments the oxidation of Fe(II) by molecular oxygen is the predominant iron converting process. Aerobic iron-oxidizing microorganisms (*e.g. Gallionella*, *Leptothrix*, *Syderoxydans* and *Mariprofundus* genera) are therefore restricted to micro-aerobic environments where the chemical oxidation rates are sufficiently slow to allow microorganisms to successfully compete with abiotic iron oxidation [11,14-16]. Biotic Fe(II) oxidation at 50 μM O_2 was shown to contribute only 20 % to the iron oxidation, though decreasing O_2 concentration to 15 μM its contribution increased to more than 80 % [14]. At more anoxic conditions, iron oxidation is dominated by anaerobic phototrophic (*e.g. Rhodobacter*, *Rhodomicrobium*, *Chlorobium*, *Rhodovulum*, *Thiodictyon* and *Rhodopseudomonas* genera) [16,17] and nitrate-reducing iron-oxidizing microorganisms (*e.g. Ferroglobus*, *Acidovorax* and *Aquabacterium*) [16,18,19]. Competition with chemical oxidation of Fe(II) by nitrite is only

relevant at elevated nitrite concentrations and in low pH environments [20]. These organisms do not compete with each other since they inhabit different niches and rely on different energy sources (chemical and light energy) or different electron acceptors (O_2, NO_3^-).

Under acidic conditions, Fe(II) is more stable and persists for a longer period of time in the environment even in the presence of O_2. This allows aerobic acidophilic Fe(II)-oxidizing bacteria (*e.g. Acidithiobacillus*; *Acidiferrobacter* and *Ferrovum* genera) to compete with the abiotic oxidation of Fe(II) by O_2 [16,21].

In all cases, microorganisms capable of iron oxidation have to cope with the issue of encrustation due to the formation of insoluble Fe(III) species [22]. The sole exception are the acidophilic Fe(II)-oxidizing bacteria, since Fe(III) is soluble at low pH values.

Iron-oxidation is only one-side of the coin. To close the biogeochemical iron cycle, Fe(III), which at circumneutral pH is mostly trapped in the form of insoluble iron oxides, has to be reduced in order to provide Fe(II) for re-oxidation. This Fe(III) can be either reduced biologically through microorganisms [10,13,23] or chemically by hydrogen sulfide, which is a common end product of microbial sulfur and sulfate reduction [24]. Insoluble Fe(III) species are reduced mostly in anaerobic conditions either by anaerobes (*e.g. Geobacter* and *Geothrix* genera) [25-27] or by facultative anaerobes (*e.g. Shewanella* genus) [28,29]. These dissimilatory iron reducing bacteria are able to perform the biochemically challenging electron transfer to the extracellular insoluble Fe(III) oxides and produce soluble Fe(II). Although there are Fe(III)-reducing bacteria which can couple the reduction of Fe(III) to the oxidation of complex organic compounds, it has been suggested that fermentative

microorganisms break down these compounds and Fe(III)-reducing bacteria use these fermentative end products as carbon sources [30]. Both, *Geobacter* and *Shewanella* have become model organisms to study the biochemical mechanisms of iron reduction and extracellular electron transfer in general [23,31].

Soluble Fe(II) can diffuse once again to the oxic/anoxic interface where it becomes re-oxidized to Fe(III), which precipitates in the form of ferric iron minerals, re-starting this remarkably dynamic and complex biogeochemical cycle. It has been estimated that in sediments each iron atom goes through approximately 100 cycles of oxidation/reduction prior to permanent incorporation [24].

THE GENUS *SHEWANELLA*

Organisms currently assigned to the genus *Shewanella* have been recognized for over 80 years, having first been isolated from the surface of rotten butter in 1931 by Derby & Hammer and given the tentative name *Achromobacter putrefaciens* [32]. Over the next several decades, these bacteria received little attention, with the exception being the constant name changes. In 1941, the taxon was renamed to *Pseudomonas* (*Pseudomonas putrefaciens*) [33] but in 1960 a new classification scheme proposed by Shewan *et al.* [34] reinforced reclassification into the genus *Pseudomonas*. Though, it was only in 1977 that this bacterium was placed with other non-fermentative marine bacteria into the genus *Alteromonas* [35], as *Alteromonas putrefaciens*. In 1985, based on 5S rRNA sequence data collected by MacDonell & Colwell a new reclassification was proposed [36]. This time a new genus *Shewanella* was created to honor Dr. James Shewan for his contributions in the study of these

microorganisms. *Alteromonas putrefaciens* was placed into this genus as *Shewanella putrefaciens* and there has been no further reclassifications made up to date at the level of the genus. Although, most newly discovered *Shewanella* strains were initially classified as *S. putrefaciens,* DNA:DNA hybridization and 16S rRNA sequences has resulted in approximately 60 species assigned to this genus [37,38].

It was only in 1988, with the discovery of the vast array of respiratory electron acceptors (*e.g.* manganese and iron) of some members of the *Shewanella* genus, that these microorganisms started to find a prominent position within the scientific community [39]. These findings strongly suggested that this genus could play important roles in the biogeochemistry of the planet but also in several biotechnological applications, such as microbial fuel cells (MFCs) and bioremediation of environments contaminated by toxic heavy metals [37,40,41]. Presently, these microorganisms have become models for dissimilatory metal reduction studies and a *Shewanella* Federation has been established to study these metabolically versatile bacteria (http://shewanella.org/).

Members of the genus *Shewanella* are facultative anaerobic Gram-negative γ-Proteobacteria. They generally possess a single polar flagellum and a rod shape with 2–3 μm in length and 0.5–0.6 μm in diameter [42] (Figure 1.2).

The vast majority of the *Shewanella* isolates are from marine environments with only a few species being cultured from non-marine environments (*e.g. S. putrefaciens* and *S. oneidensis*). These non-marine species still seem to require the addition of some salt for maximal growth under laboratory conditions [42]. This allows the conjecture of a potential marine origin for all *Shewanella* species.

For example, in the case of *S. oneidensis* MR-1, this specie was isolated in 1988 from the sediments of Lake Oneida (NY, USA) [39]. Although this is a freshwater lake, in 1835 with the construction of the Erie Canal System an opening for the contamination of this lake with seawater arose. Under laboratory conditions it has been observed that *S. oneidensis* MR-1 presents higher growth rates with the addition of salt up to 0.3 M NaCl (seawater concentration is ≈ 0.6 M) [43]. This seems to indicate that this bacterium is still not fully adapted to freshwater environments and that it diverged from its marine origin very recently (< 200 years).

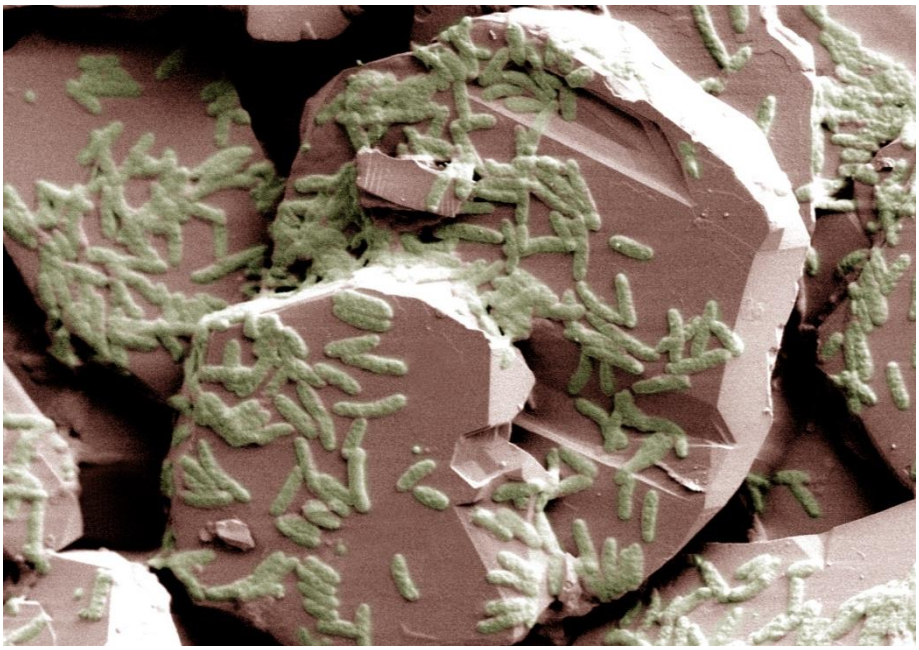

Figure 1.2. *S. oneidensis* MR-1 growing on the surface of the hematite (iron oxide). Image from http://www.pnnl.gov.

One of the major traits of the *Shewanella* species is their capacity to grow at low temperatures (< 5 ºC) even though their optimal growth temperature is above 16 ºC (*e.g.* ≈30 ºC in the case of *S. oneidensis* MR-1) [44]. This ability is useful in environments with large temperature fluctuations. For example, in

Lake Oneida the water temperature ranges from 25 ºC in the summer to 5 ºC in the winter (the lake freezes over completely). The combination of the low depth (average depth of 7 m) with an efficient mixture of the lake's water by winds, makes the water-column temperature usually the same from top to bottom [45].

Another major trait is the ability of the *Shewanella* genus to utilize an enormous variety of organic and inorganic compounds as a final electron acceptor (Table 1.1). This has allowed them to thrive in a wide range of aquatic habitats, both marine and freshwater, and play a role in several biogeochemical redox cycles. Since many of these compounds are toxic or highly insoluble, they do not enter the bacteria and are extracellularly reduced by terminal reductases localized on the outer-membrane of the cell [46]. Their respiratory capability is by far the most diverse ever described, with the possible list of known electron acceptors still incomplete [37].

In contrast to their versatility with regard to electron acceptors, the *Shewanella* genus tends to be rather limited in its ability to use carbon sources. Most *Shewanella* species only grow on carbon sources, such as glucose, *N*-acetylglucosamine, formate, pyruvate, succinate and lactate [28].

In 2001, the genome of *S. oneidensis* MR-1was sequenced primarily due to its position as a model organism for dissimilatory metal reduction and its potential role in several biotechnologies [47]. Since that date approximately 20 other *Shewanella* genomes have been sequenced.

Analysis of the *S. oneidensis* MR-1 genome revealed that the chromosome encodes for 41 putative *c*-type cytochromes (9 in the cytoplasmic membrane, 27 in the periplasm, and 5 in the outer membrane) [48,49]. The capability to transfer electrons to a vast range of electron acceptors (*e.g.* insoluble metals

and toxic compounds) under anoxic conditions is presumably due to this large number of *c*-type cytochromes.

The ability to grow *Shewanella* robustly under oxygen conditions, the large quantity of sequenced genomes, and their easy genetic manipulation makes these bacteria ideal to work with in the laboratory.

Table 1.1. Some of the electron acceptors utilized by *Shewanella*. Adapted from [28].

Electron acceptor	Reduction products
Oxygen	H_2O
Nitrate	NO_2^-, NO, N_2O, N_2 and NH_4^+
Nitrite	NO, N_2O, N_2 and NH_4^+
Mn (IV) Solid	Mn (II) Soluble
Mn (III) Chelate	Mn (II) Soluble
Mn (III) Solid	Mn (II) Soluble
VO_2^+	VO^{2+}
Fe (III) Chelate	Fe (II) Soluble
$Fe(OH)_3$ Ferrihydrite	Fe (II) Soluble
FeO(OH) Goethite	Fe (II) Soluble
Fe_2O_3 Hematite	Fe (II) Soluble
Fe_3O_4 Magnetite	Fe (II) Soluble
Fe (III) Clay smectite	Fe (II) Soluble
SO_3^{2-}	H_2S
$S_2O_3^{2-}$	H_2S
Sulfur (S^0)/Polysulfide	H_2S
U (VI) Soluble	U (IV) Solid
Cr (VI) Soluble	Cr (III) Solid
Selenite	Se^0 Solid
Arsenate	Arsenite, As^0
Tc (VII) Soluble	Tc (IV) Solid
Iodate	Iodide
Trimethylamine-*N*-oxide (TMAO)	Trimethyl amine
Dimethylsulfoxide (DMSO)	Dimethylsulfide
Fumarate	Succinate
Glycine	Alanine

STRATEGIES USED BY *SHEWANELLA* FOR EXTRACELLULAR ELECTRON TRANSFER

Microorganisms that perform extracellular respiration have developed several strategies for transferring electrons to a terminal acceptor localized outside the cell. The molecular mechanisms of electron transfer to these extracellular substrates can be divided broadly in indirect electron transfer and direct electron transfer [23] (Figure 1.3). The study and elucidation of these mechanisms have led to a better understanding on how extracellular electron transfer occurs in these organisms.

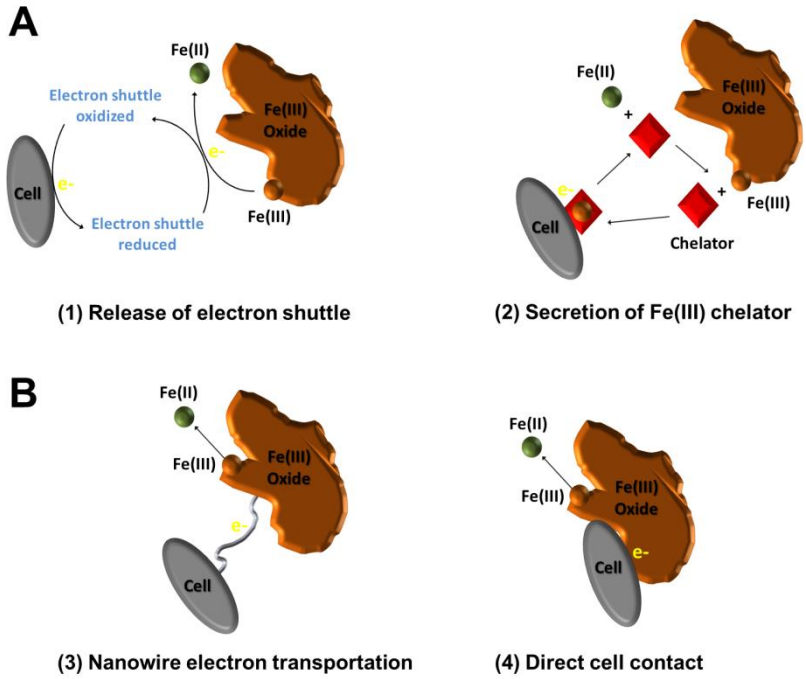

Figure 1.3. Strategies that may be employed by the *Shewanella* genus for electron transfer to insoluble extracellular electron acceptors. Extracellular electron transfer can occur by indirect contact (**A**) through electron transfer mediated by electron shuttle compounds (**1**) or through the secretion of metal chelators (**2**). Extracellular electron transfer can also occur by direct contact (**B**) through cell appendages known as nanowires (**3**) or through direct cell contact via outer-membrane multiheme cytochromes (**4**).

Indirect electron transfer. Evidence for indirect electron transfer to extracellular substrates was reported as early as 2000 [50]. Indirect electron transfer has been proposed to take place via electron shuttles (*e.g.* flavins) (Figure 1.3-A1) and metal chelators (*e.g.* siderophores) (Figure 1.3-A2), and is used by cells in the bacterial biofilm that cannot contact directly with the surface of the extracellular electron acceptor [23].

Electron shuttles. Electron shuttles can be exogenous (*e.g.* humic acids) or endogenous (*e.g.* flavins). The possible involvement of endogenous electron shuttles in reduction of poorly soluble metal minerals by *Shewanella* was first proposed by Newman & Kolter [50]. Evidence to further support the participation of electron shuttles in the dissimilatory iron respiration of *S. oneidensis* MR-1 metal reducing bacteria was also found by Lies *et al.* [29]. They demonstrated that iron oxide entrapped within nanoporous glass beads could be reduced by this bacterium. Similarly, work performed by Nevin & Lovley revealed, although in a different organism, that *Geothrix fermentans* could produce an electron shuttle with characteristics of a water-soluble quinone [51]. The ability of flavins to enhance iron reduction was first examined by Myers & Myers [52]. These workers showed that addition of flavin mononucleotide (FMN) increased ferric reductase activity in *S. oneidensis* MR-1. More recent evidences, showing that flavins are responsible for indirect extracellular electron transfer have been reported. These confirm that not only the *Shewanella* genus is capable of secreting flavins but also that the existence of flavins, such as riboflavin, FMN and flavin adenine dinucleotide (FAD) in the growth media increases greatly the iron reduction rates of poorly soluble iron oxides [53-55].

Kinetic results showed that direct contact between the outer-membrane multiheme cytochromes (*e.g.* OmcA and MtrC) and insoluble iron substrates or MFC anodes could not account for the rates of electron transfer observed when using whole cells assays [56,57]. This gap in electron transfer rates was resolved with the addition of flavins. This demonstrated that outer-membrane cytochromes are not the only elements responsible for the electron transfer to insoluble iron at relevant kinetic rates and that direct and indirect electron transfer occur in tandem in *S. oneidensis* MR-1 [56]. Moreover, recently it has been shown that the outer-membrane cytochromes account for at least 95 % of the reduction of extracellular flavins at physiological relevant rates [58].

With reduction potentials of −219 mV (FMN and FAD) and −208 mV (riboflavin) [59], these flavins have the potential to act as efficient extracellular redox mediators for the reduction of metal oxides at neutral pH (redox couple ferrihydrite/Fe^{2+} has a reduction potential ranging from −100 to +100 mV [60]). Thus, this gives S*hewanella* species that are able to secrete and utilize flavins as electron shuttles an advantage in environments that contain poorly soluble metal oxides but lack exogenous redox mediators, such as humic acids. Another advantage of flavin secretion by *Shewanella* species is their potential application in the construction of MFCs without addition of costly exogenous redox mediators [61]

Metal chelators. Several studies have shown that reduction of Fe(III) oxides is enhanced upon addition of synthetic chelators, although experimental evidence for this occurring with chelators of microbial origin is still limited [62,63]. Nevertheless, soluble organic-Fe(III) complexes have been detected in cultures of *S. putrefaciens* strain 200 grown with iron oxides in the absence of exogenous chelating compounds [64]. Moreover, while flavins

function as electron shuttling agents in the *Shewanella* genus, these molecules also possess metal chelating capacity [53]. Therefore, it is possible that these electron shuttles may act as endogenous metal chelators.

Another type of endogenous iron-binding agent is siderophores. These chelating compounds are produced by various organisms in response to iron limitation and have a very high affinity towards Fe(III) [65]. However, the relevance of siderophores in dissimilatory metal reducing processes has been questioned on the basis of the inadequate redox potential of the chelated metal [66]. More recently, deletion mutants on siderophore biosynthesis pathways as well as of their receptors and reductases in *S. oneidensis* MR-1 showed that they do not have a main role in dissimilatory metal reduction even though soluble forms of Fe(III) are detected [67].

Direct electron transfer. Early studies with *S. oneidensis* MR-1 supported a mechanism of physical contact for growth on insoluble manganese oxide [39,68]. Work developed by Lower *et al.* [69] revealed the first experimental evidence for this mechanism in *Shewanella*. These workers were able to show, using atomic force microscopy (AFM), that there was preferential binding of the metal oxide to *Shewanella* cells anaerobically grown in contrast to aerobically grown cells. A recent vivid demonstration has been reported, by recording a movie under a microscope of insoluble MnO_2 dissolution by *S. oneidensis* MR-1. Individual cells are seen touching and swimming away from the metal oxide that is slowly being dissolved [70]. This direct contact can be mediated via electrically conducting appendages called pili or nanowires [71-75] (Figure 1.3-B3). Electrical contact can also occur by redox proteins protruding from the cell surface (Figure 1.3-B4). A great number of multiheme cytochromes are found in organisms capable of dissimilatory metal reduction,

with several of them directly implicated in direct extracellular electron transfer [46,76,77].

Nanowire electron conductivity. Electron transfer via direct contact in *Shewanella* can be mediated by electrically conductive pili, also known as nanowires, which are hypothesized to assist in the electron transfer from the bacterial cells to extracellular electron acceptors (Figure 1.4) [73]. Scanning tunneling microscopy (STM) showed various thin filaments with about 8 nm in diameter and tens of microns in length.

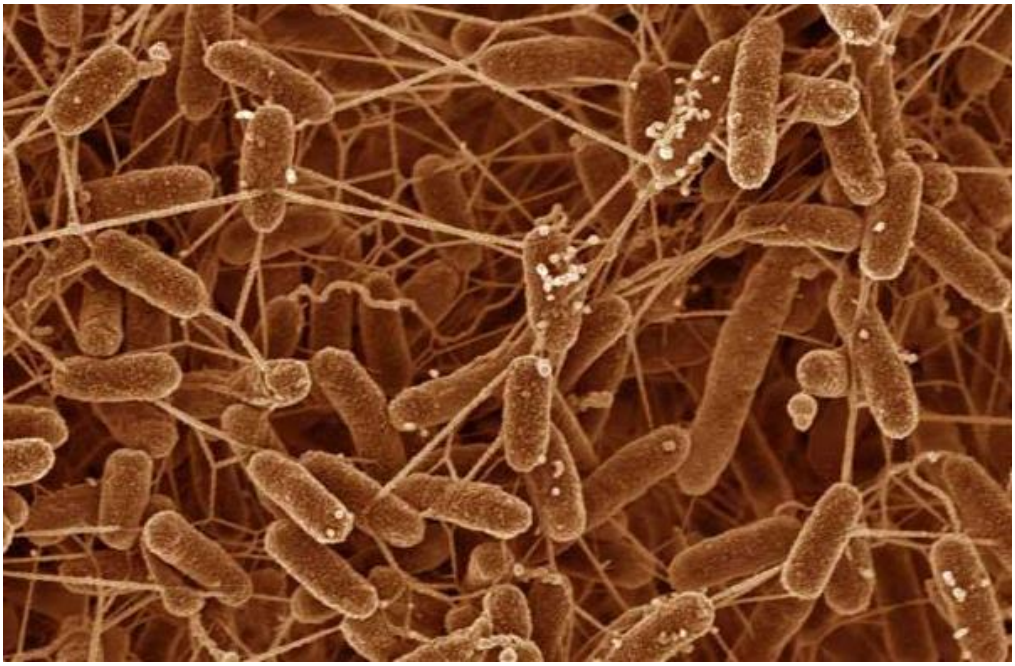

Figure 1.4. Electrically conductive nanowires from *S. oneidensis* MR-1. Image from http://www.newscientist.com/article/dn9526-bacteria-made-to-sprout-conducting-nanowires.html

Other organisms such as *Geobacter* sp. also produce microbial nanowires [78]. In terms of morphology *Shewanella* and *Geobacter* nanowires are similar and are thought to be partially composed of *c*-type cytochromes [31,72,73,75,78]. This was demonstrated in *Shewanella* by deleting the genes

coding for the outer-membrane cytochromes, MtrC and OmcA, resulting in non-conductive pili structures [73]. Also, deleting the *gspG* gene which is involved in the type II secretion pathway, that is required for the proper export of the outer-membrane cytochromes MtrC and OmcA to the cell exterior [79,80], resulted in non-conductive pili structures. Recently, it was concluded that *Shewanella* nanowires were not essential for extracellular electron transfer to metal oxides or anode surfaces and should play a role in aiding contact between bacterial cells in the biofilm or with the metal oxide [80,81]. For example, *S. oneidensis* MR-1 strains deficient in the flagellum and in the pil type IV pili generated more current in MFCs than wild-type strain, while strains deficient in the msh type IV pili, showed only a 20% decrease in current output relative to the wild-type [80].

Direct cell contact via outer-membrane cytochromes. Evidence for this extracellular electron transfer mechanism in *Shewanella* was first observed by Lower *et al.* [69]. These workers were able to show binding of *Shewanella* whole cells, grown anaerobically using ferric iron as an electron acceptor, to goethite (a species of iron oxide). They inferred that a putative terminal iron reductase with ≈150 kDa was involved in the binding process. In *S. oneidensis* MR-1 the likely candidate proteins for this putative terminal iron reductase include the outer-membrane (OM) decaheme cytochromes OmcA and MtrC, which are both extracellulary exposed and combined have a molecular weight of ≈160 kDa (Table 1.2) [82]. More recently, it was also shown that both these OM cytochromes bind with high affinity to hematite (a species of iron oxide) through a direct contact mechanism and are able to efficiently transfer electrons to it [83-86].

PROTEINS INVOLVED IN DISSIMILATORY IRON REDUCTION

To transfer electrons to extracellular insoluble metals, *Shewanella* utilizes an extensive network of *c*-type cytochromes that spans from the cytoplasmic membrane to the outer-membrane [48,49]. Of course, not all the 41 putative *c*-type cytochromes are required simultaneously. Using a variety of genetic (*e.g.* knock-out studies) and biochemical techniques (*e.g.* protein characterization), some of the components involved have been identified (Table 1.2; Figure 1.5). The so called "minimal setup" of redox proteins which are believed to be responsible for the ability to transfer electrons to extracellular ferric iron will be discussed below.

Table 1.2. Cytochromes involved in dissimilatory iron reduction in *Shewanella*. Abbreviations: Cytoplasmic Membrane (CM), Periplasm (P), Outer Membrane (OM), Electron Transfer (ET), not detected (n.d.)

Protein	Molecular mass (kDa)	Cofactors	Localization	Function	References
CymA	21	4 hemes	CM/P	ET to various reductases	[87-89]
STC (CctA)	12	4 hemes	P	Implicated in Fe reduction	[90-92]
FccA (Fcc_3)	64	4 hemes	P	Fumarate terminal reductase/Implicated in Fe reduction	[92-95]
MtrA	37	10 hemes	P/OM	Implicated in Fe reduction	[96,97]
MtrB	78	n.d.	OM	Localization of MtrA, MtrC and OmcA	[97-99]
MtrC (OmcB)	75	10 hemes	OM	Potential terminal Fe reductase	[100-103]
OmcA	85	10 hemes	OM	Potential terminal Fe reductase	[100,103]

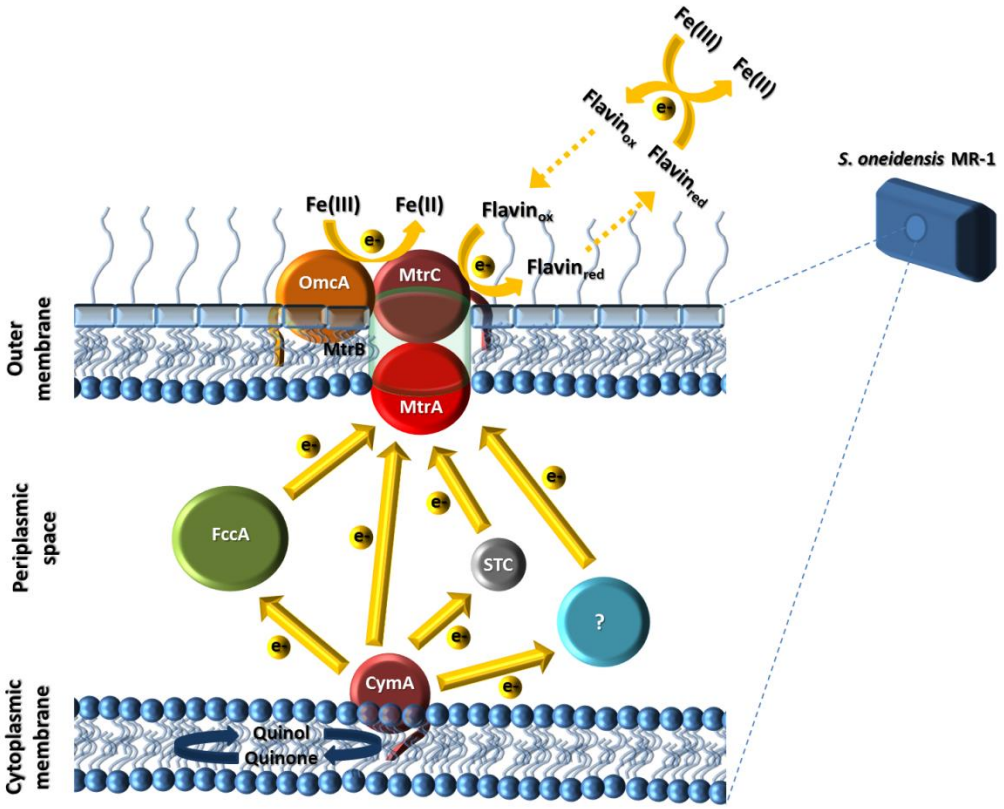

Figure 1.5. Schematic representation of the components involved in the dissimilatory iron reduction in *S. oneidensis* MR-1. Solid unidirectional arrows represent possible electron transfer steps. Dashed arrows indicate electron shuttle movements.

Electron transfer at the cytoplasmic membrane. Electron transfer at the cytoplasmic membrane (CM) involves the linkage of dehydrogenases responsible for oxidation of carbon sources in the cytoplasm (*e.g.* formate dehydrogenase), through a lipid soluble quinone pool, to electron transfer proteins (*e.g.* cytochromes) bound to the CM [104]. This mechanism generates a proton-electrochemical gradient that will be used to produce ATP via the ATP synthase [105].

Quinones, such as menaquinones ($E^{o\prime} \approx -80$ mV) and ubiquinones ($E^{o\prime} \approx +80$ mV), were shown to be required for anaerobic respiration in *Shewanella* [89]. Genetic studies where deletion of the *menD* and *menB* genes involved in the biosynthesis of menaquinone produced a phenotype incapable of iron respiration [89,106]. This revealed the role of menaquinone and not ubiquinone in the metal respiration. The origin of this specificity and its physiological relevance remain to be established, although a detailed structural and biochemical characterization of the electron transfer protein involved in electron transfer across the CM may reveal the answer. Presently, it is well known that the CM electron transfer protein involved in metal respiration is a tetraheme *c*-type cytochrome protein called CymA [87-89].

Cytoplasmic membrane cytochrome CymA. CymA is 21 kDa tetraheme *c*-type cytochrome bound by a α-helical anchor to the periplasmic side of the CM in *Shewanella*. It has been identified as a member of the NapC/NirT protein family and demonstrated to be able to bind quinol (K_d = 0.1-1 μM [107]) and function as a quinol oxidase [89,108,109]. As such, CymA plays a role as an electron transfer intermediate between the menaquinone pool and the various downstream periplasmic electron transfer proteins. Deletion of the *cymA* gene encoding this protein severely disabled reduction of a variety of substrates including Fe(III)/Mn(IV) oxides, fumarate, nitrate, and DMSO [87,88], allowing the proposal that CymA is one of the major hubs for electron transfer to the periplasm. Also, several studies have demonstrated CymA's ability to interact with multiple periplasmic cytochrome partners [108,110].

Although no structural characterization is presently available (Figure 1.6), recent studies have shown that this tetraheme cytochrome has three low-

spin hemes with bis–histidine axial ligation and one high-spin heme with a histidine–water axial ligation [89]. This high-spin heme forms an intrinsic part of the quinol oxidation site. Also, site-directed mutagenesis experiments revealed that the amino acid Lysine-91 is essential for quinol interaction with CymA from *Shewanella* sp strain ANA-3 [107].

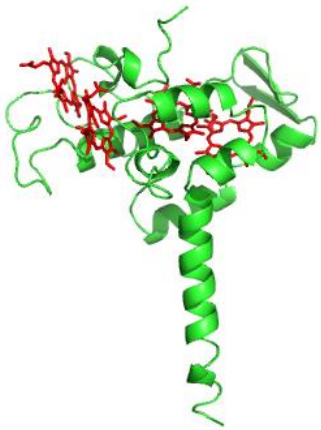

Figure 1.6. Homology model of CymA to *Desulfovibrio vulgaris* NrfH (PDB code 2J7A), tetraheme cytochrome subunit of nitrite reductase NrfAH. Model was made using SWISS-MODEL [111,112].

Redox properties have also been determined for CymA from *S. oneidensis* MR-1, with macroscopic midpoint potentials at pH 7.0 of approximately -110, -190 and -265 mV for the three low-spin hemes and -240 mV for the high-spin heme [89]. These potentials are below that of the menaquinol/menaquinone couple ($E^{o\prime} \approx$ -80 mV), and thus electron transfer only becomes efficient when the menaquinol/menaquinone balance is shifted towards menaquinol. Although once the electrons enter the heme network, electron flow to the metal oxides becomes thermodynamically favorable due to progressively less negative redox potentials of the electron transfer proteins involved [113].

Further confirmation of its relevance in iron reduction was obtained by heterologous expression of CymA, where the production of this cytochrome was sufficient to endow *E. coli* with the ability to reduce soluble ferric iron [114].

Electron transfer across the periplasmic space. The reduction of substrates incapable of diffusion into the periplasm, such as insoluble metal oxides, require the reducing equivalents generated at the CM to be transferred across the periplasmic space of *Shewanella* (≈235 Å wide [115]) by means of intermediate electron transfer proteins (*e.g.* multiheme cytochromes). Two highly abundant periplasmic cytochromes from the *Shewanella* genus have been implicated to some degree in this process, one is the tetraheme flavocytochrome *c* FccA (also known as Fcc_3) [92,95] and the other is the small tetraheme cytochrome *c* STC (also known as CctA) [90,92,116].

Flavocytochrome *c* FccA. FccA is a 64 kDa tetraheme *c*-type flavocytochrome that has been shown biochemically to be a unidirectional fumarate reductase with a FAD cofactor in the active site and is responsible for the reduction of fumarate to succinate in the *Shewanella* genus [117]. This enzyme is unique in comparison to other fumarate reductases since it is a monomeric soluble periplasmic protein. X-ray crystal structures of FccA from *S. frigidimarina* NCIMB400 and *S. oneidensis* MR-1 are available [118,119] (Figure 1.7), showing that these proteins fold into three domains. An N-terminal cytochrome domain with four bis–histidine low-spin *c*-type hemes, a C-terminal flavoprotein domain with a non-covalently bound FAD group and a clamp domain that may control the access to the active site of the enzyme. The hemes found in the N-terminal cytochrome domain of FccA are arranged in a quasi-linear architecture that allows an efficient conduction of the electrons across the length of the domain [94,118,119]. Electron transfer to the active site is performed by heme IV, which is located in close proximity (≈5 Å) to the FAD cofactor (Figure 1.7).

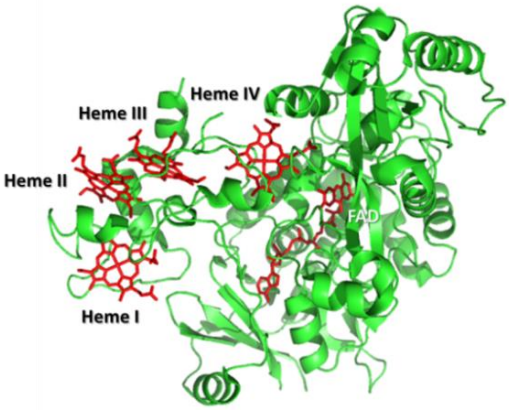

Figure 1.7. Cytochrome representation made with PyMOL using the structure of FccA (PDB code 1D4D) from *S. oneidensis* MR-1. The Roman numerals correspond to the order of heme attachment to the polypeptide chain.

Redox properties have been obtained for FccA from *S. frigidimarina* NCIMB400 and *S. oneidensis* MR-1, revealing similarities between these two ortholog proteins [94]. The microscopic reduction potentials of the hemes from both FccA were shown to cover a similar potential range: -148 to -270 mV and -145 to -286 mV for *S. frigidimarina* NCIMB400 and *S. oneidensis* MR-1, respectively. Also, for both proteins the heme redox interactions are dominated by the interaction between hemes II and III (+65 and +95 mV, for *S. frigidimarina* NCIMB400 and *S. oneidensis* MR-1, respectively). Futhermore, the effect of protonation on the reduction potentials of the hemes (redox–Bohr effect), in both FccA, is small and of similar magnitude for all the hemes.

Several studies have showed both *in vitro* and *in vivo* the occurrence of electron transfer between CymA and FccA [95,108,120]. Intriguingly, recent studies have revealed that FccA is one of the most prominent cytochromes in the periplasmic space of *S. oneidensis* MR-1 grown anaerobically with ferric iron as the electron acceptor [95]. Also, these studies demonstrated that FccA could transfer electrons to MtrA, an outer-membrane associated decaheme cytochrome implicated in iron reduction [95]. Thus, due to its high abundance and its connection with CymA and MtrA, FccA can be suggested as a possible

candidate for electron shuttling in the periplasm during extracellular respiration of metal oxides. Additional data in support of this role is reported in this thesis.

Small tetraheme cytochrome STC. STC is a highly abundant small tetraheme cytochrome *c* with a molecular weight of 12 kDa from the periplasm of *Shewanella* [116]. Presently high resolution crystal structures of STC from *S. oneidensis* MR-1 are available (Figure 1.8), for both reduced and oxidized state [91]. For *S. frigidimarina* NCIMB400 a nuclear magnetic resonance (NMR) solution structure of STC was recently determined for the reduced state [121]. Comparison of the structures from these two proteins showed that the general fold is similar and the relative positions of the heme groups are well conserved [121]. The arrangement of the pairs of hemes in perpendicular and parallel geometries allows the required distance between the cofactors for a controlled intramolecular transfer of the electrons [122]. Also, all four hemes are low-spin and have a bis–histidine axial ligation to the polypeptide chain [91,121].

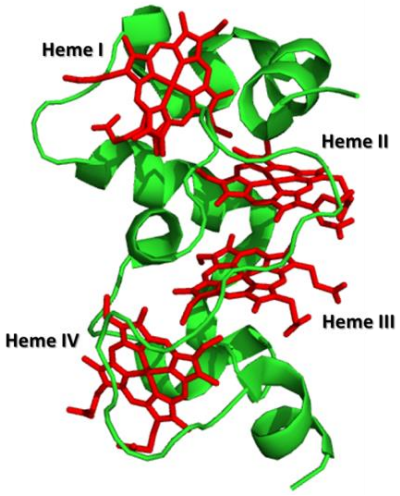

Figure 1.8. Cytochrome representation made with PyMOL using the structure of STC (PDB code 1M1Q) from *S. oneidensis* MR-1. The Roman numerals correspond to the order of heme attachment to the polypeptide chain.

Redox properties have been obtained for STC, with the microscopic reduction potentials for the four hemes of STC from *S. frigidimarina* NCIMB400 being determined by Pessanha *et al.* [123]. In the fully reduced and protonated protein state the hemes presented the following redox potentials -190, -212, -199; -229 mV for hemes I, II, III and IV, respectively. These are modulated by redox interactions between the four hemes (covering a range of 8 to 56 mV) and by interactions between the hemes and a protonable center (-4 to -36 mV) located in close proximity to heme III. All of the interactions are clearly dominated by electrostatic effects and the microscopic reduction potential of heme III is the one most affected by the oxidation of the other hemes and by the protonation state of the molecule. Also, in the case of STC from *S. oneidensis* MR-1, Harada *et al.* [124] determined the reduction potentials of the four hemes and their pairwise interactions at high non-physiological pH (pH 9.1). However, the effect of pH on the reduction potentials of the hemes (redox-Bohr effect) was not taken in consideration and the interactions between hemes suggest the presence of significant positive cooperatives that are difficult to reconcile with the minor redox-linked changes observed in the structures [91].

The implication of STC as an integral component in the iron respiration pathway was identified in *S. frigidimarina* NCIMB400 based on gene knock-out experiments [90]. In *S. oneidensis* MR-1 knock-out of the *cctA* gene gave origin to a marginally defective phenotype in iron reduction [125,126]. Thus, it is possible that STC could be one of the electron transfer proteins responsible for passing electrons across the periplasmic space, from the CymA cytochrome to the outer-membrane metal reductases, in extracellular electron transfer although further characterization is needed to determine its physiological function.

Electron transfer across the outer-membrane. In order to reduce insoluble electron acceptors, electrons must pass through the outer-membrane (OM) and reach the cell exterior. Several redox proteins from *Shewanella* have been shown to be associated or bound to the OM. Of these the MtrCAB-OmcA protein complex has been determined to be required for maximal extracellular iron reduction rates [46,99,101,127,128]. The genes encoding for this protein complex are clustered in the following sequential order *omcA-mtrC-mtrA-mtrB*.

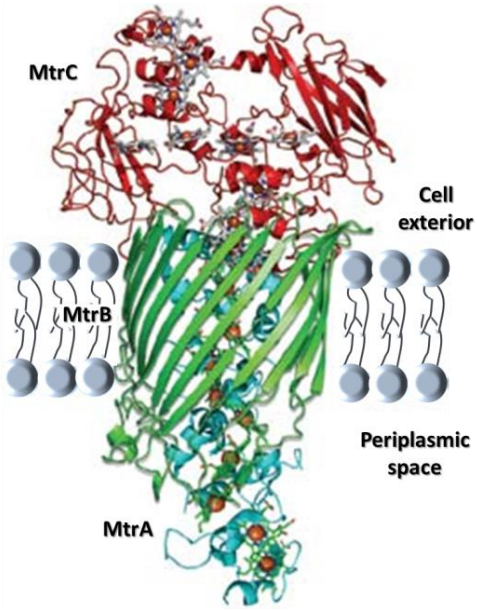

Figure 1.9. Representation of the MtrCAB complex. Adapted from [129]. The structure of the decaheme cytochrome MtrC (red) is based on that of MtrF (PDB code 3PMQ). The structure of MtrA (blue) is based on that of two pentaheme NrfB monomers (PDB code 2OZY) fused end to end. The degree to which the multiheme cytochromes are embed into the porin MtrB (green) sheath is not currently known and this cartoon is therefore purely illustrative.

Outer-membrane decaheme cytochromes MtrC and OmcA. MtrC (previously known as OmcB) and OmcA are two OM anchored cytochromes with 75 kDa and 85 kDa, respectively [82,100,101]. Both cytochromes were shown to have 10 low-spin *c*-type hemes and to be extracellularly exposed [82,102,109,130]. Treatment by proteinase K significantly degraded MtrC and OmcA by 31 % and 71 %, respectively [82]. This indicates that MtrC is not as exposed to the extracellular environment as OmcA, which is coherent with the

fact that MtrC becomes partly buried upon association with the β-barrel protein MtrB (Figure 1.9).

Several studies have shown that these two OM cytochromes are highly expressed by *S. oneidensis* MR-1 under ferric iron reducing conditions [101,127,128] and are capable of direct electron transfer to iron oxides [84-86]. Disruption of the *mtrC* or *omcA* genes did not affect the growth of *S. oneidensis* MR-1 on soluble terminal electron acceptors, such as fumarate, nitrate and DMSO [100]. In contrast, reduction of insoluble iron oxides and electron transfer to MFC anodes was severely diminished [58,102,126,127,130,131]. A series of knock-out mutations of all the outer-membrane cytochromes and subsequent expression of each one individually, showed that MtrC is pivotal for extracellular electron transfer and that mutants containing only the OmcA cytochrome were not capable of transferring electrons to iron [128]. This fact suggests that while OmcA is an iron terminal reductase [56,100], its contact with the periplasmic redox chain is mediated by MtrC [128]. Recent studies have additionally shown that MtrC is responsible for most of the electron transfer to carbon electrodes, while OmcA is involved in cellular attachment to solid surfaces and plays a smaller role in electron transfer [58]. This is coherent with data obtained by antibody functionalized atomic force microscopy (AFM) tips that showed OmcA in the interface between the cell and insoluble substrate, while MtrC displays a more uniform distribution across the cell surface [130]. Furthermore, the binding strength of OmcA to ferric iron oxide was shown to be approximately twice that for MtrC, while the binding frequency of MtrC to the iron oxide was twice that for OmcA [83,84]. Both MtrC and OmcA polypeptides contain a putative hematite-binding motif (Ser/Thr-Pro-Ser/Thr) [132].

In vivo cross-linking studies revealed that MtrC interacts with the *β*-barrel protein MtrB forming in combination with the decaheme cytochrome MtrA an OM membrane protein complex MtrCAB, with a 1:1:1 stoichiometry (Figure 1.9) [133]. Also, the cross-linking assays demonstrated that MtrC and OmcA physically interact with each other on the bacterial cells [133,134], although the stoichiometry of this interaction is still unclear. *In vitro* studies performed by *Shi et al.* showed that MtrC and OmcA form a stable complex with a dissociation constant smaller than 0.5 μM [103]. These workers also verified that the physical interaction between MtrC and OmcA synergistically boosts the metal reductase activity of these OM cytochromes [103].

Ross *et al.* revealed that purified MtrC and OmcA reduced iron oxides at much slower rates compared to measurements with intact *Shewanella* cells [56]. However, these workers also showed that with the addition of flavins, rates can be increased to values comparable to those measured with intact cells [56]. These results suggest an electron shuttle role for flavins during MtrC and OmcA mediated reduction of ferric iron oxides.

Potentiometric titrations revealed that both MtrC and OmcA titrate over a broad range of redox potentials from +100 mV to -500 mV and -20 mV to -320 mV, respectively [102,103,113].

Recently a crystal structure of the OM decaheme *c*-type cytochrome MtrF has been determined [135]. MtrF is a paralog of MtrC and OmcA, with an amino-acid identity compared to MtrF of 34 % and 25 %, respectively [126]. MtrF also has the ability to reduce metals and MFC anodes but its physiological function was recently proposed to be reduction based detoxification of radionuclides [128,136]. The MtrF structure has provided the unprecedented molecular structural evidence for understanding how the

function of the OM cytochromes MtrC and OmcA [135]. The ten hemes are organized across four domains in a unique crossed formation in which a staggered 65 Å octaheme chain transects the length of the protein and is bisected at the middle by a 45 Å tetraheme chain (Figure 1.9). Each heme is within 7 Å from each other, allowing efficient electron transfer among the hemes. Structural characteristics of MtrF support the idea that the extracellularly exposed cytochromes, such as MtrC and OmcA, transfer electrons directly to the surface of Fe(III) oxides *via* their solvent-exposed hemes (hemes V and X in the case of MtrF). Furthermore, they support that these OM cytochromes can also reduce and use flavins for the reduction of insoluble iron oxide (*via* hemes II and VII in the case of MtrF) [135].

Decaheme cytochrome MtrA. MtrA is a 37 kDa periplasmic cytochrome with 10 bis–histidine low-spin *c*-type hemes, associated with the OM *via* the integral membrane protein complex MtrCAB (Figure 1.9) [46,77,96,133,137]. *In vivo* cross-linking assays have shown that MtrA interacts on the periplasmic side with the OM *ß*-barrel protein MtrB [133]. Also, it has been shown that MtrA forms a stable protein complex with a dissociation constant smaller than 0.1 μM with its OM partners, MtrB and MtrC [137]. Pitts *et al.* showed that overexpression of MtrA in *E. coli*, allow this bacterium to gain the ability to reduce soluble chelated ferric iron [96]. It is so far the only soluble multiheme cytochrome that was shown to be necessary for ferric iron reduction [101,125,126].

Shewanella contains several other periplasmic decaheme cytochromes homologous to MtrA. These are the MtrD, the DmsE and the gene product of SO4360 with an amino-acid identity compared to MtrA of 68 %, 64 % and 53 %, respectively [126]. These paralogs, although involved in other extracellular

electron transfer pathways [128,138], were shown to be able to replace a MtrA knock-out mutant and restore iron reduction competency [126].

Using small-angle X-ray scattering it was recently shown that MtrA is shaped like an extended molecular "wire" with overall dimensions 104 Å x 20 Å x 50 Å [139]. Given the thickness of the Gram-negative OM is ≈70 Å [140], the estimated length of MtrA is sufficient for transferring electrons heme-to-heme across the entire OM. Potentiometric redox titrations have showed that MtrA reduces over a potential range of -100 mV to -400 mV at pH 7.5 [96].

In vitro assays have revealed that MtrA can be directly reduced by CymA [95,110]. However, *in vitro* studies performed by Schuetz *et al.* also showed that MtrA is able to interact and receive electrons from the periplasmic cytochrome FccA [95]. Until now, it remains unknown if MtrA dissociates from the MtrCAB complex and interacts directly with the cytoplasmic membrane CymA or if a more complex *c*-type cytochrome network exists in the periplasm of *Shewanella*.

Outer-membrane *ß*-barrel protein MtrB. MtrB is a 78 kDa *β*-barrel protein with no heme cofactors, essential for the extension of the electron transfer chain from MtrA to the OM in the *Shewanella* genus [99]. Its pore size estimated to be larger than 30 Å x 40 Å, and can in principle embed at least partially, MtrA and MtrC (Figure 1.9) [139]. The role of MtrB in metal reduction was first demonstrated by Beliaev & Saffarini [99], where a MtrB knock-out mutant strain was shown to have lost its ability to reduce Fe(III) and Mn(IV) oxides. Furthermore, MtrB knock-out mutants in *S. oneidensis* MR-1 showed mislocalization of the OM decaheme cytochromes MtrC and OmcA [98]. Also, it was demonstrated that decaheme cytochrome MtrA is only associated with the OM when MtrB is expressed [141].

Several other OM β-barrel proteins homologous to MtrB are expressed by *Shewanella*. These are the MtrE, the DmsF and the gene product of SO4359 with an amino-acid identity compared to MtrB of 35 %, 35 % and 25 %, respectively [126]. Only the paralog MtrE was shown to be able to replace a MtrB knock-out mutant and restore iron reduction capability [126].

Schicklberger *et al.*, using knock out mutations and subsequent monitoring of complex assembly, showed the existence of a synergetic relationship between MtrA and MtrB [97]. The assembly of the MtrAB subcomplex stabilizes MtrB, while subcomplex MtrBC does not assemble in the absence of MtrA. Three other stable modules similar to MtrAB have been identified in *S. oneidensis* MR-1, all of which are thought to be involved in some type of extracellular electron transfer pathway [126,128,138]. Moreover, gene clusters encoding for homologous MtrAB modules are phylogenetically distributed among organisms capable of electron exchange with the extracellular environment [141]. Both metal-reducing (*e.g. Shewanella* and *Geobacter* genera) and metal-oxidizing (*e.g. Rhodopseudomonas* and *Sideroxydans* genera) bacteria have homologous MtrAB modules [77,141-143]. This emphasizes the hypothesis of the MtrAB module being essential for both outwards and inwards extracellular electron transfer [129].

TRANSIENT ELECTRON TRANSFER PROTEIN COMPLEXES

Interactions between proteins are highly relevant for biological processes, such as electron transfer. The study of the biophysical aspects behind the protein complex formation allows a better understanding of how these interactions occur. One of these aspects is the equilibrium dissociation constant between proteins ($K_d = \frac{k_{off}}{k_{on}}$), where k_{off} and k_{on} are the dissociation

and association rate constants, respectively. The strength, duration and nature of the interaction correlates with the biological function of the proteins involved. Dissociation constants cover a wide range of values, with weak transient interactions characterized by a K_d values in the micromolar range, while permanent interactions have K_d values in the nanomolar range (Figure 1.10) [144].

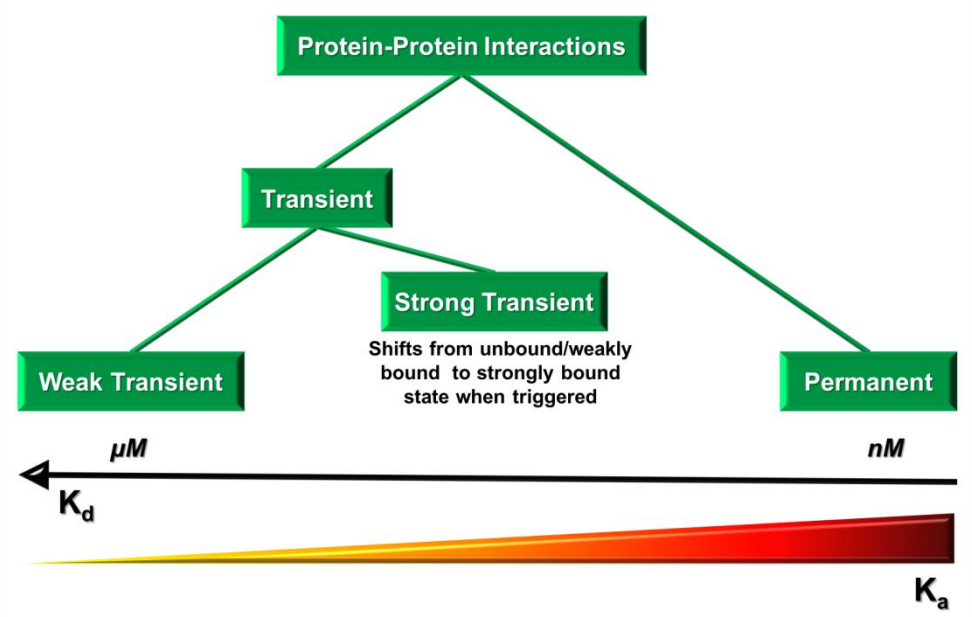

Figure 1.10. Different types of protein-protein interactions. The dissociation constant (K_d) is inversely related to the binding affinity (K_a). While weakly transient proteins interactions show a fast bound-unbound equilibrium with K_d values typically in the μM range, permanent interactions have strong binding affinities (K_d values typically in the nM range). Adapted from [145].

Interactions between redox proteins form the basis of the path for controlled flow of electrons. Electron transport between membrane-bound proteins from *Shewanella* (*e.g.* CymA and MtrCAB), are facilitated by soluble electron transfer protein shuttles (*e.g.* STC and FccA). This should occur through transient interactions between the periplasmic components, in order

to maintain a continuous electron current between the membranes. To maintain the necessary high-turnover conditions in the periplasmic space, the k_{off} of the redox complexes must be high ($\geq 10^3$ s^{-1}) [146]. Also, according to the Marcus theory [147], the rate of electron transfer (k_{et}) decreases exponentially with the distance between the redox centers. Hence, for electron transfer to occur, the redox partners need to be associated with some degree of specificity, to bring the redox centers sufficiently close together (at least a distance of 14 Å [148]). Consequently, k_{on} values for electron transfer partners must also be high (in the range of 10^7–10^9 M^{-1} s^{-1}) [146]. Considering the high k_{on} and k_{off} values, this results in K_d values in the μM-mM range and complex lifetimes in the millisecond timescale for these redox proteins.

The fact that the electron shuttle proteins have to be reactive with at least two redox partners requires these proteins to be able to recognize and bind different molecular surfaces. If the binding site becomes optimized toward one partner, the affinity for the other would be reduced. On the other hand, if the binding site is too promiscuous, electrons will be transferred unspecifically in the periplasm and the respiratory pathway will be disrupted [149]. As a result, in transient electron transfer complexes, a delicate equilibrium between turnover rate and specificity needs to be established.

Factors contributing to (transient) protein-protein interactions. When two proteins collide, they occupy the same solvent shell even in the absence of intermolecular attraction. This non-specific association is called the encounter complex [150]. Surrounded by water molecules, these proteins rapidly test several possible conformations within the encounter complex [151].

Electrostatic attractions between the opposite charged amino-acids from the different redox partners complement the encounter complex formation, by

accelerating the association rate and prolonging its lifetime. These can also assist with the orientation of the proteins to originate reactive collisions [152]. However, while electrostatic attractions promote the kinetics of binding, its contribution to the thermodynamics is not as favorable due to the reduction of entropy upon protein complex formation [152,153]. In contrast, electrostatic interactions that are predominately repulsive lower the lifetime of the encounter complex and prevent the formation of a reactive redox protein complex, avoiding the occurrence of promiscuous electron transfer.

Another important aspect is that upon association, the loss of translational and rotational entropy of the proteins is compensated by the increase in the entropy of the system with the release of water molecules from the protein surface. Thus, desolvation provides a driving force for complex formation and can lead to a substantial increase in k_{on} when complementary electrostatics are weak [154,155]. In electron transfer proteins that have distinct hydrophobic patches surrounding their redox cofactors, this effect is likely to play a major role in the transient protein complex formation [156].

Also, the size of the binding site interface influences the transient protein complex formation. Binding sites are normally confined to a specific region, representing only a small fraction of the total protein surface. In the case of electron-transfer proteins, their reactive binding site consists of just a few amino acids neighboring the redox cofactor. The smaller size of this interface and the lack of close packing between the proteins lowers to a certain degree the affinity and the specificity, thus contributing to the rapid turnover rates and high k_{off} values typical of transient redox protein complexes [157,158].

Together, these biophysical features promote the formation of the transient protein-protein complex but also enable its rapid dissociation.

BIOTECHNOLOGICAL OUTLOOK

The capability of the *Shewanella* genus to transfer electrons to a wide range of extracellular electron acceptors makes these microorganisms potential candidates to be used in different biotechnological applications, such as microbial energy generation and bioremediation of environments contaminated by toxic heavy metals. The improvement of these biotechnological applications is strongly linked with the physiology of these microorganisms. Thus, a better understanding of their extracellular electron transfer metabolism, besides the described biogeochemical relevance, will ultimately enhance the way biotechnological applications involving *Shewanella* species are presently built.

Microbial Fuel Cells (MFCs). MFCs are devices that utilize microorganisms to produce electrical current while metabolizing nutrients in the medium. These devices consist of an anode that is kept under anoxic conditions and that receives the electrons from the bioenergetic metabolism of the microorganisms growing on its surface. MFCs also contain a cathode that transfers electrons to a terminal electron acceptor. The electrons flow from the anode to the cathode passing through an external circuit to perform electrical work. There is a wide variety of designs and the anode and cathode may be in a single compartment or separated by a physical barrier that is permeable to ions that close the circuit (Figure 1.11) [159-161].

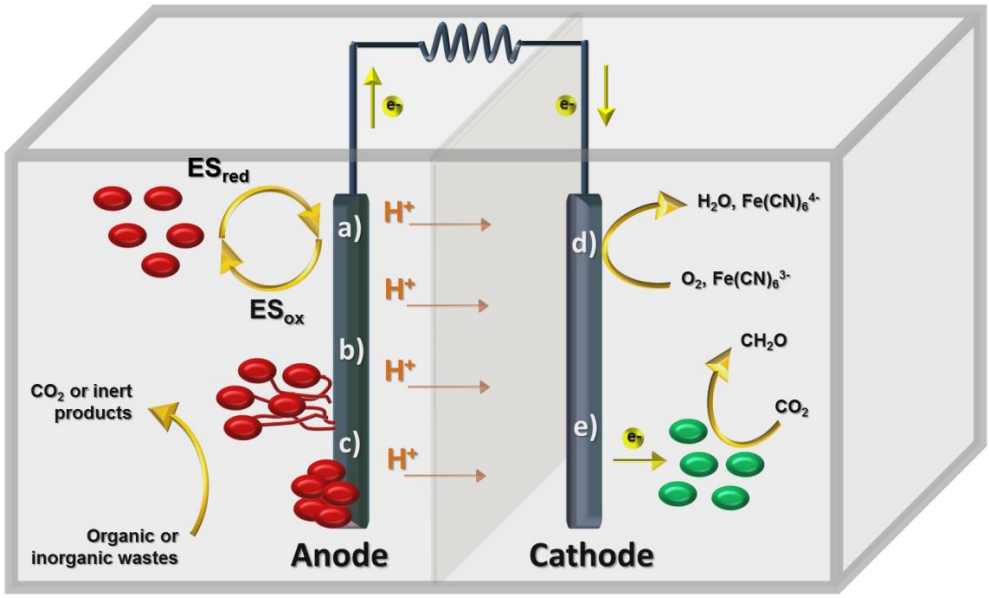

Figure 1.11. Schematic representation of a MFC. Bacteria at the anode chamber (red ellipsoids) feed on organic or inorganic wastes and transfer electrons to the anode through: **a)** Electron Shuttles (ES), **b)** Nanowires or **c)** Directly through outer membrane cytochromes. The protons produced flow through the selectively permeable membrane to the cathode chamber and the electrons flow through an electrical circuit to the cathode. The electrons are then transferred to the final electron acceptor. This can be **d)** Abiotic or **e)** Biotic (Green ellipsoids).

Research on microbial fuel cells leading to real world applications has surged in recent years [162,163]. It is accepted that practical applications of this technology require the use of atmospheric oxygen as the terminal acceptor in the cathode. Oxygen has several advantages, it is free and easily available, and has a high reduction potential. However, the disadvantage of having slow reduction kinetics creates the need for expensive catalysts, like platinum, for efficient reaction. Nevertheless, the need to reduce the costs of the device spurred the development of new materials that considerably cut the use of precious metals or even eliminate their need. A laboratory model using stainless steel anodes lead to the report of a peak current of 2.4 A/m^2 [164].

Another approach is the utilization of a second bacterial culture that receives the electrons at the cathode [165]. Design evolution is also contributing to bringing this technology closer to real world applications. Tubular cell designs that facilitate the flow of substrate have improved the Coulombic efficiency of the devices up to 75% when using acetate as substrate and a solution of ferricyanide at cathode side [166]. Of particular importance for novel designs of MFCs was the observation that once microbial biofilms had been established, it is the metabolic rate and not interfacial electron transfer the kinetically limiting step in current production [167]. In terms of microbiology, isolation and characterization of new strains or microbial communities can increase electron transfer in both the anode and cathode side of the MFC. Higher power obtained from MFCs operating with a mixed culture versus a pure culture was shown to be a consequence of lower internal resistance, and therefore dependent on the design of the MFC [168].

The capability of using organic waste, including wastewater, as substrate for MFCs has opened the possibility of producing electricity in a way that is close to carbon-neutral [169]. It also provides an alternative route for removal of organic matter in the treatment of municipal residues as well as residues derived from the food and beverage processing industries that is less power intensive and may even result in net power generation [170]. Electricity production is typically the objective when operating MFCs, but research has also lead to alternative designs and operation modes called Microbial Electrolysis Cells that can yield valuable commodities such as hydrogen or carbon based fuels [171,172]. Different processes can be linked and tuned towards electricity production or value added compounds. This allows for a versatile optimization of the most interesting outcome.

Bioremediation. Bioremediation consists in the utilization of a microorganism's metabolism for the treatment or removal of pollutants, allowing the inexpensive and effective clean-up of contaminated environments [4,173]. Among the metal reducing bacteria potentially capable of being used in this biotechnology, *Shewanella* species are exceptional candidates due to their intrinsic ability to transfer electrons to a wide range of terminal electron acceptors [28]. Toxic compounds that pollute the environment, such as halogenated organic compounds and nitramines (explosive contaminant), can be reduced by *Shewanella* and converted into less-toxic or benign compounds [37]. Also, *Shewanella* species can reduce toxic heavy metals, such as chromium (Cr), uranium (U), mercury (Hg) and arsenic (As), although the effects of this reduction may be beneficial or harmful to the environment. Reduction of soluble Cr(VI) to Cr(III) or soluble U(VI) to U(IV) results in the formation of solid metal oxides that facilitates the clean-up and prevents further spread into the groundwater [37]. However, reduction of Hg(II) to elemental Hg(0) or As(V) to As(III) leads to increased mobility and subsequent contamination of the aquifers [37].

Understanding the mechanism behind the extracellular reduction of these toxic compounds and heavy metals is crucial to optimize clean-up strategies.

Additionally, the mining industry also takes advantages of the bioprecipitation and bioleaching capabilities of the *Shewanella* genus to extract metals from ores that are too poor for other technologies [9,174].

Of all aspects involving the development of the described biotechnologies, the detailed knowledge of the molecular mechanisms that support extracellular electron transfer are the least advanced. Only now with the intense study of model organisms from the genera *Shewanella* and *Geobacter*, a few general aspects are becoming well established.

REFERENCES

[1] **Newman, D.K. and J.F. Banfield.** 2002. Geomicrobiology: how molecular-scale interactions underpin biogeochemical systems. Science *296*:1071-1077.

[2] **Cavalier-Smith, T., M. Brasier, and T.M. Embley.** 2006. Introduction: How and when did microbes change the world? Philos Trans R Soc Lond B - Biol Sci *361*:845-850.

[3] **Templeton, A.S.** 2011. Geomicrobiology of iron in extreme environments. ELEMENTS *7*:95-100.

[4] **Gadd, G.M.** 2010. Metals, minerals and microbes: geomicrobiology and bioremediation. Microbiology *156*:609-643.

[5] **Haferburg, G. and E. Kothe.** 2007. Microbes and metals: interactions in the environment. J Basic Microbiol *47*:453-467.

[6] **Lovley, D.R.** 2002. Dissimilatory metal reduction: from early Life to bioremediation. ASM News *68*:231-237.

[7] **Canfield, D.E., M.T. Rosing, and C. Bjerrum.** 2006. Early anaerobic metabolisms. Philos Trans R Soc B - Biol Sci *361*:1819-1834.

[8] **Wiatrowski, H.A. and T. Barkay.** 2005. Monitoring of microbial metal transformations in the environment. Curr Opin Biotech *16*:261-268.

[9] **Gadd, G.M.** 2000. Bioremedial potential of microbial mechanisms of metal mobilization and immobilization. Curr Opin Biotech *11*:271-279.

[10] **Emerson, D., E. Roden, and B.S. Twining.** 2012. The microbial ferrous wheel: iron cycling in terrestrial, freshwater, and marine environments. Front Microbiol *3*:383.

[11] **Kappler, A. and K.L. Straub.** 2005. Geomicrobiological cycling of iron. Rev Mineral Geochem *59*:85-108.

[12] **Schmidt, C., S. Behrens, and A. Kappler.** 2010. Ecosystem functioning from a geomicrobiological perspective – a conceptual framework for biogeochemical iron cycling. Environ Chem *7*:399-405.

[13] **Bird, L.J., V. Bonnefoy, and D.K. Newman.** 2011. Bioenergetic challenges of microbial iron metabolisms. Trends Microbiol *19*:330-340.

[14] **Druschela, G.K., D. Emerson, R. Sutkab, P. Sucheckic, and G.W.I. Luther.** 2008. Low-oxygen and chemical kinetic constraints on the geochemical niche of

neutrophilic iron(II) oxidizing microorganisms. Geochim Cosmochim Acta *72*:3358–3370.

[15] **Neubauer, S.C., D. Emerson, and J.P. Megonigal.** 2002. Life at the energetic edge: kinetics of circumneutral iron oxidation by lithotrophic iron-oxidizing bacteria isolated from the wetland-plant rhizosphere. Appl Environ Microbiol *68*:3988-3995.

[16] **Hedrich, S., M. Schlomann, and D.B. Johnson.** 2011. The iron-oxidizing proteobacteria. Microbiology *157*:1551-1564.

[17] **Widdel, F., S. Schnell, S. Heising, A. Ehrenreich, B. Assmus, and B. Schink.** 1993. Ferrous iron oxidation by anoxygenic phototrophic bacteria. Nature *362*:834-836.

[18] **Straub, K.L., M. Benz, B. Schink, and F. Widdel.** 1996. Anaerobic, nitrate-dependent microbial oxidation of ferrous iron. Appl Environ Microbiol *62*:1458-1460.

[19] **Benz, M., A. Brune, and B. Schink.** 1998. Anaerobic and aerobic oxidation of ferrous iron at neutral pH by chemoheterotrophic nitrate-reducing bacteria. Arch Microbiol *169*:159-165.

[20] **Wrage, N., G.L. Velthof, M.L. van Beusichem, and O. Oenema.** 2001. Role of nitrifier denitrification in the production of nitrous oxide. Soil Biol Biochem *33*:1723-1732.

[21] **Pronka, J.T. and D.B. Johnson.** 1992. Oxidation and reduction of iron by acidophilic bacteria. Geomicrobiol J *10*:153-171.

[22] **Kappler, A., B. Schink, and D.K. Newman.** 2005. Fe(III) minerals precipitated by nitrate-dependent Fe(II)-oxidizers Fe(III) mineral formation and cell encrustation by the nitrate-dependent Fe(II)-oxidizer strain BoFeN1. Geobiology *3*:235-245.

[23] **Gralnick, J.A. and D.K. Newman.** 2007. Extracellular respiration. Mol Microbiol *65*:1-11.

[24] **Thamdrup, B., R. Rossello-Mora, and R. Amann.** 2000. Microbial manganese and sulfate reduction in Black Sea shelf sediments. Appl Environ Microbiol *66*:2888-2897.

[25] **Lovley, D.R., K.P. Nevin, S.E. Childers, T. Mehta, and S.A. Ciufo.** 2002. Different strategies for Fe(III) oxide reduction in *Geobacter* versus *Shewanella* and *Geothrix* species. Abstr Pap Am Chem Soc *223*:U598.

[26] **Coates, J.D., D.J. Ellis, C.V. Gaw, and D.R. Lovley.** 1999. *Geothrix fermentans* gen. nov., sp. nov., a novel Fe(III)-reducing bacterium from a hydrocarbon-contaminated aquifer. Int J Syst Bacteriol *49*:1615-1622.

[27] **Mahadevan, R., D.R. Bond, J.E. Butler, A. Esteve-Nunez, M.V. Coppi, B.O. Palsson, C.H. Schilling, and D.R. Lovley.** 2006. Characterization of metabolism in the Fe(III)-reducing organism *Geobacter sulfurreducens* by constraint-based modeling. Appl Environ Microbiol *72*:1558-1568.

[28] **Nealson, K.H. and J. Scott.** 2006. Ecophysiology of the genus *Shewanella*, p. 1133-1151. *In* M. Dworkin (Ed.), The Prokaryotes. Springer-Verlag, New York.

[29] **Lies, D.P., M.E. Hernandez, A. Kappler, R.E. Mielke, J.A. Gralnick, and D.K. Newman.** 2005. *Shewanella oneidensis* MR-1 uses overlapping pathways for iron reduction at a distance and by direct contact under conditions relevant for biofilms. Appl Environ Microbiology *71*:4414-4426.

[30] **Lovley, D.R., D.E. Holmes, and K.P. Nevin.** 2004. Dissimilatory Fe(III) and Mn(IV) reduction. Adv Microb Physiol *49*:219-286.

[31] **Lovley, D.R.** 2008. Extracellular electron transfer: wires, capacitors, iron lungs, and more. Geobiology *6*:225-231.

[32] **Derby, H. and B. Hammer.** 1931. Bacteriology of butter: Bacteriological studies of surface taint butter. Iowa Agric Exp Stn Res Bull *145*:387-416.

[33] **Long, H. and B. Hammer.** 1941. Classification of organisms important in dairy products: *Pseudomonas putrefaciens*. Iowa Agric Exp Stn Res Bull *285*:176–195.

[34] **Shewan, J., G. Hobbs, and W. Hodgkiss.** 1960. A determinative scheme for the identification of certain genera of gram-negative bacteria, with special reference to the *Pseudomonadaceae*. J Appl Bacteriol *23*:379-390.

[35] **Lee, J.V., D.M. Gibson, and J.M. Shewan.** 1977. A numerical taxonomic study of some *Pseudomonas*-like marine bacteria. J Gen Microbiol *98*:439-451.

[36] **MacDonell, M. and R. Colwell.** 1985. Phylogeny of the *Vibrionaceae*, and recommendation for two new genera, *Listonella* and *Shewanella*. Syst Appl Microbiol *6*:171-182.

[37] **Hau, H.H. and J.A. Gralnick.** 2007. Ecology and biotechnology of the genus *Shewanella*. Annu Rev Microbiol *61*:237-258.

[38] **Janda, J.M. and S.L. Abbott.** 2012. The genus *Shewanella*: from the briny depths below to human pathogen. Crit Rev Microbiol *doi: 10.3109/1040841X.2012.726209*.

[39] **Myers, C.R. and K.H. Nealson.** 1988. Bacterial manganese reduction and growth with manganese oxide as the sole electron acceptor. Science *240*:1319-1321.

[40] **Logan, B.E. and J.M. Regan.** 2006. Microbial fuel cells: challenges and applications. Environ Sci Technol *40*:5172-5180.

[41] **Kim, H.J., M.S. Hyun, I.S. Chang, and B.H. Kim.** 1999. A microbial fuel cell type lactate biosensor using a metal-reducing bacterium, *Shewanella putrefaciens*. J Microbiol Biotechnol *9*:365-367.

[42] **Venkateswaran, K., D.P. Moser, M.E. Dollhopf, D.P. Lies, D.A. Saffarini, B.J. MacGregor, D.B. Ringelberg, D.C. White, et al.** 1999. Polyphasic taxonomy of the genus *Shewanella* and description of *Shewanella oneidensis sp. nov*. Int J Syst Bacteriol *49*:705-724.

[43] **Liu, Y., W. Gao, Y. Wang, L. Wu, X. Liu, T. Yan, E. Alm, A. Arkin, et al.** 2005. Transcriptome analysis of *Shewanella oneidensis* MR-1 in response to elevated salt conditions. J Bacteriol *187*:2501-2507.

[44] **Abboud, R., R. Popa, V. Souza-Egipsy, C.S. Giometti, S. Tollaksen, J.J. Mosher, R.H. Findlay, and K.H. Nealson.** 2005. Low-temperature growth of *Shewanella oneidensis* MR-1. Appl Environ Microbiol *71*:811-816.

[45] **Mills, E.L. and K.T. Holeck.** 2001. Oneida Lake: undergoing ecological change. Clearwaters *31*:22-25.

[46] **Shi, L., K.M. Rosso, T.A. Clarke, D.J. Richardson, J.M. Zachara, and J.K. Fredrickson.** 2012. Molecular underpinnings of Fe(III) oxide reduction by *Shewanella oneidensis* MR-1. Front Microbiol *3*:50.

[47] **Heidelberg, J.F., I.T. Paulsen, K.E. Nelson, E.J. Gaidos, W.C. Nelson, T.D. Read, J.A. Eisen, R. Seshadri, et al.** 2002. Genome sequence of the dissimilatory metal ion-reducing bacterium *Shewanella oneidensis*. Nat Biotechnol *20*:1118-1123.

[48] **Romine, M.F., T.S. Carlson, A.D. Norbeck, L.A. McCue, and M.S. Lipton.** 2008. Identification of mobile elements and pseudogenes in the *Shewanella oneidensis* MR-1 genome. Appl Environ Microbiol *74*:3257-3265.

[49] **Meyer, T.E., A.I. Tsapin, I. Vandenberghe, L. De Smet, D. Frishman, K.H. Nealson, M.A. Cusanovich, and J.J. van Beeumen.** 2004. Identification of 42 possible cytochrome *c* genes in the *Shewanella oneidensis* genome and characterization of six soluble cytochromes. OMICS *8*:57-77.

[50] **Newman, D.K. and R. Kolter.** 2000. A role for excreted quinones in extracellular electron transfer. Nature *405*:94-97.

[51] **Nevin, K.P. and D.R. Lovley.** 2002. Mechanisms for accessing insoluble Fe(III) oxide during dissimilatory Fe(III) reduction by *Geothrix fermentans*. Appl Environ Microbiol *68*:2294-2299.

[52] **Myers, C.R. and J.M. Myers.** 1993. Role of menaquinone in the reduction of fumarate, nitrate, iron (III) and manganese (IV) by *Shewanella putrefaciens* Mr-1. FEMS Microbiol Lett *114*:215-222.

[53] **Marsili, E., D.B. Baron, I.D. Shikhare, D. Coursolle, J.A. Gralnick, and D.R. Bond.** 2008. *Shewanella* secretes flavins that mediate extracellular electron transfer. Proc Natl Acad Sci USA *105*:3968-3973.

[54] **von Canstein, H., J. Ogawa, S. Shimizu, and J.R. Lloyd.** 2008. Secretion of flavins by *Shewanella* species and their role in extracellular electron transfer. Appl Environ Microbiol *74*:615-623.

[55] **Kotloski, N.J. and J.A. Gralnick.** 2013. Flavin electron shuttles dominate extracellular electron transfer by *Shewanella oneidensis*. mBio *4*:e00553-00512.

[56] **Ross, D.E., S.L. Brantley, and M. Tien.** 2009. Kinetic characterization of OmcA and MtrC, terminal reductases involved in respiratory electron transfer for dissimilatory iron reduction in *Shewanella oneidensis* MR-1. Appl Environ Microbiol *75*:5218-5226.

[57] **Baron, D., E. LaBelle, D. Coursolle, J.A. Gralnick, and D.R. Bond.** 2009. Electrochemical measurement of electron transfer kinetics by *Shewanella oneidensis* MR-1. J Biol Chem *284*:28865-28873.

[58] **Coursolle, D., D.B. Baron, D.R. Bond, and J.A. Gralnick.** 2010. The Mtr respiratory pathway is essential for reducing flavins and electrodes in *Shewanella oneidensis*. J Bacteriol *192*:467-474.

[59] **van der Zee, F.P.** 2002. Anaerobic azo dye reduction. Wageningen University, Wageningen, The Netherlands.

[60] **Straub, K.L., M. Benz, and B. Schink.** 2001. Iron metabolism in anoxic environments at near neutral pH. FEMS Microbiol Ecol *34*:181-186.

[61] **Kim, H.J., H.S. Park, M.S. Hyun, I.S. Chang, M. Kim, and B.H. Kim.** 2002. A mediator-less microbial fuel cell using a metal reducing bacterium, *Shewanella putrefaciens*. Enzyme Microb Tech *30*:145-152.

[62] **Lovley, D.R. and J.C. Woodward.** 1996. Mechanisms for chelator stimulation of microbial Fe(III)-oxide reduction. Chem Geol *132*:19-24.

[63] **Dollhopf, M.E., K.H. Nealson, D.M. Simon, and G.W. Luther.** 2000. Kinetics of Fe(III) and Mn(IV) reduction by the Black Sea strain of *Shewanella putrefaciens* using in situ solid state voltammetric Au/Hg electrodes. Marine Chem *70*:171-180.

[64] **Taillefert, M., J.S. Beckler, E. Carey, J.L. Burns, C.M. Fennessey, and T.J. DiChristina.** 2007. *Shewanella putrefaciens* produces an Fe(III)-solubilizing organic ligand during anaerobic respiration on insoluble Fe(III) oxides. J Inorg Biochem *101*:1760-1767.

[65] **Neilands, J.B.** 1995. Siderophores: structure and function of microbial iron transport compounds. J Biol Chem *270*:26723-26726.

[66] **Hernandez, M.E. and D.K. Newman.** 2001. Extracellular electron transfer. Cell Mol Life Sci *58*:1562-1571.

[67] **Fennessey, C.M., M.E. Jones, M. Taillefert, and T.J. DiChristina.** 2010. Siderophores are not Involved in Fe(III) solubilization during anaerobic Fe(III) respiration by *Shewanella oneidensis* MR-1. Appl Environ Microbiol *76*:2425-2432.

[68] **Myers, C.R. and K.H. Nealson.** 1988. Microbial reduction of manganese oxides - interactions with iron and sulfur. Geochim Cosmochim Acta *52*:2727-2732.

[69] **Lower, S.K., M.F. Hochella, and T.J. Beveridge.** 2001. Bacterial recognition of mineral surfaces: nanoscale interactions between *Shewanella* and alpha-FeOOH. Science *292*:1360-1363.

[70] **Harris, H.W., M.Y. El-Naggar, and K.H. Nealson.** 2012. *Shewanella oneidensis* MR-1 chemotaxis proteins and electron-transport chain components essential for congregation near insoluble electron acceptors. Biochem Soc Trans *40*:1167-1177.

[71] **Veazey, J.P., G. Reguera, and S.H. Tessmer.** 2011. Electronic properties of conductive pili of the metal-reducing bacterium *Geobacter sulfurreducens* probed by scanning tunneling microscopy. Phys Rev E *84*:060901-060904.

[72] **El-Naggar, M.Y., G. Wanger, K.M. Leung, T.D. Yuzvinsky, G. Southam, J. Yang, W.M. Lau, K.H. Nealson, and Y.A. Gorby.** 2010. Electrical transport along bacterial nanowires from *Shewanella oneidensis* MR-1. Proc Natl Acad Sci USA *107*:18127-18131.

[73] **Gorby, Y.A., S. Yanina, J.S. McLean, K.M. Rosso, D. Moyles, A. Dohnalkova, T.J. Beveridge, I.S. Chang, et al.** 2006. Electrically conductive bacterial nanowires

produced by *Shewanella oneidensis* strain MR-1 and other microorganisms. Proc Natl Acad Sci USA *103*:11358-11363.

[74] **Reguera, G., K.P. Nevin, J.S. Nicoll, S.F. Covalla, T.L. Woodard, and D.R. Lovley.** 2006. Biofilm and nanowire production leads to increased current in *Geobacter sulfurreducens* fuel cells. Appl Environ Microbiol *72*:7345-7348.

[75] **Vargas, M., N.S. Malvankar, P.L. Tremblay, C. Leang, J.A. Smith, P. Patel, O. Synoeyenbos-West, K.P. Nevin, and D.R. Lovley.** 2013. Aromatic amino acids required for pili conductivity and long range extracellular electron transport in *Geobacter sulfurreducens*. mBio *4*:e00105-00113.

[76] **Shi, L., T.C. Squier, J.M. Zachara, and J.K. Fredrickson.** 2007. Respiration of metal (hydr)oxides by *Shewanella* and *Geobacter*: a key role for multihaem *c*-type cytochromes. Mol Microbiol *65*:12-20.

[77] **Shi, L., K.M. Rosso, J.M. Zachara, and J.K. Fredrickson.** 2012. Mtr extracellular electron-transfer pathways in Fe(III)-reducing or Fe(II)-oxidizing bacteria: a genomic perspective. Biochem Soc Trans *40*:1261-1267.

[78] **Reguera, G., K.D. McCarthy, T. Mehta, J.S. Nicoll, M.T. Tuominen, and D.R. Lovley.** 2005. Extracellular electron transfer via microbial nanowires. Nature *435*:1098-1101.

[79] **Shi, L., S. Deng, M.J. Marshall, Z. Wang, D.W. Kennedy, A.C. Dohnalkova, H.M. Mottaz, E.A. Hill, et al.** 2008. Direct involvement of type II secretion system in extracellular translocation of *Shewanella oneidensis* outer membrane cytochromes MtrC and OmcA. J Bacteriol *190*:5512-5516.

[80] **Bouhenni, R.A., G.J. Vora, J.C. Biffinger, S. Shirodkar, K. Brockman, R. Ray, P. Wu, B.J. Johnson, et al.** 2010. The role of *Shewanella oneidensis* MR-1 outer surface structures in extracellular electron transfer. Electroanal *22*:856-864.

[81] **Malvankar, N.S. and D.R. Lovley.** 2012. Microbial nanowires: a new paradigm for biological electron transfer and bioelectronics. ChemSusChem *5*:1039-1046.

[82] **Myers, C.R. and J.M. Myers.** 2003. Cell surface exposure of the outer membrane cytochromes of *Shewanella oneidensis* MR-1. Lett Appl Microbiol *37*:254-258.

[83] **Lower, B.H., L. Shi, R. Yongsunthon, T.C. Droubay, D.E. McCready, and S.K. Lower.** 2007. Specific bonds between an iron oxide surface and outer membrane cytochromes MtrC and OmcA from *Shewanella oneidensis* MR-1. J Bacteriol *189*:4944-4952.

[84] **Xiong, Y., L. Shi, B. Chen, M.U. Mayer, B.H. Lower, Y. Londer, S. Bose, M.F. Hochella, et al.** 2006. High-affinity binding and direct electron transfer to solid metals by the *Shewanella oneidensis* MR-1 outer membrane *c*-type cytochrome OmcA. J Am Chem Soc *128*:13978-13979.

[85] **Meitl, L.A., C.M. Eggleston, P.J.S. Colberg, N. Khare, C.L. Reardon, and L. Shi.** 2009. Electrochemical interaction of *Shewanella oneidensis* MR-1 and its outer membrane cytochromes OmcA and MtrC with hematite electrodes. Geochim Cosmochim Acta *73*:5292–5307.

[86] **Eggleston, C.M., J. Vörös, L. Shi, B.H. Lower, T.C. Droubay, and P.J.S. Colberg.** 2008. Binding and direct electrochemistry of OmcA, an outer-membrane

cytochrome from an iron reducing bacterium, with oxide electrodes: A candidate biofuel cell system. Inorg Chim Acta *361*:769-777.

[87] **Myers, C.R. and J.M. Myers.** 1997. Cloning and sequence of cymA a gene encoding a tetraheme cytochrome c required for reduction of iron(III), fumarate, and nitrate by *Shewanella putrefaciens* MR-1. J Bacteriol *179*:1143-1152.

[88] **Myers, J.M. and C.R. Myers.** 2000. Role of the tetraheme cytochrome CymA in anaerobic electron transport in cells of *Shewanella putrefaciens* MR-1 with normal levels of menaquinone. J Bacteriol *182*:67-75.

[89] **Marritt, S.J., D.G.G. McMillan, L. Shi, J.K. Fredrickson, J.M. Zachara, D.J. Richardson, L.J.C. Jeuken, and J.N. Butt.** 2012. The roles of CymA in support of the respiratory flexibility of *Shewanella oneidensis* MR-1. Biochem Soc Trans *40*:1217-1221.

[90] **Gordon, E.H., A.D. Pike, A.E. Hill, P.M. Cuthbertson, S.K. Chapman, and G.A. Reid.** 2000. Identification and characterization of a novel cytochrome c_3 from *Shewanella frigidimarina* that is involved in Fe(III) respiration. Biochem J *349*:153-158.

[91] **Leys, D., T.E. Meyer, A.S. Tsapin, K.H. Nealson, M.A. Cusanovich, and J.J. Van Beeumen.** 2002. Crystal structures at atomic resolution reveal the novel concept of "electron-harvesting" as a role for the small tetraheme cytochrome *c*. J Biol Chem *277*:35703-35711.

[92] **Tsapin, A.I., I. Vandenberghe, K.H. Nealson, J.H. Scott, T.E. Meyer, M.A. Cusanovich, E. Harada, T. Kaizu, et al.** 2001. Identification of a small tetraheme cytochrome *c* and a flavocytochrome *c* as two of the principal soluble cytochromes *c* in *Shewanella oneidensis* strain MR1. Appl Environ Microbiol *67*:3236-3244.

[93] **Gordon, E.H., S.L. Pealing, S.K. Chapman, F.B. Ward, and G.A. Reid.** 1998. Physiological function and regulation of flavocytochrome c_3, the soluble fumarate reductase from *Shewanella putrefaciens* NCIMB400. Microbiology *144*:937-945.

[94] **Pessanha, M., E.L. Rothery, C.S. Miles, G.A. Reid, S.K. Chapman, R.O. Louro, D.L. Turner, C.A. Salgueiro, and A.V. Xavier.** 2009. Tuning of functional heme reduction potentials in *Shewanella* fumarate reductases. Biochim Biophys Acta *1787*:113-120.

[95] **Schuetz, B., M. Schicklberger, J. Kuermann, A.M. Spormann, and J. Gescher.** 2009. Periplasmic electron transfer via the *c*-type cytochromes MtrA and FccA of *Shewanella oneidensis* MR-1. Appl Environ Microbiol *75*:7789-7796.

[96] **Pitts, K.E., P.S. Dobbin, F. Reyes-Ramirez, A.J. Thomson, D.J. Richardson, and H.E. Seward.** 2003. Characterization of the *Shewanella oneidensis* MR-1 decaheme cytochrome MtrA. J Biol Chem *278*:27758-27765.

[97] **Schicklberger, M., C. Bucking, B. Schuetz, H. Heide, and J. Gescher.** 2011. Involvement of the *Shewanella oneidensis* decaheme cytochrome MtrA in the periplasmic stability of the beta-barrel protein MtrB. Appl Environ Microbiol *77*:1520-1523.

[98] **Myers, C.R. and J.M. Myers.** 2002. MtrB is required for proper incorporation of the cytochromes OmcA and OmcB into the outer membrane of *Shewanella putrefaciens* MR-1. Appl Environ Microbiol *68*:5585-5594.

[99] **Beliaev, A.S. and D.A. Saffarini.** 1998. *Shewanella putrefaciens mtrB* encodes an outer membrane protein required for Fe(III) and Mn(IV) reduction. J Bacteriol *180*:6292-6297.

[100] **Myers, J.M. and C.R. Myers.** 2001. Role for outer membrane cytochromes OmcA and OmcB of *Shewanella putrefaciens* MR-1 in reduction of manganese dioxide. Appl Environ Microbiol *67*:260-269.

[101] **Beliaev, A.S., D.A. Saffarini, J.L. McLaughlin, and D. Hunnicutt.** 2001. MtrC, an outer membrane decahaem *c* cytochrome required for metal reduction in *Shewanella putrefaciens* MR-1. Mol Microbiol *39*:722-730.

[102] **Hartshorne, R.S., B.N. Jepson, T.A. Clarke, S.J. Field, J. Fredrickson, J. Zachara, L. Shi, J.N. Butt, and D.J. Richardson.** 2007. Characterization of *Shewanella oneidensis* MtrC: a cell-surface decaheme cytochrome involved in respiratory electron transport to extracellular electron acceptors. J Biol Inorg Chem *12*:1083-1094.

[103] **Shi, L., B. Chen, Z. Wang, D.A. Elias, M.U. Mayer, Y.A. Gorby, S. Ni, B.H. Lower, et al.** 2006. Isolation of a high-affinity functional protein complex between OmcA and MtrC: Two outer membrane decaheme *c*-type cytochromes of *Shewanella oneidensis* MR-1. J Bacteriol *188*:4705-4714.

[104] **Richardson, D. and G. Sawers.** 2002. PMF through the redox loop. Science *295*:1842-1843.

[105] **Scott, J.H. and K.H. Nealson.** 1994. A biochemical study of the intermediary carbon metabolism of *Shewanella putrefaciens*. J Bacteriol *176*:3408-3411.

[106] **Saffarini, D.A., S.L. Blumerman, and K.J. Mansoorabadi.** 2002. Role of menaquinones in Fe(III) reduction by membrane fractions of *Shewanella putrefaciens*. J Bacteriol *184*:846-848.

[107] **Zargar, K. and C.W. Saltikov.** 2009. Lysine-91 of the tetraheme *c*-type cytochrome CymA is essential for quinone interaction and arsenate respiration in *Shewanella* sp strain ANA-3. Arch Microbiol *191*:797-806.

[108] **Schwalb, C., S.K. Chapman, and G.A. Reid.** 2002. The membrane-bound tetrahaem *c*-type cytochrome CymA interacts directly with the soluble fumarate reductase in *Shewanella*. Biochem Soc Trans *30*:658-662.

[109] **Field, S.J., P.S. Dobbin, M.R. Cheesman, N.J. Watmough, A.J. Thomson, and D.J. Richardson.** 2000. Purification and magneto-optical spectroscopic characterization of cytoplasmic membrane and outer membrane multiheme *c*-type cytochromes from *Shewanella frigidimarina* NCIMB400. J Biol Chem *275*:8515-8522.

[110] **Firer-Sherwood, M.A., K.D. Bewley, J.Y. Mock, and S.J. Elliott.** 2011. Tools for resolving complexity in the electron transfer networks of multiheme cytochromes *c*. Metallomics *3*:344-348.

[111] **Arnold, K., L. Bordoli, J. Kopp, and T. Schwede.** 2006. The SWISS-MODEL workspace: a web-based environment for protein structure homology modelling. Bioinformatics *22*:195-201.

[112] **Kiefer, F., K. Arnold, M. Kunzli, L. Bordoli, and T. Schwede.** 2009. The SWISS-MODEL repository and associated resources. Nucleic Acids Res *37*:D387-D392.

[113] **Firer-Sherwood, M., G.S. Pulcu, and S.J. Elliott.** 2008. Electrochemical interrogations of the Mtr cytochromes from *Shewanella*: opening a potential window. J Biol Inorg Chem *13*:849-854.

[114] **Gescher, J.S., C.D. Cordova, and A.M. Spormann.** 2008. Dissimilatory iron reduction in *Escherichia coli*: identification of CymA of *Shewanella oneidensis* and NapC of *E. coli* as ferric reductases. Mol Microbiol *68*:706-719.

[115] **Dohnalkova, A.C., M.J. Marshall, B.W. Arey, K.H. Williams, E.C. Buck, and J.K. Fredrickson.** 2011. Imaging hydrated microbial extracellular polymers: comparative analysis by electron microscopy. Appl Environ Microbiol *77*:1254-1262.

[116] **Tsapin, A.I., K.H. Nealson, T. Meyers, M.A. Cusanovich, J. Van Beuumen, L.D. Crosby, B.A. Feinberg, and C. Zhang.** 1996. Purification and properties of a low-redox-potential tetraheme cytochrome c_3 from *Shewanella putrefaciens*. J Bacteriol *178*:6386-6388.

[117] **Pealing, S.L., A.C. Black, F.D. Manson, F.B. Ward, S.K. Chapman, and G.A. Reid.** 1992. Sequence of the gene encoding flavocytochrome *c* from *Shewanella putrefaciens*: a tetraheme flavoenzyme that is a soluble fumarate reductase related to the membrane-bound enzymes from other bacteria. Biochemistry *31*:12132-12140.

[118] **Taylor, P., S.L. Pealing, G.A. Reid, S.K. Chapman, and M.D. Walkinshaw.** 1999. Structural and mechanistic mapping of a unique fumarate reductase. Nature structural biology *6*:1108-1112.

[119] **Leys, D., A.S. Tsapin, K.H. Nealson, T.E. Meyer, M.A. Cusanovich, and J.J. Van Beeumen.** 1999. Structure and mechanism of the flavocytochrome *c* fumarate reductase of *Shewanella putrefaciens* MR-1. Nat Struct Biol *6*:1113-1117.

[120] **Morris, C.J., A.C. Black, S.L. Pealing, F.D. Manson, S.K. Chapman, G.A. Reid, D.M. Gibson, and F.B. Ward.** 1994. Purification and properties of a novel cytochrome: flavocytochrome *c* from *Shewanella putrefaciens*. Biochem J *302*:587-593.

[121] **Paixão, V.B., C.A. Salgueiro, L. Brennan, G.A. Reid, S.K. Chapman, and D.L. Turner.** 2008. The solution structure of a tetraheme cytochrome from *Shewanella frigidimarina* reveals a novel family structural motif. Biochemistry *47*:11973-11980.

[122] **Smith, D.M.A., K.M. Rosso, M. Dupuis, M. Valiev, and T.P. Straatsma.** 2006. Electronic coupling between heme electron-transfer centers and its decay with distance depends strongly on relative orientation. J Phys Chem B *110*:15582-15588.

[123] **Pessanha, M., R.O. Louro, I.J. Correia, E.L. Rothery, K.L. Pankhurst, G.A. Reid, S.K. Chapman, D.L. Turner, and C.A. Salgueiro.** 2003. Thermodynamic characterization of a tetrahaem cytochrome isolated from a facultative aerobic bacterium, *Shewanella frigidimarina*: a putative redox model for flavocytochrome *c*$_3$. Biochem J *370*:489-495.

[124] **Harada, E., J. Kumagai, K. Ozawa, S. Imabayashi, A.S. Tsapin, K.H. Nealson, T.E. Meyer, M.A. Cusanovich, and H. Akutsu.** 2002. A directional electron transfer regulator based on heme-chain architecture in the small tetraheme cytochrome *c* from *Shewanella oneidensis*. FEBS Lett *532*:333-337.

[125] **Coursolle, D. and J.A. Gralnick.** 2010. Modularity of the Mtr respiratory pathway of *Shewanella oneidensis* strain MR-1. Mol Microbiol *77*:995-1008.

[126] **Coursolle, D. and J.A. Gralnick.** 2012. Reconstruction of extracellular respiratory pathways for iron(III) reduction in *Shewanella oneidensis* strain MR-1. Front Microbiol *3*:56.

[127] **Borloo, J., B. Vergauwen, L. De Smet, A. Brige, B. Motte, B. Devreese, and J. Van Beeumen.** 2007. A kinetic approach to the dependence of dissimilatory metal reduction by *Shewanella oneidensis* MR-1 on the outer membrane cytochromes *c* OmcA and OmcB. FEBS J *274*:3728-3738.

[128] **Bucking, C., F. Popp, S. Kerzenmacher, and J. Gescher.** 2010. Involvement and specificity of *Shewanella oneidensis* outer membrane cytochromes in the reduction of soluble and solid-phase terminal electron acceptors. FEMS Microbiol Lett *306*:144-151.

[129] **Richardson, D.J., J.N. Butt, J.K. Fredrickson, J.M. Zachara, L. Shi, M.J. Edwards, G. White, N. Baiden, et al.** 2012. The 'porin-cytochrome' model for microbe-to-mineral electron transfer. Mol Microbiol *85*:201-212.

[130] **Lower, B.H., R. Yongsunthon, L. Shi, L. Wildling, H.J. Gruber, N.S. Wigginton, C.L. Reardon, G.E. Pinchuk, et al.** 2009. Antibody recognition force microscopy shows that outer membrane cytochromes OmcA and MtrC are expressed on the exterior surface of *Shewanella oneidensis* MR-1. Appl Environ Microbiol *75*:2931-2935.

[131] **Bretschger, O., A. Obraztsova, C.A. Sturm, I.S. Chang, Y.A. Gorby, S.B. Reed, D.E. Culley, C.L. Reardon, et al.** 2007. Current production and metal oxide reduction by *Shewanella oneidensis* MR-1 wild type and mutants. Appl Environ Microbiol *73*:7003-7012.

[132] **Lower, B.H., R.D. Lins, Z. Oestreicher, T.P. Straatsma, M.F. Hochella, Jr., L. Shi, and S.K. Lower.** 2008. In vitro evolution of a peptide with a hematite binding motif that may constitute a natural metal-oxide binding archetype. Environ Sci Technol *42*:3821-3827.

[133] **Ross, D.E., S.S. Ruebush, S.L. Brantley, R.S. Hartshorne, T.A. Clarke, D.J. Richardson, and M. Tien.** 2007. Characterization of protein-protein interactions involved in iron reduction by *Shewanella oneidensis* MR-1. Appl Environ Microbiol *73*:5797-5808.

[134] **Zhang, H., X. Tang, G.R. Munske, N. Tolic, G.A. Anderson, and J.E. Bruce.** 2009. Identification of protein-protein interactions and topologies in living cells with chemical cross-linking and mass spectrometry. Mol Cell Proteomics *8*:409-420.

[135] **Clarke, T.A., M.J. Edwards, A.J. Gates, A. Hall, G.F. White, J. Bradley, C.L. Reardon, L. Shi, et al.** 2011. Structure of a bacterial cell surface decaheme electron conduit. Proc Natl Acad Sci USA *108*:9384-9389.

[136] **McLean, J.S., G. Wanger, Y.A. Gorby, M. Wainstein, J. McQuaid, S.I. Ishii, O. Bretschger, H. Beyenal, and K.H. Nealson.** 2010. Quantification of electron transfer rates to a solid phase electron acceptor through the stages of biofilm formation from single cells to multicellular communities. Environ Sci Technol *44*:2721-2727.

[137] **Hartshorne, R.S., C.L. Reardon, D. Ross, J. Nuester, T.A. Clarke, A.J. Gates, P.C. Mills, J.K. Fredrickson, et al.** 2009. Characterization of an electron conduit between bacteria and the extracellular environment. Proc Natl Acad Sci USA *106*:22169-22174.

[138] **Gralnick, J.A., H. Vali, D.P. Lies, and D.K. Newman.** 2006. Extracellular respiration of dimethyl sulfoxide by *Shewanella oneidensis* strain MR-1. Proc Natl Acad Sci USA *103*:4669-4674.

[139] **Firer-Sherwood, M.A., N. Ando, C.L. Drennan, and S.J. Elliott.** 2011. Solution-based structural analysis of the decaheme cytochrome, MtrA, by small-angle X-ray scattering and analytical ultracentrifugation. J Phys Chem B *115*:11208-11214.

[140] **Matias, V.R., A. Al-Amoudi, J. Dubochet, and T.J. Beveridge.** 2003. Cryo-transmission electron microscopy of frozen-hydrated sections of *Escherichia coli* and *Pseudomonas aeruginosa*. J Bacteriol *185*:6112-6118.

[141] **Hartshorne, R.S., C.L. Reardon, D. Ross, J. Nuester, T.A. Clarke, A.J. Gates, P.C. Mills, J.K. Fredrickson, et al.** 2009. Characterization of an electron conduit between bacteria and the extracellular environment. Proc Natl Acad Sci USA *106*:22169-22174.

[142] **Liu, J., Z. Wang, S.M. Belchik, M.J. Edwards, C. Liu, D.W. Kennedy, E.D. Merkley, M.S. Lipton, et al.** 2012. Identification and characterization of MtoA: a decaheme *c*-type cytochrome of the neutrophilic Fe(II)-oxidizing bacterium *Sideroxydans lithotrophicus* ES-1. Front Microbiol *3*:37.

[143] **Jiao, Y. and D.K. Newman.** 2007. The pio operon is essential for phototrophic Fe(II) oxidation in *Rhodopseudomonas palustris* TIE-1. J Bacteriol *189*:1765-1773.

[144] **Nooren, I.M. and J.M. Thornton.** 2003. Diversity of protein-protein interactions. EMBO J *22*:3486-3492.

[145] **Perkins, J.R., I. Diboun, B.H. Dessailly, J.G. Lees, and C. Orengo.** 2010. Transient protein-protein interactions: structural, functional, and network properties. Structure *18*:1233-1243.

[146] **Crowley, P.B. and M. Ubbink.** 2003. Close encounters of the transient kind: Protein interactions in the photosynthetic redox chain investigated by NMR spectroscopy. Acc Chem Res *36*:723-730.

[147] **Marcus, R.A. and N. Sutin.** 1985. Electron transfers in chemistry and biology. Biochim Biophys Acta *811*:265-322.

[148] **Moser, C.C., J.L.R. Anderson, and P.L. Dutton.** 2010. Guidelines for tunneling in enzymes. Biochim Biophys Acta *1797*:1573-1586.

[149] **Mclendon, G.** 1991. Control of biological electron-transport via molecular recognition and binding: the velcro model. Struct Bond *75*:159-174.

[150] **Berg, O.G. and P.H. Vonhippel.** 1985. Diffusion-controlled macromolecular interactions. Annu Rev Biophys Biophys Chem *14*:131-160.

[151] **Northrup, S.H. and H.P. Erickson.** 1992. Kinetics of protein-protein association explained by Brownian dynamics computer-simulation. Proc Natl Acad Sci USA *89*:3338-3342.

[152] **Sheinerman, F.B., R. Norel, and B. Honig.** 2000. Electrostatic aspects of protein-protein interactions. Curr Opin Struc Biol *10*:153-159.

[153] **Janin, J.** 1997. The kinetics of protein-protein recognition. Proteins *28*:153-161.

[154] **Chothia, C. and J. Janin.** 1975. Principles of protein-protein recognition. Nature *256*:705-708.

[155] **Camacho, C.J., S.R. Kimura, C. DeLisi, and S. Vajda.** 2000. Kinetics of desolvation-mediated protein-protein binding. Biophys J *78*:1094-1105.

[156] **Williams, P.A., V. Fulop, Y.C. Leung, C. Chan, J.W.B. Moir, G. Howlett, S.J. Ferguson, S.E. Radford, and J. Hajdu.** 1995. Pseudospecific docking surfaces on electron-transfer proteins as illustrated by pseudoazurin, cytochrome c_{550} and cytochrome cd_1 nitrite reductase. Nat Struc Biol *2*:975-982.

[157] **Wodak, S.J. and J. Janin.** 2003. Structural basis of macromolecular recognition. Adv Protein Chem *61*:9-73.

[158] **Bashir, Q., S. Scanu, and M. Ubbink.** 2011. Dynamics in electron transfer protein complexes. FEBS J *278*:1391-1400.

[159] **Logan, B.E.** 2009. Exoelectrogenic bacteria that power microbial fuel cells. Nature reviews. Microbiology *7*:375-381.

[160] **Lovley, D.R.** 2008. The microbe electric: conversion of organic matter to electricity. Curr Opin Biotech *19*:564-571.

[161] **Rabaey, K. and W. Verstraete.** 2005. Microbial fuel cells: novel biotechnology for energy generation. Trends Biotechnol *23*:291-298.

[162] **Logan, B.E.** 2010. Scaling up microbial fuel cells and other bioelectrochemical systems. Appl Microbiol Biotechnol *85*:1665-1671.

[163] **Pant, D., G. Van Bogaert, L. Diels, and K. Vanbroekhoven.** 2010. A review of the substrates used in microbial fuel cells (MFCs) for sustainable energy production. Biores Technol *101*:1533-1543.

[164] **Dumas, C., R. Basseguy, and A. Bergel.** 2008. Electrochemical activity of *Geobacter sulfurreducens* biofilms on stainless steel anodes. Electrochim Acta *53*:5235-5241.

[165] **Xing, D.F., Y. Zuo, S.A. Cheng, J.M. Regan, and B.E. Logan.** 2008. Electricity generation by *Rhodopseudomonas palustris* DX-1. Environ Sci Technol *42*:4146-4151.

[166] **Rabaey, K., P. Clauwaert, P. Aelterman, and W. Verstraete.** 2005. Tubular microbial fuel cells for efficient electricity generation. Environ Sci Technol *39*:8077-8082.

[167] **Marsili, E., J. Sun, and D.R. Bond.** 2010. Voltammetry and growth physiology of *Geobacter sulfurreducens* biofilms as a function of growth stage and imposed electrode potential. Electroanal *22*:865-874.

[168] **Watson, V.J. and B.E. Logan.** 2010. Power production in MFCs inoculated with *Shewanella oneidensis* MR-1 or mixed cultures. Biotechnol Bioeng *105*:489-498.

[169] **Rozendal, R.A., H.V.M. Hamelers, K. Rabaey, J. Keller, and C.J.N. Buisman.** 2008. Towards practical implementation of bioelectrochemical wastewater treatment. Trends Biotechnol *26*:450-459.

[170] **Fornero, J.J., M. Rosenbaum, and L.T. Angenent.** 2010. Electric power generation from municipal, food, and animal wastewaters using microbial fuel cells. Electroanal *22*:832-843.

[171] **Wagner, R.C., J.M. Regan, S.E. Oh, Y. Zuo, and B.E. Logan.** 2009. Hydrogen and methane production from swine wastewater using microbial electrolysis cells. Water Res *43*:1480-1488.

[172] **Cheng, S. and B.E. Logan.** 2007. Sustainable and efficient biohydrogen production via electrohydrogenesis. Proc Natl Acad Sci USA *104*:18871-18873.

[173] **Lovley, D.R.** 2003. Cleaning up with genomics: Applying molecular biology to bioremediation. Nat Rev Microbiol *1*:35-44.

[174] **Baranska, J.A. and Z. Sadowski.** 2013. Bioleaching of uranium minerals and biosynthesis of UO_2 nanoparticles. Physicochem Probl Miner Process *49*:71-79.

CHAPTER II

The tetraheme cytochrome from *Shewanella oneidensis* MR-1 shows thermodynamic bias for functional specificity of the hemes

This chapter was published in:

Fonseca BM, Saraiva IH, Paquete CM, Soares CM, Pacheco I, Salgueiro CA, Louro RO (2009) "The tetraheme cytochrome from *Shewanella oneidensis* MR-1 shows thermodynamic bias for functional specificity of the hemes" *J Biol Inorg Chem* **14:** 375-385.

The author of this dissertation participated in all experiments described in this chapter, except in the determination of the heme axial ligands geometry and the theoretical calculations.

ABSTRACT

Bacteria of the genus *Shewanella* contain an abundant small tetraheme cytochrome in their periplasm when growing anaerobically. Data collected for the protein isolated from *Shewanella oneidensis* MR-1 and *Shewanella frigidimarina* indicate differences in the order of oxidation of the hemes. A detailed thermodynamic characterization of the cytochrome from *Shewanella oneidensis* MR-1 in the physiological pH range was performed, with data collected in the pH range 5.5-9.0 from NMR experiments using partially oxidized samples and from redox titrations followed by visible spectroscopy. These data allow the parsing of the redox- and redox-protonation interactions that occur during the titration of hemes. The results show that electrostatic effects dominate the heme-heme interactions in agreement with modest redox-linked structural modifications, and protonation has a considerable influence on the redox properties of the hemes in the physiological pH range. Theoretical calculations using the oxidized and reduced structures of this protein reveal that the bulk redox-Bohr effect arises from the aggregate fractional titration of several of the heme propionates. This detailed characterization of the thermodynamic properties of the cytochrome shows that only a few of the multiple microscopic redox states that the protein can access, are significantly populated at physiological pH. On this basis a functional pathway for the redox activity of the small tetraheme cytochrome from *Shewanella oneidensis* MR-1 is proposed, where reduction and protonation are thermodynamically coupled in the physiological range. The differences between the small tetraheme cytochromes from the two organisms are discussed in the context of their biological role.

INTRODUCTION

The bacteria of the genus *Shewanella* have been identified as suitable candidates for bioremediation efforts of contaminated sites and energy generation in microbial fuel cells due to their capability for using a wide variety of respiratory terminal electron acceptors, including a number of toxic elements and insoluble metal compounds [1]. These organisms appear to have solved the difficulties of electron transport to these insoluble respiratory electron acceptors by developing a variety of strategies that rely on complex electron transfer chains [2]. The published genome of *S. oneidensis* MR-1 contains at least 41 genes encoding putative cytochromes [3], and some of these cytochromes have been unequivocally implicated in anaerobic respiratory processes [2]. One of the most abundant cytochromes in the periplasm of cells grown anaerobically with fumarate is the small tetraheme cytochrome *c* (STC) [4] also known as CctA [5]. This is a soluble protein with a molecular weight of approximately 12 kDa containing four hemes *c*, axially coordinated by histidines. In the case of STC from *S. oneidensis* (*So*STC), its physiological role remains undetermined [5,6], whereas in *S. frigidimarina* a knockout mutant of STC was shown to be defective for iron respiration [7]. To further compound the issue, the genetic context of the *cctA* gene in the two species is different [4] suggesting different physiological functions. In line with this, the expected redox partners of *So*STC in the iron respiration pathway, the proteins CymA and MtrA, did not reveal interactions with *So*STC through formaldehyde cross-linking experiments [5].

For *So*STC X-ray structures were reported at high pH (8.5–9.2) for the oxidized and reduced states [8]. A detailed study of the redox properties was performed also at pH 9.2 and high salt, showing that the order of oxidation is I,

II, IV, III [9]. However, protein film voltammetry shows that the reduction potentials are pH dependent [10]. Preliminary structural studies of the highly homologous STC from *S. frigidimarina* (*Sf*STC) showed that the structure of the two proteins is very similar [11,12]. However, a detailed study of the redox and acid-base properties of this protein in the pH range 5.5-8.5 revealed that the order of oxidation (IV, II, I, III) is different from that determined for *So*STC, and that there are significant effects resulting from the titration of acid-base groups in the physiological pH range. The pairwise redox interactions are dominated by electrostatic effects and the redox potentials of the hemes are modulated by pH in the physiological range (the redox-Bohr effect).

When pH modulates the reduction potential of the redox centers, the driving force for electron transfer is modified [13] and the effect can be functionally important [14]. Pairwise interactions involving hemes and acid-base groups have been shown to give rise to complex functional behavior in cytochromes c_3 from sulfate reducing bacteria [15], also the most abundant periplasmic cytochromes in these anaerobic organisms [16]. Parsing of the effects arising from interactions between redox centers from the effects arising from interactions between redox and acid-base centers requires data collected in a pH range relevant for the titration of the acid-base centers. In this work, NMR and visible spectroscopy data were used to probe the thermodynamic properties of *So*STC in the pH range of 5.5 to 9.0, in order to discriminate redox and redox-Bohr interactions. This allowed the resolution of the pending issue of how the modest redox-linked structural modifications could give rise to apparent positive cooperativities between heme pairs [8,9]. A functional interpretation of the dominant microscopic populations determined from the data is presented, and the differences observed in the redox behavior of *Sf*STC

and *So*STC in the physiological pH range are discussed in the framework of their different biochemical and genetic context.

MATERIAL AND METHODS

Bacterial growth and protein purification. Cells of *S. oneidensis* were cultivated under microaerobic conditions in a batch culture at 25 ºC, using Luria–Bertani (LB) medium supplemented with 15 mM sodium lactate and 20 mM disodium fumarate. Growth was initiated with a 1 % inoculum of an over-night grown culture incubated using the same growth conditions. The culture was allowed to grow up to an optical density (OD) of approximately 1.0. The turbidity of the culture was measured at 600 nm.

Cells were harvested by centrifugation (10,000 g; 15 min; 4 ºC). The pellet was washed with 10 mM Tris buffer (pH 7.6) containing 100 mM NaCl and then resuspended in 10 mM Tris buffer (pH 7.6) containing 500 mM sucrose, to give a final cell suspension of 5-10 g per 100 mL and incubated at room temperature for 15 min. Lysozyme was added to a final concentration of 3 mg mL^{-1} and was incubated for 15 min at room temperature. The osmotic shock was achieved by adding distilled water in a 1:1 proportion. EDTA was added to a final concentration of 1 mM. The cell suspension was incubated at room temperature for a period of approximately 30 minutes to assure that the formation of spheroplasts was complete. Magnesium sulfate was added to a final concentration of 10 mM and the cell suspension was centrifuged (20,000 g; 15 min; 4 ºC). A dark orange supernatant was obtained. A second periplasmic extraction was performed on the remaining pellet. The orange supernatant was loaded directly onto a DEAE column previously equilibrated with 50 mM Tris (pH 7.6). The fraction containing *So*STC eluted with 250-300 mM NaCl in 50

mM Tris (pH 7.6). This fraction was loaded onto a Q-Sepharose column, equilibrated previously with 10 mM Tris (pH 7.6). A salt gradient from 0 to 1M NaCl in 10 mM Tris (pH 7.6) was applied and the fraction containing *So*STC was eluted at 200 mM. The final purification step was performed on a Superdex 75 column, equilibrated with 10 mM Tris (pH 7.6) prior to use.

The chromatographic fractions were routinely analyzed by SDS-PAGE and UV-Visible spectroscopy, to select those containing the *So*STC. The purity of the protein was revealed as a single band on SDS-PAGE.

Redox titrations followed by UV-visible spectroscopy. Anaerobic redox titrations of the *So*STC followed by visible spectroscopy were performed at 298 K as described in the literature [17]. The *So*STC solution was prepared in 100 mM Tris/maleate buffer inside an anaerobic glove box (MBraun MB150-GI), kept at below 1 ppm oxygen level.

To assure equilibrium between the electrode and the redox centers of the protein, a mixture of redox mediators was used: methyl viologen, diquat, neutral red, safranine O, anthraquinone 2-sulfonate, anthraquinone 2,7-sulfonate, indigo disulfonate and indigo trisulfonate were used in all experiments. The following mediators were added to this mixture: for the titrations performed at pH 6.0 phenosafranine; for the titrations performed at pH 7.3 indigo tetrasulfonate; and for the titrations performed at pH 8.3 methylene blue, gallocyanine and indigo tetrasulfonate. The pH of the solution was measured before and after each experiment.

Different concentration ratios of protein (approximately 20 μM) *versus* mediators (between 1 and 2 μM) were tested to check for possible interactions between the protein and the mediators. Also, for each pH value the redox titrations were repeated at least three times, in the oxidative and reductive

directions, in order to check for hysteresis and reproducibility. Data analyses were performed as described in the literature [18].

NMR sample preparation and experiments. Protein for NMR experiments was lyophilized twice using $^{2}H_2O$ (99.9 % atom). The protein was dissolved in approximately 500 μL of $^{2}H_2O$ to a final concentration of approximately 1 mM and the ionic strength was adjusted to 100 mM by the addition of KCl. NMR spectra obtained before and after the lyophilization were identical, showing that the protein structure was not affected by this procedure.

Protein reduction was achieved with gaseous hydrogen through the addition of catalytic amounts of hydrogenase from *Desulfovibrio sp.* Partially oxidized samples were prepared by flushing out the hydrogen with argon from the fully reduced sample and then by adding controlled amounts of air into the NMR tube using a gas-tight syringe. The pH value of the solution was adjusted with small amounts of $NaO^{2}H$ or ^{2}HCl. This procedure was always performed inside an anaerobic glove box (MBraun MB150-GI) when working with the reduced and partially oxidized protein. The pH values reported are direct readings without correction for the isotope effect [19].

The NMR experiments were performed on Bruker spectrometers operating at 500 MHz. ^{1}H-^{13}C HMQC (Δ delay fixed at 3.2 ms) using natural abundance samples, ^{1}H-NOESY (25 ms, mixing time) and COSY spectra were collected to assign the signals of the heme substituents in the fully oxidized state. ^{1}H-NOESY spectra were collected using partially oxidized samples at 298 K in the pH range 5.5–9.0, for heme signal assignment and also thermodynamic characterization. The proton spectra were calibrated using the water signal as an internal reference.

The Bruker TopSpin program was used to visualize the NMR spectra and the CARA program [20] was used for the assignment work.

Thermodynamic characterization. To describe in detail the thermodynamics of a protein with four hemes and one acid-base center a total of 32 microscopic states are defined [15]. Considering the fully reduced protonated microscopic state as the reference, the energy of each microscopic state can be described by a sum of (1) the energies of oxidation of the hemes, (2) the energy of deprotonation of the acid-base center, (3) the interaction energies among the oxidized hemes and (4) the interaction energies between the hemes and the acid-base center known as redox-Bohr effect, in a total of 15 parameters. The relative populations of the microscopic states are given by the Boltzmann distribution derived from the relative energies of the various microscopic states [21]. The interaction energies between pairs of centers can be interpreted as cooperativities, which are positively cooperative, non-cooperative or anti cooperative depending on the sign and magnitude of the interaction, and on the nature of the interacting centers.

Since the intermolecular electron transfer rate is slow and the intramolecular electron transfer rate is fast on the NMR timescale, five stages of oxidation can be defined, each containing the microscopic states with 0, 1, 2, 3 and 4 oxidized hemes. The stages are connected by steps of one-electron transfer. The oxidation fractions (Ox) of each heme (n) in each stage of oxidation of the protein (S) can be determined from the respective paramagnetic shift ($\delta_{n,S}$) according to the expression:

$$Ox_{n,S} = \frac{\delta_{n,S} - \delta_{n,0}}{\delta_{n,4} - \delta_{n,0}}$$

These oxidation fractions allow the determination of the thermodynamic parameters relative to the fully reduced reference state ($Ox_{n,0}$). To determine absolute values for the thermodynamic parameters the total protein oxidation fractions were measured versus solution potential using redox titrations followed by visible spectroscopy. The experimental uncertainty associated with the NMR data was estimated from the line width of each NMR signal, while the data points of the redox titrations were given an uncertainty of 3 % of the total optical signal. The thermodynamic model was fit simultaneously to the NMR and UV- visible data using the Nelder-Mead Simplex algorithm implemented in MATLAB (MathWorks Inc) [22] (see Appendix D and E).

Determination of the axial ligand geometry. The ^{13}C chemical shifts of the α substituents of the hemes at 298 K and 305.7 K were fit to a semi empirical model of the heme molecular orbitals [23]. An average of values available for different cytochromes were used as diamagnetic references [24]. The values of the energy splitting (ΔE) and the orientation of the rhombic perturbation (θ) were fit and the hyperfine coupling constant was fixed at -36 MHz [23]. The fitting was performed with the Nelder-Mead Simplex algorithm implemented in MATLAB (MathWorks Inc) [22] (see Appendix E).

Theoretical calculations. The STC from *S. oneidensis* has been crystallized in the oxidized and reduced states, at pH 8.5-9.2 [8]. The oxidized (PDB code: 1M1Q) and reduced (PDB code: 1M1R) structures were both used in the calculations aiming at characterizing the equilibrium protonation and reduction of all groups in the protein. Given the high resolution of the data (0.97 and 1.02 Å for the oxidized and reduced structures, respectively), quite a number of residues and segments with multiple conformations are found. The highest occupancy conformers for both structures and the lowest occupancy

conformer for the propionate A from heme II were selected, yielding four different calculations. From the analysis of the X-ray structures [8], the major consequence of reduction is the displacement of Lys 72 from an exposed conformation to another conformation near hemes II and III, where it makes a salt bridge with the propionate A from heme II in its highest occupied conformer.

The thermodynamic equilibrium of protonation and reduction was studied using methodologies that were described elsewhere [25,26]. These are based on continuum electrostatic (CE) methods and Monte-Carlo (MC) sampling of binding states. The CE calculations were done using the package MEAD (version 2.2.0) [27,28]. The sets of atomic radii and partial charges were taken from the GROMOS96 43A1 force field [29,30], except in the case of the hemes, which were derived by quantum chemical calculations described elsewhere [31]. The dielectric constants used were 80 for the solvent and 20 for the protein, which are values within the range where pK_a prediction is optimized [32]. The solvent probe radius was 1.4 Å, the ion exclusion layer 2.0 Å, the ionic strength 0.1 M and the temperature 27 ºC. The program PETIT [25,26] was used for the MC sampling of proton and electron binding states. Site pairs were selected for double moves when at least one pairwise term was greater than 2 pK units. Averages were computed using 10^5 MC steps, while for correlations 10^6 MC steps were used.

RESULTS

Assignment of heme signals. For the fully oxidized protein, the methyl signals were cross-assigned through ^{1}H-NOESY spectra acquired using partially oxidized samples following published procedures [33]. The assignment of the heme signals, presented in Table 2.1, agrees with the

assignment of the heme methyl signals previously reported under slightly different experimental conditions [9]. In the fully oxidized protein ^{13}C signals were assigned using ^{13}C-^{1}H HMQC experiments. All the signals have chemical shifts comparable to those obtained for the homologous STC from *S. frigidimarina* [11], a consequence of the structural similarity between these two proteins.

Table 2.1. Assignment of ^{1}H and ^{13}C NMR resonances of the heme substituents of *So*STC at 305.7 K, pH 6.0.

	Heme I		Heme II		Heme III		Heme IV	
Substituent	^{1}H	^{13}C	^{1}H	^{13}C	^{1}H	^{13}C	^{1}H	^{13}C
2^1	6.50	-17.8	13.39	-34.4	17.08	-34.1	4.49	-19.3
3^1	-	-	0.65	0.1	-	-	-	-
3^2	-	-	-0.2	45.7	-	-	-	-
7^1	22.54	-29.9	14.95	-27.5	10.88	-13.2	27.23	-53.3
8^1	-	-	-1.52	-16	-2.17	-23.8	-	-
8^2	-	-	0.22	57.3	1.66	81.8	-	-
12^1	8.16	-24.0	20.83	-48.6	19.13	-47.7	9.71	-29.6
13^1	-1.75 -2.83	8.4	5.03 -	-18.4	-0.28 -3.11	26.2	2.66 -0.13	-8.2
13^2	-	-	1.00 1.17	89.1	- -	-	-1.13 -1.37	67.1
17^1	13.20 12.62	-24.5	5.57 2.53	-7.1	5.10 7.36	-3.6	10.03 7.12	-17.2
17^2	3.13 3.25	107.8	0.22 -0.05	71.5	- -	-	1.00 1.35	89.3
18^1	35.01	-65.5	22.69	-47.7	38.61	-68.7	30.02	-60.2

Geometry of the axial ligands of the hemes. The geometry of the heme ligands was deduced from the ^{13}C paramagnetic shifts [34]. In Figure 2.1 and Table 2.2, it can be seen that there is a good agreement between the geometric parameters deduced from NMR data and those observed in the crystal structure [8]. This shows that there are no significant structural differences

between the solution and crystal structures at the level of the heme core, despite the difference in sample conditions and experimental techniques. These data show that the heme core architecture is very robust and also provide an independent confirmation of the assignment of the heme signals to the structure.

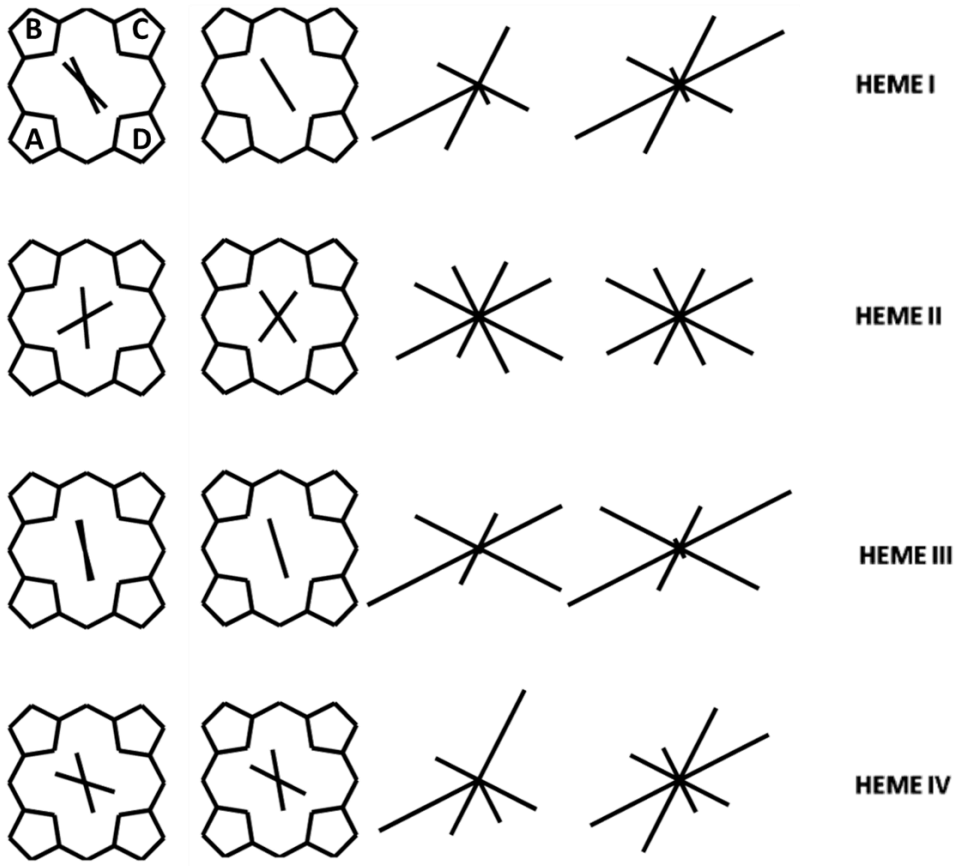

Figure 2.1. Orientation of the heme axial ligands and experimental and calculated shifts of the heme substituents. The first and second columns indicate the X-ray structure and calculated orientations of the planes of the axial histidines respectively. The heme pyrrole rings are identified according to the Fisher nomenclature as indicated on the top left. The third and fourth columns represent the experimental and calculated ^{13}C paramagnetic shifts of the heme substituents respectively. Each line is oriented from the centre of the heme to the respective carbon with a length proportional to the paramagnetic shift.

Table 2.2. Molecular orbital parameters determined by fitting the ^{13}C signals of the substituents α to the heme. To determine β the formula $\Delta E = (5 + cos4\theta)cos\beta$ was used [23]. The angles obtained from the X-ray crystal structure are shown for comparison (protein data bank code: 1M1Q).

	Heme I		**Heme II**		**Heme III**		**Heme IV**	
	NMR	X-ray	NMR	X-ray	NMR	X-ray	NMR	X-ray
θ (°)	-13.0 (0.4)	10.4	-46 (2)	-72.9	-28.3 (0.4)	-33.8	-8.5 (0.5)	-0.9
β (°)	0	18.2	71	65.7	0	6.3	53	56.8
ΔE (kJ mol^{-1})	6.0 (0.2)		1.32 (0.05)		6.3 (0.2)		3.5 (0.1)	

The largest difference between crystallographic data and the geometries deduced from NMR data is observed for heme II. This heme has the largest calculated angle between the axial histidine planes. A large predicted angle is a consequence of a small energy splitting between the frontier molecular orbitals and is associated with a reduced precision in the determination of the orientation of the rhombic perturbation. For heme II this effect is further compounded by the close proximity of heme III and its dipolar paramagnetic shifts, which distort the symmetry of the shifts of heme II substituents assumed by the model.

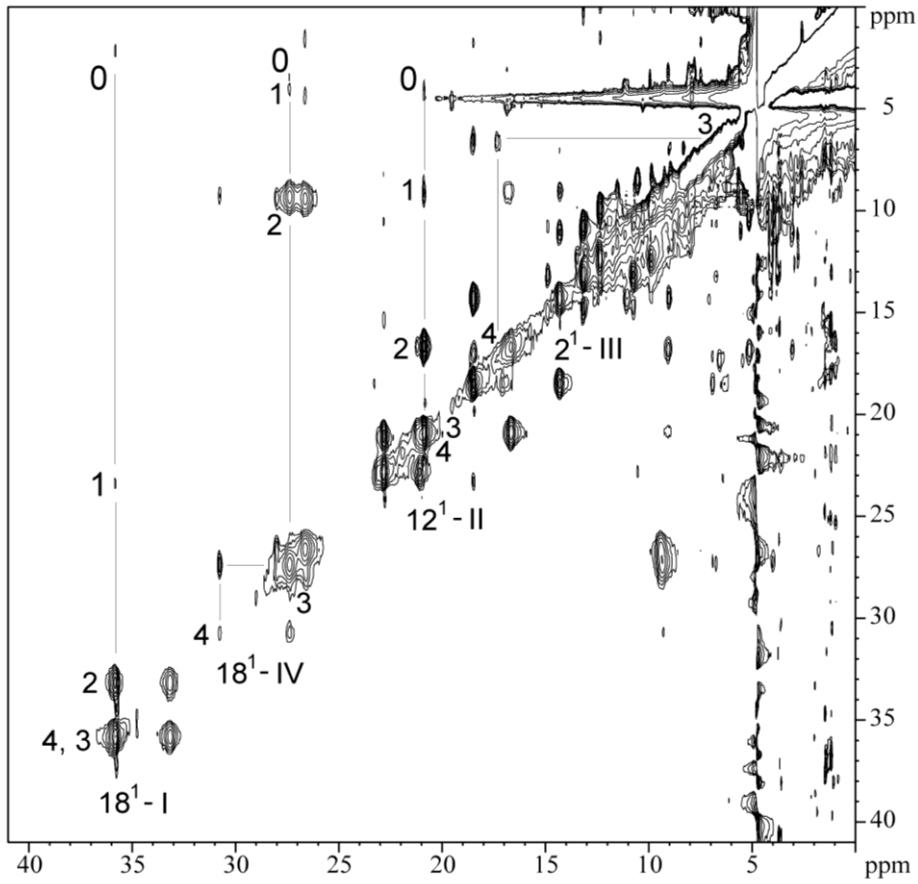

Figure 2.2. ^{1}H-NOESY spectrum of partially oxidized *So*STC at pH 6.0. Cross peaks resulting from intermolecular electron transfer are indicated for one methyl group from each heme identified using the IUPAC nomenclature (18^1CH_3-I; 12^1CH_3-II; 2^1CH_3-III; 18^1CH_3-IV) in the different stages of oxidation (0, 1, 2, 3 and 4). The roman numbers correspond to the four hemes, respectively. The cross peak to stage 0 (fully reduced) is not visible at the level of oxidation of this particular sample and its localization is indicated approximately by the end of the corresponding solid line.

Thermodynamic characterization. The NMR spectra of partially oxidized samples of *So*STC show that each heme substituent displays five discrete NMR signals (Figure 2.2). These correspond to each of the five possible macroscopic stages of oxidation that comprise microscopic states with the same number of oxidized hemes, and allow the degree of oxidation of the hemes to be monitored at each individual redox stage [35]. Care is necessary

for selecting the heme substituents that are subject to the least additional contribution to their chemical shifts resulting from the oxidation of the neighboring hemes. In this work, the heme methyl groups $18^1CH_3^I$, $7^1CH_3^{II}$, $2^1CH_3^{III}$ and $18^1CH_3^{IV}$ (Roman numerals indicating the heme by the order of attachment to the polypeptide chain) were chosen to follow the individual heme oxidation [9,36]. In order to determine the thermodynamic properties of *So*STC, the thermodynamic model was fit simultaneously to the full set of data obtained from the pH dependence of the paramagnetic chemical shifts of each heme methyl group and the data obtained for redox titrations followed by visible spectroscopy at pH 6.0, 7.3 and 8.3. The fittings are presented in Figures 2.3 and 2.4, respectively.

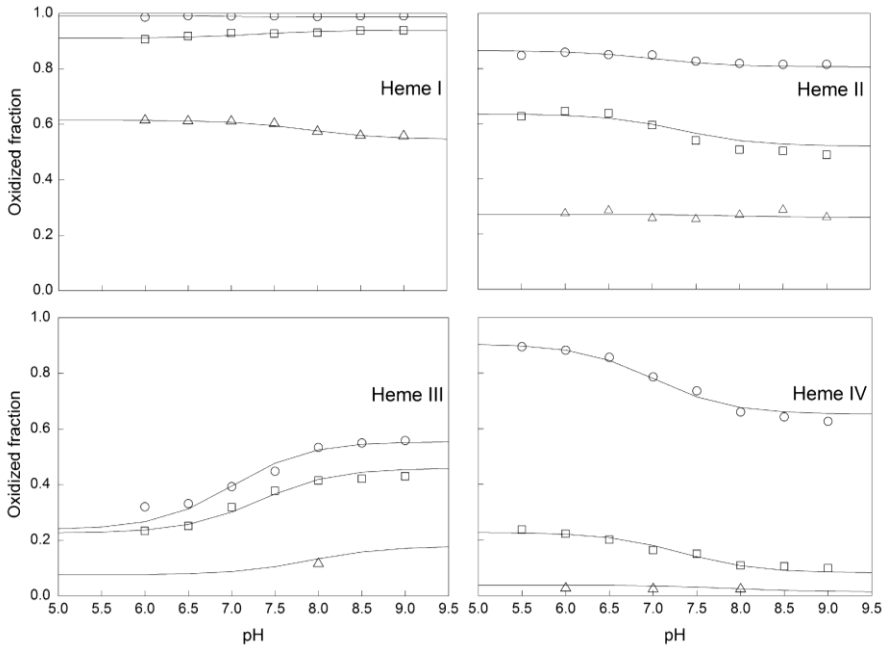

Figure 2.3. The pH dependence of the oxidized fraction of heme methyl group resonances $18^1CH_3^I$, $7^1CH_3^{II}$, $2^1CH_3^{III}$ and $18^1CH_3^{IV}$ of *So*STC. Stage 1 of oxidation (Δ); Stage 2 (□); Stage 3 (o). The oxidized fractions in the fully reduced and in the fully oxidized stage are 0 and 1, respectively. Solid lines are the result of the simultaneous fit of the thermodynamic model to the NMR and visible data as described in the Materials and Methods section.

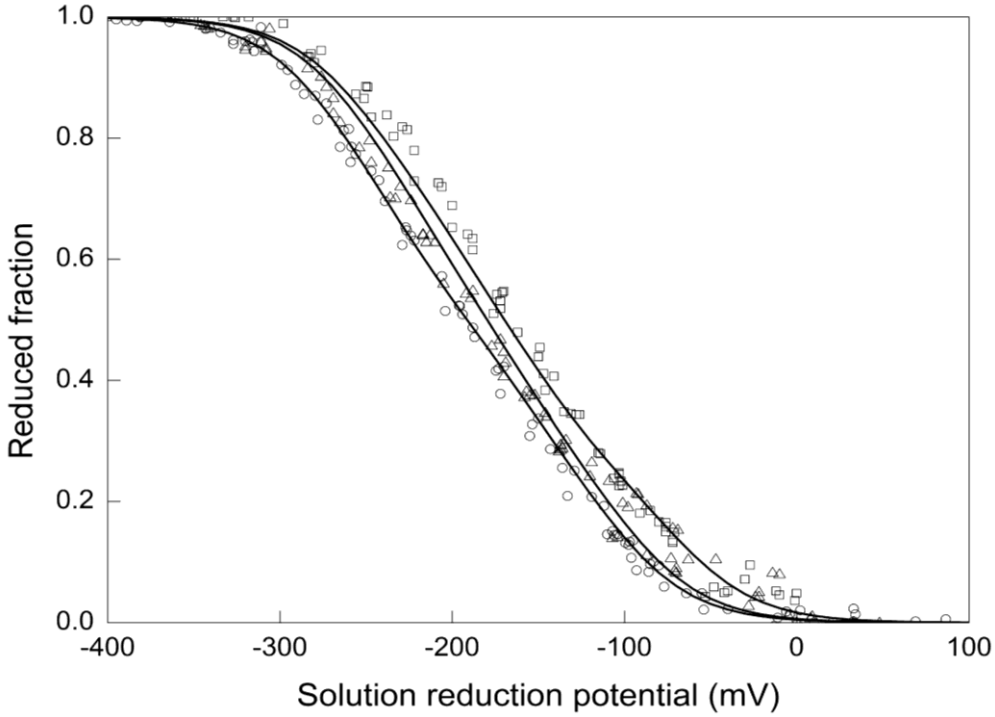

Figure 2.4. Reduced fraction of *So*STC determined by redox titrations followed by visible spectroscopy at pH 6.0 (□); 7.3 (Δ) and 8.3 (o). Solid lines are the result of the simultaneous fit of the thermodynamic model to the NMR and visible data as described in the Materials and Methods section.

The thermodynamic model shows a good agreement with the experimental data and therefore is appropriate to describe the redox and redox-Bohr properties of *So*STC in the physiological range. The thermodynamic parameters are presented in Table 2.3, together with the macroscopic pK_a values associated with the five stages of oxidation of the cytochrome.

Table 2.3. Thermodynamic parameters determined for *So*STC. A) Diagonal terms (in bold) represent the oxidation energies of the four hemes and deprotonation energies for the ionizable center in the fully reduced and protonated protein. The off-diagonal elements represent the redox and redox-Bohr interaction energies between the five centers. Standard errors are given in parentheses. All data are reported in units of meV and standard thermodynamic expressions relate the oxidation energies and deprotonation energy with reduction potentials and pK_a, respectively. **B)** Macroscopic pK_a values for the five stages of oxidation of *So*STC.

A	**Energy (meV)**				
	Heme I	**Heme II**	**Heme III**	**Heme IV**	**Ionizable center**
Heme I	**-243 (4)**	28 (2)	21 (4)	11 (3)	-31 (2)
Heme II		**-222 (4)**	72 (1)	11 (1)	-33 (2)
Heme III			**-189 (5)**	29 (1)	-56 (2)
Heme IV				**-171 (6)**	-9 (2)
Ionizable center					**500 (3)**

B				
pK_a				
Stage 0	**Stage 1**	**Stage 2**	**Stage 3**	**Stage 4**
8.5	7.9	7.3	7.0	6.3

Theoretical calculations. The order of reduction depends on the structure analyzed but is in good agreement with the data obtained in this work and those previously reported [9]. Calculations made using the oxidized and reduced structures show large changes in the redox potentials of heme II and heme III with the reduced structure generating increased redox potentials (data not shown). The stabilization of the reduced state is probably due to the conformational changes of Lys 72, which becomes closer to these two hemes upon reduction, providing another positive charge [8]. Hemes II and III show the highest redox correlation in the simulations, which is in agreement with

their interaction as deconvoluted with the experimental model. This is to be expected in view of their proximity and parallel packing.

The redox-Bohr effect is quite evident in this cytochrome and the molecular reasons for it are almost exclusively centered on the strong mutual interactions between the propionates and the heme cores where they are bound. Correlation analysis (data not shown) evidences that at pH 7, the strongest correlations between acid-base residues and hemes are: heme I – propionate D of heme I, heme II – propionate D of heme II, heme III – propionate D of heme III (the magnitude of these correlations depends heavily on the structure being analyzed). This clearly shows that the hemes being mostly affected are hemes I, II and III, confirming what was found with the experimental model. Another way to look at these effects is to look at the $pK_{1/2}$ of each protonable group under different redox states and structures. This can be seen in Figure 2.5. The three propionates mentioned above are indeed those that experience larger changes around (or close to) pH 7, confirming the correlations.

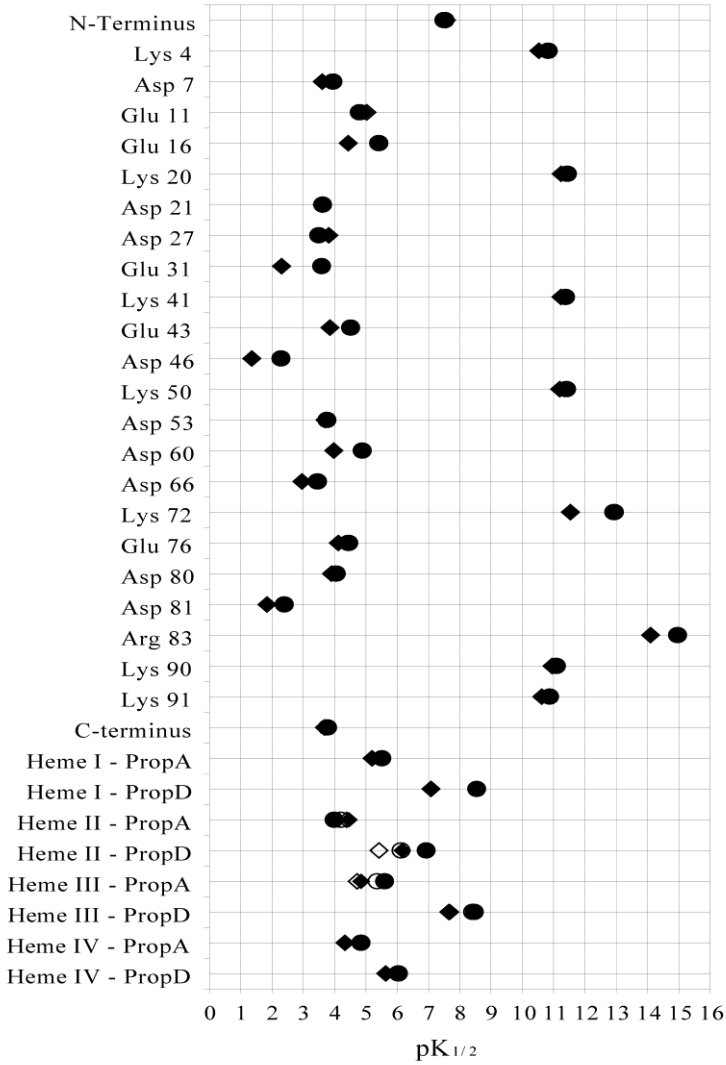

Figure 2.5. $pK_{1/2}$ (pH of half titration) for all protonatable groups in this cytochrome. Diamonds correspond to the calculations with oxidized structures and circles correspond to the ones with the reduced structures. The alternative conformer (lowest occupied) of the propionate A from heme II is represented with open symbols, while the highest occupied conformer is represented with filled symbols.

DISCUSSION

The thermodynamic parameters reported in Table 2.3 show that the reduction potentials of the hemes are negative, as expected for bis-histidinyl-ligated heme groups with substantial exposure to the solvent [37]. The positive values for the interaction between pairs of hemes, indicates negative homo-cooperativity with the oxidation of a particular heme rendering the oxidation of its neighbors more difficult. The interaction energies between the hemes and the acid-base centre are negative, a sign of positive hetero-cooperativity, whereby the oxidation of the hemes facilitates the deprotonation of the acid-base centre, and vice versa. The distance dependence of the redox interactions between pairs of hemes is similar for *So*STC and *Sf*STC, and these interactions appear to be dominated by electrostatic effects [36,38]. This indicates that other effects such as redox dependent protein reorganization does not contribute significantly to the interaction energy, and is in agreement with the modest structural differences observed among the various structures of this protein [8], the most important of which is that experienced by Lys 72. In contrast with this observation, the redox-Bohr interactions do not correlate with distance to the hemes in a clear pattern that would allow the identification of an acid-base group responsible for this effect. Figure 2.5 shows that theoretical calculations predict that several of the heme propionates are expected to display significant differences in their midpoint titrations, thereby contributing to the overall redox-Bohr effect that spans the physiological pH range (Table 2.3-B). These two pieces of evidence show that the molecular reasons for the redox-Bohr effect observed in the experimental data are complex and result from partial contribution of various acid-base groups in the protein. There is a well-known precedent for this phenomenon in the Bohr-effect of hemoglobin, where the

pH dependence of oxygen affinity is modulated by partial contributions of various acid-base groups [39]. However, the experimental data cannot define a more complex model that includes the explicit description of multiple acid-base centers [40].

The profile of oxidation of the hemes is shown in Figure 2.6. The relative order of oxidation of hemes I and IV from *So*STC is different from those from *Sf*STC [9,36], with the apparent midpoint potentials of these two hemes switched by approximately 70 mV at pH 7.0. Given the structural similarity between the two proteins this must result from the 30 % difference in the amino acid composition of these two proteins. Despite the effect that differences in amino acid composition have on the midpoint potentials of the hemes, it is interesting to note that the pairwise interactions among the hemes show similar values for *So*STC and *Sf*STC. Given the conserved nature of the heme core in these proteins, this is an indication of similar overall electrostatic environment in both proteins.

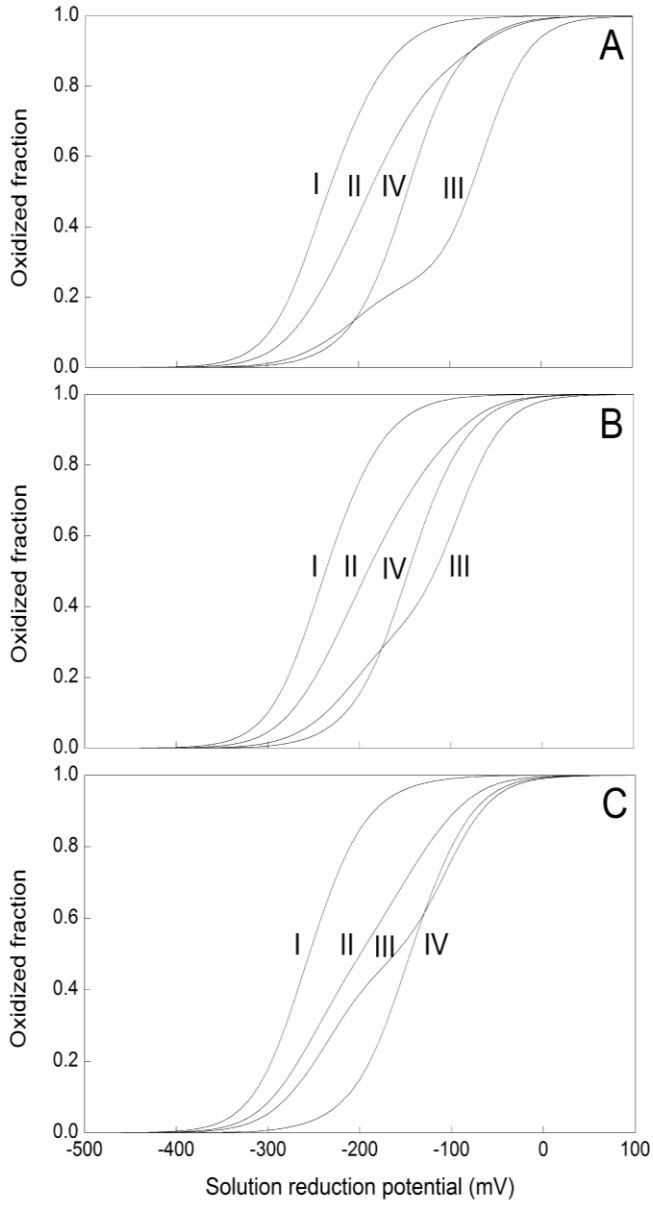

Figure 2.6. Oxidized fractions of the individual hemes of *So*STC at various pH. **A)** pH 5.5; **B)** pH 7.0; and **C)** pH 8.5. The curves were calculated using the parameters presented in Table 2.3-A.

Figure 2.6 shows that the titration of heme III is the most affected by the other hemes and by the solution pH. This heme starts to be oxidized earlier than heme IV but because of the strong redox interactions with hemes I and II,

the midpoint of its titration curve is reached at a higher value of solution potential giving an oxidation order of I, II, IV, III within the pH range of 5.5 to 8.0. As a consequence of the strong redox-Bohr effect observed for heme III, which at high pH balances the redox interactions arising from neighboring hemes, above pH 8.0 the midpoint titration of heme III occurs before that of heme IV in the experimental conditions of this work.

Figure 2.7 shows the speciation diagram for *So*STC at pH 7.0 obtained from the thermodynamic parameters listed in Table 2.3. It shows that at physiological pH, protonation is coupled to electron transfer. In the fully oxidized stage the deprotonated microscopic state is dominant, whereas for all other stages of oxidation of the protein, the protonated microscopic states are dominant. Since heme III is the most active in this redox step the data show that the redox activity of this heme is coupled thermodynamically to protonation of the cytochrome. Because of the strong redox interactions between this heme and its neighbors, and given the redox-Bohr effect on all hemes, it can be proposed that heme III plays an important role in modulating the redox properties of this protein. In Figure 2.7, all redox stages show one dominant microscopic state and therefore, a functional pathway for preferential electron transfer can be proposed for the physiological pH. Given that heme I is mostly oxidized from stage 1 to stage 4, it can be proposed that the donor can feed electrons through heme I that are redistributed to the other hemes according to the redox potentials in the sequence III, IV, II and finally I. This is a very fast process as a consequence of the short intramolecular pairwise heme distances. Because intramolecular electron reequilibration is much faster than intermolecular electron-transfer, this preferential pathway ensures that heme I is always available to receive additional electrons from the donor. Considering the structure of *So*STC, the lower accessibility of heme III,

and the similarities with the heme domain of the flavocytochrome c_3 (also known as FccA) from the same organism [41], the docking site for the electron acceptor may be located in the vicinity of heme IV. This scenario allows for fast electron donation to the acceptor since the fast intramolecular reequilibration ensures that heme IV remains reduced in the dominant populations of stages 0 to 2, and therefore the electron to be donated is at a short distance from the acceptor. Electron transfer across heme III is thermodynamically uphill in these scenarios but this has been observed to be a fast kinetic process even for more dramatic differences in driving force (see [42] for examples).

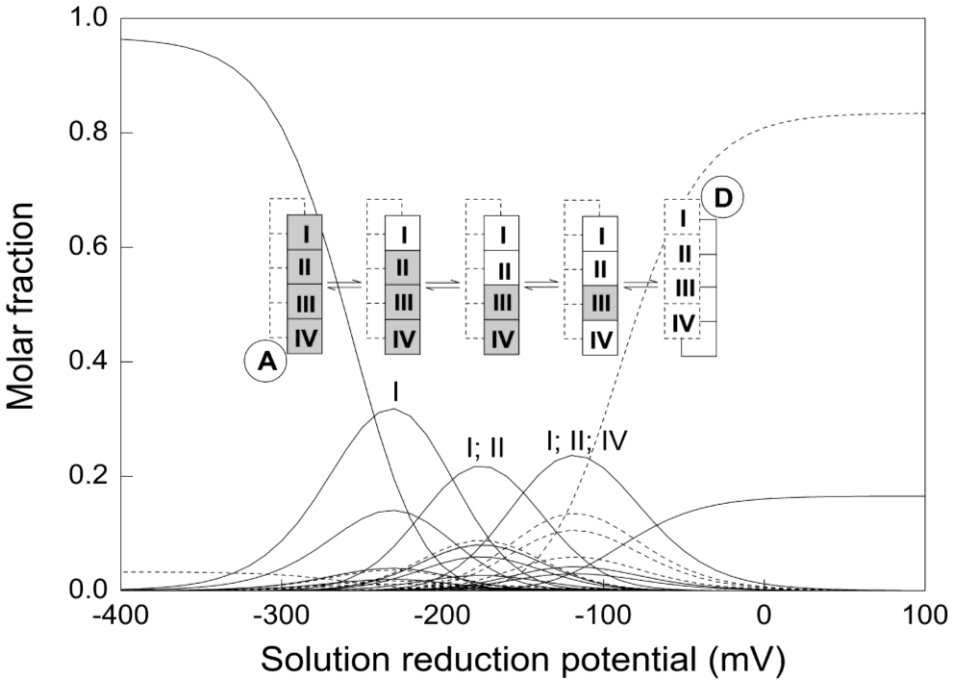

Figure 2.7. Speciation diagram of the microscopic states of *So*STC at pH 7.0. The curves were calculated as a function of the solution reduction potential using the parameters presented in Table 2.3-A. Solid lines indicate the protonated microscopic states. Dashed lines indicate the deprotonated microscopic states. Numbers above the lines indicate the oxidized hemes in the dominant microscopic states. The insert shows a diagram of the functional pathway for electron uptake and release coupled with protonation in *So*STC. (D)onor and (A)cceptor are proposed to interact in the vicinity of hemes I and IV, respectively, as discussed in the text.

The above proposal for entry and exit points takes into account the structural organization of the *So*STC, its similarity with the heme domain of FccA, and is rationalized in the context of one of the factors that regulate electron transfer, namely the driving force [13]. The detailed redox properties of the hemes measured for the isolated *So*STC are expected to be relevant in the context of docking with partners, given the precedent reported for cytochrome c_3 from *Desulfovibrio vulgaris* [43]. In that protein, the hemes are also highly exposed to the solvent and the detailed thermodynamic properties were essentially unaffected by docking with a Zn-substituted analogue of a redox partner that is redox inactive. However, recognition and binding to redox partners provide further constrains on the actual kinetics of intermolecular electron transfer process [44,45], and it has been shown that the specific contribution of different hemes for the reduction of multiheme cytochromes with dithionite can vary even for structurally homologous proteins [18].

In conclusion, the thermodynamic data reported in this work allowed the modest redox-linked structural differences observed in *So*STC to be reconciled with the apparent cooperativities by parsing the redox and protonation effects on the hemes of *So*STC in the physiological pH range. The results show that electrostatics dominate the heme-heme interactions and redox-Bohr interactions are the aggregate effect of several acid-base groups. The functional interpretation of the detailed mechanism proposed for oxidation and reduction of *So*STC relies solely on thermodynamic data and reveals an important aspect of multiredox centre proteins, which is the modulation of thermodynamic properties to generate functional specificity of the various redox centers. However, the physiological importance of the differences displayed by these

two proteins in terms of detailed redox and acid-base behavior will only be amenable to interpretation once the role of *So*STC is determined.

ACKNOWLEDGEMENTS

We thank Graeme Reid (University of Edinburgh) for supplying *Shewanella oneidensis* strain MR1A CS21a. We acknowledge CERMAX at ITQB and Rede Nacional de RMN for access to the facilities where NMR data was collected. Rede Nacional de RMN is supported with funds from FCT, Projecto de Re-Equipamento Científico, Portugal. This research was supported by the Fundação para a Ciência e Tecnologia (PPCDT/2004/BIA-PRO/58722 and PPCDT/QUI/60060/2004). BMF, IHS and CMP are the recipients of grants from Fundação para a Ciência e a Tecnologia (SFRH/BD/41205/2007 (BMF); SFRH/BD/36582/2007 (IHS); SFRH/BPD/34591/2007 (CMP)).

REFERENCES

[1] **Hau, H.H. and J.A. Gralnick.** 2007. Ecology and biotechnology of the genus *Shewanella*. Annu Rev Microbiol *61*:237-258.

[2] **Croal, L.R., J.A. Gralnick, D. Malasarn, and D.K. Newman.** 2004. The genetics of geochemistry. Annu Rev Genet *38*:175-202.

[3] **Meyer, T.E., A.I. Tsapin, I. Vandenberghe, L. De Smet, D. Frishman, K.H. Nealson, M.A. Cusanovich, and J.J. Van Beeumen.** 2004. Identification of 42 possible cytochrome *c* genes in the *Shewanella oneidensis* genome and characterization of six soluble cytochromes. OMICS: J Integ Biol *8*:57-77.

[4] **Tsapin, A.I., I. Vandenberghe, K.H. Nealson, J.H. Scott, T.E. Meyer, M.A. Cusanovich, E. Harada, T. Kaizu, et al.** 2001. Identification of a small tetraheme cytochrome *c* and a flavocytochrome *c* as two of the principal soluble cytochromes *c* in *Shewanella oneidensis* strain MR1. Appl Environ Microbiol *67*:3236-3244.

[5] **Ross, D.E., S.S. Ruebush, S.L. Brantley, R.S. Hartshorne, T.A. Clarke, D.J. Richardson, and M. Tien.** 2007. Characterization of protein-protein interactions involved in iron reduction by *Shewanella oneidensis* MR-1. Appl Environ Microbiol *73*:5797-5808.

[6] **Bretschger, O., A. Obraztsova, C.A. Sturm, I.S. Chang, Y.A. Gorby, S.B. Reed, D.E. Culley, C.L. Reardon, et al.** 2007. Current production and metal oxide reduction by *Shewanella oneidensis* MR-1 wild type and mutants. Appl Environ Microbiol *73*:7003-7012.

[7] **Gordon, E.H., A.D. Pike, A.E. Hill, P.M. Cuthbertson, S.K. Chapman, and G.A. Reid.** 2000. Identification and characterization of a novel cytochrome c_3 from *Shewanella frigidimarina* that is involved in Fe(III) respiration. Biochem J *349*:153-158.

[8] **Leys, D., T.E. Meyer, A.S. Tsapin, K.H. Nealson, M.A. Cusanovich, and J.J. Van Beeumen.** 2002. Crystal structures at atomic resolution reveal the novel concept of "electron-harvesting" as a role for the small tetraheme cytochrome *c*. J Biol Chem *277*:35703-35711.

[9] **Harada, E., J. Kumagai, K. Ozawa, S. Imabayashi, A.S. Tsapin, K.H. Nealson, T.E. Meyer, M.A. Cusanovich, and H. Akutsu.** 2002. A directional electron transfer regulator based on heme-chain architecture in the small tetraheme cytochrome *c* from *Shewanella oneidensis*. FEBS Lett *532*:333-337.

[10] **Firer-Sherwood, M., G.S. Pulcu, and S.J. Elliott.** 2008. Electrochemical interrogations of the Mtr cytochromes from *Shewanella*: opening a potential window. J Biol Inorg Chem *13*:849-854.

[11] **Louro, R.O., M. Pessanha, G.A. Reid, S.K. Chapman, D.L. Turner, and C.A. Salgueiro.** 2002. Determination of the orientation of the axial ligands and of the magnetic properties of the haems in the tetrahaem ferricytochrome from *Shewanella frigidimarina*. FEBS Lett *531*:520-524.

[12] **Pessanha, M., L. Brennan, A.V. Xavier, P.M. Cuthbertson, G.A. Reid, S.K. Chapman, D.L. Turner, and C.A. Salgueiro.** 2001. NMR structure of the haem core of a novel tetrahaem cytochrome isolated from *Shewanella frigidimarina*: identification of the haem-specific axial ligands and order of oxidation. FEBS Lett *489*:8-13.

[13] **Marcus, R.A. and N. Sutin.** 1985. Electron transfers in chemistry and biology. Biochim Biophys Acta *811*:265-322.

[14] **Christensen, H.E.M., I. Coutinho, L.S. Conrad, J.M. Hammerstad-Pedersen, G. Iversen, M.H. Jensen, J.J. Karlsson, J. Ulstrup, and A.V. Xavier.** 1994. Electron transport networks in multicentre metalloproteins. J Photochem Photobiol A: Chem *82*:103-115.

[15] **Louro, R.O.** 2007. Proton thrusters: overview of the structural and functional features of soluble tetrahaem cytochromes c_3. J Biol Inorg Chem *12*:1-10.

[16] **Legall, J., W.J. Payne, L. Chen, M.Y. Liu, and A.V. Xavier.** 1994. Localization and specificity of cytochromes and other electron-transfer proteins from sulfate-reducing bacteria. Biochimie *76*:655-665.

[17] **Correia, I.J., C.M. Paquete, A. Coelho, C.C. Almeida, T. Catarino, R.O. Louro, C. Frazao, L.M. Saraiva, et al.** 2004. Proton-assisted two-electron transfer in

natural variants of tetraheme cytochromes from *Desulfomicrobium Sp*. J Biol Chem *279*:52227-52237.

[18] **Paquete, C.M., D.L. Turner, R.O. Louro, A.V. Xavier, and T. Catarino.** 2007. Thermodynamic and kinetic characterisation of individual haems in multicentre cytochromes *c*3. Biochim Biophys Acta *1767*:1169-1179.

[19] **Delgado, R., J.J.R.F. Dasilva, M.T.S. Amorim, M.F. Cabral, S. Chaves, and J. Costa.** 1991. Dissociation-constants of bronsted acids in D_2O and H_2O - Studies on polyaza and polyoxa-polyaza macrocycles and a general correlation. Anal Chim Acta *245*:271-282.

[20] **Keller, R.** 2004. The computer aided resonance assignment tutorial. CANTINA Verlag, Goldau, Switzerland.

[21] **Turner, D.L., C.A. Salgueiro, T. Catarino, J. Legall, and A.V. Xavier.** 1996. NMR studies of cooperativity in the tetrahaem cytochrome *c*3 from *Desulfovibrio vulgaris*. Eur J Biochem *241*:723-731.

[22] **Lagarias, J.C., J.A. Reeds, M.H. Wright, and P.E. Wright.** 1998. Convergence properties of the Nelder-Mead simplex method in low dimensions. SIAM J Opt *9*:112-147.

[23] **Louro, R.O., I.J. Correia, L. Brennan, I.B. Coutinho, A.V. Xavier, and D.L. Turner.** 1998. Electronic structure of low-spin ferric porphyrins: C-13 NMR studies of the influence of axial ligand orientation. J Am Chem Soc *120*:13240-13247.

[24] **Turner, D.L.** 1995. Determination of heme electronic-structure in His-Met cytochromes-*c* by C-13-NMR - The effect of the axial ligands. Eur J Biochem *227*:829-837.

[25] **Baptista, A.M., V.H. Teixeira, and C.M. Soares.** 2002. Constant-pH molecular dynamics using stochastic titration. J Chem Phys *17*:4184-4200.

[26] **Teixeira, V.H., C.M. Soares, and A.M. Baptista.** 2002. Studies of the reduction and protonation behaviour of tetrahaem cytochromes using atomic detail. J Biol Inorg Chem *7*:200-216.

[27] **Bashford, D. and K. Gerwert.** 1992. Electrostatic calculations of the pKa values of ionizable groups in bacteriorhodopsin. J Mol Biol *224*:473-486.

[28] **Bashford, D.** 1997. An Object-Oriented Programming Suite for Electrostatic Effects in Biological Molecules, p. 233-240. *In* Y. Ishikawa, R.R. Oldehoeft, J.V.W. Reynders, and M. Tholburn (Eds.), Scientific Computing in Object-Oriented Parallel Environments. ISCOPE97, Springer, Berlin.

[29] **Scott, W.R.P., P.H. Hünenberger, I.G. Tironi, A.E. Mark, S.R. Billeter, J. Fennen, A.E. Torda, T. Huber, et al.** 1999. The GROMOS biomolecular simulation program package. J Phys Chem *103*:3596-3607.

[30] **van Gunsteren, W.F., S.R. Billeter, A.A. Eising, P.H. Hunenberger, P. Kruger, A.E. Mark, W.R.P. Scott, and I.G. Tironi.** 1996. Biomolecular simulation: The GROMOS96 manual and user guide. vdf Hochschulverlag AG, Zurich, Switzerland.

[31] **Oliveira, A.S., V.H. Teixeira, A.M. Baptista, and C.M. Soares.** 2005. Reorganization and conformational changes in the reduction of tetraheme cytochromes. Biophys J *89*:3919-3930.

[32] **Teixeira, V.H., C.A. Cunha, M. Machuqueiro, A.S. Oliveira, B.L. Victor, C.M. Soares, and A.M. Baptista.** 2005. On the use of different dielectric constants for computing individual and pairwise terms in poisson-boltzmann studies of protein ionization equilibrium. J Phys Chem B *109*:14691-14706.

[33] **Salgueiro, C.A., D.L. Turner, H. Santos, J. LeGall, and A.V. Xavier.** 1992. Assignment of the redox potentials to the four haems in *Desulfovibrio vulgaris* cytochrome c_3 by 2D-NMR. FEBS Lett *314*:155-158.

[34] **Turner, D.L., C.A. Salgueiro, P. Schenkels, J. LeGall, and A.V. Xavier.** 1995. Carbon-13 NMR studies of the influence of axial ligand orientation on haem electronic structure. Biochim Biophys Acta *1246*:24-28.

[35] **Santos, H., J.J.G. Moura, I. Moura, J. Legall, and A.V. Xavier.** 1984. NMR-Studies of electron-transfer mechanisms in a protein with interacting redox centers - *Desulfovibrio gigas* cytochrome c_3. Eur J Biochem *141*:283-296.

[36] **Pessanha, M., R.O. Louro, I.J. Correia, E.L. Rothery, K.L. Pankhurst, G.A. Reid, S.K. Chapman, D.L. Turner, and C.A. Salgueiro.** 2003. Thermodynamic characterization of a tetrahaem cytochrome isolated from a facultative aerobic bacterium, *Shewanella frigidimarina*: a putative redox model for flavocytochrome c_3. Biochem J *370*:489-495.

[37] **Dolla, A., L. Blanchard, F. Guerlesquin, and M. Bruschi.** 1994. The protein moiety modulates the redox potential in cytochromes-*c*. Biochimie *76*:471-479.

[38] **Louro, R.O., T. Catarino, C.M. Paquete, and D.L. Turner.** 2004. Distance dependence of interactions between charged centres in proteins with common structural features. FEBS Lett *576*:77-80.

[39] **Perutz, M.F., J.V. Kilmartin, K. Nishikura, J.H. Fogg, P.J. Butler, and H.S. Rollema.** 1980. Identification of residues contributing to the Bohr effect of human haemoglobin. J Mol Biol *138*:649-668.

[40] **Louro, R.O., T. Catarino, J. LeGall, D.L. Turner, and A.V. Xavier.** 2001. Cooperativity between electrons and protons in a monomeric cytochrome c_3: The importance of mechano-chemical coupling for energy transduction. ChemBioChem *2*:831-837.

[41] **Leys, D., A.S. Tsapin, K.H. Nealson, T.E. Meyer, M.A. Cusanovich, and J.J. Van Beeumen.** 1999. Structure and mechanism of the flavocytochrome *c* fumarate reductase of *Shewanella putrefaciens* MR-1. Nat Struct Biol *6*:1113-1117.

[42] **Page, C.C., C.C. Moser, X. Chen, and P.L. Dutton.** 1999. Natural engineering principles of electron tunnelling in biological oxidation-reduction. Nature *402*:47-52.

[43] **Salgueiro, C.A., L. Morgado, B. Fonseca, P. Lamosa, T. Catarino, D.L. Turner, and R.O. Louro.** 2005. Binding of ligands originates small perturbations on the

microscopic thermodynamic properties of a multicentre redox protein. FEBS J *272*:2251-2260.

[44] **Hoffman, B.M., L.M. Celis, D.A. Cull, A.D. Patel, J.L. Seifert, K.E. Wheeler, J. Wang, J. Yao, et al.** 2005. Differential influence of dynamic processes on forward and reverse electron transfer across a protein-protein interface. Proc Natl Acad Sci USA *102*:3564-3569.

[45] **Gray, H.B. and J.R. Winkler.** 2003. Electron tunneling through proteins. Q Rev Biophys *36*:341-372.

CHAPTER III

The role of intramolecular interactions in the functional control of multiheme cytochromes *c*

This chapter was published in:

Fonseca BM, Paquete CM, Salgueiro CA, Louro RO (2012) "The role of intramolecular interactions in the functional control of multiheme cytochromes *c*" *FEBS Lett* **586**: 504-509.

The author of this dissertation participated in the analysis and interpretation of the data described in this chapter. This chapter was written in honor of Professor Antonio V. Xavier, an inspiring man and scientist. It was a unique privilege to have known him.

ABSTRACT

Detailed thermodynamic and structural data measured in soluble monomeric multiheme cytochromes *c* provided the basis to investigate the functional significance of interactions between redox co-factors. The steep decay of intramolecular interactions with distance means that close proximity of the redox centers is necessary to modulate the intrinsic reduction potentials in a significant way. This ensures selection of specific populations during redox activity in addition to maintaining fast intramolecular electron transfer. Therefore, intramolecular interactions between redox co-factors play an important role in establishing the biological function of the protein by controlling how electrons flow through and are distributed among the co-factors.

INTRODUCTION

Charles A. MacMunn presented the earliest report of cytochromes in the late 19th century and the interest in these cell components grew in the 1920's when David Keilin re-identified them as key players in respiratory chains [1]. Presently, cytochromes are known to be key players in fundamental cell functions such as electron transfer, gas transport, catalysis and also cellular signalling [2,3].

Cytochromes contain heme prosthetic groups, which are coordination complexes of a tetrapyrrole porphyrin ring with an iron. These co-factors confer characteristic absorption bands in the visible wavelength range that change with redox, spin and coordination state. Depending on the type of substituent at the periphery of the porphyrin ring, cytochromes can be classified as type *a*, *b*, *c* or *d*. The heme in *c*-type cytochromes is covalently

bound through thioether bonds to cysteine residues of the polypeptide chain arranged in a typical CXXCH motif, where the histidine provides the proximal ligand to the iron [2].

The biogenesis of *c*-type cytochromes relies on complex molecular assemblies. The best characterized system is the cytochrome *c* maturation (Ccm) system that can be found in many species of Bacteria and Archaea. It is composed of eight proteins encoded by the *ccmABCDEFGH* gene cluster, which are located in the periplasm and/or cytoplasmic membrane. These proteins are responsible for the correct ligation of the heme to the apocytochrome *c*, while it is translocated to the periplasmic space. Thus, no cytoplasmic cytochrome *c* is known. These proteins are either periplasmic, associated to the cytoplasmic or outer-membrane or to extracellular electrically conductive appendages [4-7].

Although the first *c*-type cytochromes were found in aerobic or facultative anaerobic organisms [1], anaerobes contain a considerable variety of these proteins. The first cytochromes identified contained only a small number of heme co-factors [1,8,9] but a screen of the currently available genomic sequences revealed that the number of heme binding motifs per multiheme cytochrome *c* varies considerably. The most common numbers are two, three and four. Sequences containing five, eight or ten binding motifs are also relatively common. Although the protein structure with the largest number of hemes per polypeptide is a hexadecaheme cytochrome [10], genes coding for polypeptide chains that contain 43 and 45 heme binding motifs were identified in *Geobacter uraniumreducens* and *Aeromyxobacter sp*., respectively [11]. Almost all major groups of Bacteria and Archaea have multiheme cytochromes *c*. In some of these organisms, such as representatives of *Geobacter*, *Shewanella*, *Anaeromyxobacter* or *Desulfovibrio* genera, the number of multiheme

cytochromes is so elevated that it corresponds to a high percentage of their proteome, having elicited the creation of the term "cytochromome" [12,13].

The fact that so many organisms contain a large number of genes coding for multiheme cytochromes *c* and that these cytochromes can bind so many hemes begs two questions: what are the selective advantages of containing so many redox co-factors in a single polypeptide, and why did the spatial distribution of the co-factors evolve to be the way it is?

The detailed structural, thermodynamic and kinetic characterization reported in the literature for several multiheme cytochromes, following the pioneering efforts of Antonio V. Xavier [14], is reviewed here in order to formulate a proposal to answer these questions.

STRUCTURAL AND FUNCTIONAL ADVANTAGES

There are structural advantages in binding several heme co-factors to a single polypeptide. Besides contributing to the correct fold of the polypeptide chain, the hemes also confer stability to the protein structure. Structures are known of multiheme cytochromes *c* with as little as 23 amino acids per heme. The cross linkage arising from the heme *c* coordinating residues, with three bonds provided by the CXXCH motif, or four bonds in the case of hexacoordinated hemes, provides multiheme cytochromes *c* with greater stability compared with proteins of similar size [15]. The covalent binding of the *c*-type hemes prevents the statistical thermodynamic decay in affinity constants for equilibrium binding of multiple identical co-factors [16]. This means that the hemes can be stably positioned close to each other and in larger quantity per polypeptide chain. Indeed, all known multiheme cytochromes containing more than two hemes per polypeptide are of type *c* [17].

Having multiple redox centers in a single protein also provides functional advantages for electron transfer. For electrons that have to be transferred across large distances, intramolecular electron transfer within a multicenter redox protein proceeds without the need for transient recognition and binding between successive physiological partners in the crowded cellular medium. The two main parameters that define the intraprotein electron transfer are the tunneling distance and the driving force [18,19]. For a tunneling distance between pairs of redox centres shorter than approximately 14 Å, the tunneling rates remain compatible with the physiological turnover of the protein [18]. For electron transfer over larger distances the introduction of several redox centers is the only way to ensure that the electron tunneling rate remains sufficiently fast [19]. This mode of long distance electron transfer is called hopping, and it allows electrons to flow at a rate compatible with the physiological turnover even when there are endergonic steps in the overall exergonic electron transfer chain [19].

Multiheme cytochromes *c* can access a larger range of redox activity because each redox center can be tuned to be active at a different reduction potential. This contrasts with proteins containing a single redox center, which have a range of redox activity limited by the Nernst curve. There are various factors that influence the reduction potentials of hemes and allow them to be tuned over a range of 1 V (from -550 mV to +450 mV) [17]. The two most relevant are: the heme environment, namely amino acid charges, dipoles and exposure to solvent, which can shift the potential by up to 500 mV [20]; and the nature of the axial ligands, which can shift the potential by as much as 650 mV [21]. Smaller effects arise from factors such as: non-planar distortions of the heme, orientation of the axial ligands, thermodynamic proton coupling (redox-Bohr effect), and heme-heme interactions [22].

COOPERATIVE EFFECTS

Heme-heme interactions modify the reduction potentials of the hemes involved. These changes may be cooperative or anti-cooperative, with both having functional consequences. Cooperativity between co-factors is an exclusive characteristic of multicenter redox proteins. The uptake of an electron by one heme affects the affinity for electrons (reduction potentials) of the remaining oxidized hemes. When the uptake of an electron lowers the affinity for the uptake of another, the protein exhibits negative cooperativity (anti-cooperativity) and this increases the range of electrode potentials where it is redox active. Conversely, if the uptake of one electron increases the affinity for an electron at another site, the cytochrome exhibits positive cooperativity and a sharper transition in redox state of the protein. Indeed, the maximum cooperativity that can be attained by a multicenter protein is ultimately limited by the number of sites. Therefore, the increase in the number of hemes facilitates the emergence of cooperative processes [23].

The detailed characterization of the reduction potentials and interactions in multiheme cytochromes is a laborious task and has been reported for several examples. Of these, the following are soluble and monomeric in physiological conditions, the structure is known, and heme-heme interactions were determined experimentally: the triheme cytochromes c_7 (or Ppc) from the *Geobacteraceae* family [24,25]; the tetraheme cytochromes c_3 from the *Desulfovibrio* and *Desulfomicrobium* genera [26-29]; the small tetraheme cytchrome *c* (STC) [30,31] and the tetraheme flavocytochrome *c* (FccA) [32] from the *Shewanella* genus; and the diheme cytochrome c_4 from *Pseudomonas stutzeri* [33]. Figure 3.1 shows the heme architecture of the target cytochrome structural families.

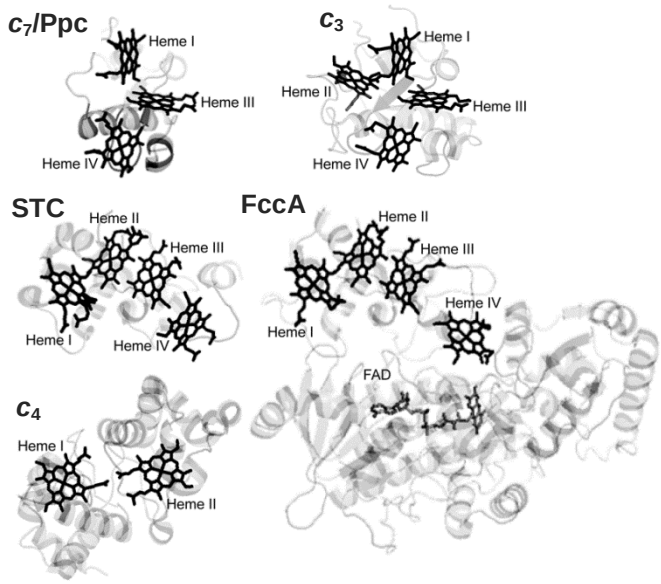

Figure 3.1. Spatial arrangement of the hemes in the various cytochrome structural families analyzed in this work. The image was prepared using the program Pymol v0.99 to display the structures with the following PDB codes, corresponding to a representative of each protein family: 3H4N (PpcD from *G. sulfurreducens*); 1UPD (cytochrome c_3 from *D. desulfuricans* ATCC 27774); 1M1Q (STC from *S. oneidensis* MR-1); 1QJD (FccA from *S. frigidimarina*); 1M70 (cytochrome c_4 from *P. stutzeri*).

DISTANCE DEPENDENCE OF ELECTROSTATIC INTERACTIONS

The experimental heme-heme interactions are composite parameters that can contain contributions from other processes. The most common is the redox-Bohr effect that arises from thermodynamic coupling between redox and acid-base groups that titrate in the physiological pH range. The heme, with a redox active iron and acid-base active propionates, is a well suited co-factor to establish such a heterotropic linkage. Whereas the electrostatic interaction between the electrons in hemes is repulsive and therefore anti-cooperative, the electrostatic interaction between electrons and protons is attractive and therefore cooperative. Consequently, the parsing of the redox-Bohr contribution is essential for correctly interpreting the values of the heme-heme

interactions [30,34]. For those cases where this was done it is possible to observe that the redox interactions between pairs of hemes show a dependence with the iron-to-iron distance that follows a simple model of shielded electrostatic interactions (Figure 3.2). This model considers a Coulombic decay enhanced by a Debye-Hückel shielding factor [35]. This is an indication that the overall dielectric environment within these multiheme cytochromes is very similar, despite the differences between the number of hemes, heme architecture and amino acid composition. Considering only the heme domain of the FccA, STC and cytochrome *c*$_3$, the overall ratio of protein length to heme for these proteins is very low, ranging from 23 to 27 amino acids. The diheme cytochrome *c*$_4$, which has a ratio of 95 amino acids per heme, displays a less effective electrostatic shielding of the hemes-heme interactions in agreement with a less hydrophilic environment.

The values of the redox interactions between pairs of hemes are typically positive as expected for the repulsive interaction between electrons. However, this simple correlation breaks down in the presence of redox-linked conformational changes that can modify the relative coordinates of the interacting centers or the electrostatic environment surrounding the interacting charges. These additional terms in the observed interaction are denominated non-Coulombic effects or mechano-chemical effects, which can enhance or diminish the electrostatic component of the interaction [28,36].

Non-Coulombic effects are evident in Figure 3.2 for data measured for the cytochromes *c*$_3$, which are the most disperse [35]. Some of the heme-heme interactions measured for these proteins even display negative values when cooperative non-Coulombic effects dominate over the electrostatic effects. These redox-linked conformational changes were identified by comparative structural studies of the oxidized and reduced forms in several cytochromes *c*$_3$.

They do not involve major structural rearrangements and were mainly associated with localized conformational changes in the side chains of amino acid residues located in the neighborhood of the heme groups and with conformational changes in the heme propionates [37-41].

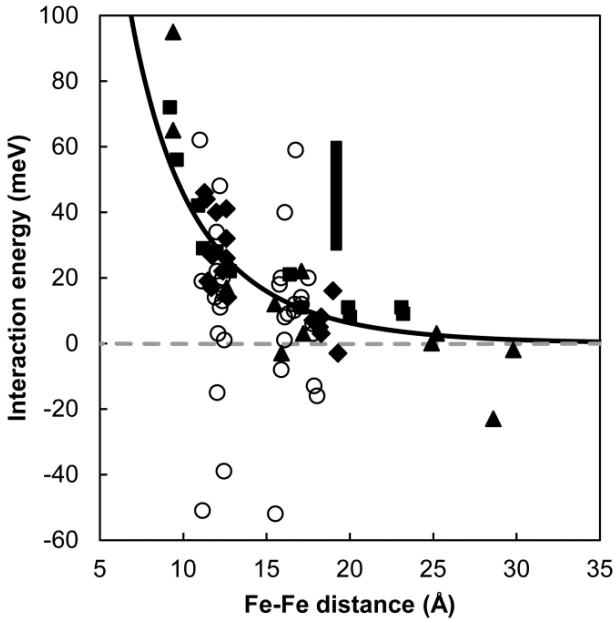

Figure 3.2. Distance dependence of the pairwise interactions between the hemes. Squares illustrate data for the STC from the *Shewanella* genus [30,31]; Triangles illustrate data for the FccA from the *Shewanella* genus [32]; Diamonds illustrate data for the cytochrome c_7/Ppc from *Desulfuromonas* and *Geobacter* genera [24,25]; the rectangle illustrates the range of the interactions reported for the cytochrome c_4 [33]; open circles illustrate data for the cytochromes c_3 from the *Desulfovibrio* and *Desulfomicrobium* genera [27-29]. Distances were measured between iron atoms from the protein structures with the following PDB codes: 1M1Q; 2K3V; 1QJD; 1D4D; 1HH5; 2LDO; 3BXU; 3H4N; 3H34; 1RWJ; 1WAD; 2CTH; 1UPD; 2BQ4; 2CY3; 1W7O; 1M70, using the program Pymol v0.99. The solid line was obtained with a Debye–Hückel model of shielded electrostatic interactions considering and effective dielectric constant of 8.6 and Debye length of 7.7 Å [42].

A FUNCTIONAL ROLE FOR INTRAMOLECULAR INTERACTIONS

Figure 3.2, shows that heme-heme interactions affect the reduction potentials of the hemes, and that this effect of up to 100 mV decays rapidly with distance.

Figure 3.1 shows that multiheme cytochromes with different physiological functions may present similar spatial arrangement of the hemes. These data suggest that the interplay of the heme reduction potentials with the redox, redox-Bohr and non-Coulombic effects, plays a role in establishing the functional specificity of each protein.

This hypothesis attributes a biological function to the heme-heme interactions in modulating the microscopic redox properties of multicenter redox proteins. Thermodynamically, this means that the population of the multiple microscopic states that mediate the progression between fully reduced and fully oxidized cytochrome is not fortuitous and has been selected to favor the physiological function.

To explore this hypothesis the redox speciation diagrams for these complex proteins need to be calculated on the basis of the experimentally determined heme reduction potentials and their interactions, pK_as of acid-base groups affected by the redox state of the protein and redox-Bohr interactions. Experimental data that allow this detailed analysis was collected for several multiheme cytochromes and are plotted in Figure 3.3. Due to the close proximity of the hemes in all these multiheme cytochromes, intramolecular electron transfer is fast on the experimental time-scale, which ensures equilibrium among all microscopic states with the same number of oxidized hemes, in what are called macroscopic stages of oxidation. The stages are linked by steps that involve the uptake or release of one electron by the

cytochrome. In the case of a multicenter protein containing *n* redox centers, *n+1* macroscopic stages of oxidation can co-exist in solution, each containing the microscopic states with the same number of oxidized hemes. The number of oxidized hemes provides the nomenclature for the macroscopic stages of oxidation from 0 for the fully reduced protein to *n+1* for the fully oxidized state. For *n+1* macroscopic stages of oxidation there are 2^{n+m} microscopic states, being m the number of redox-Bohr centers within the protein (see appendix D).

The populations of these microscopic states for 15 soluble monomeric multiheme cytochromes are reported in Figure 3.3, where the dominant microscopic states of partially oxidized stages are labeled to identify the hemes that are oxidized in each step.

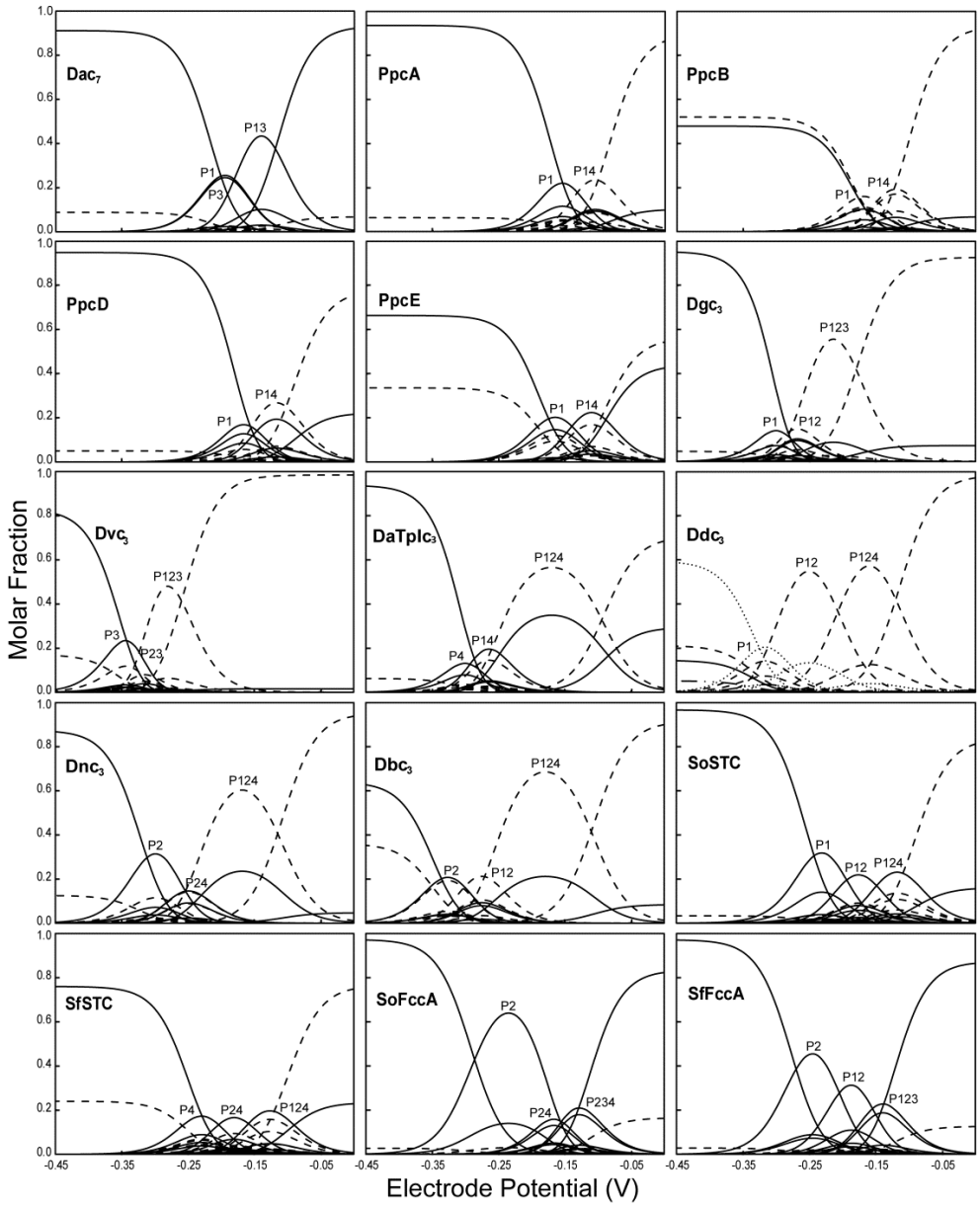

Figure 3.3. Speciation diagrams of the microscopic states of the multiheme cytochromes *c*. The curves were calculated as a function of the electrode potential (SHE) using the thermodynamic properties determined experimentally [24-32]. The solid lines indicate the protonated microscopic states while the dashed lines indicate the deprotonated microscopic states. Dotted and dash-dot lines in the panel Ddc_3 indicate a second set of redox-linked protonations. The numerals above the lines indicate the oxidized hemes in the dominant microscopic states. Panels Dac_7 and PpcA-E correspond to data from the triheme cytochrome c_7 from *Desulfuromonas acetoxidans*

and *G. sulfurreducens*, respectively, at physiological pH 7.5 [24,25]. Panels Dgc_3, Dvc_3, DaTpIc_3 Ddc_3 correspond to data from the type I tetraheme cytochrome c_3 from *D. gigas*, *D. vulgaris* Hildenbourgh, *D. africanus*, *D. desulfuricans* ATCC 27774, respectively, at physiological pH 7.0 [26-28]. Panels Dnc_3 and Dbc_3 correspond to data from the tetraheme cytochrome c_3 from *Desulfomicrobium norvegicum* and *Desulfomicrobium baculatum*, respectively, at physiological pH 6.15 [29]. Panels SoSTC and SfSTC correspond to data from the tetraheme cytochrome STC from *S. oneidensis* MR-1 and *S. frigidimarina*, respectively, at physiological pH 7.0 [30,31]. Panels SoFccA and SfFccA correspond to data from the tetraheme flavocytochrome *c* (FccA) from *S. oneidensis* MR-1 and *S. frigidimarina*, respectively, at physiological pH 7.0 [32].

Figure 3.3 shows two aspects of the interplay between intrinsic reduction potentials of the individual hemes and the intramolecular interactions. The first is that in structurally identical proteins the tuning of the reduction potentials and interactions leads to dramatic differences in the dominant microscopic states as the proteins proceed from fully reduced to fully oxidized at physiological pH. This is observed for the triheme c_7/Ppc cytochromes. Proteomics and knock-out mutant studies on the five triheme cytochromes c_7 (PpcA-E) from *Geobacter sulfurreducens* suggested that this family of cytochromes plays a crucial role in driving electron transfer from the cytoplasm to the cell exterior, and assisting the reduction of extracellular acceptors [25]. In the case of PpcB and PpcE, several microscopic states are significantly populated in stages of oxidation 1 and 2 and therefore, no preferential pathway for electron transfer can be established. In contrast, PpcA and PpcD appear to be optimized to interact with specific redox partners involving e^-/H^+ transfer via different mechanisms, where hemes I and IV are directly involved in the electron-proton coupling. In the case of PpcA, electron-proton coupling occurs between stages of oxidation 1 and 2, whereas in PpcD stages of oxidation 0 and 2 are involved in a two-electron transfer step coupled to the deprotonation of the redox-Bohr center [25]. The triheme cytochrome c_7

from *Desulfuromonas acetoxidans* was also implicated in the respiration of metals and sulfur [43,44]. In this cytochrome, no electron-proton coupling is observed in the physiological pH range but a clear selection of the intermediate stage populations is evident [24].

The second aspect is that structurally identical proteins can achieve the same functional properties via dramatically different detailed mechanisms. The tetraheme cytochromes c_3 from *Desulfovibrio* and *Desulfomicrobium* share a common architecture of the heme core, which is identical to that of cytochromes c_7 with the addition of the polypeptide section that binds heme II. The physiological function of these cytochromes is to accept electrons and protons from periplasmic hydrogenases, and deliver them to membrane-linked protein complexes, with a net energy transfer from the redox to the protonic centers [28,45]. In line with this common function and in contrast to what is observed for the triheme cytochromes, all cytochromes c_3 show a bias for some of the intermediate stage populations to be greatly diminished, an indication of positive cooperativity. Figure 3.3 shows that a variety of strategies can be used to achieve this objective. For the cytochromes c_3 from *D. gigas*, *D. vulgaris* Hildenborough, *D. africanus* and *D. desulfuricans* ATCC 27774, a clear-cut positive cooperativity between a pair of hemes occurs [46]. In all cases the positive redox cooperativity is associated with an acid-base transition giving rise to a proton-coupled two-electron step. The speciation diagram for *D. desulfuricans* is slightly more complex since two redox-linked protonation events are observed in the physiological range, leading to a greater dispersion of the populations. For the cytochromes c_3 from the *Desulfomicrobium* genus the coupling with protonation is so important, in the context of a weaker heme-heme positive cooperativity, that it has been named proton-assisted two-electron step [29].

The STC cytochrome from *Shewanella* genus, a soluble 12 kDa protein isolated from the periplasmic space, presents a distinct spatial arrangement of the hemes which forms a bent chain. Knock-out mutations of the gene implicate this protein in iron reduction [47,48] and more recently in the reduction of DMSO [49]. Analyzing the panels corresponding to STC from *S. oneidensis* (SoSTC) and from *S. frigidimarina* (SfSTC), it is possible to verify that in both cases, at physiological pH, reduction of heme III which is the least exposed heme and therefore the less likely to make direct electron transfer to a redox partner, is strongly coupled to protonation. This suggests a role as gate-keeper by modulating the electrostatic environment via redox and redox-Bohr interactions with the other hemes. The consequence is that when the protein is fully oxidized, the deprotonated microscopic state is dominant, whereas in all the other stages of oxidation, the protonated microscopic states are dominant, for both examples. In addition to this protonation step coupled with electron transfer, there is always a dominant microscopic state in every stage of oxidation, indicating that there is an ordered distribution of the electrons within the protein [30,31]. The similarities at the structural level and in metabolic role are also translated in kinetic studies performed *in-vitro* [50]. These studies show that for both SoSTC and SfSTC the heme with the more negative reduction potential is the major player in the uptake or release of electrons.

Finally, flavocytochrome *c* (FccA) is a 64 kDa soluble fumarate reductase from the *Shewanella* genus. This enzyme contains a tetraheme domain that is structurally homologous to the STC cytochrome and a flavin domain responsible for the unidirectional reduction of fumarate to succinate. This is a coupled two-electron, two-proton reaction. It is clear from the dominant microscopic states in both examples that the first pair of electrons is transferred

to the FAD catalytic site while ensuring that heme IV, located near the catalytic site, remains reduced. This reduction is achieved by intramolecular re-equilibration among the hemes which is approximately three orders of magnitude faster than the electron transfer to the FAD, ensuring the transfer of a pair of electrons necessary for the catalysis [32,51]. Interestingly, the data for these two enzymes do not show significant e^-/H^+ coupling, which reveals that proton delivery to the catalytic site is not thermodynamically linked to the redox state of the hemes [32].

The data reported in Figure 3.3 reveals clearly that for a similar heme core arrangement the combined effect of the reduction potentials and interactions brings about a detailed selection of the specific states of the protein that are active during the redox cycling. These allow for a versatile tuning of the detailed redox properties of multiheme cytochromes. Therefore, a common architecture can accommodate different functions, or alternatively a common architecture can be used to achieve a similar function by different detailed mechanisms.

CONCLUSION

The data compiled in this review argue in favor of an important role for intramolecular interactions in establishing a defined speciation during the redox cycling of multicenter cytochromes, a phenomenon called thermodynamic gating [40]. However, the electrostatic component of these interactions decays strongly with distance. As a consequence, hemes need to be located very close together to ensure an interaction magnitude that can significantly modulate their intrinsic reduction potentials. This in turn places constrains on the spatial organization of the hemes within the protein.

In conclusion, the architecture of multiheme cytochromes ensures fast intramolecular electron transfer and control over the microscopic states that are populated during the redox activity. These properties are essential to prevent the thermodynamic dissipation of the redox energy channeled through these proteins, diminishing the probability of unspecific interactions within the crowded cellular medium and guaranteeing a defined biological role.

ACKNOWLEDGEMENTS

B.M.F. and C.M.P. are the recipients of grants from Fundação para a Ciência e Tecnologia [SFRH/BD/41205/2007 (B.M.F.); SFRH/BPD/34591/2007 (C.M.P.)]. Research in the authors laboratories is supported by grants PTDC/QUI/70182/2006, PTDC/BIA-PRO 098158/2008 and MIT-Pt BS-BB/1014/2008 from Fundação para a Ciência e Tecnologia.

REFERENCES

[1] **Stone, F.M. and C.B. Coulter.** 1932. Porphyrin Compounds Derived from Bacteria. J Gen Physiol *15*:629-639.

[2] **Pettigrew, G.W. and G.R. Moore.** 1987. Cytochromes *c*: Biological Aspects. Springer Series in Molecular Biology.

[3] **Mayfield, J.A., C.A. Dehner, and J.L. DuBois.** 2011. Recent advances in bacterial heme protein biochemistry. Curr Opin Chem Biol *15*:260-266.

[4] **Schulz, H., R.A. Fabianek, E.C. Pellicioli, H. Hennecke, and L. Thony-Meyer.** 1999. Heme transfer to the heme chaperone CcmE during cytochrome *c* maturation requires the CcmC protein, which may function independently of the ABC-transporter CcmAB. Proc Natl Acad Sci USA *96*:6462-6467.

[5] **Ferguson, S.J., J.M. Stevens, J.W.A. Allen, and I.B. Robertson.** 2008. Cytochrome c assembly: A tale of ever increasing variation and mystery? Biochim Biophys Acta *1777*:980–984.

[6] **Sanders, C., S. Turkarslan, D.W. Lee, and F. Daldal.** 2010. Cytochrome *c* biogenesis: the Ccm system. Trends Microbiol *18*:266-274.

[7] **Leang, C., X.L. Qian, T. Mester, and D.R. Lovley.** 2010. Alignment of the *c*-type cytochrome OmcS along pili of Geobacter sulfurreducens. Appl Environ Microb *76*:4080-4084.

[8] **Smith, L.** 1959. Reactions of Rhodospirillum rubum extract with cytochrome *c* and cytochrome c_2. J Biol Chem *234*:1571-1574.

[9] **Postgate, J.R.** 1954. Dependence of sulphate reduction and oxygen utilization on a cytochrome in *Desulfovibrio*. Biochem J *58*:ix.

[10] **Matias, P.M., A.V. Coelho, F.M. Valente, D. Placido, J. LeGall, A.V. Xavier, I.A. Pereira, and M.A. Carrondo.** 2002. Sulfate respiration in *Desulfovibrio vulgaris* Hildenborough. Structure of the 16-heme cytochrome *c* HmcA AT 2.5-A resolution and a view of its role in transmembrane electron transfer. J Biol Chem *277*:47907-47916.

[11] **Sharma, S., G. Cavallaro, and A. Rosato.** 2010. A systematic investigation of multiheme *c*-type cytochromes in prokaryotes. J Biol Inorg Chem *15*:559-571.

[12] **Londer, Y.Y., S.E. Giuliani, T. Peppler, and F.R. Collart.** 2008. Addressing *Shewanella oneidensis* "cytochromome": the first step towards high-throughput expression of cytochromes *c*. Protein Expr Purif *62*:128-137.

[13] **Alves, A.S., C.M. Paquete, B.M. Fonseca, and R.O. Louro.** 2011. Exploration of the 'cytochromome' of *Desulfuromonas acetoxidans*, a marine bacterium capable of powering microbial fuel cells. Metallomics *3*:349-353.

[14] **Xavier, A.V.** 1983. NMR studies of cytochromes, p. 291 - 311. *In* I. Bertini, R.S. Drago, and C. Luchinat (Eds.), The Coordination Chemistry of Metalloenzymes. D. Reidel Pub. Co., Dordrecht, Holland.

[15] **Florens, L., P. Bianco, J. Haladjian, M. Bruschi, I. Protasevich, and A. Makarov.** 1995. Thermal stability of the polyheme cytochrome c_3 superfamily. FEBS Lett *373*:280-284.

[16] **Cantor, C.R. and P.R. Schimmel.** 1980. Biophysical Chemistry Part III: The behavior of biological macromolecules. W H Freeman, New York.

[17] **Reedy, C.J., M.M. Elvekrog, and B.R. Gibney.** 2008. Development of a heme protein structure-electrochemical function database. Nucleic Acids Res *36*:307-313.

[18] **Moser, C.C., J.L. Anderson, and P.L. Dutton.** 2010. Guidelines for tunneling in enzymes. Biochim Biophys Acta *1797*:1573-1586.

[19] **Gray, H.B. and J.R. Winkler.** 2010. Electron flow through metalloproteins. Biochim Biophys Acta *1797*:1563-1572.

[20] **Tezcan, F.A., J.R. Winkler, and H.B. Gray.** 1998. Effects of ligation and folding on reduction potentials of heme proteins. J Am Chem Soc *120*:13383-13388.

[21] **Raphael, A.L. and H.B. Gray.** 1991. Semisynthesis of Axial-Ligand (Position-80) Mutants of Cytochrome *c*. J Am Chem Soc *113*:1038-1040.

[22] **Moore, G.R. and G.W. Pettigrew.** 1990. Cytochromes *c*: Evolutionary, Structural and Physicochemical Aspects. Springer-Verlag, Berlin.

[23] **Wyman, J. and S.J. Gill.** 1990. The Binding Polynomial, p. 63-121. *In* A. Kelly (Ed.), Binding and Linkage - Functional Chemistry of Biological Macromolecules. University Science Books, Mill Valley, CA.

[24] **Correia, I.J., C.M. Paquete, R.O. Louro, T. Catarino, D.L. Turner, and A.V. Xavier.** 2002. Thermodynamic and kinetic characterization of trihaem cytochrome c_3 from *Desulfuromonas acetoxidans*. Eur J Biochem *269*:5722-5730.

[25] **Morgado, L., M. Bruix, M. Pessanha, Y.Y. Londer, and C.A. Salgueiro.** 2010. Thermodynamic characterization of a triheme cytochrome family from *Geobacter sulfurreducens* reveals mechanistic and functional diversity. Biophys J *99*:293-301.

[26] **Paquete, C.M., P.M. Pereira, T. Catarino, D.L. Turner, R.O. Louro, and A.V. Xavier.** 2007. Functional properties of type I and type II cytochromes c_3 from *Desulfovibrio africanus*. Biochim Biophys Acta *1767*:178-188.

[27] **Paquete, C.M., D.L. Turner, R.O. Louro, A.V. Xavier, and T. Catarino.** 2007. Thermodynamic and kinetic characterisation of individual haems in multicentre cytochromes c_3. Biochim Biophys Acta *1767*:1169-1179.

[28] **Louro, R.O., T. Catarino, J. LeGall, D.L. Turner, and A.V. Xavier.** 2001. Cooperativity between electrons and protons in a monomeric cytochrome c_3: the importance of mechano-chemical coupling for energy transduction. Chembiochem *2*:831-837.

[29] **Correia, I.J., C.M. Paquete, A. Coelho, C.C. Almeida, T. Catarino, R.O. Louro, C. Frazao, L.M. Saraiva, et al.** 2004. Proton-assisted two-electron transfer in natural variants of tetraheme cytochromes from *Desulfomicrobium sp.* J Biol Chem *279*:52227-52237.

[30] **Fonseca, B.M., I.H. Saraiva, C.M. Paquete, C.M. Soares, I. Pacheco, C.A. Salgueiro, and R.O. Louro.** 2009. The tetraheme cytochrome from *Shewanella oneidensis* MR-1 shows thermodynamic bias for functional specificity of the hemes. J Biol Inorg Chem *14*:375-385.

[31] **Pessanha, M., R.O. Louro, I.J. Correia, E.L. Rothery, K.L. Pankhurst, G.A. Reid, S.K. Chapman, D.L. Turner, and C.A. Salgueiro.** 2003. Thermodynamic characterization of a tetrahaem cytochrome isolated from a facultative aerobic bacterium, *Shewanella frigidimarina*: a putative redox model for flavocytochrome c_3. Biochem J *370*:489-495.

[32] **Pessanha, M., E.L. Rothery, C.S. Miles, G.A. Reid, S.K. Chapman, R.O. Louro, D.L. Turner, C.A. Salgueiro, and A.V. Xavier.** 2009. Tuning of functional heme reduction potentials in *Shewanella* fumarate reductases. Biochim Biophys Acta *1787*:113-120.

[33] **Conrad, L.S., J.J. Karlsson, and J. Ulstrup.** 1995. Electron transfer and spectral alpha-band properties of the di-heme protein cytochrome c_4 from *Pseudomonas stutzeri*. Eur J Biochem *231*:133-141.

[34] **Paixão, V.B., H. Vis, and D.L. Turner.** 2010. Redox linked conformational changes in cytochrome c_3 from *Desulfovibrio desulfuricans* ATCC 27774. Biochemistry *49*:9620-9629.

[35] **Louro, R.O., T. Catarino, C.M. Paquete, and D.L. Turner.** 2004. Distance dependence of interactions between charged centres in proteins with common structural features. FEBS Lett *576*:77-80.

[36] **Xavier, A.V.** 2002. A mechano-chemical model for energy transduction in cytochrome *c* oxidase: the work of a Maxwell's God. FEBS Lett *532*:261-266.

[37] **Brennan, L., D.L. Turner, A.C. Messias, M.L. Teodoro, J. LeGall, H. Santos, and A.V. Xavier.** 2000. Structural basis for the network of functional cooperativities in cytochrome c_3 from *Desulfovibrio gigas*: Solution structures of the oxidised and reduced states. J Mol Biol *298*:61-82.

[38] **Messias, A.C., D.H.W. Kastrau, H.S. Costa, J. LeGall, D.L. Turner, H. Santos, and A.V. Xavier.** 1998. Solution structure of *Desulfovibrio vulgaris* (Hildenborough) ferrocytochrome c_3: Structural basis for functional cooperativity. J Mol Biol *281*:719-739.

[39] **Pieulle, L., X. Morelli, P. Gallice, E. Lojou, P. Barbier, M. Czjzek, P. Bianco, F. Guerlesquin, and E.C. Hatchikian.** 2005. The type I/type II cytochrome *c*$_3$ complex: an electron transfer link in the hydrogen-sulfate reduction pathway. J Mol Biol *354*:73-90.

[40] **Louro, R.O., I. Bento, P.M. Matias, T. Catarino, A.M. Baptista, C.M. Soares, M.A. Carrondo, D.L. Turner, and A.V. Xavier.** 2001. Conformational component in the coupled transfer of multiple electrons and protons in a monomeric tetraheme cytochrome. J Biol Chem *276*:44044-44051.

[41] **Harada, E., Y. Fukuoka, T. Ohmura, A. Fukunishi, G. Kawai, T. Fujiwara, and H. Akutsu.** 2002. Redox-coupled conformational alternations in cytochrome *c*$_3$ from *D. vulgaris* Miyazaki F on the basis of its reduced solution structure. J Mol Biol *319*:767-778.

[42] **Louro, R.O. and C.M. Paquete.** 2010. Molecular details of multielectron transfer: the case of multiheme cytochromes from metal respiring organisms. Dalton Trans *39*:4259-4266.

[43] **Roden, E.E. and D.R. Lovley.** 1993. Dissimilatory Fe(III) reduction by the marine microorganism *Desulfuromonas acetoxidans*. Appl Environ Microbiol *59*:734-742.

[44] **Pereira, I.A., I. Pacheco, M.Y. Liu, J. Legall, A.V. Xavier, and M. Teixeira.** 1997. Multiheme cytochromes from the sulfur-reducing bacterium *Desulfuromonas acetoxidans*. Eur J Biochem *248*:323-328.

[45] **Louro, R.O., T. Catarino, J. LeGall, and A.V. Xavier.** 1997. Redox-Bohr effect in electron/proton energy transduction: cytochrome *c*$_3$ coupled to hydrogenase works as a 'proton thruster' in *Desulfovibrio vulgaris*. J Biol Inorg Chem 2:488-491.

[46] **Louro, R.O.** 2007. Proton thrusters: overview of the structural and functional features of soluble tetrahaem cytochromes *c*$_3$. J. Biol. Inorg. Chem. *12*:1-10.

[47] **Gordon, E.H., A.D. Pike, A.E. Hill, P.M. Cuthbertson, S.K. Chapman, and G.A. Reid.** 2000. Identification and characterization of a novel cytochrome *c*$_3$ from *Shewanella frigidimarina* that is involved in Fe(III) respiration. Biochem J *349*:153-158.

[48] **Leys, D., T.E. Meyer, A.S. Tsapin, K.H. Nealson, M.A. Cusanovich, and J.J. Van Beeumen.** 2002. Crystal structures at atomic resolution reveal the novel concept of "electron-harvesting" as a role for the small tetraheme cytochrome *c*. J Biol Chem *277*:35703-35711.

[49] **Coursolle, D. and J.A. Gralnick.** 2010. Modularity of the Mtr respiratory pathway of *Shewanella oneidensis* strain MR-1. Mol Microbiol *77*:995–1008.

[50] **Paquete, C.M., I.H. Saraiva, E. Calcada, and R.O. Louro.** 2010. Molecular basis for directional electron transfer. J Biol Chem *285*:10370-10375.

[51] **Turner, K.L., M.K. Doherty, H.A. Heering, F.A. Armstrong, G.A. Reid, and S.K. Chapman.** 1999. Redox properties of flavocytochrome *c*$_3$ from *Shewanella frigidimarina* NCIMB400. Biochemistry *38*:3302-3309.

CHAPTER IV

Mind the gap: cytochrome interactions reveal electron pathways across the periplasm of *Shewanella oneidensis* MR-1

This chapter was published in:

Fonseca BM, Paquete CM, Neto SE, Pacheco I, Soares CM, Louro RO (2013) "Mind the gap: cytochrome interactions reveal electron pathways across the periplasm of *Shewanella oneidensis* MR-1" *Biochem J* **449:** 101-108.

The author of this dissertation participated in all experiments described in this chapter, except in the determination of the protein electrostatic surface potentials.

ABSTRACT

Extracellular electron transfer is the key metabolic trait that enables some bacteria to play a significant role in the biogeochemical cycling of metals and in bioelectrochemical devices such as microbial fuel cells. In *Shewanella oneidensis* MR-1, electrons generated in the cytoplasm by catabolic processes must cross the periplasmic space to reach terminal oxidoreductases found at the cell surface. Lack of knowledge on how these electrons flow across the periplasmic space is one of the unresolved issues related with extracellular electron transfer. Using NMR to probe protein-protein interactions, kinetic measurements of electron transfer and electrostatic calculations, we were able to identify protein partners and their docking sites, and determine the dissociation constants. The results showed that both STC and FccA interact with their redox partners, CymA and MtrA, through a single heme avoiding the establishment of stable redox complexes capable of spanning the periplasmic space. Furthermore, we verified that the most abundant periplasmic cytochromes STC, FccA and ScyA do not interact with each other and this likely the consequence of negative surface charges in these proteins. This reveals the co-existence of two non-mixing redox pathways that lead to extracellular electron transfer in *Shewanella oneidensis* MR-1 established through transient protein interactions.

INTRODUCTION

Metal reducing organisms are attracting widespread attention from the scientific and engineering communities due to the key role that they play in the biogeochemical cycling of metals, and in novel biotechnological processes for

bioremediation of contaminated sites, sustainable energy production, or synthesis of added-value compounds from waste [1-4].

Shewanella oneidensis MR-1 is one of the most studied metal reducing organisms. This Gram negative ɣ-proteobacterium is one of the most versatile organisms with respect to the use of terminal electron acceptors [5,6]. In addition to gaseous oxygen it can use soluble compounds such as fumarate and also insoluble compounds, such as metal oxides or even electrode surfaces in bioelectrochemical devices [6-8]. Reduction of insoluble compounds requires the delivery of electrons to the cell surface. In Gram negative bacteria, electrons from the quinone pool located in the cytoplasmic membrane must cross the periplasmic space to reach the terminal reductases located in the external membrane [9].

Proceeding outwards, the quinone pool reduces the 21 kDa tetraheme cytochrome CymA attached to the cytoplasmic membrane that acts as a hub for electron distribution to multiple periplasmic partners [10-12]. Among these, MtrA is a 35 kDa decaheme periplasmic protein that has a definite phenotype in metal reduction in *S. oneidensis* MR-1. It was shown to be mostly associated to the outer membrane and has a maximum length of 104 Å determined by SAXS [13-16]. This cytochrome is encoded by a polycistronic operon that also includes the *mtrC*, *mtrB* and *omcA* genes [16]. MtrB is a transmembrane *β*-barrel protein, which provides a conduit that enables contact between MtrA and the cytochromes MtrC and OmcA. These are attached to the outer surface of the external membrane and function as terminal metal oxidoreductases [17].

The periplasmic space of *S. oneidensis* MR-1 was recently measured to be 235 Å wide [18] which is too wide for electron transfer to proceed by direct contact between CymA and the MtrCAB-OmcA complex. Therefore, MtrA must be able to diffuse within the periplasmic space or additional redox

proteins are necessary to establish the transfer of electrons across the periplasmic gap.

The most abundant periplasmic proteins found in anaerobically grown *S. oneidensis* MR-1 are the small tetraheme cytochrome *c* (STC, also known as CctA), the monoheme cytochrome c_5 (ScyA) and the flavocytochrome *c* (FccA) [19,20]. Their genes are up-regulated during extracellular respiration [21] but individual gene deletion mutants of these proteins have thus far failed to confirm a phenotype in metal reduction [15,22,23]. No clear physiological role has been attributed to STC yet [15,24], whereas ScyA is considered to be the electron donor to the diheme cytochrome *c* peroxidase (CcpA) [25]. FccA is the unique fumarate reductase in *S. oneidensis* MR-1 and it also appears to contribute to metal reduction [26,27].

The identification of the redox partners involved in bridging the periplasmic gap between CymA and MtrCAB-OmcA complex is one of the key remaining issues in the understanding of extracellular metal respiration by *S. oneidensis* MR-1 [28]. Complexes of redox proteins typically have a transient nature, since they need to balance the requirement for fast electron transfer with fast turnover, making their interaction studies more challenging [29]. NMR spectroscopy is exquisitely sensitive to the presence of transient protein-protein interactions and can probe very weak interactions between redox proteins by either chemical shift perturbation or relaxation enhancement methods [29,30]. NMR has the unique added advantage of allowing the identification of the docking regions between the partners when resonance assignments are available.

In this work, protein-protein interactions involving the most abundant cytochromes from the periplasmic space of *S. oneidensis* MR-1 were identified

and used to propose an organization for the electron transfer network across the periplasmic space.

MATERIAL AND METHODS

Bacterial strains and growth conditions. The bacterial strains used in this work, *S. oneidensis* LS82 and *Escherichia coli* LS246, were kindly provided by Liang Shi from PNNL (Richland, WA, USA). *S. oneidensis* LS82 overexpresses the tetraheme cytochrome CymA and *E. coli* LS246 overexpresses the decaheme cytochrome MtrA. The strain *S. oneidensis* LS82 was grown at 30 ºC in Terrific Broth (TB) containing 50 μg mL^{-1} kanamycin in 5 L Erlenmeyer flasks containing 2 L of medium at 150 rpm. Cells were allowed to grow for 24 h before harvesting. The strain *E. coli* LS246 was grown at 30 ºC in TB medium containing 100 μg mL^{-1} ampicillin and 35 μg mL^{-1} chloramphenicol in 5 L Erlenmeyer flasks containing 1 L of medium at 180 rpm. After reaching an optical density at 600 nm of approximately 0.6, the cells were induced with 0.1 mM isopropyl-1-thio-β-D-galactopyranoside (IPTG). After induction, cells were allowed to grow under the same conditions for 16 h before harvesting.

Protein purification. Cells were harvested by centrifugation at 10,000 g for 15 min at 4 ºC. The cell pellet was washed and resuspended in 20 mM Tris-HCl buffer, pH 7.5, containing a protease inhibitor cocktail (Roche). Cell disruption was obtained by two passages through a French Press at a pressure of 1000 psi. Cell debris were removed by centrifugation at 10,000 g for 15 min at 4 ºC. The supernatant was ultracentrifuged at 200,000 g for 1 h at 4 ºC. The supernatant obtained from this procedure contained the soluble protein fraction and the pellet contained the membrane protein fraction.

The soluble protein fraction obtained from the *E. coli* LS246 cell growth, containing the MtrA cytochrome, was loaded directly onto a diethylaminoethyl (DEAE) column (GE Healthcare) previously equilibrated with 20 mM Tris (pH 7.6). A salt gradient from 0 to 1 M NaCl in 20 mM Tris buffer (pH 7.6) was applied and the fraction containing MtrA was eluted at 150 mM NaCl. This fraction was dialysed and loaded onto a Q-Sepharose column (GE Healthcare), equilibrated previously with 20 mM Tris buffer (pH 7.6). The fraction containing MtrA was eluted at 200 mM NaCl. This fraction was subsequently dialysed and loaded onto a hydroxylapatite (HTP) column (Bio-Rad Laboratories), pre-equilibrated with 10 mM potassium phosphate buffer (pH 7.6). MtrA was eluted with 50 mM of potassium phosphate buffer (pH 7.6).

The soluble protein fraction obtained from the *S. oneidensis* LS82 cell growth, containing the cytochrome ScyA, STC and FccA, was loaded directly onto a DEAE column previously equilibrated with 20 mM Tris buffer (pH 7.6). A salt gradient from 0 to 1 M NaCl in 20 mM Tris buffer (pH 7.6) was applied and the fractions containing the cytochromes ScyA, FccA and STC were eluted at 70 mM NaCl, 200 mM NaCl, and 250 mM NaCl, respectively. These fractions were dialysed and loaded separately onto a Q-Sepharose column, equilibrated previously with 20 mM Tris buffer (pH 7.6). Fractions containing the cytochromes ScyA, FccA and STC were eluted at 50 mM NaCl, 150 mM NaCl, and 200 mM NaCl, respectively. Fractions were loaded separately onto a HTP column, pre-equilibrated with 10 mM potassium phosphate buffer (pH 7.6), after dialysis. While the fractions containing the cytochromes ScyA and STC did not bind to the column and were eluted in the washout volume, the fraction containing FccA was eluted with 100 mM of potassium phosphate buffer (pH 7.6).

The membrane pellet obtained from the *S. oneidensis* LS82 cells was homogenized and solubilized in 20 mM Tris buffer (pH 7.6) containing a protease inhibitor cocktail and 4 % (w/v) n-dodecyl β-D-maltoside (DDM) at 4 ºC overnight. The insoluble material was removed by ultracentrifugation at 200,000 g for 1 h at 4 ºC, and the supernatant was used to purify CymA cytochrome using the procedure reported in the literature [31].

The chromatographic fractions were routinely analyzed by SDS-PAGE and UV–visible spectroscopy to select those containing the protein of interest. The purity of the protein was revealed as a single band in the gel. Fractions containing pure cytochrome samples had a typical absorbance ratio, $A_{Soret\ Peak}/A_{280nm}$, larger than 4.5 (See Appendix A).

NMR sample preparation and titrations. The protein samples were lyophilized twice using $^{2}H_2O$ (99.9 atom %). NMR spectra obtained before and after the lyophilization were identical, showing that the protein structure was not affected by this procedure. All protein samples were dissolved in $^{2}H_2O$ (99.9 atom %) and contained 20 mM potassium phosphate buffer (pH 7.6) with an ionic strength of 100 mM adjusted by the addition of potassium chloride. Cytochrome stock samples had a protein concentration of 1 mM.

NMR experiments were performed at 25 ºC on a Bruker Avance II 500 MHz NMR spectrometer equipped with a TXI probe. Samples containing 100 μM of one cytochrome were titrated against increasing concentrations of another cytochrome. ^{1}H-1D-NMR spectra were recorded for each addition. All cytochromes were in the fully oxidized state except the high potential monoheme cytochrome ScyA which was maintained fully reduced by the addition of 200 μM of ascorbic acid to the buffer.

Data analysis and binding affinities. In low-spin paramagnetic heme proteins, the methyl substituents at the periphery of the hemes show NMR resonances that are well separated from the protein envelope. This makes them convenient targets for chemical shift perturbation measurements. Furthermore, in the case of STC and FccA these signals have been assigned to specific hemes in the structure allowing the identification of the docking sites [32,33]. In reduced diamagnetic hemes such as that found in the monoheme cytochrome ScyA, the ring currents of the heme shift the meso protons outside of the protein envelope [34]. Thus, the NMR signals from the meso protons of the heme were followed instead.

The NMR spectra were processed and analyzed with Bruker TopSpin program. Chemical shifts are reported in parts per million (ppm) and the proton spectra were calibrated using the water signal as internal reference. Only chemical shift perturbations equal or larger than 0.025 ppm were considered significant [30]. The chemical shift perturbations ($\Delta\delta_{bind}$) of the NMR signals from a cytochrome (Cyt_A) resulting from the complex formation with another cytochrome (Cyt_B) were plotted against the molar ratio (R) of [Cyt_B]/[Cyt_A]. The data were fitted using least squares minimization to a 1:1 binding model using the following equation (See Appendix B) [35]:

$$\Delta\delta_{bind} = \frac{1}{2}\Delta\delta^{\infty}_{bind}\left(\mathrm{A} - \sqrt{(\mathrm{A}^2 - 4\mathrm{R})}\right) \qquad \text{(Eq. 4.1a)}$$

$$\mathrm{A} = 1 + \mathrm{R} + \frac{\mathrm{K}_d([\mathrm{Cyt}_A]_0\mathrm{R} + [\mathrm{Cyt}_B]_0)}{[\mathrm{Cyt}_A]_0[\mathrm{Cyt}_B]_0} \qquad \text{(Eq. 4.1b)}$$

Where $\Delta\delta^{\infty}_{bind}$ is the maximal chemical shift perturbation of the NMR signals resulting from the complex formation between Cyt_A and Cyt_B and K_d is the dissociation constant. [Cyt_A]$_0$ is the initial concentration of Cyt_A, [Cyt_B]$_0$ is

the stock concentration of Cyt_B. When several methyl signals belonging to an individual heme were clearly visible, the data obtained for all methyl signals were used to define the dissociation constant. Experimental uncertainty was estimated from the spectral resolution of the NMR acquisition.

Spectroscopic assay of interprotein electron transfer. Electron transfer involving FccA from *S. oneidensis* MR-1 was measured inside an anaerobic glove box (Coy Labs model type B), using a UV/Visible spectrophotometer (Shimadzu model UV-1800) to collect spectra in the range of 250-800 nm.

A 1 mL cuvette was prepared using 20 mM potassium phosphate buffer (pH 7.6) and 100 mM KCl with each of the target proteins at an approximate concentration of 1 μM. In the case of CymA, DDM (0.03 %) was added to the potassium phosphate buffer to avoid precipitation of the protein. To reduce the target proteins a concentrated solution of sodium dithionite was added in small amounts and the absorbance monitored at 314 nm to control for excess dithionite that could interfere with the results. A large excess of fumarate was added (approximately 1 mM) and the sample checked for the absence of changes in absorbance at 552 nm. The reaction was initiated by the addition of catalytic amounts of FccA (approximately 1 nM) and spectral changes were monitored over time. Experiments were performed with constant stirring, and the temperature was kept at 25 ºC using an external thermostating bath.

Protein electrostatic surface potential calculations. The structures of STC (PDB code 1M1Q), FccA (PDB code 1D4D) and ScyA (PDB code 1KX2), were used to perform electrostatic surface potential calculations considering a fully oxidized state for STC and FccA and a fully reduced state for ScyA, mimicking the experimental conditions used for studying the protein

interactions. Protein and co-factor partial charges were set using the GROMOS 43A1 force field [36]. Electrostatic potential calculations were performed with the MEAD package [37] that solves the Poisson-Boltzmann equation for a given system. The ionic strength used was 0 mM and the internal and external dielectric constants used were 2 and 80, respectively. The electrostatic potential was mapped at the proteins' surface using PyMOL [38].

RESULTS

NMR titrations and binding affinities. NMR spectroscopy is exquisitely sensitive to changes in chemical environment. When two proteins bind in fast exchange, the signals of the nuclei that are close to the binding site suffer a change in position according to the bound fraction. For electron transfer to occur at physiologically relevant rates between cytochromes, one heme in the donor and one heme in the acceptor must be in close proximity [39,40]. Thus, changes in the chemical shifts of the signals from hemes are among the best to monitor protein-protein interactions that are relevant for electron transfer. Figure 4.1 illustrates this phenomenon by presenting the spectral changes for the 18^{1} methyl signal (IUPAC-IUB nomenclature) from heme IV ($18^{1}CH_{3}^{IV}$) of STC in the presence of increasing amounts of MtrA. The broadening of the signals arises from the increased fraction of the bound species which is heavier. Primary NMR spectra for the free and bound forms of the cytochromes that display interactions are presented in Appendix C.

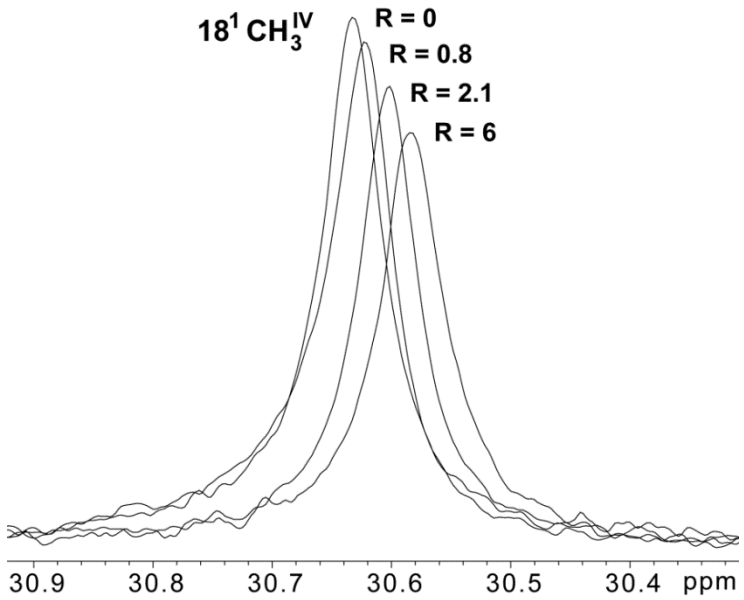

Figure 4.1. ^{1}H-1D NMR spectral changes of the signal from methyl 18^{1} belonging to heme IV of STC in the presence of increasing amounts of MtrA. The methyl group is identified using the IUPAC-IUB nomenclature for hemes. The Roman numeral corresponds to the order of heme binding to the polypeptide chain. The R value corresponds to the molar ratio of [MtrA]/[STC].

All the signals from STC, FccA and ScyA that are clearly visible in the NMR spectra were analyzed, and those that show changes resulting from interactions with putative partner proteins are reported in Figure 4.2.

Table 4.1 reports all pairs of proteins tested and the K_d values determined for those that showed interaction. The heme from STC or FccA that has signals showing greater perturbations in the chemical shifts provided the identification of the docking site, and is also indicated in Table 4.1.

All K_d values presented in Table 4.1 are consistent with weak transient interactions [41,42] as expected for redox partners and are of similar magnitude to other K_d values reported in the literature for the interaction between cytochromes [30,43].

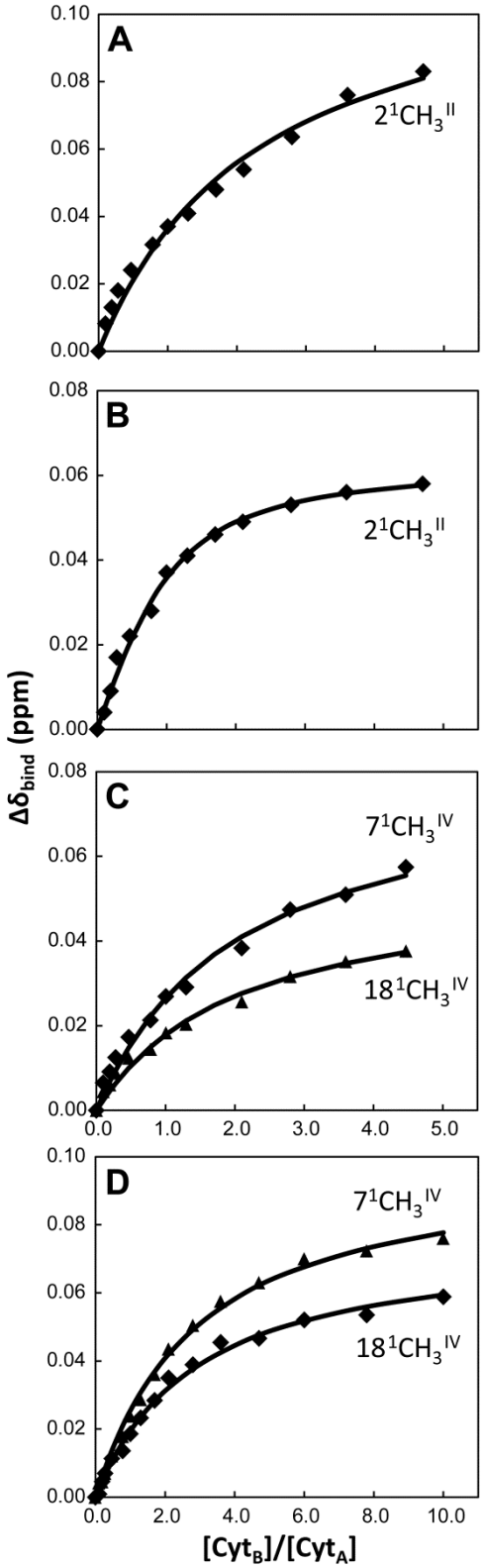

Figure 4.2. Binding curves of periplasmic cytochromes from *S. oneidensis* MR-1 that show interactions monitored by ^{1}H-NMR. **A)** FccA vs CymA; **B)** FccA vs MtrA; **C)** STC vs CymA; **D)** STC vs MtrA. The chemical shift perturbations of the heme methyl signals are plotted as a function of the molar ratio of the interacting proteins. Nomenclature is as in Figure 4.1. The solid lines represent the best global fit to the 1:1 binding model (Equation 4.1).

Table 4.1. Pairwise interactions tested for cytochromes found in the periplasm of *S. oneidensis* MR-1. * The dissociation constants were calculated as described in the Materials and Methods section and standard errors were calculated from the diagonal elements of the covariance matrix and are reported between brackets. † The heme belonging to STC or FccA displaying the greatest changes is reported. The Roman numerals correspond to the order of heme attachment to the polypeptide chain.

Cytochrome complex	K_d [μM] *	Docking site †
FccA *vs* CymA	398 (5)	Heme II
FccA *vs* MtrA	35 (14)	Heme II
FccA *vs* STC	—	—
FccA *vs* ScyA	—	—
STC *vs* CymA	250 (17)	Heme IV
STC *vs* MtrA	572 (5)	Heme IV
STC *vs* FccA	—	—
STC *vs* ScyA	—	—
ScyA vs MtrA	—	—

Spectroscopic assay of interprotein electron transfer. The interaction data obtained from the NMR experiments involving FccA were confirmed spectrophotometrically. The fumarate reductase activity of FccA, which is lacking in the other periplasmic cytochromes, was used to measure the re-oxidation of the partner cytochrome by catalytic FccA in the presence of excess fumarate.

Figure 4.3 shows that catalytic amounts of FccA can re-oxidise CymA and MtrA in the presence of excess fumarate, but not STC or ScyA. In the case of ScyA, the initial spectrum was already partially reduced due to the high reduction potential of this monoheme cytochrome.

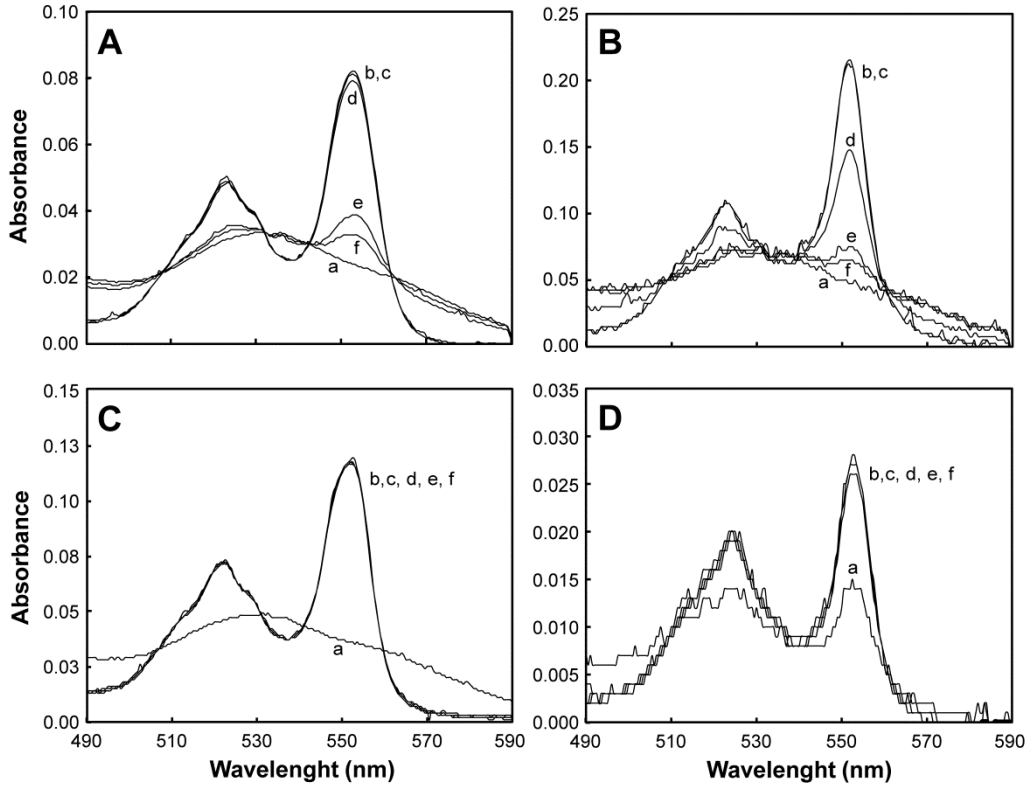

Figure 4.3. UV-visible spectroscopy of reduced periplasmic cytochromes in the presence of fumarate and catalytic amounts of FccA. UV-visible spectra of the cytochrome as purified (**a**), after reduction with dithionite (**b**) and subsequent addition of fumarate (**c**). After addition of FccA to the mixture, spectra were acquired at: 0 min (**d**), 2 min (**e**) and 5 min (**f**). Panels **A)**, **B)**, **C)** and **D)** represent FccA vs CymA, FccA vs MtrA, FccA vs STC, FccA vs ScyA, respectively.

Protein electrostatic surface potential characteristics. Electrostatic potential calculations show that STC, FccA and ScyA have, overall, surfaces displaying negative potential (Figure 4.4). STC shows very negative potentials in the whole protein with a small exception around the C-terminus fairly distant from the hemes. In FccA the heme containing domain also shows strongly negative surface potentials, whereas in the ScyA the protein shows a negative surface potential, with a neutral zone near the heme edge.

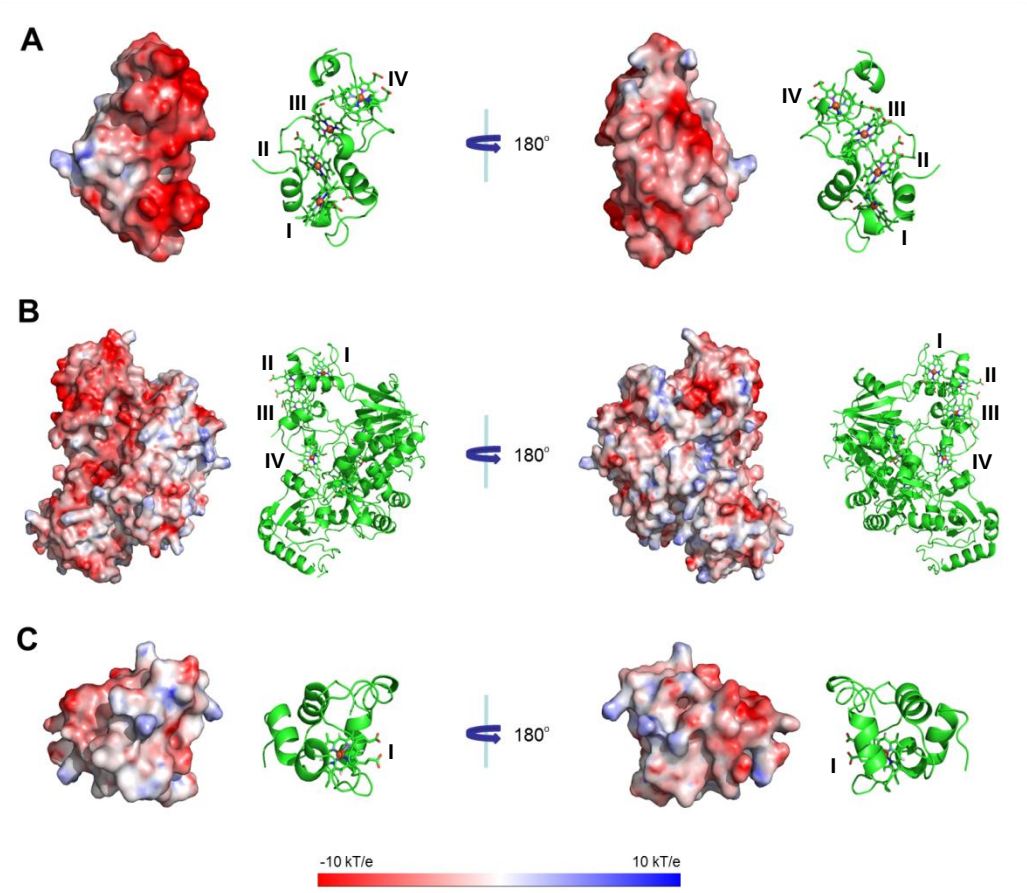

Figure 4.4. Electrostatic potential mapping on the protein's surface of the most abundant periplasmic cytochromes of *S. oneidensis* MR-1. Panel **A)**, **B)** and **C)** represent STC (PDB code 1M1Q), FccA (PDB code 1D4D) and ScyA (PDB code 1KX2), respectively. Electrostatic potentials were calculated (see Materials and Methods section for details) considering a fully oxidized state for STC and FccA and a fully reduced state for ScyA. The Roman numeral corresponds to the order of heme binding to the polypeptide chain.

DISCUSSION

Of all the aspects of the extracellular electron transfer performed by metal reducing bacteria, the organization of the trans-periplasmic redox network that has remained poorly understood. In order to try to unravel this

issue, several approaches have been used to study interactions among the numerous periplasmic *c*-type cytochromes. While attempts to cross-link these cytochromes have failed, most likely due to the highly dynamic transient nature of the interactions [24], studies performed with proteins attached to electrodes or other surfaces have been more successful and allowed the identification of some partners [11,44]. However, this approach may lead to false negatives since the orientation of the cytochrome on the surface may prevent the access of partners in physiological orientations.

In order to overcome these limitations, we probed the interactions between periplasmic cytochromes from *S. oneidensis* MR-1, using the perturbation of the chemical shifts of the NMR signals belonging to the most abundant proteins in the periplasmic space (STC, ScyA, and FccA) [19,20] as a probe for interaction between these proteins and their physiological redox partners.

NMR docking studies are done in conditions where electron transfer between the interacting partners is not taking place during the measurement. Notwithstanding, the vast body of literature on the subject shows the power of this approach for obtaining physiological and structural insights on the details of interactions between redox partners [29,43]. Furthermore, the relevance of the results for physiological electron transfer in the present case was independently supported by the observation of fumarate reduction only for those proteins that showed interaction with FccA in the NMR data (Figure 4.3). Table 4.2 summarizes the results obtained in this work and places them in the context of previous information available in the literature.

Table 4.2. Pairwise interactions tested for cytochromes found in the periplasm of *S. oneidensis* MR-1

Cytochrome complex	Interaction	Reference or Source
FccA *vs* CymA	+	This study; [10,27]
FccA *vs* MtrA	+	This study; [27]
FccA *vs* STC	-	This study
FccA *vs* ScyA	-	This study
FccA *vs* CcpA	-	[25]
STC *vs* CymA	+	This study; [44]
STC *vs* MtrA	+	This study
STC *vs* ScyA	-	This study
CymA *vs* ScyA	+	[25]
CymA *vs* MtrA	+	[27,44]
CymA *vs* DmsE	+	[44]
CymA *vs* CcpA	-	[25]
ScyA *vs* MtrA	-	This study
ScyA *vs* CcpA	+	[25]
MtrA *vs* CcpA	-	[25]

CymA plays a central role in the respiratory chain of *Shewanella*, by coupling the oxidation of menaquinol to a broad variety of multiheme cytochromes in the periplasmic space [10]. This was also shown by the NMR data obtained in this work, where CymA displayed interactions with both STC and FccA. The magnitude of the K_d values obtained between CymA and STC or CymA and FccA (Table 4.1) reveals the formation of weak complexes that prevent the blockage of access to CymA by the various redox partners. The results also indicate that both STC and FccA interact with the decaheme cytochrome MtrA, where FccA has a stronger affinity for MtrA than STC. Taking into consideration the importance of MtrA in metal respiration, these results indicate that both FccA and STC participate in metal reduction in *S. oneidensis* MR-1. This conclusion is consistent with gene knock-out experiments

where STC was shown to play a small role in iron reduction [16,45]. This observation may be a consequence of the stronger affinity of FccA for MtrA that leads to a longer lifetime of the complex and lower turnover rate of electron transfer relative to STC. Also, knock-out of the gene encoding for FccA showed that ferric iron reduction was faster in the deletion mutant than in the wild-type strain [27]. In this context, the absence of clear phenotypes in knock-out mutants of *Shewanella* may be due to the presence of both cytochromes in the periplasmic space [20,46] as well as some other of the 41 *c*-type cytochromes coded in the *S. oneidensis* MR-1 genome. This allows functional redundancy as previously reported for the decaheme cytochromes [16].

This electron transfer scenario is also favored by the structural and electrostatic similarities between the heme domain of FccA and STC. The electrostatic calculations show that both proteins have very negative surfaces in the regions that would be relevant for electron transfer. This provides a rational for the lack of interaction between FccA and STC both in the NMR data and in the electron transfer assay. The two proteins are highly abundant in the periplasmic space and interact with the same partners, but do not exchange electrons with each other. Therefore, electrons in the pool of STC molecules in the periplasm will not equilibrate with those in the pool of FccA molecules. Interestingly, this occurs in the absence of physical barriers and in the presence of overlapping ranges of redox activity of both proteins [33,47]. In these conditions it is the tuning of the surface electrostatics of the proteins that serves to maintain segregated electron transfer pathways across the periplasmic space.

Likewise, the monoheme cytochrome ScyA that is also produced in high amounts in the periplasm of *Shewanella* under oxygen limited conditions [20], also has negative electrostatic surface potentials. It does not interact with STC,

FccA or MtrA, showing the presence of a third segregated redox pathway that in this case does not lead to metal reduction. These results lend further support to the proposal that ScyA mediates electron transfer between CymA and the cytochrome *c* peroxidase CcpA [25].

This study also enabled, for the first time, the identification of the hemes in STC and FccA that are responsible for electron transfer with their periplasmic redox partners. FccA interacts with CymA and MtrA in the vicinity of heme II, while interactions between STC and CymA or MtrA occur near heme IV. The region around heme IV from STC displays the strongest negative potentials (Figure 4.4-A), making it a good candidate to interact with a redox partner displaying presumably positively charged potentials at the surface. Similarly, the zone corresponding to heme II in FccA is also the one displaying the highest negative potentials (Figure 4.4-B). Unfortunately, an experimentally determined structure of CymA does not exist and MtrA has been structurally characterized only by SAXS. Therefore, it is not possible presently to determine whether CymA and MtrA contain surface regions of positive potential where they can establish interaction with their negatively charged redox partners. Furthermore, although STC and FccA bind to CymA and MtrA through different hemes, until structures of CymA and MtrA are available, it remains to be known whether STC and FccA compete for the same docking positions in CymA and MtrA or if they bind to different positions.

Nonetheless, an important insight on the organization of the transperiplasmic redox network emerges from these results. As had been previously observed for STC with inorganic electron donors and acceptors [48], entry and exit of electrons appears to occur through the same heme, implying that ternary complexes are not formed (Figure 4.5). Therefore, both STC and FccA must reorient to present the same heme (heme IV in the case of

STC and heme II in the case of FccA) to CymA and MtrA as they glide back and forth in the periplasmic space with a movement akin to that of a boomerang.

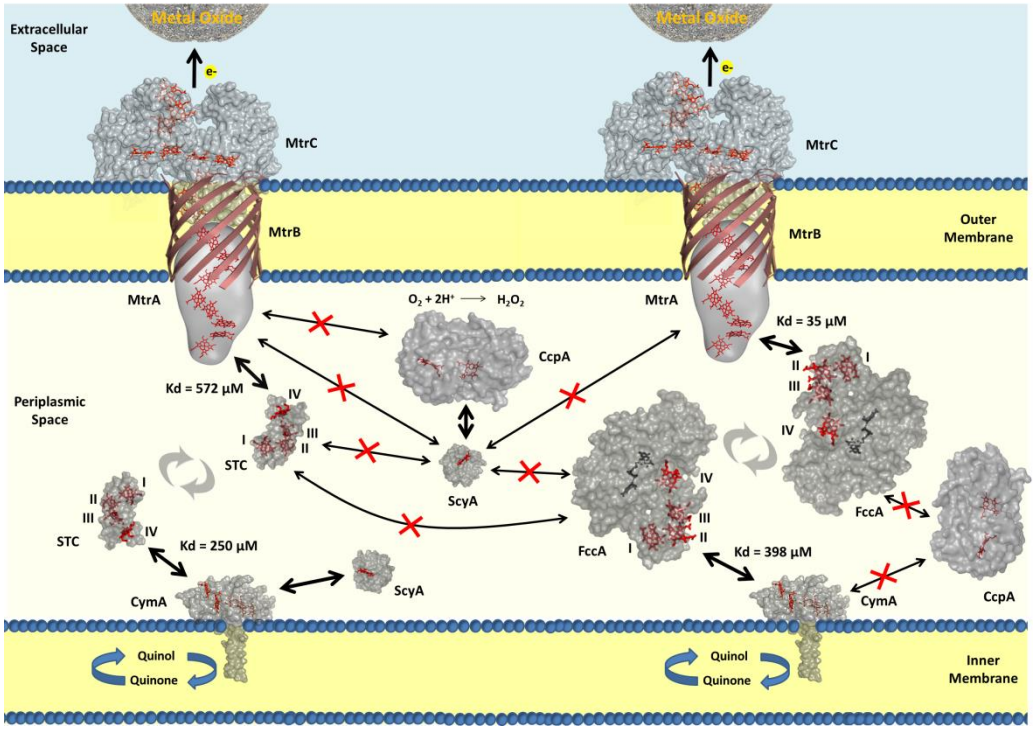

Figure 4.5. Cartoon depicting the interactions that occur between the most abundant periplasmic cytochromes of *S. oneidensis* MR-1. Arrows in bold indicate the interactions that occur between the cytochromes and point to the possible docking site. The dissociation constants (K_d) corresponding to each interaction are positioned next to their respective arrow. Interactions that do not occur are represented by a red X in the middle of the arrow. The Roman numerals correspond to the order of heme attachment to the polypeptide chain. Cytochrome representations were made with PyMOL [38] using the structures of STC (PDB code 1M1Q), FccA (PDB code 1D4D), ScyA (PDB code 1KX2), CcpA (PDB code 3O5C) and the SAXS model of MtrA. For MtrC and CymA, models were made with SWISS-MODEL [49,50] using as template the structures of MtrF (PDB code 3PMQ) and NrfH (PDB code 2J7A), respectively.

To conclude, this work filled important gaps in the knowledge of the interaction network of periplasmic cytochromes of *S. oneidensis* MR-1. The results show for the first time that there are two clearly segregated pathways to transfer electrons across the periplasmic gap to the outer-membrane metal reductases, one involving STC and the other involving FccA. This finding provides a rational for the lack of clear phenotypes of deletion mutants of these two proteins. The fact that in each of these cytochromes it is the same heme that contacts the donor (CymA) and the acceptor (MtrA), and the large dissociation constants measured show that a stable multi-protein complex capable of bridging the periplasmic gap does not exist. However, these findings beg the question, of whether the two pathways involving STC and FccA that share the same cell compartment, serve any other purpose than the maintenance of redundancy in this essential physiological trait of extracellular electron transfer. Experiments to address this issue in particular in the context of proposals for these proteins as electron storage devices are being planned.

ACKNOWLEDGEMENTS

We thank Liang Shi from PNNL (Richland, WA, USA) for the bacterial strains used in this work. BMF and CMP are the recipients of grants (SFRH/BD/41205/2007) and (SFRH/BPD/34591/2007) from Fundação para a Ciência e a Tecnologia (FCT), respectively. Research in the author's laboratories was supported by FCT grants (PTDC/BIA-PRO 098158/2008) and (MIT-Pt BS-BB/1014/2008). This work was also supported by FCT through grant (PEst-OE/EQB/LA0004/2011). The NMR data were collected at The Portuguese National NMR Network (REDE/1517/RMN/2005), supported by "Programa Operacional Ciência e Inovação (POCI) 2010" and FCT.

REFERENCES

[1] **Lovley, D.R.** 2006. Bug juice: harvesting electricity with microorganisms. Nat Rev Microbiol *4*:497-508.

[2] **Summers, Z.M., H.E. Fogarty, C. Leang, A.E. Franks, N.S. Malvankar, and D.R. Lovley.** 2010. Direct exchange of electrons within aggregates of an evolved syntrophic coculture of anaerobic bacteria. Science *330*:1413-1415.

[3] **Logan, B.E. and K. Rabaey.** 2012. Conversion of wastes into bioelectricity and chemicals by using microbial electrochemical technologies. Science *337*:686-690.

[4] **Biffinger, J.C., L.A. Fitzgerald, R. Ray, B.J. Little, S.E. Lizewski, E.R. Petersen, B.R. Ringeisen, W.C. Sanders, et al.** 2011. The utility of *Shewanella japonica* for microbial fuel cells. Biores Technol *102*:290-297.

[5] **Myers, C.R. and K.H. Nealson.** 1988. Bacterial manganese reduction and growth with manganese oxide as the sole electron-acceptor. Science *240*:1319-1321.

[6] **Hau, H.H. and J.A. Gralnick.** 2007. Ecology and biotechnology of the genus *Shewanella*. Annu Rev Microbiol *61*:237-258.

[7] **Richter, K., M. Schicklberger, and J. Gescher.** 2012. Dissimilatory reduction of extracellular electron acceptors in anaerobic respiration. Appl Environ Microb *78*:913-921.

[8] **Richardson, D.J., J.N. Butt, J.K. Fredrickson, J.M. Zachara, L. Shi, M.J. Edwards, G. White, N. Baiden, et al.** 2012. The 'porin-cytochrome' model for microbe-to-mineral electron transfer. Mol Microbiol *85*:201-212.

[9] **Gralnick, J.A. and D.K. Newman.** 2007. Extracellular respiration. Mol Microbiol *65*:1-11.

[10] **Schwalb, C., S.K. Chapman, and G.A. Reid.** 2003. The tetraheme cytochrome CymA is required for anaerobic respiration with dimethyl sulfoxide and nitrite in *Shewanella oneidensis*. Biochemistry *42*:9491-9497.

[11] **McMillan, D.G.G., S.J. Marritt, J.N. Butt, and L.J.C. Jeuken.** 2012. Menaquinone-7 is specific cofactor in tetraheme quinol dehydrogenase CymA. J Biol Chem *287*:14215-14225.

[12] **Zargar, K. and C.W. Saltikov.** 2009. Lysine-91 of the tetraheme *c*-type cytochrome CymA is essential for quinone interaction and arsenate respiration in *Shewanella sp.* strain ANA-3. Arch Microbiol *191*:797-806.

[13] **Firer-Sherwood, M.A., N. Ando, C.L. Drennan, and S.J. Elliott.** 2011. Solution-based structural analysis of the decaheme cytochrome, MtrA, by small-angle X-ray scattering and analytical ultracentrifugation. J Phys Chem B *115*:11208-11214.

[14] **Pitts, K.E., P.S. Dobbin, F. Reyes-Ramirez, A.J. Thomson, D.J. Richardson, and H.E. Seward.** 2003. Characterization of the *Shewanella oneidensis* MR-1 decaheme cytochrome MtrA. J Biol Chem *278*:27758-27765.

[15] **Bretschger, O., A. Obraztsova, C.A. Sturm, I.S. Chang, Y.A. Gorby, S.B. Reed, D.E. Culley, C.L. Reardon, et al.** 2007. Current production and metal oxide reduction by *Shewanella oneidensis* MR-1 wild type and mutants. Appl Environ Microb *73*:7003-7012.

[16] **Coursolle, D. and J.A. Gralnick.** 2010. Modularity of the Mtr respiratory pathway of *Shewanella oneidensis* strain MR-1. Mol Microbiol *77*:995-1008.

[17] **Hartshorne, R.S., C.L. Reardon, D. Ross, J. Nuester, T.A. Clarke, A.J. Gates, P.C. Mills, J.K. Fredrickson, et al.** 2009. Characterization of an electron conduit

between bacteria and the extracellular environment. Proc Natl Acad Sci USA *106*:22169-22174.

[18] **Dohnalkova, A.C., M.J. Marshall, B.W. Arey, K.H. Williams, E.C. Buck, and J.K. Fredrickson.** 2011. Imaging hydrated microbial extracellular polymers: comparative analysis by electron microscopy. Appl Environ Microb *77*:1254-1262.

[19] **Tsapin, A.I., I. Vandenberghe, K.H. Nealson, J.H. Scott, T.E. Meyer, M.A. Cusanovich, E. Harada, T. Kaizu, et al.** 2001. Identification of a small tetraheme cytochrome *c* and a flavocytochrome *c* as two of the principal soluble cytochromes c in *Shewanella oneidensis* strain MR1. Appl Environ Microb *67*:3236-3244.

[20] **Meyer, T.E., A.I. Tsapin, I. Vandenberghe, L. de Smet, D. Frishman, K.H. Nealson, M.A. Cusanovich, and J.J. van Beeumen.** 2004. Identification of 42 possible cytochrome *c* genes in the *Shewanella oneidensis* genome and characterization of six soluble cytochromes. OMICS *8*:57-77.

[21] **Rosenbaum, M.A., H.Y. Bar, Q.K. Beg, D. Segre, J. Booth, M.A. Cotta, and L.T. Angenent.** 2012. Transcriptional analysis of *Shewanella oneidensis* MR-1 with an electrode compared to Fe(III)-citrate or oxygen as terminal electron acceptor. Plos One *7*:1-13.

[22] **Gao, H., S. Barua, Y. Liang, L. Wu, Y. Dong, S. Reed, J. Chen, D. Culley, et al.** 2010. Impacts of *Shewanella oneidensis c*-type cytochromes on aerobic and anaerobic respiration. Microb Biotechnol *3*:455-466.

[23] **Coursolle, D. and J.A. Gralnick.** 2012. Reconstruction of extracellular respiratory pathways for iron(III) reduction in *Shewanella oneidensis* strain MR-1. Front Microbiol *3*:56.

[24] **Ross, D.E., S.S. Ruebush, S.L. Brantley, R.S. Hartshorne, T.A. Clarke, D.J. Richardson, and M. Tien.** 2007. Characterization of protein-protein interactions involved in iron reduction by *Shewanella oneidensis* MR-1. Appl Environ Microb *73*:5797-5808.

[25] **Schutz, B., J. Seidel, G. Sturm, O. Einsle, and J. Gescher.** 2011. Investigation of the electron transport chain to and the catalytic activity of the diheme cytochrome *c* peroxidase CcpA of *Shewanella oneidensis*. Appl Environ Microb *77*:6172-6180.

[26] **Gordon, E.H., S.L. Pealing, S.K. Chapman, F.B. Ward, and G.A. Reid.** 1998. Physiological function and regulation of flavocytochrome c_3, the soluble fumarate reductase from *Shewanella putrefaciens* NCIMB 400. Microbiology *144*:937-945.

[27] **Schuetz, B., M. Schicklberger, J. Kuermann, A.M. Spormann, and J. Gescher.** 2009. Periplasmic electron transfer via the *c*-type cytochromes MtrA and FccA of *Shewanella oneidensis* MR-1. Appl Environ Microb *75*:7789-7796.

[28] **Shi, L., K.M. Rosso, T.A. Clarke, D.J. Richardson, J.M. Zachara, and J.K. Fredrickson.** 2012. Molecular underpinnings of Fe(III) oxide reduction by *Shewanella oneidensis* MR-1. Front Microbiol *3*:50.

[29] **Prudencio, M. and M. Ubbink.** 2004. Transient complexes of redox proteins: structural and dynamic details from NMR studies. J Mol Recognit *17*:524-539.

[30] **Diaz-Moreno, I., A. Diaz-Quintana, M. Ubbink, and M.A. De la Rosa.** 2005. An NMR-based docking model for the physiological transient complex between cytochrome *f* and cytochrome c_6. FEBS Lett *579*:2891-2896.

[31] **Marritt, S.J., T.G. Lowe, J. Bye, D.G. McMillan, L. Shi, J. Fredrickson, J. Zachara, D.J. Richardson, et al.** 2012. A functional description of CymA, an electron-transfer hub supporting anaerobic respiratory flexibility in *Shewanella*. Biochem J *444*:465-474.

[32] **Fonseca, B.M., I.H. Saraiva, C.M. Paquete, C.M. Soares, I. Pacheco, C.A. Salgueiro, and R.O. Louro.** 2009. The tetraheme cytochrome from *Shewanella oneidensis* MR-1 shows thermodynamic bias for functional specificity of the hemes. J Biol Inorg Chem *14*:375-385.

[33] **Pessanha, M., E.L. Rothery, C.S. Miles, G.A. Reid, S.K. Chapman, R.O. Louro, D.L. Turner, C.A. Salgueiro, and A.V. Xavier.** 2009. Tuning of functional heme reduction potentials in *Shewanella* fumarate reductases. Biochim Biophys Acta *1787*:113-120.

[34] **Bartalesi, I., I. Bertini, P. Hajieva, A. Rosato, and P.R. Vasos.** 2002. Solution structure of a monoheme ferrocytochrome *c* from *Shewanella putrefaciens* and structural analysis of sequence-similar proteins: functional implications. Biochemistry *41*:5112-5119.

[35] **Worrall, J.A., W. Reinle, R. Bernhardt, and M. Ubbink.** 2003. Transient protein interactions studied by NMR spectroscopy: the case of cytochrome *c* and adrenodoxin. Biochemistry *42*:7068-7076.

[36] **Scott, W.R.P., P.H. Hünenberger, I.G. Tironi, A.E. Mark, S.R. Billeter, J. Fennen, A.E. Torda, T. Huber, et al.** 1999. The GROMOS biomolecular simulation program package. J Phys Chem A *103*:3596-3607.

[37] **Bashford, D. and M. Karplus.** 1990. pKa's of ionizable groups in proteins: atomic detail from a continuum electrostatic model. Biochemistry *29*:10219-10225.

[38] **Delano, W.L.** 2003. The PyMol molecular graphics system. Delano Scientific LLC, San Carlos, CA, USA.

[39] **Gray, H.B. and J.R. Winkler.** 2010. Electron flow through metalloproteins. Biochim Biophys Acta *1797*:1563-1572.

[40] **Moser, C.C., S.E. Chobot, C.C. Page, and P.L. Dutton.** 2008. Distance metrics for heme protein electron tunneling. Biochim Biophys Acta *1777*:1032-1037.

[41] **Bashir, Q., S. Scanu, and M. Ubbink.** 2011. Dynamics in electron transfer protein complexes. FEBS J *278*:1391-1400.

[42] **Perkins, J.R., I. Diboun, B.H. Dessailly, J.G. Lees, and C. Orengo.** 2010. Transient protein-protein interactions: structural, functional, and network properties. Structure *18*:1233-1243.

[43] **Meschi, F., F. Wiertz, L. Klauss, A. Blok, B. Ludwig, A. Merli, H.A. Heering, G.L. Rossi, and M. Ubbink.** 2011. Efficient electron transfer in a protein network lacking specific interactions. J Am Chem Soc *133*:16861-16867.

[44] **Firer-Sherwood, M.A., K.D. Bewley, J.Y. Mock, and S.J. Elliott.** 2011. Tools for resolving complexity in the electron transfer networks of multiheme cytochromes *c*. Metallomics *3*:344-348.

[45] **Gordon, E.H.J., A.D. Pike, A.E. Hill, P.M. Cuthbertson, S.K. Chapman, and G.A. Reid.** 2000. Identification and characterization of a novel cytochrome c_3 from *Shewanella frigidimarina* that is involved in Fe(III) respiration. Biochem J *349*:153-158.

[46] **Romine, M.F., T.S. Carlson, A.D. Norbeck, L.A. McCue, and M.S. Lipton.** 2008. Identification of mobile elements and pseudogenes in the *Shewanella oneidensis* MR-1 genome. Appl Environ Microb *74*:3257-3265.

[47] **Firer-Sherwood, M., G.S. Pulcu, and S.J. Elliott.** 2008. Electrochemical interrogations of the Mtr cytochromes from *Shewanella*: opening a potential window. J Biol Inorg Chem *13*:849-854.

[48] **Paquete, C.M., I.H. Saraiva, E. Calcada, and R.O. Louro.** 2010. Molecular basis for directional electron transfer. J Biol Chem *285*:10370-10375.

[49] **Arnold, K., L. Bordoli, J. Kopp, and T. Schwede.** 2006. The SWISS-MODEL workspace: a web-based environment for protein structure homology modelling. Bioinformatics *22*:195-201.

[50] **Kiefer, F., K. Arnold, M. Kunzli, L. Bordoli, and T. Schwede.** 2009. The SWISS-MODEL repository and associated resources. Nucleic Acids Res *37*:D387-D392.

CHAPTER V

Efficient and selective isotopic labeling of hemes to facilitate the study of multiheme proteins

This chapter was published in:

Fonseca BM, Tien M, Rivera M, Shi L, Louro RO (2012) "Efficient and selective isotopic labeling of hemes to facilitate the study of multiheme proteins" *BioTechniques Rapid Dispatches* **doi:** 10.2144/000113859.

The author of this dissertation participated in all experiments described in this chapter, except in the synthesis of the labeled δ-aminolevulinic acid.

ABSTRACT

Specific isotopic labeling of hemes provides a unique opportunity to characterize the structure and function of heme-proteins. Unfortunately, present day methods do not allow efficient labeling in high yields of multiheme cytochromes *c*, which are of great biotechnological interest. Here, a method for production of recombinant multiheme cytochromes *c* in *Escherichia coli* with isotopically labeled hemes is reported. A small tetraheme cytochrome of 12 kDa from *Shewanella oneidensis* MR-1 was used to demonstrate the method, achieving a production of 4 mg of pure protein per liter. This method achieves, in a single step, efficient expression and incorporation of hemes isotopically labeled in specific atom positions adequate for spectroscopic characterization of these complex heme proteins. It is, furthermore, of general application to heme proteins opening new possibilities in the characterization of this important class of proteins.

INTRODUCTION

Heme proteins hold a special place in the development of modern Biochemistry. Hemoglobin is aptly considered an honorary enzyme despite its physiological role as a diatomic gas transporter [1]. Indeed, heme proteins perform ubiquitous cell functions such as electron transfer (cytochromes) [2-4], energy transduction (cytochrome *c* oxidase) [5,6], catalysis (P450 and peroxidases) [7-10] or molecular sensing (chemotactic proteins) [11]. One class of heme proteins has recently gathered considerable attention, being the focus of a Biogeochemistry Grand Challenge of the U.S. Department of Energy. These are multiheme cytochromes *c*, which mediate electron transfer at the microbe-mineral interface in geological settings and at the microbe-electrode

interface in bioelectrochemical devices [12,13]. These cytochromes have been shown to play major roles in cellular respiration and to exist in almost all major groups of Bacteria and Archaea [14]. In some of these organisms, such as representatives of *Geobacter, Shewanella, Anaeromyxobacter* or *Desulfovibrio* genera, the number of multiheme cytochromes is so elevated that it corresponds to a high percentage of their proteome, having elicited the creation of the term "cytochromome" [15,16]. For *Geobacter* and *Shewanella* many of these are known to be essential for the extracellular respiration that is at the core of electricity production in microbial fuel cells [17].

Given their biological importance, considerable efforts have gone into the development of efficient methods for their recombinant production to facilitate their molecular characterization and/or their use in medical or biotechnological applications [12,16-18]. In comparison to other types of cytochromes, multiheme cytochromes *c* are more difficult to express correctly on two accounts: the various hemes must be covalently attached, through thioether linkages, to the polypeptide chain at the CXX(XX)CH binding site; and also the correct distal axial ligand must be connected to the iron in the nascent protein. This is essential in order to obtain the native fold of the protein. For this to occur properly in Gram negative bacteria, specific molecular assembly helper proteins, collectively known as the Cytochrome *c* maturation proteins CcmA-H (*ccm* cluster), are needed [19,20]. These proteins are responsible for the correct ligation of the heme to the apoprotein, while it is translocated to the periplasmic space. This cytochrome *c* biogenesis system is denominated as system I and is the most complex of the presently known cytochrome *c* biogenesis systems, allowing the maturation of a variety of *c*-type cytochromes under different conditions [20-22].Among many systems available for

recombinant protein expression, the bacterium *E. coli* is one of the most attractive hosts, due to the advantage of fast growth at a high density in an inexpensive medium, well characterized genetics and the availability of a large number of cloning vectors. With the insertion of a plasmid containing the ccm cluster [23,24], *E. coli* becomes capable of expressing *c*-type cytochromes with correctly inserted hemes under aerobic conditions. Also, under these conditions *E.coli* has the advantage of expressing only the recombinant *c*-type cytochromes. This simplifies considerably the protein purification procedure in comparison to other expression hosts described in the literature [25-29], which also produce their own native *c*-type cytochromes under the expression conditions used.

Multiheme cytochromes *c* are also more difficult to analyze with respect to their detailed functional properties, due to the multiple combinations of electron distribution that can occur among the various hemes. Since the heme co-factors are the functional components of multiheme proteins, their specific isotopic labeling is an attractive strategy to analyze the structure and function of these proteins. Towards this end, several approaches have been developed involving the supplementation of the growth media with specifically labeled heme co-factors [30,31] or with isotopically labeled heme precursor δ-aminolevulinic acid (dALA) [31-33]. Also, to guarantee that the uptake of these substituents is efficient, bacterial strains that are incapable of synthetizing hemes co-factors were created by deleting genes that are responsible for biosynthesis of dALA in the cell, such as the *hemA* gene (See Appendix F) [33,34].

However, the methods presently published do not allow isotopic labeling of the hemes in multiheme *c*-type cytochromes [30-33], preventing the

study of these more complex cytochromes. Here, a method that allows efficient expression of recombinant multiheme cytochromes *c* with specific isotopic labeling in the various hemes is reported. This method will bring an enormous advantage for the characterization of this important class of proteins by several spectroscopic techniques.

Nuclear magnetic resonance (NMR), resonance Raman, and FTIR, are among the spectroscopic methods capable of probing the structure and function of multiheme cytochromes *c*. All stand to benefit from the spectral simplification afforded by the isotopic labeling of specific heme carbons.

MATERIAL AND METHODS

Chemical reagents. All chemical reagents were obtained from Sigma or Sigma-Aldrich with the exception of the BugBuster® protein extraction reagent (Merck KGaA) and the Complete protease inhibitor cocktail tablets (Roche).

Synthesis of labeled dALA. The method reported by Bunce *et al.* [35] was used to synthesize 1,2-^{13}C-labeled dALA. This compound gives rise to hemes with ^{13}C labeled atoms in the methyl positions and also at the *β*- and carboxylate carbons of the propionate groups [36].

Construction of the *hemA* knockout in *E. coli* strain JM109(DE3). The *E. coli* strain JM109(DE3) was purchased from Promega. In order to generate a Δ*hemA* mutant in *E. coli* JM109(DE3), the method developed by Datsenko & Wanner to disrupt chromosomal genes was used [37]. First the *hemA* gene was replaced with a kanamycin resistance (*kan*) gene which was then subsequently excised. In order to do this the plasmid pKD4 was used as a template and the region that contained the *kan* resistance gene flanked by Flp recombination

target (FRT) sites was amplified. Primers homologous to the flanking sites of the *kan* gene were constructed. These also carried nucleotide extensions homologous to the chromosomal regions adjacent to the *hemA* gene (forward: 5′-CAGACTAACCCTATCAACGTTGGTATTATTTCCCGCAGACGTGTAGG CTGGAGCTGCTTC-3′ and reverse: 5′-GGCGTAAATGCACCCTGTAAAAAA AGAAAATGATGTACTGCATATGAATATCCTCCTTAG-3′). The PCR product consisted of the *kan* gene flanked by 40 bp sequences homologous to the regions adjacent to the *hemA* gene of *E. coli*. Before inserting the amplified region, the *E. coli* cells were transformed with the plasmid pKD46 in order to obtain better transformation and recombination rates. This plasmid contains the genes of the phage λ Red protein recombination system. Kanamycin resistant clones were selected on Luria-Bertani (LB) medium supplemented with 50 mg L^{-1} dALA and 50 mg L^{-1} kanamycin. The *kan* gene was subsequently eliminated using the helper plasmid pCP20 which encodes for the Flp recombinase and promotes recombination at the FRT sites. This step allows the excision of the antibiotic gene from the chromosome since it is flanked by the FRT sites, leaving behind only a small residual scar. Successful disruption of the *hemA* gene was verified by PCR. This *hemA* knockout *E. coli* mutant was denominated LS542.

Construction of the *E. coli* strains used for protein expression. The plasmid pEC86 [23], containing the *ccmABCDEFGH* (cytochrome *c* maturation) genes, was introduced via electroporation into LS542 to create LS543.

Expression vectors pET21a-stC(D2N) [38] and pKP1 [39] containing the genes encoding for the mutant STC(D2N) and native MtrA, respectively, were subsequently introduced into LS543. These strains were denominated LS543-STC(D2N) and LS544, respectively.

In order to compare expression levels between the *hemA* knockout *E. coli* mutant strain and the wild-type (wt) strain *E. coli* JM109(DE3) the plasmids pEC86 and pET21a-stC(D2N) were also introduced into wt. This strain was denominated ROL002.

With exception of the wild-type, all the other strains were grown in media supplemented with 50 mg L^{-1} of dALA. The supplementation of the media with dALA is essential for growth of the mutant strains.

Optimization of protein expression. To optimize the expression, the *E. coli* strains LS543-STC(D2N), LS544 and ROL002 were tested using several overexpression methods for cytochromes. In all the cases, controlled modifications of temperature, dALA concentration, IPTG concentration and induction period were performed.

The overexpression of proteins in a rich medium with an induction step at a certain OD_{600nm} was tested [24]. This was done using LB medium (10 g L^{-1} tryptone, 5 g L^{-1} yeast extract, 10 g L^{-1} NaCl) and also in Terrific Broth (TB) medium (12 g L^{-1} tryptone, 24 g L^{-1} Yeast extract, 4 mL glycerol, 2.31 g L^{-1} KH_2PO_4, 12.54 g L^{-1} K_2HPO_4) supplemented with 35 mg L^{-1} chloramphenicol, 100 mg L^{-1} ampicillin and 50 mg L^{-1} dALA. Cells were grown overnight at 30 ºC and 180 rpm and 1 % of this culture served as inoculum for the fresh medium. Batches of fresh medium were supplemented with different concentrations of dALA, ranging from 20 mg L^{-1} to 200 mg L^{-1}, in order to determine the best dALA concentration to overexpress the protein. The culture was then allowed to grow at 180 rpm, at a defined temperature (25 ºC, 30 ºC or 37 ºC) until an $OD_{600nm} \approx 0.8$ was reached. The protein expression was induced by addition of different concentrations of IPTG, ranging from 0 to 1 mM.

The method developed by Fernandes *et al.* [40] for isotopic labeling of *c*-type multiheme cytochromes was also tested. The cells were first grown in 1 L of LB medium supplemented with 50 mg L^{-1} dALA, 35 mg L^{-1} chloramphenicol and 100 mg L^{-1} ampicillin at 30 ºC and 180 rpm. After achieving an OD_{600nm} ≈ 1.5 the cells were harvested by centrifugation at 6400 g for 30 min. The cell pellet was washed twice with a salt solution containing 15 g L^{-1} KH_2PO_4, 38 g L^{-1} $Na_2HPO_4 \cdot H_2O$, and 2.5 g L^{-1} NaCl, in order to remove nutrients left behind by the rich medium. The cells were subsequently resuspended in 250 mL of minimal medium containing 5 g L^{-1} NH_4Cl, 0.5 g L^{-1} $MgSO_4$, 0.01 g L^{-1} $CaCl_2$, 1 mg L^{-1} $MnCl_2 \cdot 4H_2O$, 2.8 mg L^{-1} $FeSO_4 \cdot 7H_2O$, 1x BME vitamins solution, 4 g L^{-1} glucose or 7 mL L^{-1} 50 % glycerol stock solution as carbon source, supplemented with 35 mg L^{-1} chloramphenicol, 100 mg L^{-1} ampicillin and 1 mM dALA. Cells were allowed to recover for a period of 1 h before inducing protein expression. Different concentrations of IPTG, ranging from 0 to 1 mM, and also different temperatures (25 ºC, 30 °C or 37 ºC) were used.

The auto-induction method developed by Studier [41] that had previously been used to produce heme proteins in *E. coli* [42] was also tested. The cells were first grown overnight in LB medium supplemented with 50 mg L^{-1} dALA, 35 mg L^{-1} chloramphenicol and 100 mg L^{-1} ampicillin at 30 ºC and 180 rpm. 1 % of this culture served as inoculum. The auto-induction medium was made by adding 50 mL of a stock solution 20x NPS (1 M Na_2HPO4, 1 M KH_2PO_4, 500 mM $(NH_4)_2SO_4$), 20 mL of a stock solution 50x 5052 (25 % glycerol, 2.5 % glucose, 10 % α-lactose monohydrate) to 1 liter of LB or TB medium supplemented with 1 mM $MgSO_4$, 0.1 mM $FeSO_4$, 35 mg L^{-1} chloramphenicol, and 100 mg L^{-1} ampicillin. The optimal dALA concentration was determined, by testing concentrations varying from 20 mg L^{-1} to 200 mg L^{-1}. Different

temperatures (25 ºC, 30 ºC and 37 ºC) were also tested in order to optimize protein expression.

In order to test different induction periods, aliquots (1 mL) were taken each hour from each different culture condition and centrifuged to collect the cell pellet. The pellets were subsequently lysed using BugBuster® protein extraction reagent. The supernatants were run on a sodium dodecyl sulfate polyacrylamide gel electrophoresis (SDS-PAGE) and the gels were stained using the heme staining procedure developed by Francis & Becker [43].

The gels were visualized and the stained protein bands were compared and analyzed for their intensity using the ImageJ v1.44 program (http://rsbweb.nih.gov/ij/index.html).

All growth conditions and analysis were performed in triplicate.

Protein production and purification. The auto-induction method previously described was used to overexpress the mutant STC(D2N) multiheme cytochrome in *E. coli* strain LS543-STC(D2N). The LB auto-induction medium was supplemented with 35 mg L^{-1} chloramphenicol, 100 mg L^{-1} ampicillin, 50 mg L^{-1} of unlabeled dALA to produce unlabeled hemes, or 50 mg/L of 1,2-^{13}C-labeled dALA [35] to produce specific isotopically labeled hemes.

The cells were grown for 27 h at 30 ºC and 180 rpm in conical flasks filled with 1/5 of the total volume. Expression of STC(D2N) was induced spontaneously by depletion of the glucose present in the medium. There was a clear change in the medium's color to orange. The bacterial cells were harvested by centrifugation at 4 ºC and at 10,000 g for 15 min. The cell pellet was disrupted by gentle stirring for 20 min at room temperature with 5 mL BugBuster® protein extraction reagent per gram of wet cell paste supplemented

with a protease inhibitor cocktail. Cell debris were removed by centrifugation at 16,000 g for 20 min at 4 ºC. The supernatant containing the soluble extract was loaded directly onto a Q-Sepharose column (GE Healthcare), equilibrated previously with 10 mM Tris buffer (pH 7.6). A salt gradient from 0 to 1 M NaCl in 10 mM Tris (pH 7.6) was applied and the fraction containing STC(D2N) was eluted at 200 mM. The final purification step was performed on a hydroxylapatite (HTP) column (Bio-Rad Laboratories), pre-equilibrated with 10 mM phosphate buffer (pH 7.6). The fraction containing STC(D2N) did not bind to the column and was eluted in the washout volume.

The chromatographic fractions were routinely analyzed by SDS-PAGE and UV–visible spectroscopy to select those containing STC(D2N). The purity of the protein was confirmed by a single band on SDS-PAGE. Pure samples present an absorption ratio A_{408nm}/A_{280nm} of approximately 4.5 in the UV-visible spectrum.

NMR sample preparation and experiments. Protein for NMR experiments was lyophilized twice using $^{2}H_2O$ (99.9 atom %). The protein was dissolved in approximately 500 μL of $^{2}H_2O$ to a final concentration of approximately 0.5 mM in 10 mM phosphate buffer at pH 7.0. The pH value reported is a direct reading without correction for the isotope effect. NMR spectra obtained before and after the lyophilization were identical, showing that the protein structure was not affected by this procedure. The NMR experiments were performed with Bruker Avance and Avance II spectrometers operating at 500 MHz (Bruker BioSpin). 2D-^{1}H-^{13}C heteronuclear multiple quantum correlation (HMQC) spectra were obtained with 2048 points covering a spectral width of 39.7 kHz in the ^{1}H dimension and 256 increments with TPPI to give a spectral width of 34 kHz in the ^{13}C

dimension, using a Δ delay fixed at 3.2 ms, with 16 scans, at a temperature of 25 ºC. 1D-^{1}H spectra were always performed before and after each 2D spectrum, in order to verify that no changes had occurred in the protein sample. Partially reduced samples were prepared by flushing out the oxygen from the NMR tube with nitrogen gas and subsequently adding controlled amounts of a freshly prepared 10 mM sodium dithionite solution using a gastight syringe. The ^{1}H spectra were calibrated using the water signal as an internal reference. The Bruker TopSpin program (Bruker BioSpin) was used to visualize and analyze the NMR spectra.

RESULTS AND DISCUSSION

Isotopic labeling of hemes using labeled dALA was originally reported by Druyan *et al.* [44] which labeled hemes of cytochromes belonging to the rat liver. Wachenfeldt *et al.* [45] and Rivera *et al.* [32] used isotopic labeled dALA to label hemes of monoheme cytochromes from Bacteria. This was achieved by expressing the protein in a minimal medium supplemented with isotopically labeled dALA. This proved the concept for this type of strategy, although expression in minimal media has a much lower yield relative to expression in complex media, such as LB. However, using this method in a complex medium would lead to expression of proteins containing hemes produced from unlabeled sources available in the medium, decreasing the efficiency of isotopic labeling. A method for isotopic labeling of multiheme cytochromes *c* using complex medium was proposed by Fernandes *et al.* [40] that uses two steps of growth. Cells are initially grown in rich medium, harvested, washed, and resuspended in minimal medium supplemented with dALA. However this procedure is experimentally cumbersome and not very efficient since the

overexpression step also occurs in minimal medium, which limits greatly the expression yields.

Although Woodward *et al.* [30] and Bryson *et al.* [33] reported strategies to isotopically label hemes, using mutants of *E. coli* incapable of synthesizing either the heme or dALA, respectively, these methods are limited with respect to the type of cytochromes that can be expressed. In particular, *c*-type cytochromes could not be obtained. Nonetheless, these developments opened the possibility of using rich media, such as LB, supplemented with heme or dALA under aerobic conditions to overexpress cytochromes.

Taking advantage of this progress, an *E. coli* mutant unable to synthesize dALA was created. The commercially available strain JM109(DE3) which had already proven its value for correctly overexpressing large multiheme cytochromes *c* efficiently was used as source organism [39]. This modified strain was then transformed with the vector pEC86 containing the *ccmABCDEFGH* (cytochrome *c* maturation) genes, that endows *E. coli* with the ability to correctly incorporate hemes in multiheme cytochromes *c*, when growing aerobically [23]. This increases the versatility of this novel Δ*hemA E. coli* strain with respect to the type of cytochromes it can express efficiently, versus previous methods [30,32,33].

Deletion of the *hemA* gene does not affect the capability of the *E. coli* strains to express multiheme cytochromes efficiently, provided that the expression medium is supplemented with dALA. This was verified by comparing the multiheme cytochrome expression in the wt *E. coli* JM109(DE3) strain containing pEC86 with the expression in the Δ*hemA E. coli* strain LS543 (Figure 5.1-A). For this, an expression vector containing a gene for the 12 kDa small tetraheme cytochrome (STC) from *S. oneidensis* MR-1, mutated in a

surface aspartate to an asparagine (D2N) was inserted in both strains. This modification does not affect the structure of the mutant *versus* native form, as determined by the pattern of the paramagnetic shifts in the NMR spectra collected in oxidized state (Figure 5.2-B,C) but is expected to affect the interaction with physiological partners due to changes in surface electrostatics [38].

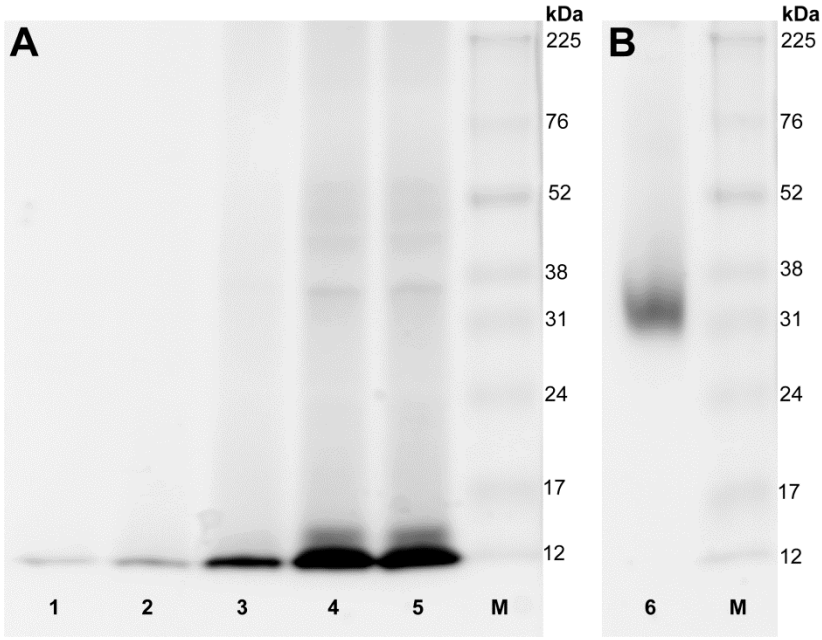

Figure 5.1. Expression tests of the different protein production strategies used. Equal amount of cell culture from the best condition of each strategy was collected and the supernatant obtained from the cell lysis is presented in the heme stained SDS-PAGE gel. For all expression strategies, 30 ºC proved to be the optimal temperature. Panel **A)** Overexpression of STC(D2N). **lane 1)** Protein expression in Δ*hemA E. coli* LS543-STC(D2N) strain using minimal medium with glucose as carbon source; **lane 2)** Protein expression in Δ*hemA E. coli* LS543-STC(D2N) strain using minimal medium with glycerol as carbon source; **lane 3)** Protein expression in Δ*hemA E. coli* LS543-STC(D2N) strain using LB medium; **lane 4)** Protein expression in Δ*hemA E. coli* LS543-STC(D2N) strain using 27 h auto-induction LB medium; **lane 5)** Protein expression in wild-type *E. coli* ROL002 strain using 27 h auto-induction in LB medium. Panel **B)** Overexpression of MtrA. **lane 6)** Protein expression in Δ*hemA E. coli* LS544 strain using 48 h auto-induction LB medium. In both panels **lane M)** corresponds to the pre-stained protein molecular weight marker.

Moreover, to confirm that the Δ*hemA E. coli* LS543 strain is capable of expressing larger and more complex multiheme cytochromes *c*, an expression vector containing the gene of the decaheme cytochrome MtrA from *S. oneidensis* MR-1 of approximately 37 kDa, was used. Figure 5.1-B shows that the resulting Δ*hemA E. coli* LS544 strain is also capable of expressing this protein, opening the door to the detailed characterization of these larger multiheme *c*-type cytochromes.

The auto-induction method developed by Studier [41] showed the best expression yields compared to the other protein expression methods tested (Figure 5.1-A). This approach has the advantage of allowing the induction to occur gradually. This gradual process is essential for correct incorporation of the hemes, and allows the cultures to reach higher cell densities, thereby increasing the protein yield. A yield of approximately 4 mg of pure STC(D2N) per liter of cell culture was obtained. To the best of our knowledge, to present date, this is the highest yield obtained for isotopically labeled multiheme cytochromes [40], and is comparable to other strategies used for overexpressing non-labeled multiheme cytochromes *c* [25,26,46].

Thus, this expression method allows the efficient production of specifically isotopic labeled hemes and also their correct incorporation into a multiheme cytochrome *c* (Figure 5.2 and Figure 5.3).

Using 1,2-^{13}C-labeled dALA, causes the incorporation of ^{13}C at the methyl groups at the periphery of the heme macrocycle and also at the *β*- and carboxylate carbons of the propionate groups (Figure 5.2-A) (See Appendix F). Figure 5.2 shows that adventitious unlabeled carbons in the methyl positions is below the detection limit of NMR experiments as can be confirmed by verifying the lack of residual peaks at the center of each doublet in spectra

obtained without ^{13}C decoupling (Figure 5.2-A). In low-spin paramagnetic cytochromes, the heme methyls are reasonably sharp and typically located in a clean spectral region in the ^{13}C dimension (Figure 5.3). This allows for a simple identification of these NMR signals that facilitates their assignment since the remainder of the protein contains ^{13}C only at natural abundance (≈ 1%).

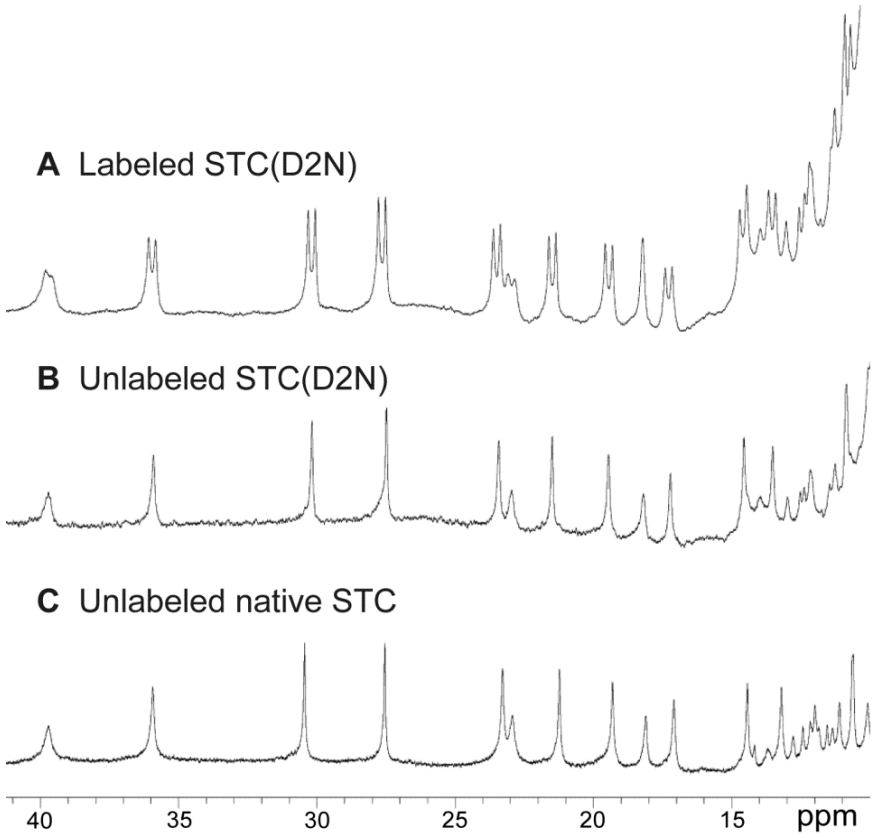

Figure 5.2. High frequency region of the 1D-^{1}H NMR spectra of STC at pH 7.0 and 25 ºC. A) Specific isotopic labeled STC(D2N) with ^{13}C incorporated in the methyl groups and also in the *β*- and carboxylate carbons of the propionate groups of the heme, overexpressed in the Δ*hemA E. coli* LS543-STC(D2N) strain. Data collected without ^{13}C decoupling; **B)** Unlabeled mutant STC(D2N) overexpressed in the Δ*hemA E. coli* LS543-STC(D2N) strain; **C)** Unlabeled native STC expressed in *S. oneidensis* MR-1.

This now opens the possibility to characterize in detail the structure and function of multiheme cytochromes containing a large number of hemes thanks to the greater spectral dispersion obtained in the ^{13}C frequency *versus* the ^{1}H frequency (Figure 5.3). The position of the heme methyl signals in low-spin paramagnetic hemes can be used to determine the orientation of the axial ligands and the placement of the magnetic axes system associated with the unpaired electron [47]. When a multiheme cytochrome is titrated, the position of the methyl signals changes in ways that can be related with the oxidized fraction allowing for the determination of the relative reduction potentials of the hemes (See Appendix D) [48]. The specific ^{13}C labeling enabled by the method reported here is further suitable for characterizing proteins of large size or containing numerous paramagnetic centers [49] because it allows the use of direct heteronuclear detection experiments such as ^{13}C-^{13}C NOESY, which may be more suitable than ^{1}H based experiments in these cases.

Also, since dALA is a versatile labeling source for hemes, with different labeled carbons in dALA, different kinds of information can be obtained. For instance, considering NMR applications, using 5-^{13}C-labeled dALA the heme carbons attached to the meso protons can be labeled. Measurements of the residual dipolar coupling (RDC) of these signals provide information on the relative spatial orientation of the hemes [50].

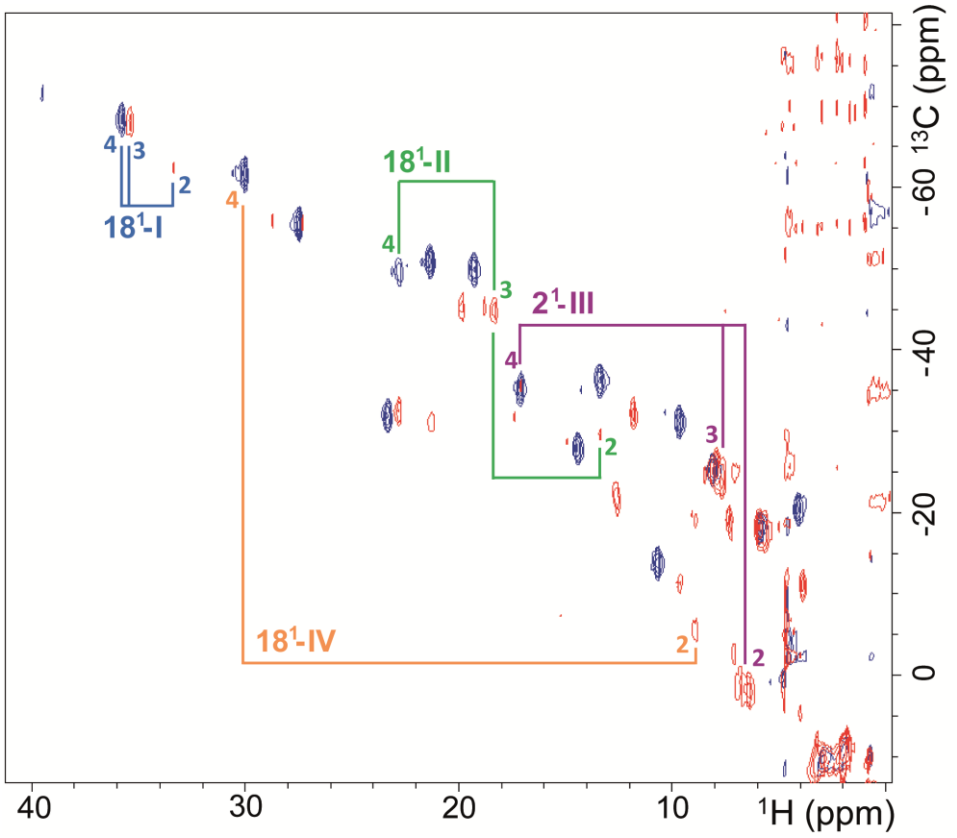

Figure 5.3. Methyl region of the 2D-^{1}H–^{13}C HMQC NMR spectra of the STC(D2N) with ^{13}C specifically incorporated in the methyl groups and also in the β- and carboxylate carbons of the propionate groups of the heme macrocycle. The blue contours correspond to the fully oxidized sample and the red contours correspond to the partially reduced sample. In the partially reduced spectrum, signals resulting from cytochromes containing different number of oxidized hemes that coexist in solution can be observed because intermolecular electron exchange is slow. In order to not overcrowd the figure only one methyl signal for each heme of STC(D2N) is labeled. The methyl group from each heme was identified using the IUPAC nomenclature (18^{1}CH$_3$-I; 18^{1}CH$_3$-II; 2^{1}CH$_3$-III; 18^{1}CH$_3$-IV); in the different stages of oxidation (4, 3, and 2). Stage numbers correspond to the number of oxidized hemes in the protein where the signal arises, with 4 being the fully oxidized protein. The Roman numerals correspond to the four hemes in the cytochrome, numbered according to the order of the CXXCH attachment to the polypeptide chain.

A further general advantage of the method described here when applied to NMR spectroscopy is that the need for a highly concentrated sample or even, a pure sample, may be eliminated. Under aerobic conditions *E. coli* only expresses the cytochrome of interest, assuring the specific and efficient use of the labeled dALA in the biosynthesis of the hemes for this protein. Therefore, the ^{13}C NMR spectrum is dominated by the signals of the labeled hemes. This advantage may facilitate the future characterization of multiheme *c*-type cytochromes that are difficult to express and purify, such as those associated to cell membranes, and may also allow the *in cell* characterization of cytochromes.

In conclusion, a strategy to efficiently produce multiheme cytochromes labeled at selected carbons in the hemes was developed. The simplicity of the method and its ability to produce isotopically labeled multiheme *c*-type cytochromes with a yield comparable to that obtained from the expression of unlabeled proteins, makes this approach potentially applicable to many different heme proteins. This is true even for those cytochromes that are not of the *c*-type and therefore dispense the need for covalent attachment of the heme to the polypeptide chain. The methodology will also enable the detailed structural and functional characterization of large multiheme cytochromes. A detailed characterization of these proteins, which mediate microbe-mineral or microbe-electrode contact, is essential to develop rationally designed bioelectrochemical devices and bioengineered systems for bioenergy production and bioremediation of environmental contaminants [13].

ACKNOWLEDGEMENTS

The plasmid pEC86 used in this work was a gift from Prof. L Thöny-Meyer. BMF is the recipient of a PhD fellowship from Fundação para a Ciência e Tecnologia (FCT) (SFRH/BD/41205/2007). LS was supported by the Subsurface Biogeochemical Research program/Office of Biological and Environmental Research, U.S. Department of Energy. Research in the author's laboratories was supported by grants PTDC/BIA-PRO 098158/2008, MIT-Pt BS-BB/1014/2008 from FCT awarded to ROL, and a grant from the National Science Foundation (MCB-0818488) awarded to MR. This work was also supported by FCT through grant PEst-OE/EQB/LA0004/2011. The NMR data were collected at The Portuguese National NMR Network (REDE/1517/RMN/2005), supported by "Programa Operacional Ciência e Inovação (POCI) 2010" and FCT.

REFERENCES

[1] **Brunori, M.** 1999. Hemoglobin is an honorary enzyme. Trends Biochem Sci *24*:158-161.

[2] **Paquete, C.M. and R.O. Louro.** 2010. Molecular details of multielectron transfer: the case of multiheme cytochromes from metal respiring organisms. Dalton Trans *39*:4259-4266.

[3] **Rodgers, K.R. and G.S. Lukat-Rodgers.** 2004. Electron Transfer: Cytochromes, p. 17-60. *In* J. McCleverty, and T.J. Meyer (Eds.), Comprehensive Coordination Chemistry II. Pergamon press, Oxford.

[4] **Gray, H.B. and J.R. Winkler.** 2010. Electron flow through metalloproteins. Biochim Biophys Acta *1797*:1563-1572.

[5] **Konstantinov, A.A.** 2012. Cytochrome *c* oxidase: Intermediates of the catalytic cycle and their energy-coupled interconversion. FEBS Lett *586*:630-639.

[6] **Yoshikawa, S., K. Muramoto, and K. Shinzawa-Itoh.** 2011. Proton-pumping mechanism of cytochrome *c* oxidase. Annu Rev Biophys *40*:205-223.

[7] **Poulos, T.L.** 2010. Thirty years of heme peroxidase structural biology. Arch Biochem Biophys *500*:3-12.

[8] **Rittle, J. and M.T. Green.** 2010. Cytochrome P450 compound I: capture, characterization, and C-H bond activation kinetics. Science *330*:933-937.

[9] **Poulos, T.L.** 1995. Cytochrome P450. Curr Opin Struct Biol *5*:767-774.

[10] **Wade, R.C., D. Motiejunas, K. Schleinkofer, Sudarko, P.J. Winn, A. Banerjee, A. Kariakin, and C. Jung.** 2005. Multiple molecular recognition mechanisms. Cytochrome P450 - a case study. Biochim Biophys Acta *1754*:239-244.

[11] **Pokkuluri, P.R., M. Pessanha, Y.Y. Londer, S.J. Wood, N.E. Duke, R. Wilton, T. Catarino, C.A. Salgueiro, and M. Schiffer.** 2008. Structures and solution properties of two novel periplasmic sensor domains with c-type heme from chemotaxis proteins of *Geobacter sulfurreducens*: implications for signal transduction. J Mol Biol *377*:1498-1517.

[12] **Lovley, D.R.** 2006. Bug juice: harvesting electricity with microorganisms. Nat Rev Microbiol *4*:497-508.

[13] **Summers, Z.M., H.E. Fogarty, C. Leang, A.E. Franks, N.S. Malvankar, and D.R. Lovley.** 2010. Direct exchange of electrons within aggregates of an evolved syntrophic coculture of anaerobic bacteria. Science *330*:1413-1415.

[14] **Sharma, S., G. Cavallaro, and A. Rosato.** 2010. A systematic investigation of multiheme *c*-type cytochromes in prokaryotes. J Biol Inorg Chem *15*:559-571.

[15] **Londer, Y.Y., S.E. Giuliani, T. Peppler, and F.R. Collart.** 2008. Addressing *Shewanella oneidensis* "cytochromome": the first step towards high-throughput expression of cytochromes *c*. Protein Expr Purif *62*:128-137.

[16] **Alves, A.S., C.M. Paquete, B.M. Fonseca, and R.O. Louro.** 2011. Exploration of the 'cytochromome' of *Desulfuromonas acetoxidans*, a marine bacterium capable of powering microbial fuel cells. Metallomics *3*:349-353.

[17] **Lovley, D.R.** 2006. Microbial fuel cells: novel microbial physiologies and engineering approaches. Curr Opin Biotechnol *17*:327-332.

[18] **Xuan, J., X.-D. Jia, L.-P. Jiang, E.S. Abdel-Halim, and J.-J. Zhu.** 2012. Gold nanoparticle-assembled capsules and their application as hydrogen peroxide biosensor based on hemoglobin. Bioelectrochemistry *84*:32-37.

[19] **Schulz, H., R.A. Fabianek, E.C. Pellicioli, H. Hennecke, and L. Thony-Meyer.** 1999. Heme transfer to the heme chaperone CcmE during cytochrome c maturation requires the CcmC protein, which may function independently of the ABC-transporter CcmAB. Proc Natl Acad Sci USA *96*:6462-6467.

[20] **Stevens, J.M., D.A. Mavridou, R. Hamer, P. Kritsiligkou, A.D. Goddard, and S.J. Ferguson.** 2011. Cytochrome *c* biogenesis system I. FEBS J *278*:4170-4178.

[21] **Feissner, R.E., C.L. Richard-Fogal, E.R. Frawley, J.A. Loughman, K.W. Earley, and R.G. Kranz.** 2006. Recombinant cytochromes *c* biogenesis systems I and II and analysis of haem delivery pathways in *Escherichia coli*. Mol Microbiol *60*:563-577.

[22] **Kranz, R.G., C. Richard-Fogal, J.S. Taylor, and E.R. Frawley.** 2009. Cytochrome *c* biogenesis: mechanisms for covalent modifications and trafficking of heme and for heme-iron redox control. Microbiol Mol Biol Rev *73*:510-528.

[23] **Arslan, E., H. Schulz, R. Zufferey, P. Kunzler, and L. Thony-Meyer.** 1998. Overproduction of the *Bradyrhizobium japonicum c*-type cytochrome subunits of the *cbb*$_3$ oxidase in *Escherichia coli*. Biochem Biophs Res Commun *251*:744-747.

[24] **Londer, Y.Y.** 2011. Expression of recombinant cytochromes *c* in *E. coli*. Methods Mol Biol *705*:123-150.

[25] **Ozawa, K., A.I. Tsapin, K.H. Nealson, M.A. Cusanovich, and H. Akutsu.** 2000. Expression of a tetraheme protein, *Desulfovibrio vulgaris* Miyazaki F cytochrome c_3, in *Shewanella oneidensis* MR-1. Appl Environ Microbiol *66*:4168-4171.

[26] **Shi, L., J.T. Lin, L.M. Markillie, T.C. Squier, and B.S. Hooker.** 2005. Overexpression of multi-heme *c*-type cytochromes. BioTechniques *38*:297-299.

[27] **Pollock, W.B., M. Loutfi, M. Bruschi, B.J. Rapp-Giles, J.D. Wall, and G. Voordouw.** 1991. Cloning, sequencing, and expression of the gene encoding the high-molecular-weight cytochrome *c* from *Desulfovibrio vulgaris* Hildenborough. J Bacteriol *173*:220-228.

[28] **Kern, M. and J. Simon.** 2011. Production of recombinant multiheme cytochromes *c* in *Wolinella succinogenes*. Methods Enzymol *486*:429-446.

[29] **Park, I. and B.C. Kim.** 2011. Homologous overexpression of omcZ, a gene for an outer surface *c*-type cytochrome of *Geobacter sulfurreducens* by single-step gene replacement. Biotechnol Lett *33*:2043-2048.

[30] **Woodward, J.J., N.I. Martin, and M.A. Marletta.** 2007. An *Escherichia coli* expression-based method for heme substitution. Nat Methods *4*:43-45.

[31] **Schiött, T., M. Throne-Holst, and L. Hederstedt.** 1997. *Bacillus subtilis* CcdA-defective mutants are blocked in a late step of cytochrome *c* biogenesis. J Bacteriol *179*:4523-4529.

[32] **Rivera, M. and F.A. Walker.** 1995. Biosynthetic preparation of isotopically labeled heme. Anal Biochem *230*:295-302.

[33] **Bryson, D., P.L. Lim, A. Lawson, S. Manjunath, and G.M. Raner.** 2011. Isotopic labeling of the heme cofactor in cytochrome P450 and other heme proteins. Biotechnol Lett *33*:2019-2026.

[34] **Chen, W., C.S. Russell, Y. Murooka, and S.D. Cosloy.** 1994. 5-Aminolevulinic acid synthesis in *Escherichia coli* requires expression of *hemA*. J Bacteriol *176*:2743-2746.

[35] **Bunce, R.A., C.L. Schilling III, and M. Rivera.** 1997. Synthesis of [1,2-^{13}C]- and [2,3-^{13}C]-labeled δ-aminolevulinic acid. J Labelled Comp Radiopharm *39*:669–675.

[36] **Rivera, M. and G.A. Caignan.** 2004. Recent developments in the ^{13}C NMR spectroscopic analysis of paramagnetic hemes and heme proteins. Anal Bioanal Chem *378*:1464-1483.

[37] **Datsenko, K.A. and B.L. Wanner.** 2000. One-step inactivation of chromosomal genes in *Escherichia coli* K-12 using PCR products. Proc Natl Acad Sci U S A *97*:6640-6645.

[38] **Qian, Y., C.M. Paquete, R.O. Louro, D.E. Ross, E. Labelle, D.R. Bond, and M. Tien.** 2011. Mapping the iron binding site(s) on the small tetraheme cytochrome of *Shewanella oneidensis* MR-1. Biochemistry *50*:6217-6224.

[39] **Pitts, K.E., P.S. Dobbin, F. Reyes-Ramirez, A.J. Thomson, D.J. Richardson, and H.E. Seward.** 2003. Characterization of the *Shewanella oneidensis* MR-1

decaheme cytochrome MtrA: expression in *Escherichia coli* confers the ability to reduce soluble Fe(III) chelates. J Biol Chem *278*:27758-27765.

[40] **Fernandes, A.P., I. Couto, L. Morgado, Y.Y. Londer, and C.A. Salgueiro.** 2008. Isotopic labeling of *c*-type multiheme cytochromes overexpressed in *E. coli*. Protein Expr Purif *59*:182-188.

[41] **Studier, F.W.** 2005. Protein production by auto-induction in high density shaking cultures. Protein Expr Purif *41*:207-234.

[42] **Zal, F., T. Harnois, M. Rousselot, and H. Rogniaux.** 2009. High-level production of recombinant *Arenicola marina* globin chains in *Escherichia Coli*: A new generation of blood substitute. Artificial Cells, Blood Substitutes and Biotechnol *37*:106-116.

[43] **Francis, R.T., Jr. and R.R. Becker.** 1984. Specific indication of hemoproteins in polyacrylamide gels using a double-staining process. Anal Biochem *136*:509-514.

[44] **Druyan, R., Debernar.B, and Rabinowi.M.** 1969. Turnover of cytochromes labeled with delta-aminolevulinic acid-^{3}H in rat liver. J Biol Chem *244*:5874-5878.

[45] **von Wachenfeldt, C. and L. Hederstedt.** 1990. *Bacillus subtilis* 13-Kilodalton cytochrome *c*-550 encoded by *ccc*A consists of a membrane-anchor and a heme domain. J Biol Chem *265*:13939-13948.

[46] **Londer, Y.Y., P.R. Pokkuluri, J. Erickson, V. Orshonsky, and M. Schiffer.** 2005. Heterologous expression of hexaheme fragments of a multidomain cytochrome from *Geobacter sulfurreducens* representing a novel class of cytochromes *c*. Protein Expr Purif *39*:254-260.

[47] **Louro, R.O., I.J. Correia, L. Brennan, I.B. Coutinho, A.V. Xavier, and D.L. Turner.** 1998. Electronic structure of low-spin ferric porphyrins: ^{13}C NMR studies of the influence of axial ligand orientation. J Am Chem Soc *120*:13240-13247.

[48] **Salgueiro, C.A., D.L. Turner, H. Santos, J. LeGall, and A.V. Xavier.** 1992. Assignment of the redox potentials to the four haems in *Desulfovibrio vulgaris* cytochrome c_3 by 2D-NMR. FEBS Lett *314*:155-158.

[49] **Bertini, I., I.C. Felli, R. Kummerle, D. Moskau, and R. Pierattelli.** 2004. ^{13}C-^{13}C NOESY: an attractive alternative for studying large macromolecules. J Am Chem Soc *126*:464-465.

[50] **Erbil, W.K., M.S. Price, D.E. Wemmer, and M.A. Marletta.** 2009. A structural basis for H-NOX signaling in *Shewanella oneidensis* by trapping a histidine kinase inhibitory conformation. Proc Natl Acad Sci USA *106*:19753-19760.

CHAPTER VI

Future perspectives and concluding remarks

FUTURE PERSPECTIVES AND CONCLUDING REMARKS

The ability to transfer electrons to insoluble substrates is thought to be as old as Life itself [1,2]. These ancient redox cycles sustain nowadays microbial metabolism in more specialized niches and have only recently started to be a focus of interest by the scientific community due to their potential application in several biotechnologies. Using as model organisms bacteria from the *Geobacter* and *Shewanella* genera, our understanding on how extracellular electron transfer occurs has increased greatly over this past decade [3-13]. Here, multiheme *c*-type cytochromes have continuously revealed themselves as key players, creating an efficient redox network that stretches from the cytoplasmic membrane, across the periplasmic space and through the outer-membrane, transferring electrons directly or indirectly to their insoluble acceptors. In this thesis, various *c*-type cytochromes from the periplasmic space of *S. oneidensis* MR-1 were studied in order to try to unravel the mystery of how electrons travel between the cellular membranes during extracellular electron transfer.

Of the possible periplasmic candidates, some such as the cytoplasmic membrane tetraheme cytochrome *c*, CymA, and the decaheme outer-membrane associated cytochrome *c*, MtrA, have been shown unequivocally to be involved in extracellular electron transfer through knock-out mutants [14-16] and transcriptional studies [17]. Studies involving *in vitro* assays have shown that electron transfer can occur between these two multiheme cytochromes and several publications have postulated a direct electron transfer route between CymA and MtrA [3,18,19]. This process seems quite unlikely to happen within the bacterial cell. Firstly, the periplamic space of *S. oneidensis* MR-1 is approximately 235 Å wide [20], which creates a gap that both MtrA

(with a length of 104 Å [21]) and CymA (with a length of approximately 40 Å; measured using a theoretical structural model of CymA based on the homology with the protein structure of NrfH (PDB code 2J7A)) combined cannot bridge. Secondly, both cytochromes are bound to their respective membranes, CymA by its anchoring helix [22] and MtrA due to the formation of a stable protein complex (dissociation constant smaller than 0.1 μM) with the outer-membrane proteins MtrB (*β*-barrel protein) and MtrC (decaheme cytochrome) [23,24]. Therefore, additional redox proteins are necessary to establish the transfer of electrons across the periplasmic space.

Other periplasmic *c*-type cytochromes that also showed up-regulation during growth conditions involving extracellular electron transfer [17] were chosen as potential candidates to bridge the gap between CymA and MtrA.

The periplasmic monoheme cytochrome c_5 (ScyA), which is highly abundant during extracellular electron transfer to iron compounds and electrodes [17,25], was used in interaction assays to verify if it could interact with MtrA. This interaction was not observed. Also, interactions between ScyA and two other up-regulated periplasmic cytochromes [17,18], the small tetraheme cytochrome *c* (STC) and the tetraheme flavocytochrome *c* (FccA), were shown here not to occur [26]. These results suggest that ScyA has no role in extracellular electron transfer and help solidify the suggestion made by Schutz, B. *et al.* [25] that ScyA shuttles specifically electrons between CymA and the diheme cytochrome *c* peroxidase (CcpA). Those authors verified that ScyA was capable of interaction with both, CymA and CcpA, while CcpA was incapable of interaction with other periplasmic cytochromes (CymA, MtrA, and FccA) besides the ScyA.

The question that arises is why then would *S. oneidensis* MR-1 produce high quantities of ScyA under conditions that require extracellular electron

transfer to metals or electrodes? *S. oneidensis* was isolated from aquatic sediments within the oxic/anoxic interface rich in iron compounds [27,28]. These environmental conditions are prosperous for reactive oxygen species to be formed via the Fenton reaction. Thus, it seems to be of extreme advantage for *S. oneidensis* MR-1 to have a specific electron transport chain composed of highly abundant cytochromes, powered with electrons from the menaquinol pool, in order to guarantee a rapid detoxification of the periplasmic space and possibly even use hydrogen peroxide as a terminal electron acceptor.

The tetraheme cytochrome STC, which had been until now only postulated as an electron shuttle between CymA and MtrA [3,29], was shown here for the first time to interact with both these redox partners [26]. Also, another highly abundant tetraheme cytochrome, the FccA, was shown to interact with these redox proteins (CymA and MtrA) [26] while not interacting with its highly abundant periplasmic companion STC. Thus, establishing what seems to be two separate electron transfer pathways from CymA to the outer-membrane cytochrome MtrA. The existence of these two possible pathways seems to justify why single gene knock-out mutations of these cytochromes have failed to confirm a phenotype in metal reduction [30-32]. To confirm this and verify if these two cytochromes are the only ones capable of transferring electrons to the outer-membrane decaheme cytochrome MtrA, double gene knock-out mutations would have to be performed.

Dissociation constants (K_d) for the previous pairwise interactions were obtained in this work [26]. K_d values for the interactions with CymA (CymA-STC; CymA-FccA) had the same order of magnitude. This similarity between the values maybe indicative of CymA's function as a periplasmic electron hub, transferring electrons to several redox partners belonging to different respiratory chains [33,34] or perhaps due to the structural similarities between

STC and the heme domain of FccA [35]. To try to comprehend better this matter, further interaction experiments between CymA and its other redox partners, such as ScyA, should be performed to verify if K_d values are kept similar or if there is higher affinity to some over others.

Interactions with MtrA gave rise to K_d values with one order of magnitude difference between the STC-MtrA and the FccA-MtrA interaction, with the last one being the smaller. The higher affinity of FccA towards MtrA was a surprising result since this flavocytochrome *c* was shown to be the unique fumarate reductase in the *Shewanella* genus [22,36]. The potential key role of this cytochrome in extracellular metal reduction was also argued in Schutz, B. *et al.* [18], where a bidirectional electron transfer between FccA and MtrA was observed. Hence, it seems that FccA could be the electron shuttle between CymA and MtrA, having a dual function within the periplasm of *S. oneidensis* MR-1. The fact that the availability of exogenous fumarate is usually low in the sedimentary environments in which these species predominate [37,38] and that the reduction of iron species is generally thermodynamically more favorable (Table 6.1), allows the proposal that electrons ought to preferably flow from CymA to FccA and subsequently to MtrA. Only in situations where less thermodynamically favorable metal oxides are available should fumarate, if present, be reduced by FccA. During fumarate reduction, this cytochrome is kept reduced by receiving electrons from CymA (reduced by the menaquinol pool) or from MtrA (previously reduced by STC or FccA) [18,36]. Ross, D.E. *et al.* [36] showed that electron transfer to FccA occurs primarily through CymA instead of MtrA. This info is inconsistent with the binding data reported in this thesis, where a higher affinity of FccA towards MtrA (one order of magnitude larger than with CymA) was observed. This could be due to the experimental approach used by Ross, D.E. *et al.* [36], where

electrons are forced into the bacterial cell by an electrode poised at −0.36 V versus standard hydrogen electrode (SHE). These growth conditions are more suitable for metal oxidizers than for metal reducers (*e.g. Shewanella* and *Geobacter* genera) [39,40]. In the *Shewanella* genus, multiheme cytochromes have evolved to be more favorable for "downhill" electron flow towards the extracellular insoluble acceptors [41], which limits the driving force for electrons to flow inwards. This makes the transfer of electrons from MtrA to FccA less efficient, even though FccA has a higher affinity towards MtrA in comparison with CymA.

Table 6.1. Reduction potentials and free energies of relevant reduction pairs. E_{env}* indicates environmentally relevant midpoint potentials: pH 7 except where noted, standard concentrations except for solid iron minerals, for which Fe^{2+} concentration is assumed to be 100 μM. ΔG calculations assume standard conditions and pH 7, except in the case of iron minerals, where Fe^{2+} concentration is 100 μM. Adapted from [40].

Terminal electron acceptors	E_{env}* (V)	ΔG (kJ mol^{-1})
Fumarate/succinate	+0.033	–6.4
Fe^{3+}/Fe^{2+} (pH 2)	+0.77	–74.2
Fe(III)-citrate/Fe(II)-citrate	+0.385	–37.1
Fe(III)-NTA/Fe(II)-NTA	+0.372	–35.9
Ferrihydrite $_{(solid)}/Fe^{2+}$	+0.1 to –0.1	–9.6 to 9.6
α-FeOOH $_{(solid)}/Fe^{2+}$	–0.274	26.4
α-$Fe_2O_{3\ (solid)}/Fe^{2+}$	–0.287	55.4
$Fe_3O_{4\ (solid)}/Fe^{2+}$	–0.314	60.6

The pairwise cytochrome complex STC-MtrA, although having a much smaller affinity could still occur *in vivo* due to the high abundance of STC in the periplasmic space. Both STC and FccA have a very similar reduction potential range [42,43]. Thus, STC seems be able to maintain an efficient and rapid electron flow from CymA to MtrA in situations where FccA for some

given reason is unable (*e.g.* knock-out mutation). Another option is that STC is involved in other extracellular electron transfer pathways that use paralogs of MtrA [44]. The high homology between these decaheme cytochromes (MtrA; MtrD; DmsE; SO4360) and the fact that they can compensate knock-out mutants of each other, by forming a hybrid protein complex with their homologue's subunits [15], is indicative of similar docking sites in these cytochromes. To test if STC has a higher affinity towards one of these decaheme cytochromes, further interaction studies should be done with the different possible combinations of STC/MtrA paralog. These MtrA paralog interaction studies should also be perform using FccA, to try to verify if specificity exists in the periplasmic electron transfer step of the different extracellular electron transfer pathways of *S. oneidensis* MR-1.

Moreover, to make all the interaction studies mentioned above more biologically relevant, reconstitution of decaheme cytochrome MtrA (or its paralogs) with its respective β-barrel protein in phospholipid bilayer nanodiscs could be done. This provides a more native environment to the decaheme cytochrome. Similarly, interaction studies with CymA stand to benefit from the use of phospholipid bilayer nanodiscs, avoiding the addition of detergent which has been shown to affect its protein structure [45].

In this thesis, it was also shown that both STC and FccA, re-orient themselves to present always the same heme (heme IV in the case of STC and heme II in the case of FccA) for interaction, avoiding the formation of ternary complexes. Previously published data had already indicated this possibility in the case of STC [46]. To gain some insight on the docking site of their membrane redox partners (e.g. CymA and MtrA) and verify if the same site is used for both STC and FccA or if specific docking sites exist, competitive binding assays should be done.

The present lack of thermodynamic and kinetic knowledge on most of the multiheme cytochromes involved in extracellular electron transfer has limited the ability to fully understand how this challenging process occurs.

In the case of STC, kinetic studies were done by Paquete C.M. *et al.* [46] while a detailed thermodynamic characterization was performed and presented here in this thesis [42]. The determination of the microscopic thermodynamic properties of STC showed that its hemes are capable of receiving and transferring electrons between CymA and MtrA [41]. Also, it showed that the redox–Bohr interactions are the aggregate effect of several acid–base groups and that electrostatics dominate the heme–heme interactions. In addition, these last interactions were shown to play a major role in the modulation of the thermodynamic properties of STC, allowing only a few of the multiple microscopic redox states that this protein can access to be significantly populated at physiological pH (electrons populate the hemes in the following order: heme III, heme IV, heme II and finally heme I).

The microscopic thermodynamic properties of STC reported in this thesis were compared with other thermodynamic data from multiheme cytochromes belonging to *Shewanella* and other genera, where it was possible to observe that in all cases heme-heme intramolecular interactions seem to play an important role in controlling how electrons flow through and are distributed among the hemes [47]. As a consequence, hemes not only require to be located at the correct distance from each other to guarantee rapid electron transfer [48,49] but also to ensure an interaction magnitude that can significantly modulate their intrinsic reduction potentials and establish the biological function of the protein. These two constraints deeply reduce the spatial organization possibilities of the hemes within the protein.

To date no detailed thermodynamic characterization of CymA and MtrA has been obtained. This mainly has to do with the lower spectral discrimination of these proteins compared to the previous multiheme cytochromes (STC and FccA) (Figure 6.1).

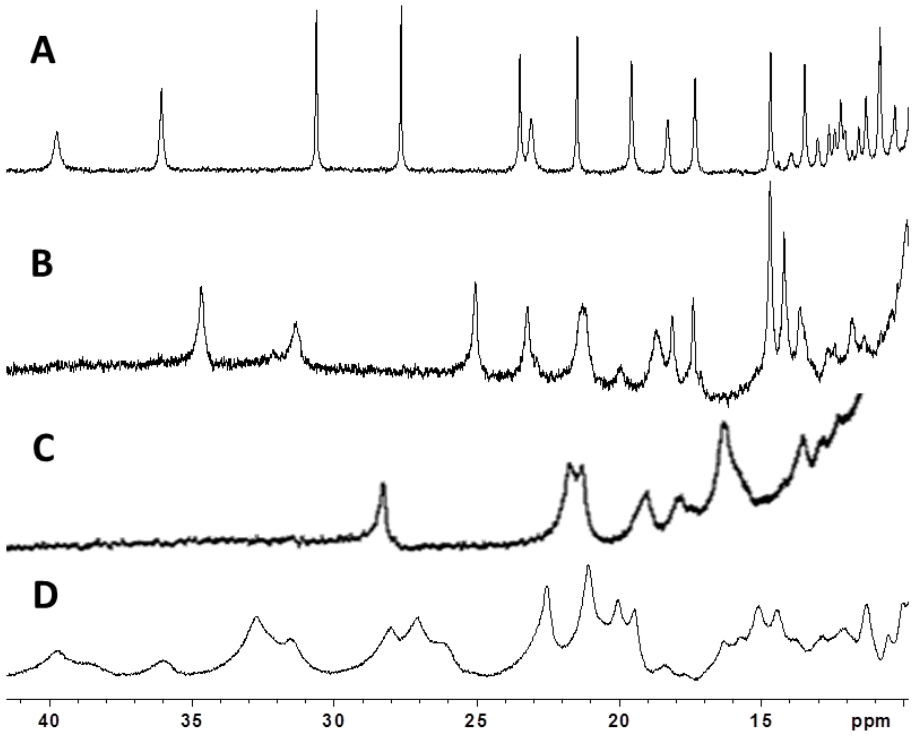

Figure 6.1. Comparison of ^{1}H-NMR spectral quality for various multiheme cytochromes. A) STC with 12 kDa and containing four hemes; **B)** FccA with 64 kDa and four hemes; **C)**. CymA with 21 kDa and containing four hemes, solubilized with 0.03 % DDM detergent; **D)** MtrA with 37 kDa and containing ten hemes.

Figure 6.1 shows that while the NMR spectrum of STC (12kDa; 4 hemes) gives origin to sharp well dispersed heme methyl signals (Figure 6.1-A), in the case of FccA (64 kDa; 4 hemes) these signals are much broader (Figure 6.1-B). This line broadening of the signals is owed to the slower tumbling time of this

larger cytochrome. Slow tumbling times leads to a more rapid decay of the NMR signal due to fast relaxation of the magnetization.

Although CymA (21 kDa; 4 hemes) is much smaller than FccA, the use of detergents (which form large micelles) to solubilize this cytoplasmic membrane bound cytochrome gives rise to a very large particle. Thus, NMR spectra of this multiheme cytochrome have poorly resolved heme methyl signals (Figure 6.1-C), making its thermodynamic characterization very difficult.

The case of MtrA (37 kDa; 10 hemes) is different from that of CymA since MtrA is only outer-membrane associated and is soluble without the addition of surfactants. The reason for the poorer spectral resolution compared to NMR spectra obtained with FccA (≈ 2 times the size of MtrA), is that this multiheme cytochrome has 10 hemes (Figure 6.1-D). A decaheme cytochrome has 40 heme methyl signals (4 methyl substituents per heme) in the same spectral widow as the 16 methyl signals expected for a tetraheme cytochrome. This increment in spectral complexity leads to the overlap of the majority of these signals and makes the thermodynamic characterization of this cytochrome also very challenging.

To overcome these difficulties and increase spectral resolution in more challenging multiheme cytochromes, such as CymA and MtrA, the use of ^{13}C instead of ^{1}H NMR experiments was proposed. Recent developments in NMR probe sensitivity and pulse programs for ^{13}C direct detection were shown to be successful with paramagnetic proteins [50]. These experiments although being less sensitive than ^{1}H (^{13}C nuclei has a smaller magnetic moment than ^{1}H), have a much larger chemical shift range and also give rise to sharper signals (^{13}C nuclei has a slower relaxation than ^{1}H). This makes the spectrum less crowded and greatly increases its resolution.

In order to apply this approach, isotopic ^{13}C labeling of these cytochromes is necessary to increase the experimental sensitivity (natural abundance of ^{13}C is ≈ 1 %). Up to this work, the methods described in the literature for isotopic labeling of multiheme cytochromes were not very efficient and also had the disadvantage, in this case, of labeling the entire protein and wasting expensive ^{13}C resources in regions that would not be investigated [51]. For the detailed thermodynamic characterization of these multiheme cytochromes only the NMR signals from their functional components (hemes) are analyzed, a more ingenious method is required. In this thesis a state-of-the-art method is described [52]. The method brings together tools in molecular biology, organic synthesis, and metabolic regulation to assemble a coherent and simple strategy for the efficient isotopic labeling of specific carbon atoms in the hemes of multiheme cytochromes. Also, the specific isotopic labeling of different carbons in the heme allows different kinds of information to be obtained. This opens the door for the exploration of the functional properties of these more challenging cytochromes.

Furthermore, to assist with the analysis of the spectral data obtained, site-direct mutagenesis should be performed, changing the axial coordinated distal histidine residues of the hemes to a methionine [53]. This will alter the environment around the heme and therefore the position of its signals in the NMR spectra. Comparing wild-type protein spectra with spectra obtained using the mutants will allow the distinction between signals belonging to each individual heme and their subsequent assignment. This last step is necessary for the detailed thermodynamic characterization of these complex cytochromes.

In conclusion, this thesis provides significant insights into the question of how electrons cross the periplasmic space of *S. oneidensis* in the extracellular electron transfer process. The discovery of three co-existing non-mixing redox pathways established through transient cytochrome interactions showed that electron transfer in the crowded periplasmic space of *S. oneidensis* MR-1 is carefully controlled. This happens even when the cytochromes have over-lapping thermodynamic properties, such as the case of STC (reported here) [42] and FccA [43]. Furthermore, this thesis opened the door for the functional characterization of the more challenging multiheme cytochromes, such as the membrane cytochromes involved in the extracellular electron transfer process. This final point will allow a better understanding on the how these cytochromes interact and transfer electrons with their periplasmic electron shuttles partners.

As any research work, this thesis provides only some closure to the extracellular electron transfer issue, with a lot of future work still ahead in order to completely understand this highly dynamic and complex electron transfer network.

COMMENTS ON BIOTECHNOLOGICAL APPLICATIONS

The detailed functional characterization of the multiheme cytochromes from microorganisms capable of extracellular electron transfer (*e.g. Shewanella* and *Geobacter* genera) will ultimately lead to more rational design and optimized biotechnological applications which use these organisms. This optimization can be biological or technological, using different approaches such as molecular biology to tune the reduction potentials of hemes belonging to multiheme cytochromes involved in the electron transfer pathway [54] or

surface enhancement of electrodes in MFCs [55] for contact improvement between the outer-membrane cytochromes and the electrode. Either way, all stand to benefit from the studies and methods presented in this thesis and from the full characterization of these complex electron transfer pathways.

REFERENCES

[1] **Richardson, D.J.** 2000. Bacterial respiration: a flexible process for a changing environment. Microbiol *146*:551-571.

[2] **Craddock, P.R. and N. Dauphas.** 2011. Iron and carbon isotope evidence for microbial iron respiration throughout the Archean. Earth Planet Sci Lett *303*:121–132.

[3] **Shi, L., K.M. Rosso, T.A. Clarke, D.J. Richardson, J.M. Zachara, and J.K. Fredrickson.** 2012. Molecular underpinnings of Fe(III) oxide reduction by *Shewanella oneidensis* MR-1. Front Microbiol *3*:50.

[4] **Shi, L., K.M. Rosso, J.M. Zachara, and J.K. Fredrickson.** 2012. Mtr extracellular electron-transfer pathways in Fe(III)-reducing or Fe(II)-oxidizing bacteria: a genomic perspective. Biochem Soc Trans *40*:1261-1267.

[5] **Brutinel, E.D. and J.A. Gralnick.** 2012. Shuttling happens: soluble flavin mediators of extracellular electron transfer in *Shewanella*. Appl Microbiol Biotechnol *93*:41-48.

[6] **Richter, K., M. Schicklberger, and J. Gescher.** 2012. Dissimilatory reduction of extracellular electron acceptors in anaerobic respiration. Appl Environ Microbiol *78*:913-921.

[7] **Richardson, D.J., M.J. Edwards, G.F. White, N. Baiden, R.S. Hartshorne, J. Fredrickson, L. Shi, J. Zachara, et al.** 2012. Exploring the biochemistry at the extracellular redox frontier of bacterial mineral Fe(III) respiration. Biochem Soc Trans *40*:493-500.

[8] **Richardson, D.J., J.N. Butt, J.K. Fredrickson, J.M. Zachara, L. Shi, M.J. Edwards, G. White, N. Baiden, et al.** 2012. The 'porin-cytochrome' model for microbe-to-mineral electron transfer. Mol Microbiol *85*:201-212.

[9] **Roden, E.E.** 2012. Microbial iron-redox cycling in subsurface environments. Biochem Soc Trans *40*:1249-1256.

[10] **Smith, J.A., D.R. Lovley, and P.L. Tremblay.** 2013. Outer cell curface components essential for Fe(III) oxide reduction by *Geobacter metallireducens*. Appl Environ Microbiol *79*:901-907.

[11] **Lovley, D.R.** 2012. Long-range electron transport to Fe(III) oxide via pili with metallic-like conductivity. Biochem Soc Trans *40*:1186-1190.

[12] **Aklujkar, M., M.V. Coppi, C. Leang, B.C. Kim, M.A. Chavan, L.A. Perpetua, L. Giloteaux, A. Liu, and D. Holmes.** 2013. Proteins involved in electron transfer to Fe(III) and Mn(IV) oxides by *Geobacter sulfurreducens* and *Geobacter uraniireducens*. Microbiol *doi: 10.1099/mic.0.064089-0*.

[13] **Shrestha, P.M., A.E. Rotaru, Z.M. Summers, M. Shrestha, F. Liu, and D.R. Lovley.** 2013. Transcriptomic and genetic analysis of direct interspecies electron transfer. Appl Environ Microbiol *doi: 10.1128/AEM.03837-12*.

[14] **Gao, H., S. Barua, Y. Liang, L. Wu, Y. Dong, S. Reed, J. Chen, D. Culley, et al.** 2010. Impacts of *Shewanella oneidensis c*-type cytochromes on aerobic and anaerobic respiration. Microb Biotechnol *3*:455-466.

[15] **Coursolle, D. and J.A. Gralnick.** 2012. Reconstruction of extracellular respiratory pathways for iron(III) reduction in *Shewanella oneidensis* strain MR-1. Front Microbiol *3*:56.

[16] **Bretschger, O., A. Obraztsova, C.A. Sturm, I.S. Chang, Y.A. Gorby, S.B. Reed, D.E. Culley, C.L. Reardon, et al.** 2007. Current production and metal oxide reduction by *Shewanella oneidensis* MR-1 wild type and mutants. Appl Environ Microbiol *73*:7003-7012.

[17] **Rosenbaum, M.A., H.Y. Bar, Q.K. Beg, D. Segre, J. Booth, M.A. Cotta, and L.T. Angenent.** 2012. Transcriptional analysis of *Shewanella oneidensis* MR-1 with an electrode compared to Fe(III)citrate or oxygen as terminal electron acceptor. Plos One *7*:e30827.

[18] **Schuetz, B., M. Schicklberger, J. Kuermann, A.M. Spormann, and J. Gescher.** 2009. Periplasmic electron transfer via the *c*-type cytochromes MtrA and FccA of *Shewanella oneidensis* MR-1. Appl Environ Microbiol *75*:7789-7796.

[19] **Firer-Sherwood, M.A., K.D. Bewley, J.Y. Mock, and S.J. Elliott.** 2011. Tools for resolving complexity in the electron transfer networks of multiheme cytochromes *c*. Metallomics *3*:344-348.

[20] **Dohnalkova, A.C., M.J. Marshall, B.W. Arey, K.H. Williams, E.C. Buck, and J.K. Fredrickson.** 2011. Imaging hydrated microbial extracellular polymers: comparative analysis by electron microscopy. Appl Environ Microbiol *77*:1254-1262.

[21] **Firer-Sherwood, M.A., N. Ando, C.L. Drennan, and S.J. Elliott.** 2011. Solution-based structural analysis of the decaheme cytochrome, MtrA, by small-angle X-ray scattering and analytical ultracentrifugation. J Phys Chem B *115*:11208-11214.

[22] **Schwalb, C., S.K. Chapman, and G.A. Reid.** 2002. The membrane-bound tetrahaem *c*-type cytochrome CymA interacts directly with the soluble fumarate reductase in *Shewanella*. Biochem Soc Trans *30*:658-662.

[23] **Hartshorne, R.S., C.L. Reardon, D. Ross, J. Nuester, T.A. Clarke, A.J. Gates, P.C. Mills, J.K. Fredrickson, et al.** 2009. Characterization of an electron conduit between bacteria and the extracellular environment. Proc Natl Acad Sci USA *106*:22169-22174.

[24] **Ross, D.E., S.S. Ruebush, S.L. Brantley, R.S. Hartshorne, T.A. Clarke, D.J. Richardson, and M. Tien.** 2007. Characterization of protein-protein interactions involved in iron reduction by *Shewanella oneidensis* MR-1. Appl Environ Microbiol *73*:5797-5808.

[25] **Schutz, B., J. Seidel, G. Sturm, O. Einsle, and J. Gescher.** 2011. Investigation of the electron transport chain to and the catalytic activity of the diheme cytochrome *c* peroxidase CcpA of *Shewanella oneidensis*. Appl Environ Microbiol *77*:6172-6180.

[26] **Fonseca, B.M., C.M. Paquete, S.E. Neto, I. Pacheco, C.M. Soares, and R.O. Louro.** 2013. Mind the gap: cytochrome interactions reveal electron pathways across the periplasm of *Shewanella oneidensis* MR-1. Biochem J *449*:101-108.

[27] **Hau, H.H. and J.A. Gralnick.** 2007. Ecology and biotechnology of the genus *Shewanella*. Annu Rev Microbiol *61*:237-258.

[28] **Myers, C.R. and K.H. Nealson.** 1988. Bacterial manganese reduction and growth with manganese oxide as the sole electron-acceptor. Science *240*:1319-1321.

[29] **Gordon, E.H.J., A.D. Pike, A.E. Hill, P.M. Cuthbertson, S.K. Chapman, and G.A. Reid.** 2000. Identification and characterization of a novel cytochrome c_3 from *Shewanella frigidimarina* that is involved in Fe(III) respiration. Biochem J *349*:153-158.

[30] **Bretschger, O., A. Obraztsova, C.A. Sturm, I.S. Chang, Y.A. Gorby, S.B. Reed, D.E. Culley, C.L. Reardon, et al.** 2007. Current production and metal oxide reduction by *Shewanella oneidensis* MR-1 wild type and mutants. Appl Environ Microbiol *73*:7003-7012.

[31] **Gao, H., S. Barua, Y. Liang, L. Wu, Y. Dong, S. Reed, J. Chen, D. Culley, et al.** 2010. Impacts of *Shewanella oneidensis c*-type cytochromes on aerobic and anaerobic respiration. Microb Biotechnol *3*:455-466.

[32] **Coursolle, D. and J.A. Gralnick.** 2012. Reconstruction of extracellular respiratory pathways for iron(III) reduction in *Shewanella oneidensis* strain MR-1. Front Microbiol *3*:56.

[33] **Zargar, K. and C.W. Saltikov.** 2009. Lysine-91 of the tetraheme *c*-type cytochrome CymA is essential for quinone interaction and arsenate respiration in *Shewanella sp.* strain ANA-3. Arch Microbiol *191*:797-806.

[34] **Marritt, S.J., T.G. Lowe, J. Bye, D.G. McMillan, L. Shi, J. Fredrickson, J. Zachara, D.J. Richardson, et al.** 2012. A functional description of CymA, an electron-transfer hub supporting anaerobic respiratory flexibility in *Shewanella*. Biochem J *444*:465-474.

[35] **Tsapin, A.I., I. Vandenberghe, K.H. Nealson, J.H. Scott, T.E. Meyer, M.A. Cusanovich, E. Harada, T. Kaizu, et al.** 2001. Identification of a small tetraheme cytochrome *c* and a flavocytochrome *c* as two of the principal soluble cytochromes *c* in *Shewanella oneidensis* strain MR1. Appl Environ Microbiol *67*:3236-3244.

[36] **Ross, D.E., J.M. Flynn, D.B. Baron, J.A. Gralnick, and D.R. Bond.** 2011. Towards electrosynthesis in *Shewanella*: energetics of reversing the mtr pathway for reductive metabolism. Plos One *6*:e16649.

[37] **Butler, J.E., R.H. Glaven, A. Esteve-Nunez, C. Nunez, E.S. Shelobolina, D.R. Bond, and D.R. Lovley.** 2006. Genetic characterization of a single bifunctional enzyme for fumarate reduction and succinate oxidation in *Geobacter sulfurreducens* and engineering of fumarate reduction in *Geobacter metallireducens*. J Bacteriol *188*:450-455.

[38] **Lovley, D.R. and F.H. Chapelle.** 1995. Deep Subsurface Microbial Processes. Rev Geophys *33*:365-381.

[39] **Weber, K.A., L.A. Achenbach, and J.D. Coates.** 2006. Microorganisms pumping iron: anaerobic microbial iron oxidation and reduction. Nat Rev Microbiol *4*:752-764.

[40] **Bird, L.J., V. Bonnefoy, and D.K. Newman.** 2011. Bioenergetic challenges of microbial iron metabolisms. Trends Microbiol *19*:330-340.

[41] **Firer-Sherwood, M., G.S. Pulcu, and S.J. Elliott.** 2008. Electrochemical interrogations of the Mtr cytochromes from *Shewanella*: opening a potential window. J Biol Inorg Chem *13*:849-854.

[42] **Fonseca, B.M., I.H. Saraiva, C.M. Paquete, C.M. Soares, I. Pacheco, C.A. Salgueiro, and R.O. Louro.** 2009. The tetraheme cytochrome from Shewanella oneidensis MR-1 shows thermodynamic bias for functional specificity of the hemes. J Biol Inorg Chem *14*:375-385.

[43] **Pessanha, M., E.L. Rothery, C.S. Miles, G.A. Reid, S.K. Chapman, R.O. Louro, D.L. Turner, C.A. Salgueiro, and A.V. Xavier.** 2009. Tuning of functional heme reduction potentials in *Shewanella* fumarate reductases. Biochim Biophys Acta *1787*:113-120.

[44] **Coursolle, D. and J.A. Gralnick.** 2010. Modularity of the Mtr respiratory pathway of *Shewanella oneidensis* strain MR-1. Mol Microbiol *77*:995–1008.

[45] **Louro, R.O. and C.M. Paquete.** 2012. The quest to achieve the detailed structural and functional characterization of CymA. Biochem Soc Trans *40*:1291-1294.

[46] **Paquete, C.M., I.H. Saraiva, E. Calcada, and R.O. Louro.** 2010. Molecular basis for directional electron transfer. J Biol Chem *285*:10370-10375.

[47] **Fonseca, B.M., C.M. Paquete, C.A. Salgueiro, and R.O. Louro.** 2012. The role of intramolecular interactions in the functional control of multiheme cytochromes *c*. FEBS Lett *586*:504-509.

[48] **Moser, C.C., J.L. Anderson, and P.L. Dutton.** 2010. Guidelines for tunneling in enzymes. Biochim Biophys Acta *1797*:1573-1586.

[49] **Gray, H.B. and J.R. Winkler.** 2010. Electron flow through metalloproteins. Biochim Biophys Acta *1797*:1563-1572.

[50] **Bertini, I., I.C. Felli, R. Kummerle, D. Moskau, and R. Pierattelli.** 2004. ^{13}C-^{13}C NOESY: an attractive alternative for studying large macromolecules. J Am Chem Soc *126*:464-465.

[51] **Fernandes, A.P., I. Couto, L. Morgado, Y.Y. Londer, and C.A. Salgueiro.** 2008. Isotopic labeling of *c*-type multiheme cytochromes overexpressed in *E. coli*. Protein Expr Purif *59*:182-188.

[52] **Fonseca, B.M., M. Tien, M. Rivera, L. Shi, and R.O. Louro.** 2012. Efficient and selective isotopic labeling of hemes to facilitate the study of multiheme proteins. BioTechniques Rapid Dispatches *doi: 10.2144/000113859 1-7.*

[53] **Reyes, C., F. Qian, A. Zhang, S. Bondarev, A. Welch, M.P. Thelen, and C.W. Saltikov.** 2012. Characterization of axial and proximal histidine mutations of the decaheme cytochrome MtrA from *Shewanella sp.* strain ANA-3 and implications for the electron transport system. J Bacteriol *194*:5840-5847.

[54] **Voigt, P. and E.W. Knapp.** 2003. Tuning heme redox potentials in the cytochrome *c* subunit of photosynthetic reaction centers. J Biol Chem *278*:51993-52001.

[55] **Wei, J., P. Liang, and X. Huang.** 2011. Recent progress in electrodes for microbial fuel cells. Biores Technol *102*:9335-9344.

Appendices

APPENDIX A: PERIPLASMIC *C*-TYPE CYTOCHROMES FROM *SHEWANELLA ONEIDENSIS* MR-1

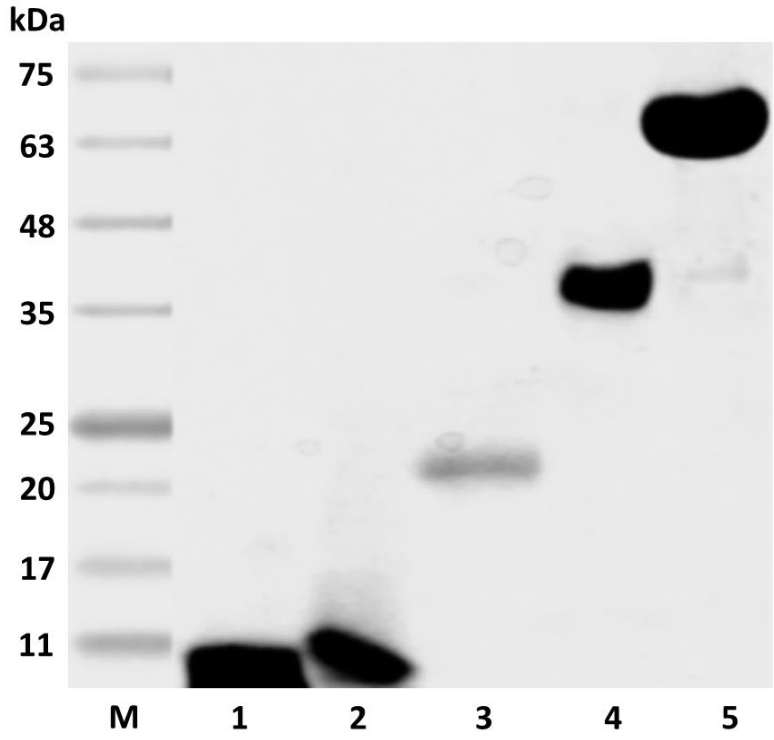

Figure A.1. 12% SDS-PAGE gel loaded with the purified periplasmic *c*-type cytochromes from *S. oneidensis* MR-1. Lane 1) monoheme cytochrome c_5 (ScyA); **Lane 2)** small tetraheme cytochrome *c* (STC); **Lane 3)** tetraheme cytochrome *c* CymA; **Lane 4)** decaheme cytochrome *c* MtrA; **Lane 5)** tetraheme flavocytochrome *c* (FccA); **Lane M)** corresponds to the protein molecular weight marker. The protein gel was double-stained using the procedure developed by Francis and Becker [1], firstly with the heme-dependent peroxidase activity protocol and secondly with the Coomassie blue staining protocol.

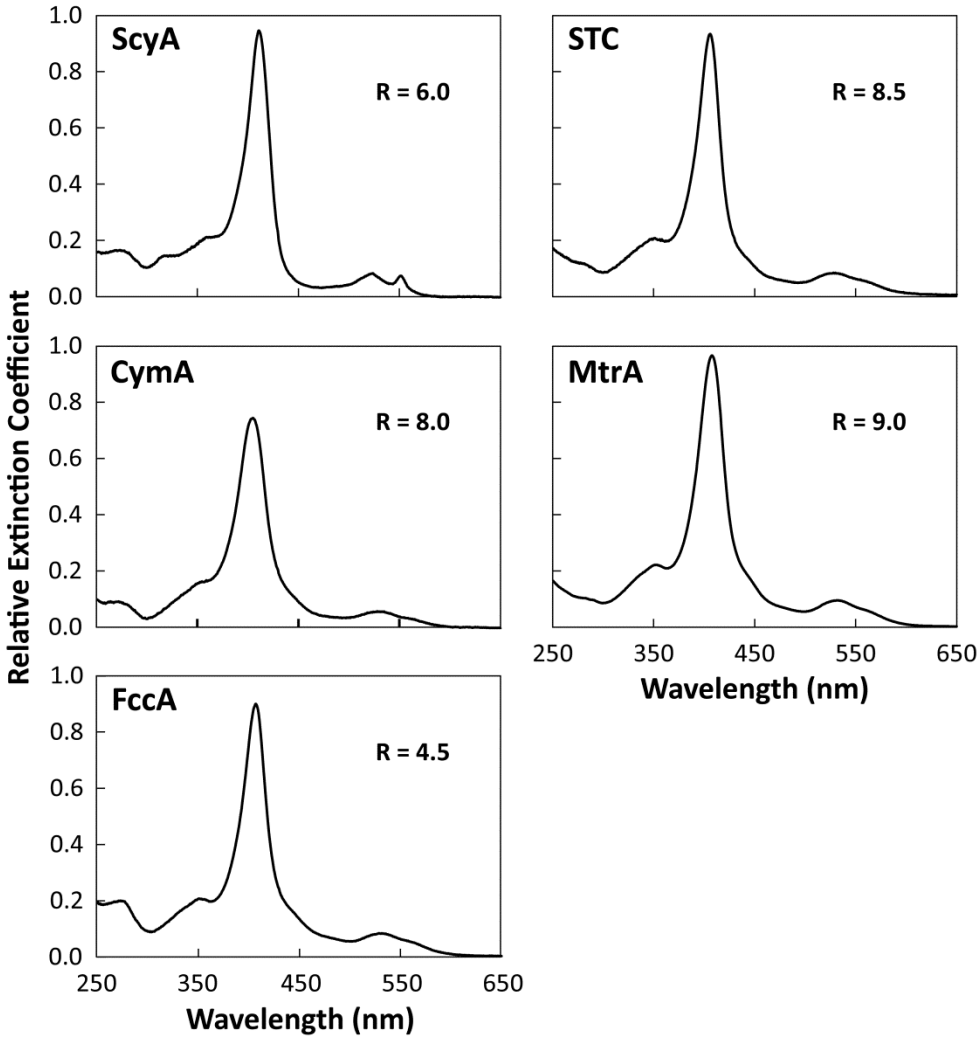

Figure A.2. UV-Visible absorption spectra of the periplasmic *c*-type cytochromes from *S. oneidensis* MR-1. All pure cytochrome samples contained 20 mM potassium phosphate buffer (pH 7.6) with an ionic strength of 100 mM adjusted by the addition of KCl. The CymA sample also contained 0.03 % DDM. The pure sample absorbance ratio (R), $A_{\text{Soret Peak}}/A_{280\text{nm}}$, is shown inside the respective panel.

APPENDIX B: BINDING MODEL EQUATION DEDUCTION

In a simple redox partner binding equilibrium, assuming that both the electron donor and acceptor have only one binding site, the equilibrium equation is represented by the following:

$$[A] + [B] \rightleftarrows [AB] \quad \text{(Eq. B.1)}$$

This thermodynamic equilibrium is characterized by the dissociation constant (K_d), which for the simplest case of a 1:1 binding redox complex is defined as:

$$K_d = \frac{[A][B]}{[AB]} \quad \text{(Eq. B.2)}$$

The terms [A], [B] and [AB] correspond to the equilibrium concentrations of non-bound protein A, non-bound protein B and the complexed state AB, respectively. K_d has the units of concentration.

Total protein concentration is given by the sum of their respective non-bound and complexed state concentrations, where $[A_T]$ and $[B_T]$ correspond to the total concentration of protein A and B, respectively.

$$[A_T] = [A] + [AB] \quad \text{(Eq. B.3)}$$

$$[B_T] = [B] + [AB] \quad \text{(Eq. B.4)}$$

These total protein concentrations are well known and are defined by the investigator during the NMR titration. Therefore, the key for the determination of K_d will be to relate the known solution composition $[A_T]$ and $[B_T]$ to the equilibrium concentrations [A], [B] and [AB].

Performing NMR experiments allows the distinction between the free non-bound protein and the bound protein state. In the case of highly dynamic systems such as transient electron transfer protein complexes, the exchange between the free and bound forms occurs at a fast rate on the NMR timescale.

Therefore, the NMR chemical shift (δ_{obs}) of the signals of the chosen observational target (*e.g.* protein A) is the mole fraction (χ) weighted average of the NMR parameters of the free (δ_A) and bound states (δ_{AB}). These mole fractions range from 0 to 1 over the course of the NMR titration.

$$\delta_{obs} = \delta_A \chi_A + \delta_{AB} \chi_{AB} \quad \text{(Eq. B.5)}$$

As mole fractions can be described as the proportion of a species present in the free or bound state relative to its total amount, it is possible to write equation B.5 as follows:

$$\delta_{obs} = \delta_A \frac{[A]}{[A_T]} + \delta_{AB} \frac{[AB]}{[A_T]} \quad \text{(Eq. B.6)}$$

Since it is not practical to express the NMR parameters in terms of absolute peak positions (δ_{obs}; δ_A; δ_{AB}), but rather in terms of changes that occur in these parameters during the NMR titration, such as the chemical shift perturbation of the NMR signals relative to the free protein state caused by the addition of an interacting redox partner. Hence:

$$\Delta\delta_{obs} = \Delta\delta_{bind} = \delta_{obs} - \delta_A \quad \text{(Eq. B.7)}$$

In the limiting case of the above expression, we have the chemical shift difference between the bound and free protein state.

$$\Delta\delta_{bind}^{\infty} = \Delta\delta_{max} = \delta_{AB} - \delta_A \quad \text{(Eq. B.8)}$$

Considering the position of the NMR signal belonging to protein A without the addition of its redox partner (free form) as the starting point for the NMR titration ($\delta_A = 0$), then equations B.7 and B.8 can be written as follows:

$$\Delta\delta_{bind} = \delta_{obs} \quad \text{(Eq. B.9)}$$

$$\Delta\delta_{bind}^{\infty} = \delta_{AB} \quad \text{(Eq. B.10)}$$

Taking into account equations B.9 and B.10 and δ_A as the reference position ($\delta_A = 0$), it is possible to write equation B.6 as follows:

$$\Delta\delta_{\text{bind}} = \Delta\delta^{\infty}_{bind}\frac{[\text{AB}]}{[\text{A}_\text{T}]} \quad \text{(Eq. B.11)}$$

Using equations B.2, B.3 and B.4, it is possible to reorganize and express the complexed state concentration [AB] as a function of $[A_T]$, $[B_T]$ and K_d, as shown next:

$$K_d = \frac{([A_T]-[AB])([B_T]-[AB])}{[AB]} \quad \text{(Eq. B.12)}$$

$$K_d = \frac{[A_T][B_T]-[A_T][AB]-[AB][B_T]+[AB]^2}{[AB]} \quad \text{(Eq. B.13)}$$

$$K_d\,[AB] = [A_T][B_T] - ([A_T] + [B_T])[AB] + [AB]^2 \quad \text{(Eq. B.14)}$$

$$0 = [A_T][B_T] - ([A_T] + [B_T] + K_d)[AB] + [AB]^2 \quad \text{(Eq. B.15)}$$

$$[AB] = \frac{([A_T]+[B_T]+K_d)-\sqrt{([A_T]+[B_T]+K_d)^2 - 4[A_T][B_T]}}{2} \quad \text{(Eq. B.16)}$$

To accurately calculate total protein concentrations ($[A_T]$; $[B_T]$) and correct for the dilution effect that occurs during the NMR titration due to the addition of small volumes of concentrated protein B to the initial solution containing protein A, the following equations were used:

$$[A_T] = \frac{[A]_0\,V_0}{V_T} \quad \text{(Eq. B.17)}$$

$$[B_T] = \frac{[B]_0\,V_{ad}}{V_T} \quad \text{(Eq. B.18)}$$

$$V_T = V_0 + V_{ad} \quad \text{(Eq. B.19)}$$

The term $[A]_0$ corresponds to the initial concentration of protein A before any addition occurs, while the term $[B]_0$ corresponds to the stock concentration of protein B. Total solution volume (V_T) is given by the sum of the initial solution volume (V_0) and the volume of concentrated protein B solution added (V_{ad}) during the titration.

Using the equations B.17 and B.18 and reorganizing them, it is possible to express total protein A concentration $[A_T]$ as a function of $[A]_0$, $[B]_0$ and the $[B_T]/[A_T]$ molar ratio (R), as shown in the following equation:

$$[A_T] = \frac{[A]_0\,[B]_0}{R\,[A]_0 + [B]_0} \quad \text{(Eq. B.20)}$$

Substituting equations B.16 and B.20 in equation B.11 and considering the $[B_T]/[A_T]$ molar ratio (R), the following equation can be obtained:

$$\Delta\delta_{bind} = \frac{1}{2}\Delta\delta^{\infty}_{bind}\left(1 + R + \frac{K_d\,(R\,[A]_0 + [B]_0)}{[A]_0\,[B]_0} - \sqrt{\left(1 + R + \frac{K_d\,(R\,[A]_0 + [B]_0)}{[A]_0\,[B]_0}\right)^2 - 4R}\right) \quad \text{(Eq. B.21)}$$

In order to simplify visually the previous equation, it is possible to consider that,

$$A = 1 + R + \frac{K_d\,(R\,[A]_0 + [B]_0)}{[A]_0\,[B]_0} \quad \text{(Eq. B.22)}$$

and write equation B.21 as follows:

$$\Delta\delta_{bind} = \frac{1}{2}\Delta\delta^{\infty}_{bind}\left(A - \sqrt{A^2 - 4R}\right) \quad \text{(Eq. B.23)}$$

This final equation was used to determine the two unknown parameters, K_d and $\Delta\delta^{\infty}_{bind}$. This was done by fitting equation B.23 to the binding curve obtained from plotting the chemical shift perturbations ($\Delta\delta_{bind}$) that occur to the NMR signals from protein A during the titration against the $[B_T]/[A_T]$ molar ratio (R). Although $\Delta\delta^{\infty}_{bind}$ can be measured directly from NMR spectrum obtained under conditions of a fully saturated binding site, this is rarely done due to the risk of introducing a greater variance in the calculated K_d value.

APPENDIX C: NMR BINDING TITRATIONS

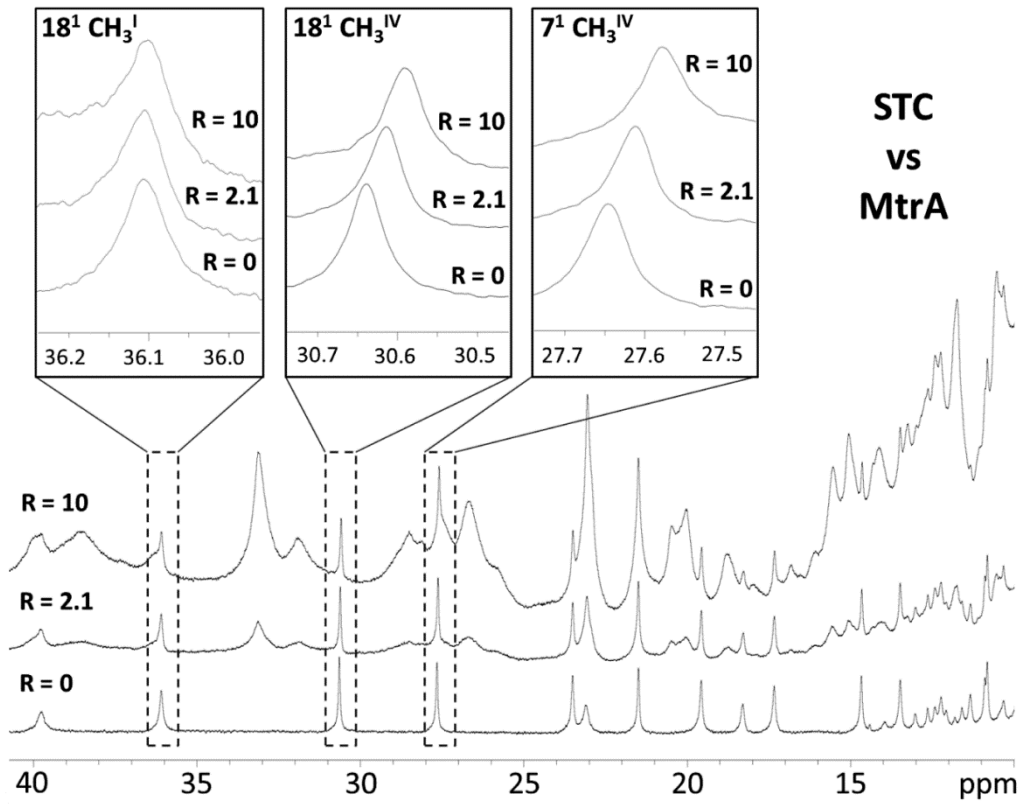

Figure C.1. ^{1}H-1D NMR spectral changes of STC in the presence of increasing amounts of MtrA. The methyl group is identified using the IUPAC-IUB nomenclature for hemes. The Roman numeral corresponds to the order of heme binding to the polypeptide chain. The R value corresponds to the molar ratio of [MtrA]/[STC]. Boxes show examples of methyl signals without significant chemical shift perturbation (18^{1}-CH_3^{I}) and with significant changes (18^{1}-CH_3^{IV}; 7^{1}-CH_3^{IV}).

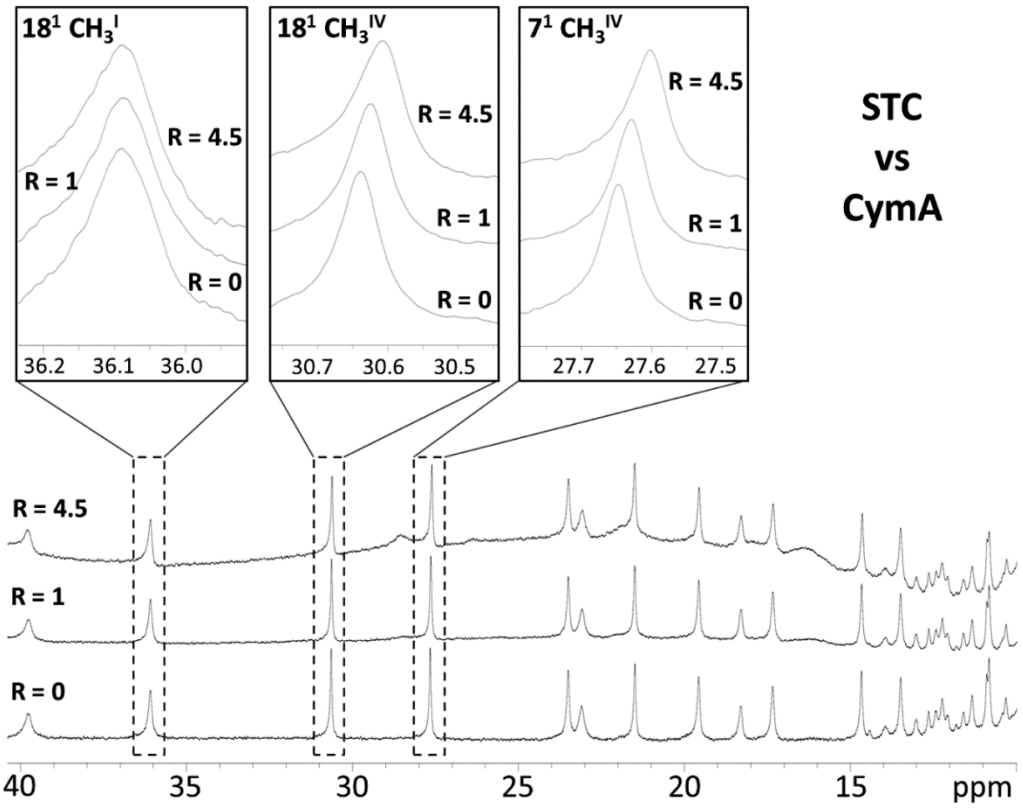

Figure C.2. ^{1}H-1D NMR spectral changes of STC in the presence of increasing amounts of CymA. The methyl group is identified using the IUPAC-IUB nomenclature for hemes. The Roman numeral corresponds to the order of heme binding to the polypeptide chain. The R value corresponds to the molar ratio of [CymA]/[STC]. Boxes show examples of methyl signals without significant chemical shift perturbation (18^{1}-CH_3^{I}) and with significant changes (18^{1}-CH_3^{IV}; 7^{1}-CH_3^{IV}).

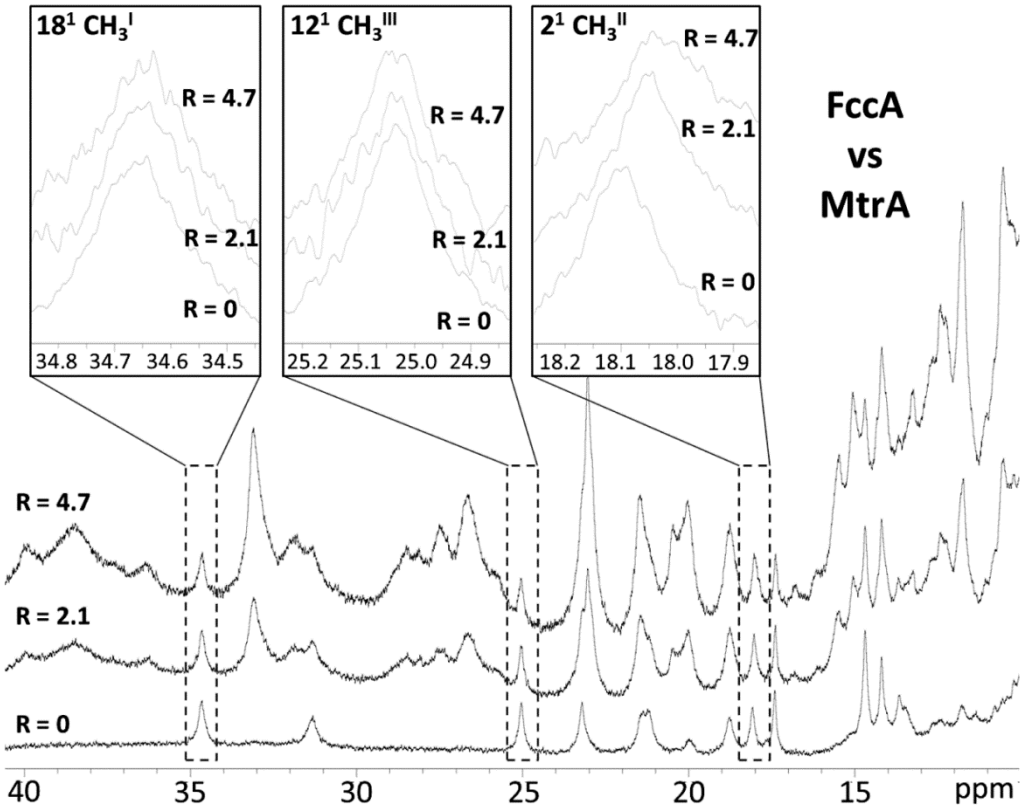

Figure C.3. ^{1}H-1D NMR spectral changes of FccA in the presence of increasing amounts of MtrA. The methyl group is identified using the IUPAC-IUB nomenclature for hemes. The Roman numeral corresponds to the order of heme binding to the polypeptide chain. The R value corresponds to the molar ratio of [MtrA]/[FccA]. Boxes show examples of methyl signals without significant chemical shift perturbation (18^{1}-CH_3^{I}; 12^{1}-CH_3^{III}) and with significant changes (2^{1}-CH_3^{II}).

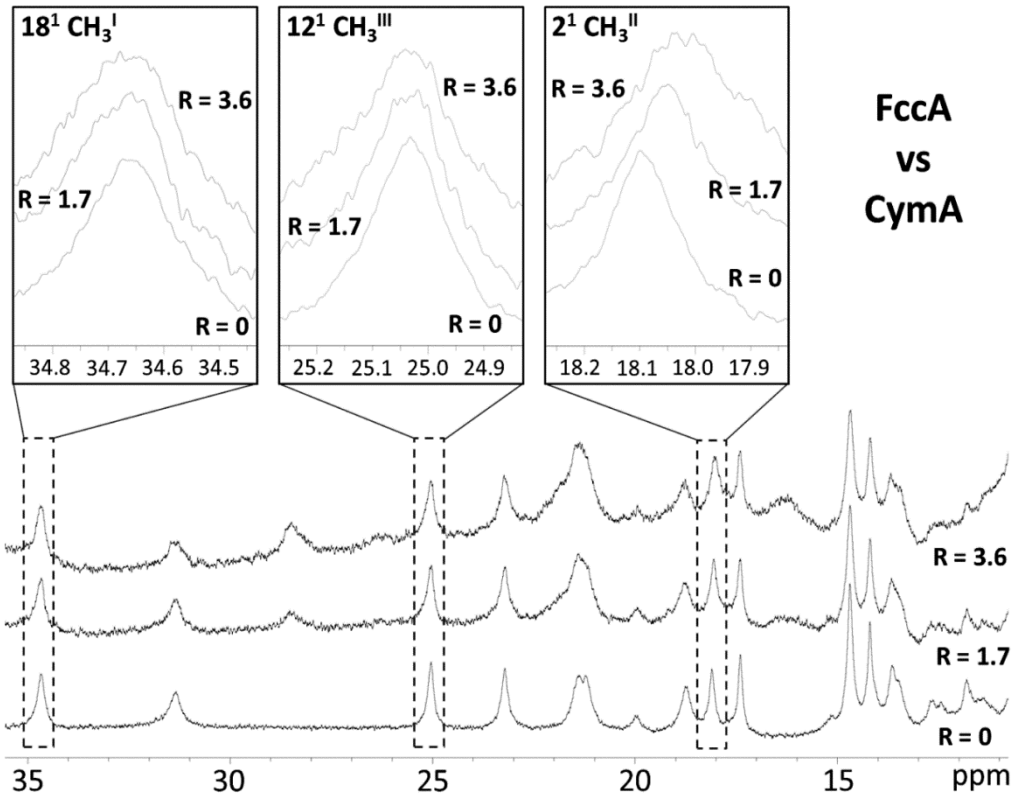

Figure C.4. ^{1}H-1D NMR spectral changes of FccA in the presence of increasing amounts of CymA. The methyl group is identified using the IUPAC-IUB nomenclature for hemes. The Roman numeral corresponds to the order of heme binding to the polypeptide chain. The R value corresponds to the molar ratio of [CymA]/[FccA]. Boxes show examples of methyl signals without significant chemical shift perturbation (18^{1}-CH_3^{I}; 12^{1}-CH_3^{III}) and with significant changes (2^{1}-CH_3^{II}).

APPENDIX D: THE THERMODYNAMIC STUDY OF MULTIHEME CYTOCHROMES

During the uptake or release of multiple electrons, several possible combinations exist for their redistribution within the redox populations of the protein (microscopic states). In the case of a multiheme cytochrome with *n* number hemes and *m* number of ionizable centers, the number of possible microscopic states is 2^{n+m}. These can be grouped in *n*+1 possible stages of oxidation, numbered 0, 1, 2, 3, …, *n*; according to the number of oxidized hemes that are found in the populations of the microscopic states that make up each stage of oxidation (Figure D.1) [2].

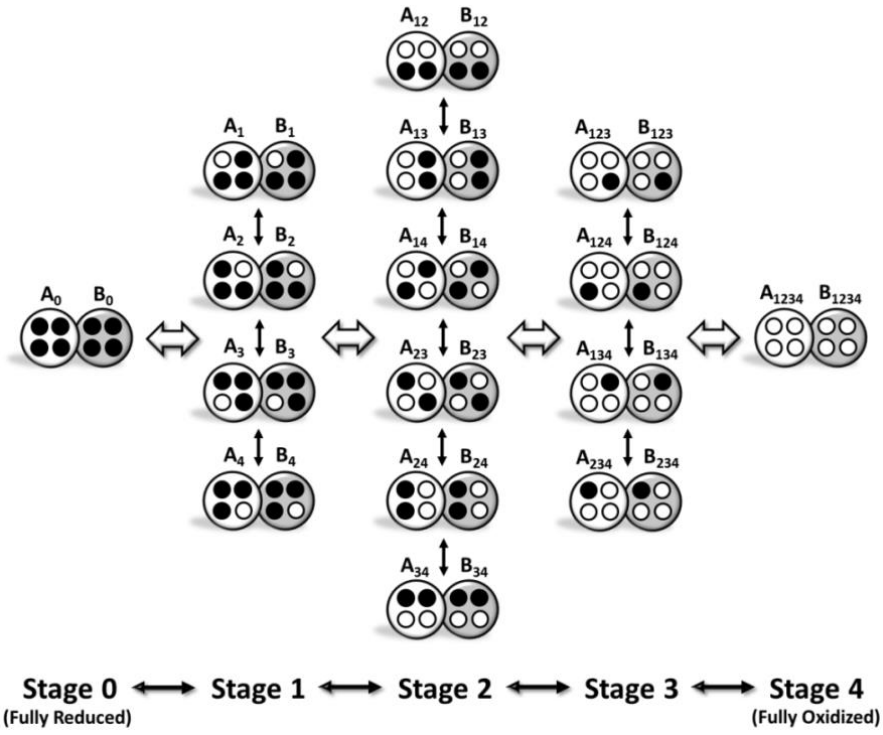

Figure D.1. Schematic representation of the microscopic states of a protein with four redox centers and one ionizable center. The four small circles represent the four redox centers, black when reduced and white when oxidized. A and B represent protonated and deprotonated microstates, respectively. Subscripts indicate the centers that are

oxidized in each microstate. A total of 64 possible electron transfer steps link the fully reduced to the fully oxidized protein. Electron exchange between the microscopic states belonging to the same stage of oxidation is fast (small black arrows), while electron exchange between the microscopic states belonging to different stages of oxidation is slow (large white arrows). The steps between each stage of oxidation represent transitions of one electron, corresponding to the macroscopic states of the protein.

For the small tetraheme cytochrome *c* (STC) from *Shewanella oneidensis* MR-1, the simplest thermodynamic model that fits the observed behavior requires a network of redox interactions between the four hemes and one protonation site, which accounts for the pH dependence of the reduction potentials of the hemes (Figure D.2). This five center model gives origin to a total of 32 possible microscopic states for this cytochrome, divided into five macroscopic stages of oxidation (Figure D.1).

In order to define in detail the thermodynamic properties of such a protein it is necessary to determine the energies of the 32 microscopic states in combination with the solution potential and pH. These energies can be expressed as sums of energies of oxidation of the hemes or of deprotonation of the ionizable centers, plus the interactions between these centers. If one neglects the interaction terms involving more than two centers, this gives a total of 15

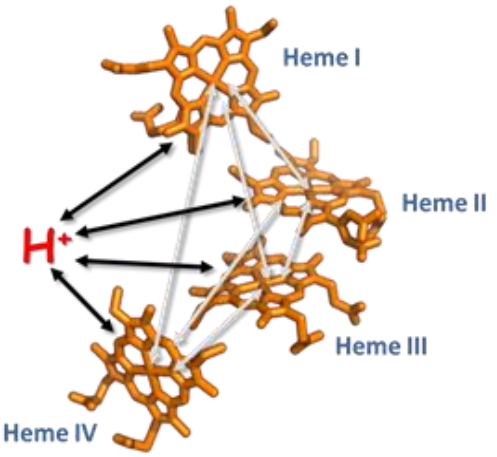

Figure D.2. Schematic representation of the pairwise interactions between the centers of the multiheme cytochrome STC from *S. oneidensis* MR-1. The Roman numerals correspond to the order of heme attachment to the polypeptide chain.

thermodynamic parameters: four reduction potentials, one pK_a, six heme-heme interactions and four heme-ionizable center interactions (redox-Bohr effect) (Figure D.2) [3].

Since the model considers different physical units (reduction potential and pH), using the Gibbs free energy equation allows us to express the redox potentials and the dissociation constant of the protonation site in terms of the energy of the microscopic states.

$$\Delta G = -nF\Delta E \quad \text{(Eq. D.1)}$$

$$\Delta G = -2.3RT\, logK_a \quad \text{(Eq. D.2)}$$

Considering the fully reduced and protonated microscopic state (A_0) as the reference state, the energy of each of the other 31 microscopic states relative to A_0 is given by the sum of the relevant energetic parameters plus a term $-nFE$ to account for the effect of the solution potential E in the different stages of oxidation. Also, a term to account for the proton chemical potential, $-2.3RT\, pH$, is added in the case of the deprotonated microscopic states [4].

The energies of the protonated microscopic states (A), one for each stage of oxidation are given by the following equations:

Stage 1 $$G_{Ai} = g_i - FE \quad \text{(Eq. D.3)}$$

Stage 2 $$G_{Aij} = g_i + g_j + g_{ij} - 2FE \quad \text{(Eq. D.4)}$$

Stage 3 $$G_{Aijk} = g_i + g_j + g_k + g_{ij} + g_{ik} + g_{jk} - 3FE \quad \text{(Eq. D.5)}$$

Stage 4 $$G_{Aijkl} = g_i + g_j + g_k + g_l + g_{ij} + g_{ik} + g_{il} + g_{jk} + g_{jl} + g_{kl} - 4FE \quad \text{(Eq. D.6)}$$

Where, g_i, g_j, g_k, g_l correspond to the relative energies of oxidation of the 4 individual hemes (i, j, k, l = I-IV; $i < j < k < l$) which are proportional to their respective reduction potentials (Equation D.1); and the energetic parameters

corresponding to the interactions between the hemes are given by the heme-heme interaction energies g_{ij}, g_{ik}, g_{il}, g_{jk}, g_{jl}, g_{kl}.

For the deprotonated microscopic states (B) the energies are given by the following equations:

Stage 1 $$G_{Bi} = G_{Ai} + g_H + g_{iH} - 2.3RT\,pH \quad \text{(Eq. D.7)}$$

Stage 2 $$G_{Bij} = G_{Aij} + g_H + g_{iH} + g_{JH} - 2.3RT\,pH \quad \text{(Eq. D.8)}$$

Stage 3 $$G_{Bijk} = G_{Aijk} + g_H + g_{iH} + g_{jH} + g_{kH} - 2.3RT\,pH \quad \text{(Eq. D.9)}$$

Stage 4 $$G_{Bijkl} = G_{Aijkl} + g_H + g_{iH} + g_{jH} + g_{kH} + g_{lH} - 2.3RT\,pH \quad \text{(Eq. D.10)}$$

Where, g_H is the ionization energy of the fully reduced protein, which is related to the pK_a of the ionizable group in the reference state (Equation D.2); and the energetic parameters corresponding to the interactions between the hemes and the ionizable center are given by the heme-ionizable center interaction energies g_{iH}, g_{jH}, g_{kH}, g_{lH}.

Having expressed the energies of 32 possible microscopic states in terms of the 15 thermodynamic parameters needed to define the model, it is possible to express the populations of all microscopic states relative to the reference state A_0 population (P_{A0}) using the Boltzmann distribution and the relative energies. This gives origin to the following equations for the relative populations of the protonated microscopic states and deprotonated microscopic states:

Stage 1 $$\frac{P_{Ai}}{P_{A0}} = e^{\left(\frac{-G_{Ai}}{RT}\right)} \quad ; \quad \frac{P_{Bi}}{P_{A0}} = e^{\left(\frac{-G_{Bi}}{RT}\right)} \quad \text{(Eq. D.11 and D.12)}$$

Stage 2 $$\frac{P_{Aij}}{P_{A0}} = e^{\left(\frac{-G_{Aij}}{RT}\right)} \quad ; \quad \frac{P_{Bij}}{P_{A0}} = e^{\left(\frac{-G_{Bij}}{RT}\right)} \quad \text{(Eq. D.13 and D.14)}$$

Stage 3 $$\frac{P_{Aijk}}{P_{A0}} = e^{\left(\frac{-G_{Aijk}}{RT}\right)} \quad ; \quad \frac{P_{Bijk}}{P_{A0}} = e^{\left(\frac{-G_{Bijk}}{RT}\right)} \quad \text{(Eq. D.15 and D.16)}$$

Stage 4 $\frac{P_{Aijkl}}{P_{A0}} = e^{\left(\frac{-G_{Aijkl}}{RT}\right)}$; $\frac{P_{Bijkl}}{P_{A0}} = e^{\left(\frac{-G_{Bijkl}}{RT}\right)}$ (Eq. D.17 and D.18)

Also, according to the model the addition of negative or positive terms leads to a decrease or increase in the overall energy of the microscopic states, respectively. This originates an increase in their relative populations when the interacting energies are negative (positive cooperativity) or a decrease when the interacting energies are positive (negative cooperativity).

Using the ionization energy of the fully reduced protein, g_H, and the heme-ionizable center interaction energies, g_{iH}, g_{jH}, g_{kH}, g_{lH}, it is also possible to calculate the macroscopic pK_a^{stage} value for each stage of oxidation of the protein.

Stage 0 $K_a^0 = e^{\left(\frac{-g_H}{RT}\right)}$ (Eq. D.19)

Stage 1 $K_a^1 = \frac{\sum P_{Ai}\, e^{\left(\frac{-(g_H + g_{iH})}{RT}\right)}}{\sum P_{Ai}}$ (Eq. D.20)

Stage 2 $K_a^2 = \frac{\sum P_{Aij}\, e^{\left(\frac{-(g_H + g_{iH} + g_{jH})}{RT}\right)}}{\sum P_{Aij}}$ (Eq. D.21)

Stage 3 $K_a^3 = \frac{\sum P_{Aijk}\, e^{\left(\frac{-(g_H + g_{iH} + g_{jH} + g_{kH})}{RT}\right)}}{\sum P_{Aijk}}$ (Eq. D.22)

Stage 4 $K_a^4 = e^{\left(\frac{-(g_H + g_{iH} + g_{jH} + g_{kH} + g_{lH})}{RT}\right)}$ (Eq. D.23)

In order to obtain experimental data on the relative populations of the microscopic states one can use NMR spectroscopy. The differences between the cytochrome spectra in the reduced and oxidized states make this powerful technique highly suitable to study thermodynamically the hemes, which can be probed individually.

These differences in the spectra occur to due to changes in the electronic structure of each heme with the oxidation state, axial ligands and coordination state of its iron atom. In the case of STC, the octahedral coordination of the iron and the bis-histidine axial ligands of its hemes favors the diamagnetic low-spin form (S=0) in the reduced state (Fe(II)) and the paramagnetic low-spin form (S=1/2) in the oxidized state (Fe(III)) [5]. In both situations, it is possible to obtain well-resolved NMR spectra of the hemes although in the reduced state the majority of these signals are located within the protein's spectral envelope. In the oxidized state, the signals belonging to some of the heme's substituents, particularly those from the methyl groups are shifted to high frequency and appear isolated from the protein's polypeptide chain spectral envelope. This shift to high frequency (paramagnetic shift) occurs due to the delocalization of the unpaired electron through the porphyrin ring π orbitals of the heme (contact shifts) and also due to the influence of its magnetic moment on the neighboring nuclei magnetic fields (pseudo-contact shifts) [6,7].

Spectral differences between the sets of signals belonging to each oxidized heme are mainly due to the orientation of their axial ligands. Depending on the angle that the planes of the axial ligands make between each other, the electronic cloud of the heme is more delocalized to some of its substituents in relation to others [8]. This endows each heme with a unique pattern for its substituents' NMR signals, allowing the linkage of a specific group of signals to an individual heme in the protein structure.

In order to assign each heme signal to its respective heme substituent, 2D-NMR NOESY spectra must be performed. This assignment is done by following in the spectrum, cross-peaks between the diagonal signals of the different heme substituents [9,10]. Since these cross-peaks appear due to cross-relaxation between nuclei that are spatially close to each other (nuclear

Overhauser effect – nOe), this allows us to connect each substituent signal to its respective substituent neighbors' signal. Using longer mixing times when acquiring the NOESY spectrum allows the cross-relaxation between nuclei to travel larger distances and therefore, observe nOe cross-peaks between heme substituents that are further away (Figure D.3). Interheme nOe cross-peaks provide information on which hemes are neighboring each other.

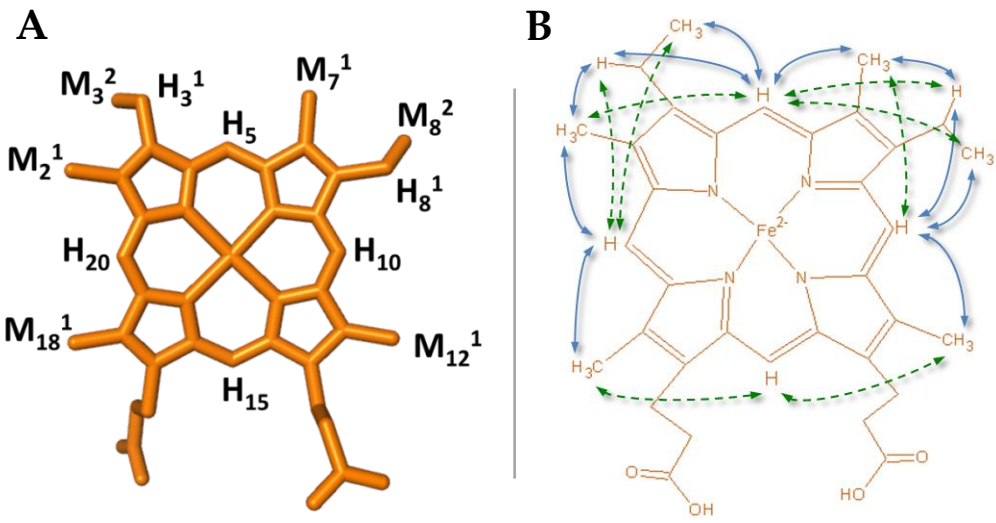

Figure D.3. Diagram of a *c*-type heme. **A)** Numbered according to the IUPAC-IUB nomenclature for tetrapyrroles [11]. **B)** Representation of intraheme connectivity between heme substituents that originate nOe cross-peaks. Solid and broken lines represent the cross-peaks that are possible to observe in NOESY experiments using short or long mixing times, respectively.

Analyzing NOESY spectra obtained with a partially oxidized sample, besides the nOe cross-peaks mentioned above, it is also possible to observe chemical exchange cross-peaks. Their existence depends on the rate of conversion between the possible redox populations (microscopic states) in relation to the NMR timescale. While electron exchange between the microscopic states belonging to different stages of oxidation (intermolecular exchange) is slow on the NMR timescale, exchange between microscopic states

belonging to the same stage of oxidation (intramolecular exchange) is fast (Figure D.1). Thus, this gives origin to five NMR signals for each heme substituent, one for each stage of oxidation, connected in the spectrum through their chemical exchange cross-peaks.

Since the NMR spectrum has the weighted contributions of all the possible microscopic states of the multiheme cytochrome, the paramagnetic chemical shifts displayed by the heme signals are governed by the weighted average of microscopic states that possess that particular heme oxidized at that stage of oxidation. Thus, the observed changes in the chemical shifts of the signals belonging to a specific heme with each stage of oxidation are proportional to the fraction of oxidation of that particular heme [2,4]. The following equation can be used to define the fractions of oxidation of each heme i (i=I-IV) in each stage of oxidation of the protein (*Stage*) using the observed chemical shift of a methyl group signal belonging to heme i (δ_i^{Stage}) in stages of oxidation 0 to 4, respectively.

$$Fraction\ of\ Oxidation\ {}_i^{Stage} = \frac{\delta_i^{Stage} - \delta_i^0}{\delta_i^4 - \delta_i^0} \qquad \text{(Eq. D.24)}$$

Following the resonance positions of the chemical exchange cross-peaks of one methyl group from each heme, it is possible to monitor the hemes through all the different stages of oxidation at various pH values and extract information about their relative energies of oxidation and respective interaction energies, pH dependence and the order of reduction of the hemes [2,4,12,13]. The choice of the methyl group to be followed is important and it should preferably point towards the protein surface to minimize paramagnetic contributions caused by nearby oxidized hemes (extrinsic shifts) [12].

From the analysis of the NMR data alone it is not possible to determine all the 15 energetic parameters needed to define the thermodynamic model. Due to the impracticality of measuring the solution reduction potential inside the NMR tube, the parameters obtained from these data are relative to the reference state (A_0).

Taking into account that the oxidation step between the stages of oxidation involves a one electron transfer it is possible, using only three chosen methyl groups' fractions of oxidation, to determine the fraction of oxidation of the fourth methyl group.

$$\sum_{i=I}^{IV} \frac{(\delta_i^{Stage} - \delta_i^0)}{(\delta_i^4 - \delta_i^0)} = Stage \qquad \text{(Eq. D.25)}$$

This means that only 9 independent observable variables can be extracted from the NMR spectra for each pH value. An additional 3 independent observable variables are obtained from the macroscopic pK_a values of the intermediate stages of oxidation (1 to 3), from analyzing NMR data performed at different pH values. Thus, a total of 12 independent observable variables can be obtained by NMR data, making it insufficient to determine the 15 energetic parameters needed to characterize the protein.

The remaining independent observable variables were obtained from potentiometric titrations followed by visible spectroscopy performed at different specific pH values [14]. These allow us to calibrate the relative redox energies and heme-heme interacting energies and the deprotonation energy of the fully reduced protein.

To simulate the redox titration curves, the fraction of oxidation of the protein is plotted as a function of the solution potential for each pH value. The fraction of oxidation is given by the total sum of the microscopic states'

populations from each stage of oxidation ($\sum P^{Stage}$) weighted by the number of oxidized hemes, divided by the total sum of the microscopic states' populations multiplied by four.

$$Fraction\ of\ oxidation\ = \frac{\sum P^1 + 2\sum P^2 + 3\sum P^3 + 4\sum P^4}{4(\sum P^1 + \sum P^2 + \sum P^3 + \sum P^4)} \quad \text{(Eq. D.26)}$$

The calibration of the relative energies is done through the addition of Δe to all the g_i (i = I-IV), which corresponds to the change in the base value of the redox energies, and through the addition of ΔI to all the g_{ij} (i, j, k, l = I-IV; $i < j < k < l$), which corresponds to the change in the base value of the heme-heme interacting energies. These two terms obtained from the experimental data complete the set of 15 independent observable variables necessary to define the parameters of the model. This final adjustment of the absolute values of the reference energies has a purely linear effect on all of the thermodynamic parameters of the model. For the cases of the interaction energies between the hemes and the ionizable center, g_{iH}, g_{jH}, g_{kH}, g_{lH}, the values obtained from the NMR data are already absolute and do not need any type of calibration, since the pH value is accurately measured before and after each NMR experiment.

The term Δe defines the position of the redox titration curve whereas ΔI defines the shape of the curve. Positive ΔI values result in titration curves with a shallower slope, characteristic of negative heme-heme cooperativities, while negative ΔI values result in steeper titration curves characteristic of more positive cooperativities between the hemes.

The energies of the protonated and deprotonated microscopic states after calibration (G'_A and G'_B, respectively) are related to their corresponding energies before calibration (G_A and G_B, respectively) through the following equations.

Stage 1 $G'_{Ai} = G_{Ai} + \Delta e$; $G'_{Bi} = G_{Bi} + \Delta e$ (Eq. D.27 and D.28)

Stage 2 $G'_{Aij} = G_{Aij} + 2\Delta e + \Delta I$; $G'_{Bij} = G_{Bij} + 2\Delta e + \Delta I$ (Eq. D.29 and D.30)

Stage 3 $G'_{Aijk} = G_{Aijk} + 3\Delta e + 3\Delta I$; $G'_{Bijk} = G_{Bijk} + 3\Delta e + 3\Delta I$ (Eq. D.31 and D.32)

Stage 4 $G'_{Aijkl} = G_{Aijkl} + 4\Delta e + 6\Delta I$; $G'_{Bijkl} = G_{Bijkl} + 4\Delta e + 6\Delta I$ (Eq. D.33 and D.34)

Since the term that includes the adjustment of the base values is the same for all microscopic states belonging to the same stage of oxidation, substituting equations D.27-34 in equations D.11-18, it is possible to express the change in the total sum of the microscopic populations of a stage of oxidation ($\sum P^{Stage\,\prime}$; *Stage* = 1-4) as follows:

Stage 1 $\sum P^{1\prime} = e^{\left(\frac{-\Delta e}{RT}\right)} \sum P^{1}$ (Eq. D.35)

Stage 2 $\sum P^{2\prime} = e^{\left(\frac{-(2\Delta e + \Delta I)}{RT}\right)} \sum P^{2}$ (Eq. D.36)

Stage 3 $\sum P^{3\prime} = e^{\left(\frac{-(3\Delta e + 3\Delta I)}{RT}\right)} \sum P^{3}$ (Eq. D.37)

Stage 4 $\sum P^{4\prime} = e^{\left(\frac{-(4\Delta e + 6\Delta I)}{RT}\right)} \sum P^{4}$ (Eq. D.38)

It is also possible to define the macroscopic redox potential E_{Stage} for the equilibrium between the stages of oxidation *Stage-1* and *Stage* using the Nernst equation.

$$E_{Stage} = E - \frac{RT}{F} ln \frac{\sum P^{Stage}}{\sum P^{Stage-1}} \quad \text{(Eq. D.39)}$$

For the cases where $\sum P^{Stage-1}$ (the sum of all the microscopic states that belong to the stage of oxidation *Stage-1*) is identical to $\sum P^{Stage}$ (the sum of all

the microscopic states that belong to the stage of oxidation *Stage*), the macroscopic redox potential E_{Stage} is equal to the solution potential *E*.

The substitution of equations D.35-38 in equation D.39 it is possible to express the calibrated macroscopic redox potentials E'_{Stage} as a function of the calibration terms, Δe and ΔI.

Stage 1 $$E'_1 = E_1 + \frac{\Delta e}{F}$$ (Eq. D.40)

Stage 2 $$E'_2 = E_2 + \frac{\Delta e + \Delta I}{F}$$ (Eq. D.41)

Stage 3 $$E'_3 = E_3 + \frac{\Delta e + 2\Delta I}{F}$$ (Eq. D.42)

Stage 4 $$E'_4 = E_4 + \frac{\Delta e + 3\Delta I}{F}$$ (Eq. D.43)

Having obtained the necessary experimental data from NMR and UV-visible spectroscopy, the 15 thermodynamic parameters of the model can be easily determined by fitting of the equations to all the data simultaneously using a computer routine (see Appendix E).

APPENDIX E: MATLAB ROUTINES

Thermodynamic parameters:

Matlab routine used for determination of the thermodynamic parameters via simultaneous fitting of the experimental data obtained from the NMR and the potentiometric redox titrations. The function "hemes" (file hemes.m) uses the "Chi2" function (file Chi2.m) to calculate the respective standard errors.

File hemes.m

```
function Results = hemes(NMRdata, TITRATIONdata, SETTINGS)

% HEME PROTEIN THERMODYNAMIC MODEL PARAMETER DETERMINATION
% -----------Nelder-Mead Simplex Minimization-------------
%
% In order to determine the thermodynamic parameters of a heme protein,
% the present function uses the function Chi2.m to calculate the
% chi-squared value of the differences between experimental and theoretic
% values of NMR and Titration experiments.
%
% The chi-squared value is then minimized with the function fminsearch from
% MATALAB that uses the Nelder-Mead Simplex algorithm, determining the
% thermodynamic parameters of the model.
%
% The model may have any number of heme groups or proton groups and the
% parameters are calculated RELATIVE TO THE FULY REDUCED UNPROTONATED PROTEIN.
%
% The experimental results must be inputed with two tab delimeted .txt files,
% one for the NMR and one for the Titrations. The model settings must be
% defined by a third tab delimited .txt file.
%
% IMPORTANT: the names of this three files are the three input variables of
% the hemes function and must be input by the correct order.
%
% The NMR FILE must be defined by a string containing the file name
% (strings are written between apostrophes). This string must be the FIRST
% input variable of the function hemes.
% The file must have the following form:
%
%   In the first row must be the pHs of the experiments in an ascending order.
%   Below the respective pH must be the oxidation fractions for each oxidaton
stage
%   in an ascending order down the table grouped by heme in a descending order
%   down the table (see below).
%
%   In the same file, next to this table a similar one must be present with
%   the respective linewidths (the pH values must be repeated in the first
%   row).
%
%   Below is examplefied for a tetraheme protein with five different pH
%   experiments. The roman numbers represent the oxidation fractions or
%   linewidths of the respective oxidation stages. Unkown fraction must be
%   inserted with NaN and the respective linewidth 1.
%
```

```
%   pH1   pH2   pH3   pH4   pH5        pH1   pH2   pH3   pH4   pH5
%   I     I     I     I     I          I     I     I     I     I       |
%   II    II    II    II    II         II    II    II    II    II      |_Heme4
%   III   III   III   III   III        III   III   III   III   III     |
%   IV    IV    IV    IV    IV         IV    IV    IV    IV    IV      |
%   I     I     I     I     I          I     I     I     I     I         |
%   II    II    II    II    II         II    II    II    II    II        |_Heme3
%   III   III   III   III   III        III   III   III   III   III       |
%   IV    IV    IV    IV    IV         IV    IV    IV    IV    IV        |
%   I     I     I     I     I          I     I     I     I     I       |
%   II    II    II    II    II         II    II    II    II    II      |_Heme2
%   III   III   III   III   III        III   III   III   III   III     |
%   IV    IV    IV    IV    IV         IV    IV    IV    IV    IV      |
%   I     I     I     I     I          I     I     I     I     I         |
%   II    II    II    II    II         II    II    II    II    II        |_Heme1
%   III   III   III   III   III        III   III   III   III   III       |
%   IV    IV    IV    IV    IV         IV    IV    IV    IV    IV        |
%
% The TITRATION FILE must be defined by a string compose of the file name
% (strings are written between apostrophes). This string is the SECOND
% input variable of the hemes function.
% The file must have the following form:
%
%   In the first cell of the first colunm must be the pH of the Titration.
%
%   Bellow the first cell must be the potential values of the points of the
%   Titration. Right to the potential values must be the respective
%   oxidation fractions (the first cell of this second column must be blank
%   next to the pH).
%
%   Repeat this structure to the right for each Titration done. Titration
%   must be in order of increasing pH value from left to right (it is
%   possible to have several titration at the same pH).
%
%   Bellow is examplefied with two Titrations
%
%   pH1                       pH2
%   potential   ox fraction   potential   ox fraction
%   potential   ox fraction   potential   ox fraction
%   potential   ox fraction   potential   ox fraction
%   .           .             .           .
%   .           .             .           .
%   .           .             .           .
%
% The SETTINGS FILE is define by a string composed of the file name
% (strings are writen between apostrophes). This string is the THIRD input
% variable of the hemes function.
% The file must have a single column with the following form:
%
%   first row - temperature in Kelvin
%
%   second row - number of heme groups
%
%   third row - number of protons
%
%   fourth row - units of the potential values of the TITRATION file
%   (this entry must be either "V" or "mV" (without coats)).
%
%   following rows - initial estimation values in the following order
%
%             - heme potentials (ascending order of heme number down the
colunm).
%                  - pK values (ascending order of proton down the colunm).
%                  - heme interactions (first heme1 with the others, next
%                   heme2 with the others and so on).
```

```
%                  - redox-Bohr effects for the first proton with all
%                   the hemes starting with heme1 and repeat for all the
%                   protons.
%
%   Bellow is exemplified with four hemes and two protons:
%
%       temperature
%       number of hemes
%       number of protons
%       mV                  (or V)
%       E1
%       E2
%       E3
%       E4
%       pK1
%       pK2
%       i12
%       i13
%       i14
%       i23
%       i24
%       i34
%       i1H1
%       i2H1
%       i3H1
%       i4H1
%       i1H2
%       i2H2
%       i3H2
%       i4H2
%
% The function originates a structure variable with the results:
%
%     - optimized parameters
%     - standard errors of the optimized parameters
%     - final chi-squared value of the minimization
%     - p-value of the hypothesis test
%     - pK values for each of the redox stages from 0 to the top
%     - final chi-squared value with nmr data
%     - final chi-squared value with titrations data
%     - degrees of freedom
%     - final least-squares value of the minimization
%     - final least-squares value with the nmr data
%     - final least-squares value with the titrations data
%
%
%
% An output tab delimited ASCII file is created with the  name of the NMRdata
file followed
% by 'OUT'. This file contains the seven first output variables.
%
% It is possible to use this file in a plot mode to get curves for known
proteins.
% In this case:
%
%   -as the first argument put the settings file with the parameters in place
%    of the initial estimation
%   -as the second argument insert the string 'plot'
%   -as the third argument insert a row vector with the desired pH values
%   (it has to be more than one)
%
% ------------------------------------------------------------------------

% constants
```

```
R = 8.314;  % PGC
F = 96490;  % Faraday constant

% check mode

if size(TITRATIONdata,2) ~= 4
    cue = 0;
elseif all(TITRATIONdata ~= 'plot')
    cue = 0;
else
    cue = 1;
end

if cue   % plot mode
    pH = SETTINGS;
    if ~isnumeric(pH)
        error('Insert pH row vector in third argument')
    end
    if size(pH,2) == 1
        error('More then one pH value required')
    end
    TitrationpH = pH;

        % settings

    settings = textread(NMRdata, '%s');

    units = settings{4};

    T = str2num(settings{1});

    % Model characteristics

    NumberOfHemes = str2num(settings{2});

    NumberOfProtons = str2num(settings{3});

    NumberOfMicrostates = 2^(NumberOfHemes + NumberOfProtons);

    NumberOfParameters = NumberOfHemes + NumberOfProtons +
size(combntns(1:NumberOfHemes,2),1) + NumberOfHemes*NumberOfProtons;

    % to fixate desired parameters and only optimize the res two matrix can be
used: r and fix.
    % Known parameters (1 in the respective position of r means known value)

    r = zeros(1,NumberOfParameters);

    % The fix matrix contains the known parameters in the respective position

    fix = zeros(NumberOfParameters,1);

else % optimization mode

    % settings

    settings = textread(SETTINGS, '%s');

    units = settings{4};

    if strcmp(units, 'mV')
        units = 1000;
    elseif strcmp(units, 'V')
        units = 1;
    else
```

```
       warning('Define potential units (mV or V).')
    end

    T = str2num(settings{1});

    % Model characteristics

    NumberOfHemes = str2num(settings{2});

    NumberOfProtons = str2num(settings{3});

    NumberOfMicrostates = 2^(NumberOfHemes + NumberOfProtons);

    NumberOfParameters = NumberOfHemes + NumberOfProtons +
size(combntns(1:NumberOfHemes,2),1) + NumberOfHemes*NumberOfProtons;

    % to fixate desired parameters and only optimize the res two matrix can be
used: r and fix.
    % Known parameters (1 in the respective position of r means known value)

    r = zeros(1,NumberOfParameters);

    % The fix matrix contains the known parameters in the respective position

    fix = zeros(NumberOfParameters,1);

    % initial estimation

    x0 = [];
    for m = 1:NumberOfParameters-sum(r==1)
        x0 = [x0; str2num(settings{4+m})];
    end

    % algorithm termination conditions

    TolFun = 1e-7;
    TolX = 1e-7;
    MaxIter = 20000;



    % Titration oxidation fractions and standard deviation

    N = dlmread(TITRATIONdata, '\t');

        % titration file formatting check (this check can only find some errors
        % not all).

        for m = 1:size(N,2)/2
            if N(1,2*m) ~= 0
                error('Titration data file wrongly structured')
            end
        end
        if round(size(N,2)/2) ~= size(N,2)/2
            error('Titration data file wrongly structured')
        end

    fid = fopen(TITRATIONdata);
    M = textscan(fid,'',size(N,1)-1, 'delimiter', '\t',
'headerlines',1,'headercolumns',0,'returnonerror',0,'emptyvalue',NaN);
    for m = 1:size(N,2)/2
        Titrationexpdata{m,1} = M{1,2*m}';
        Titrationexpdata{m,1}(Titrationexpdata{m,1}~=Titrationexpdata{m,1}) =
[];
    end
```

```
    Titrationstdd = 0.03; % titration experimental error

    % different pH's of the titrations

    fid = fopen(TITRATIONdata);
    TitrationpH = textscan(fid, '%n', size(N,2)-1, 'delimiter', '\t');
    TitrationpH = TitrationpH{1}';
    TitrationpH(TitrationpH~=TitrationpH) = [];
    fclose('all');

    % different Potentials's of the titrations

    if strcmp(units, 'mV')
        units = 1000;
    elseif strcmp(units, 'V')
        units = 1;
    else
       warning('Define potential units (mV or V).')
    end

    for m = 1:size(N,2)/2
        Potentials{m,1} = M{1,2*m-1}'/units;
        Potentials{m,1}(Potentials{m,1}~=Potentials{m,1}) = [];
    end

    % NMR oxidation fractions and standard deviations

    fid = load(NMRdata);

        % NMR file formatting check (this check can only find some errors
        % not all).

        if round(size(fid,2)/2) ~= size(fid,2)/2
            error('NMR data file wrongly structured')
        end
        if any(fid(1, 1:size(fid,2)/2) ~= fid(1, size(fid,2)/2+1:size(fid,2)))
            error('NMR pH values are different between fractions and
linewidths')
        end

    expdata = fid(2:size(fid,1),1:size(fid,2)/2);

    stdd = fid(2:size(fid,1), size(fid,2)/2+1:size(fid,2));

    % different pH's of the NMR experiments
    % n = number of experiments

    pH = fid(1, 1:size(fid,2)/2);
end

n = size(pH, 2);

% binary matrix to obtain the energies of the microstates without pH:
% E = mb * x
% x = vector of parameters

%   mb determination

mb = [];

        % Potential part of mb

for m = 1:NumberOfHemes
    a = [];
```

```
    for o = 1:2^(m-1)
        a = [a; zeros(2^(NumberOfHemes+1)/2^m,1);
ones(2^(NumberOfHemes+1)/2^m,1)];
    end
    mb = [mb, a];
end

        % pK part of mb

a=[];
for m = 1:2^(NumberOfHemes+1)
    if rem(m,2) & m ~= 2
        a = [a
            0];
    else
        a = [a
            1];
    end
end

mb = [mb, a];

if NumberOfProtons > 1
    for m = 2:NumberOfProtons
        mb = [mb zeros(size(mb,1),1)
            mb ones(size(mb,1),1)];
    end
end

        % Potential interaction part of mb

NumberOfInteractions = 0;
for m = 1:NumberOfHemes
    for o = m+1:NumberOfHemes
       mb(:,size(mb,2)+1) = mb(:,m) .* mb(:,o);
       NumberOfInteractions = NumberOfInteractions + 1;
    end
end

        % Proton interaction part of mb

for m = 1:NumberOfProtons
    for o = 1:NumberOfHemes
       mb(:,size(mb,2)+1) = mb(:,o) .* mb(:,NumberOfHemes+m);
    end
end

% Resizing the binary matrix mb0 for the fixed parameters.

mb0 = mb;

for m = 1:NumberOfParameters
    if r(1,m) ~= 0
        mb0(:,m-(NumberOfParameters-size(mb0,2))) = [];
    end
end

% pH components of the energies of the microstates:
% E = mb * x + EpH

if NumberOfProtons > 1
    EpH = sum((mb(:,NumberOfHemes+1:NumberOfHemes+NumberOfProtons))')' *
(2.3*R*T/F*pH);
else
    EpH = mb(:,NumberOfHemes+1) * (2.3*R*T/F*pH);
```

```
end

% binary matrixes to obtain oxidation fractions from microstates
% Fr = (mb1 * P)./(mb2 * P)          with P = exp(-F/(R*T) * E).

S = sum(mb(:,1:NumberOfHemes)')'; % oxidation stage

a = S * ones(1,NumberOfHemes) .* mb(:,1:NumberOfHemes);

mb1 = [];
for m = 1:NumberOfHemes
    for o = 1:NumberOfHemes
        mb1 =[mb1, (a(:,NumberOfHemes+1-m) == o)];
    end
end
mb1 = mb1';

mb02 = [];
for m = 1:NumberOfHemes
    mb02 = [mb02, (S == m)];
end
mb2 = [];
for m = 1:NumberOfHemes
    mb2 = [mb2, mb02];
end
mb2 = mb2';


if cue
    x = [];
    for m = 1:NumberOfParameters-sum(r==1)
        x = [x; str2num(settings{4+m})];
    end
else
    % parameter determination through Nelder-Mead SIMPLEX algorithm (fminserch
    % function)


    options = optimset('MaxFunEvals', size(x0,2)*MaxIter, 'MaxIter',
size(x0,2)*MaxIter, 'TolFun', TolFun,...
        'TolX', TolX);

    format long e

    [x, chi2, exitflag, output] = fminsearch(@(x) Chi2(x, mb, mb1, mb2,
Potentials, R, T, F, expdata, Titrationexpdata, stdd, Titrationstdd, mb0, fix,
TitrationpH, EpH, n, NumberOfMicrostates, NumberOfHemes), x0, options);


    format short

    output.message
end

% pK values at the different redox stages

E0 = mb0 * x + mb * fix;
E = E0 * ones(1,n) + EpH;
P = exp(-F/(R*T) * E);

pKa = [];
for q = 0:NumberOfHemes
    P1 = P(:,1);
    P1(find(S~=q)) = [];
    P1d = [];
```

```
    P1p = [];
    for m = 1:2:size(P1,1)
        P1d = [P1d; P1(m)];
        P1p = [P1p; P1(m+1)];
    end
    pKa = [pKa; -log10( sum(P1d)/sum(P1p) ) + pH(1)];
end

if cue
else
    % Chi square discrimination between NMR and Titration and Chi squared test

    E0 = mb0 * x + mb * fix;
    E = E0 * ones(1,n) + EpH;
    P = exp(-F/(R*T) * E);
    Fr = (mb1 * P) ./ (mb2 * P);
    B = Fr - expdata;
    B(B~=B)=0;
    NMR = sum((sum(((B)./stdd).^2)));  % chi-squared of the NMR expriments
    LSnmr = sum(sum(B.^2));            % least-squares of the NMR experiments


    E0 = mb0 * x + mb * fix;

    TITRATION = 0;
    LStitration = 0;
    for m = 1:size(TitrationpH,2)
        E = E0 * ones(1, size(Potentials{m,1},2));
        EE = -1*(sum( mb(:,1:NumberOfHemes)')' * ones(1,
size(Potentials{m,1},2))) .* (ones(NumberOfMicrostates,1) * Potentials{m,1})
+...
        mb(:,NumberOfHemes+1) * ones(1, size(Potentials{m,1},2)) * (2.3*R*T/F *
TitrationpH(1,m));
        Fr1 = sum( (exp(-F/(R*T) * ( E + EE ) )) .* (
sum(mb(:,1:NumberOfHemes)')' * ones(1,size(Potentials{m,1},2))/NumberOfHemes )
);
        Fr2 = sum(exp(-F/(R*T) * ( E + EE ) ));
        FrE = Fr1 ./ Fr2;
        A = FrE - Titrationexpdata{m,1};
        A(A~=A) = 0;

        TITRATION = TITRATION + sum( sum( (A / Titrationstdd).^2));   %  chi-
squared of the titrations
        LStitration = LStitration + sum(sum(A.^2));                   %  least-
squares of the titrations
    end

    LS = LStitration + LSnmr; % least-squares of both experiments

            % degrees of freedom calculation (df)

    a = expdata;
    b = [];
    c = [];
    for m = 0:NumberOfHemes-1
        b = [b; 1 + m*NumberOfHemes];
        c = [c; (NumberOfHemes-1)*(m+1)];
    end
    a(b,:) = [];
    a(c,:) = [];

    df = (NumberOfHemes-2)*NumberOfHemes*size(pH,2) + size([Potentials{:,1}],2)
- sum(sum(isnan(a))) - size(x,1);

    p = chi2cdf(chi2, df);   % p-value of the hypothesis test
```

```
    % derivation for the determination of the curvature matrix (alfa)

            %NMR part of function

    E0 = mb0 * x + mb * fix;
    E = E0 * ones(1,n) + EpH;
    P0 = exp(-F/(R*T) * E0);
    P = exp(-F/(R*T) * E);
    Fr = (mb1 * P) ./ (mb2 * P);

            % NMR derivative

    h = 0.000000000000001;
    dFr = zeros(NumberOfHemes^2, size(x,1));
    NMRalfa = zeros(size(x,1), size(x,1));

    for m = 1:n
        Frdx = [];
        for o = 1:size(x,1)
            Dx = zeros(size(x));
            Dx(o,1) = h;
            E0 = mb0 * (x+Dx) + mb * fix;
            E = E0 + EpH(:,m);
            P0 = exp(-F/(R*T) * E0);
            P = exp(-F/(R*T) * E);
            Frdx = [Frdx, (mb1 * P) ./ (mb2 * P)];
        end
        dFr =  ( Fr(:,m) * ones(1,size(x,1)) - Frdx )  ./  h  ./ (stdd(:,m) *
ones(1,size(x,1)));
        NMRalfa = NMRalfa + (dFr' * dFr);
    end


            % Titration part of function

    E0 = mb0 * x + mb * fix;

    FrE = {};
    for m = 1:size(TitrationpH,2)
        E = E0 * ones(1,size(Potentials{m,1},2));
        EE = -1*(sum( mb(:,1:NumberOfHemes)')' * ones(1,
size(Potentials{m,1},2))) .* (ones(NumberOfMicrostates,1) * Potentials{m,1})
+...
        mb(:,NumberOfHemes+1) * ones(1, size(Potentials{m,1},2)) * (2.3*R*T/F *
TitrationpH(1,m));
        Fr1 = sum( (exp(-F/(R*T) * ( E + EE ) )) .* (
sum(mb(:,1:NumberOfHemes)')' * ones(1,size(Potentials{m,1},2))/NumberOfHemes )
);
        Fr2 = sum(exp(-F/(R*T) * ( E + EE ) ));
        FrE{m,1} = [Fr1 ./ Fr2];
    end

            %Titration derivative

    h = 0.000000000000001;
    dFrE = zeros(1, size(x,1));
    Titrationalfa = zeros(size(x,1), size(x,1));

    for m = 1:size(TitrationpH,2)
        for q = 1:size(Potentials{m,1},2)
            FrEdx = [];
            for o = 1:size(x,1)
                Dx = zeros(size(x));
                Dx(o,1) = h;
```

```
                E = mb0 * (x+Dx) + mb * fix;
                Fr1 = [];
                Fr2 = [];
                EE = -1*(sum( mb(:,1:NumberOfHemes)')' * Potentials{m,1}(1,q))
+...
                mb(:,NumberOfHemes+1) * (2.3*R*T/F * TitrationpH(1,m));
                Fr1 = sum( (exp(-F/(R*T) * ( E + EE )) .* (
sum(mb(:,1:NumberOfHemes)')'/NumberOfHemes ) ));
                Fr2 = sum(exp(-F/(R*T) * ( E + EE ) ));
                FrEdx = [FrEdx, Fr1 ./ Fr2];
            end
            dFrE =  (FrE{m,1}(1,q) * ones(1,size(x,1)) - FrEdx) / h /
Titrationstdd;
            Titrationalfa = Titrationalfa + (dFrE' * dFrE);
        end
    end

        % Standard Errors determination

    alfa = NMRalfa + Titrationalfa;  % final curvature matrix

    stderr = (diag(inv(alfa))).^0.5;  % standard errors
end

%Ploting

   % NMR

% CalcEpH is a matrix for ploting the teoretic curves
% m = number of points
% c = pH for teoretic curves

NMRPlot = figure('Name', 'NMR', 'NumberTitle', 'off');
m = 1000;
c = pH(1):(pH(n)-pH(1))/(m-1):pH(n);

CalcEpH = ( mb(:,NumberOfHemes+1) * ones(1,size(c,2)) ) .* (
ones(NumberOfMicrostates,1) * 2.3*R*T/F*c );

CalcE0 = mb0 * x + mb * fix;           %
CalcE = CalcE0 * ones(1,m) + CalcEpH;  %
CalcP0 = exp(-F/(R*T) * CalcE0);       %  Function
CalcP = exp(-F/(R*T) * CalcE);         %
POP = (mb1 * CalcP) ./ (mb2 * CalcP);  %

w = [c;POP];
save([NMRdata(:,1:size(NMRdata,2)-4) '_NMRplot.txt'], 'w', '-ASCII', '-TABS'); %
file for NMR figure ploting

b = 1:NumberOfHemes;
for q = 0:NumberOfHemes-1
    for o = 1:NumberOfHemes-1
        subplot(round(NumberOfHemes/2),2,NumberOfHemes-q)
        hold all
        if cue
        else
            errorbar(pH, expdata(NumberOfHemes*q+o,:),
stdd(NumberOfHemes*q+o,:), '.')
        end
        plot(c, POP(NumberOfHemes*q+o,:), '-')
        axis ([pH(1) pH(n) 0 1])
        xlabel('pH')
        ylabel('Oxidation Fraction')
        title(['Heme', num2str(b(NumberOfHemes-q))])
    end
```

```
end
% legend('Stage 2',' ', 'Stage 3',' ', 'Stage 4',' ')



    % Titration

TitrationPlot1 = figure('Name', 'Titrations', 'NumberTitle', 'off');

a = 1;
TitrationRep = [];
while sum(TitrationRep) < size(TitrationpH,2)
    a = sum(TitrationpH == TitrationpH(1,sum(TitrationRep)+1));
TitrationRep = [TitrationRep, a];
end

if cue
else
    a = 1;
    for m = 1:size(TitrationRep,2)
        PlotPotentials{m,1} = [Potentials{a:sum(TitrationRep(1,1:m)),1}];
        a = sum(TitrationRep(1,1:m)) + 1;
    end
    a = 1;
    for m = 1:size(TitrationRep,2)
        PlotTitrationexpdata{m,1} =
[Titrationexpdata{a:sum(TitrationRep(1,1:m)),1}];
        a = sum(TitrationRep(1,1:m)) + 1;
    end

    for m = 1:size(TitrationRep,2)
        subplot(2,round(size(TitrationRep,2)/2),m)
        hold all
        plot(PlotPotentials{m,1}, PlotTitrationexpdata{m,1}, '.')
        title(['pH', num2str(TitrationpH(1,sum(TitrationRep(1,1:m))))])
        xlabel('E / V')
        ylabel('Populations')
        axis ([min([PlotPotentials{m,1}]) max([PlotPotentials{m,1}]) 0 1])
    end
end

E0 = mb0 * x + mb * fix;

c = -1:0.005:1;
w = c;
for m = 1:size(TitrationRep,2)
    E = E0 * ones(1,size(c,2));
    EE = -1*(sum( mb(:,1:NumberOfHemes)')' * ones(1, size(c,2))) .*
(ones(NumberOfMicrostates,1) * c) +...
    mb(:,NumberOfHemes+1) * ones(1, size(c,2)) * (2.3*R*T/F *
TitrationpH(1,sum(TitrationRep(1,1:m))));
    Fr1 = sum( (exp(-F/(R*T) * ( E + EE ) )) .* ( sum(mb(:,1:NumberOfHemes)')' *
ones(1,size(c,2))/NumberOfHemes ) );
    Fr2 = sum(exp(-F/(R*T) * ( E + EE ) ));
    FrE = [Fr1 ./ Fr2];
    w = [w; FrE]; % variable for titration ploting file
    subplot(2,round(size(TitrationRep,2)/2),m)
    hold on
    plot(c, FrE)
    xlabel('E / V')
    ylabel('Populations')
    axis ([-1 1 0 1])
end
```

```
save([NMRdata(:,1:size(NMRdata,2)-4) '_Titrationplot.txt'], 'w', '-ASCII', '-
TABS'); % file for titration ploting

TitrationPlot2 = figure('Name', 'Titrations', 'NumberTitle', 'off');

hold all
for m = 1:size(TitrationRep,2)
    c = -1:0.005:1;
    E = E0 * ones(1,size(c,2));
    EE = -1*(sum( mb(:,1:NumberOfHemes)')' * ones(1, size(c,2))) .*
(ones(NumberOfMicrostates,1) * c) +...
    mb(:,NumberOfHemes+1) * ones(1, size(c,2)) * (2.3*R*T/F *
TitrationpH(1,sum(TitrationRep(1,1:m))));
    Fr1 = sum( (exp(-F/(R*T) * ( E + EE ) )) .* ( sum(mb(:,1:NumberOfHemes)')' *
ones(1,size(c,2))/NumberOfHemes ) );
    Fr2 = sum(exp(-F/(R*T) * ( E + EE ) ));
    FrE = [Fr1 ./ Fr2];
    plot(c, FrE)
end
title('')
xlabel('E / V')
ylabel('Populations')
axis ([-1 1 0 1])
hold off

StagePopulations = figure('Name', 'Stage Populations', 'NumberTitle', 'off');  %
plot stage populations

c = -1:0.005:1;
w = c;
for m = 1:size(TitrationRep,2)
    E = E0 * ones(1,size(c,2));
    EE = -1*(sum( mb(:,1:NumberOfHemes)')' * ones(1, size(c,2))) .*
(ones(NumberOfMicrostates,1) * c) +...
    mb(:,NumberOfHemes+1) * ones(1, size(c,2)) * (2.3*R*T/F *
TitrationpH(1,sum(TitrationRep(1,1:m))));
    Fr1 = (exp(-F/(R*T) * ( E + EE ) )) .* ( sum(mb(:,1:NumberOfHemes)')' *
ones(1,size(c,2))/NumberOfHemes );
    Fr2 = exp(-F/(R*T) * ( E + EE ) );
    subplot(2,round(size(TitrationRep,2)/2),m)
    for o = 0:NumberOfHemes
        hold all
        FrE = [sum( Fr2(find(sum(mb(:,1:NumberOfHemes),2) == o),:)) ./
sum(Fr2)];
        plot(c, FrE)
        leg{o+1} = ['Stage ', num2str(NumberOfHemes-o)];
        w = [w; FrE]; % variable for StagePopulation plot file
    end
    title(['pH' num2str(TitrationpH(1,sum(TitrationRep(1,1:m))))])
    fliplr(0:NumberOfHemes);
    legend(leg)
    xlabel('E / V')
    ylabel('Populations')
    axis ([-1 1 0 1])
end

save([NMRdata(:,1:size(NMRdata,2)-4) '_StagePopulationsplot.txt'], 'w', '-
ASCII', '-TABS'); % file for StagePopulation ploting


HemeRedoxFractions = figure('Name', 'Heme Reduction Fractions', 'NumberTitle',
'off');  % plot Heme Reduction Fractions

clear leg
c = -1:0.005:1;
```

```
w = c;
for m = 1:size(TitrationRep,2)
    E = E0 * ones(1,size(c,2));
    EE = -1*(sum( mb(:,1:NumberOfHemes)')' * ones(1, size(c,2))) .*
(ones(NumberOfMicrostates,1) * c) +...
    mb(:,NumberOfHemes+1) * ones(1, size(c,2)) * (2.3*R*T/F *
TitrationpH(1,sum(TitrationRep(1,1:m))));
    Fr1 = (exp(-F/(R*T) * ( E + EE ) )) .* ( sum(mb(:,1:NumberOfHemes)')' *
ones(1,size(c,2))/NumberOfHemes );
    Fr2 = exp(-F/(R*T) * ( E + EE ) );
    subplot(2,round(size(TitrationRep,2)/2),m)
    for o = 1:NumberOfHemes
        hold all
        FrE = [sum( Fr2(find(mb(:,o) == 0),:)) ./ sum(Fr2)];
        plot(c, FrE)
        leg{o} = ['Heme ', num2str(o)];
        w = [w; FrE]; % variable for Heme Reduction Fractions plot file
    end
    title(['pH' num2str(TitrationpH(1,sum(TitrationRep(1,1:m))))])
    fliplr(0:NumberOfHemes);
    legend(leg)
    xlabel('E / V')
    ylabel('Reduction Fraction')
    axis ([-1 1 0 1])
end

save([NMRdata(:,1:size(NMRdata,2)-4) '_HemeReductionFractionsplot.txt'], 'w', '-
ASCII', '-TABS'); % file for Heme Reduction Fractions ploting


MicrostatePopulation = figure('Name', 'Microstate Popupations', 'NumberTitle',
'off');

micro =[1 2];
for o = 1:2^NumberOfHemes-1
    micro = [micro; micro(size(micro,1),:) + 2];
end
if NumberOfProtons > 1
    for m = 1:2^(NumberOfProtons-1)-1
        micro = [micro, micro(:, size(micro,2)-1:size(micro,2)) +
2*2^NumberOfHemes];
    end
end

clear leg
c = -1:0.005:1;
w = c;
for m = 1:size(TitrationRep,2)
    E = E0 * ones(1,size(c,2));
    EE = -1*(sum( mb(:,1:NumberOfHemes)')' * ones(1, size(c,2))) .*
(ones(NumberOfMicrostates,1) * c) +...
    mb(:,NumberOfHemes+1) * ones(1, size(c,2)) * (2.3*R*T/F *
TitrationpH(1,sum(TitrationRep(1,1:m))));
    Fr1 = (exp(-F/(R*T) * ( E + EE ) )) .* ( sum(mb(:,1:NumberOfHemes)')' *
ones(1,size(c,2))/NumberOfHemes );
    Fr2 = exp(-F/(R*T) * ( E + EE ) );
    subplot(2,round(size(TitrationRep,2)/2),m)
    for o = 1:2^NumberOfHemes
        hold all
        FrE = [sum( Fr2(micro(o,:),:)) ./ sum(Fr2)];
        plot(c, FrE)
        leg{o} = [num2str( abs(mb(micro(o,1),1:NumberOfHemes)-1) )];
        w = [w; FrE]; % variable for Microstatepopulation plot file
    end
    title(['pH' num2str(TitrationpH(1,sum(TitrationRep(1,1:m))))])
```

```
    fliplr(0:NumberOfHemes);
    for o = 1:2^NumberOfHemes
        for p = 1:size(leg{o},2)
            if leg{o}(p) == '1'
                leg{o}(p) = 'R';
            elseif leg{o}(p) == '0'
                leg{o}(p) = 'O';
            end
        end
    end
    legend(leg)
    xlabel('E / V')
    ylabel('Populations')
    axis ([-1 1 0 1])
end

save([NMRdata(:,1:size(NMRdata,2)-4) '_MicroStatePopulationsplot.txt'], 'w', '-
ASCII', '-TABS'); % file for MicroStatePopulation ploting


MicrostatePopulation_pKa = figure('Name', 'Microstate Popupations with pKa',
'NumberTitle', 'off');

clear leg
c = -1:0.005:1;
w = c;
for m = 1:size(TitrationRep,2)
    E = E0 * ones(1,size(c,2));
    EE = -1*(sum( mb(:,1:NumberOfHemes)')' * ones(1, size(c,2))) .*
(ones(NumberOfMicrostates,1) * c) +...
    mb(:,NumberOfHemes+1) * ones(1, size(c,2)) * (2.3*R*T/F *
TitrationpH(1,sum(TitrationRep(1,1:m))));
    Fr1 = (exp(-F/(R*T) * ( E + EE ) )) .* ( sum(mb(:,1:NumberOfHemes)')' *
ones(1,size(c,2))/NumberOfHemes );
    Fr2 = exp(-F/(R*T) * ( E + EE ) );
    subplot(2,round(size(TitrationRep,2)/2),m)
    for o = 1:NumberOfMicrostates
        hold all
        FrE = Fr2(o,:) ./ sum(Fr2);
        plot(c, FrE)
        leg{o} = [num2str( abs(mb(o,1:NumberOfHemes+NumberOfProtons)-1) )];
        w = [w; FrE]; % variable for Microstatepopulation plot file
    end
    title(['pH' num2str(TitrationpH(1,sum(TitrationRep(1,1:m))))])
    fliplr(0:NumberOfHemes);
    for o = 1:size(leg,2)
        for p = 1:size(leg{o},2) - NumberOfProtons
            if leg{o}(p) == '1'
                leg{o}(p) = 'R';
            elseif leg{o}(p) == '0'
                leg{o}(p) = 'O';
            end
        end
        if leg{o}(1,size(leg{o},2)) == '1'
            leg{o}(1,size(leg{o},2)) = '-';
        else
            leg{o}(1,size(leg{o},2)) = 'H';
        end
    end
    legend(leg)
    xlabel('E / V')
    ylabel('Populations')
    axis ([-1 1 0 1])
end
```

```
save([NMRdata(:,1:size(NMRdata,2)-4) '_MicroStatePopulations_pKa_plot.txt'],
'w', '-ASCII', '-TABS'); % file for MicroStatePopulation ploting


if cue
    for m = 0:NumberOfHemes
        a = ['Results.pKaSTAGE' num2str(m) '=pKa(m+1);'];
        eval(a);
    end
else
    NMRdata(size(NMRdata,2)-3:size(NMRdata,2)) = [];

    a=x'; b=stderr'; c=chi2; d=p; e=pKa'; f=NMR; g=TITRATION;
    save([NMRdata 'OUT' '.txt'], 'a', 'b', 'c', 'd', 'e', 'f', 'g', '-ASCII', '-
TABS') % output file

    for m = 1:NumberOfHemes
        a = ['Results.E' num2str(m) '= [x(m) stderr(m)];'];
        eval(a);
    end
    for m = NumberOfHemes+1:NumberOfHemes+NumberOfProtons
        a = ['Results.pKa' num2str(m-NumberOfHemes) '= [x(m) stderr(m)];'];
        eval(a);
    end
    b = 1;
    for o = 1:NumberOfHemes-1
        for m = o+1:NumberOfHemes
            a = ['Results.i' num2str(o) num2str(m) '=
[x(NumberOfHemes+NumberOfProtons+b) stderr(NumberOfHemes+NumberOfProtons+b)];'];
            eval(a);
            b = b + 1;
        end
    end
    b = 1;
    for o = 1:NumberOfProtons
        for m = 1:NumberOfHemes
            a = ['Results.i' num2str(m) 'H' num2str(o) '=
[x(NumberOfHemes+NumberOfProtons+NumberOfInteractions+b)
stderr(NumberOfHemes+NumberOfProtons+NumberOfInteractions+b)];'];
            eval(a);
            b = b + 1;
        end
    end
    for m = 0:NumberOfHemes
        a = ['Results.pKaSTAGE' num2str(m) '=pKa(m+1);'];
        eval(a);
    end


    Results.Chisquared = chi2;
    Results.pvalue = p;
    Results.NMRChisquared = NMR;
    Results.DegreesOfFreedom = df;
    Results.LeastSquares = LS;
    Results.LSofNMR = LSnmr;
    Results.LSofTitrations = LStitration;
end
```

File Chi2.m

```
function f = Chi2(x, mb, mb1, mb2, Potentials, R, T, F, expdata,
Titrationexpdata, stdd, Titrationstdd, mb0, fix, TitrationpH, EpH, n,
NumberOfMicrostates, NumberOfHemes)

E0 = mb0 * x + mb * fix;

f = 0;
for m = 1:size(TitrationpH,2)
    E = E0 * ones(1, size(Potentials{m,1},2));
    EE = -1*(sum( mb(:,1:NumberOfHemes)')' * ones(1, size(Potentials{m,1},2)))
.* (ones(NumberOfMicrostates,1) * Potentials{m,1}) +...
    mb(:,NumberOfHemes+1) * ones(1, size(Potentials{m,1},2)) * (2.3*R*T/F *
TitrationpH(1,m));
    Fr1 = sum( (exp(-F/(R*T) * ( E + EE ) )) .* ( sum(mb(:,1:NumberOfHemes)')' *
ones(1,size(Potentials{m,1},2))/NumberOfHemes ) );
    Fr2 = sum(exp(-F/(R*T) * ( E + EE ) ));
    FrE = Fr1 ./ Fr2;
    A = FrE - Titrationexpdata{m,1};
    A(A~=A) = 0;

    f = f + sum( sum( (A / Titrationstdd).^2));
end


E0 = mb0 * x + mb * fix;
E = E0 * ones(1,n) + EpH;
P = exp(-F/(R*T) * E);
Fr = (mb1 * P) ./ (mb2 * P);
B = Fr - expdata;
B(B~=B) = 0;

f =  f + sum((sum(((B)./stdd).^2)))
```

Heme axial ligand geometries:

Matlab routine used to determine the orientation of the heme axial ligands based on the 13C chemical shifts of the heme substituents. The function "carbonCS" (file carbon.m) uses the function "ANGLES13C" (file ANGLES13C.m).

File carbonCS.m

```
function param = carbonCS(file, cue)

data = dlmread(file);
if ~exist('cue')
    cue = 'n';
end

T = data(1,1:(size(data,1)-1)/8);

R = 8.3143;
```

```
k = 1.38*10^-23;
gama = 6.7282*10^7;
mb = 9.27*10^-24;
g = 2;
diaref = [12.1
36.5
12.1
36.5
12.1
22.5
22.5
12.1];

shifts = data(2:size(data,1),:);

if cue == 'y'
    x0 = input('Initial estimation =');
    if isempty(x0) == 1
        x0 = [3000 0 36];
    end
elseif isempty(cue) | cue == 'n'
    x0 = input('Initial estimation =');
    if isempty(x0) == 1
        x0 = [3000 0];
    end
end
bw = ones(4,1);

l = 1;
for o = 1:size(data,2)
    s=1; cs = [];
    for r = 1:size(T,2)
        cs = [cs shifts(s:s+7,o)];
        s = s + size(cs,1);
    end

    options = optimset('MaxFunEvals', size(x0,2)*2000, 'MaxIter',
size(x0,2)*2000, 'TolFun', 1e-10,...
        'TolX', 1e-10);

    format long g
    [par, mq, exitflag, output] = fminsearch(@(z) ANGLES13C(z, cs, T, R, diaref,
cue), x0, options);
    format short g
    exitflag

    if cue == 'y'
        alpha = zeros(3);
    elseif isempty(cue) | cue == 'n'
        alpha = zeros(2);
    end

    for m = 1:size(T,2) % for different temperatures

        dE = par(1);
        theta = par(2);
        if cue == 'y'
            Qcc = par(3);
        elseif isempty(cue) | cue == 'n'
            Qcc = 36;
        end

        K = Qcc / (2 * k * T(m) * gama / 10^12 / pi / g / mb);
        R = 8.3143;
        beta = rad2deg(acos(dE/1000/(5+cos(4*deg2rad(theta)))));
```

```
        Fc =[(-0.071*cos(deg2rad(theta)) - 0.137*sin(deg2rad(theta)))^2 + (-
0.071*sin(deg2rad(theta)) + 0.137*cos(deg2rad(theta)))^2 * exp(dE/(R*T(m)));
             ( 0.071*cos(deg2rad(theta)) - 0.137*sin(deg2rad(theta)))^2 + (
0.071*sin(deg2rad(theta)) + 0.137*cos(deg2rad(theta)))^2 * exp(dE/(R*T(m)));
             ( 0.137*cos(deg2rad(theta)) - 0.071*sin(deg2rad(theta)))^2 + (
0.137*sin(deg2rad(theta)) + 0.071*cos(deg2rad(theta)))^2 * exp(dE/(R*T(m)));
             ( 0.137*cos(deg2rad(theta)) + 0.071*sin(deg2rad(theta)))^2 + (
0.137*sin(deg2rad(theta)) - 0.071*cos(deg2rad(theta)))^2 * exp(dE/(R*T(m)))] .*
(K / (1 + exp(dE/(R*T(m)))));



        % derivation

        dtheta = 2 .* [(-0.071*cos(deg2rad(theta)) - 0.137*sin(deg2rad(theta)))
* ( 0.071*sin(deg2rad(theta)) - 0.137*cos(deg2rad(theta)))   +   (-
0.071*sin(deg2rad(theta)) + 0.137*cos(deg2rad(theta))) * (-
0.071*cos(deg2rad(theta)) - 0.137*sin(deg2rad(theta))) * exp(dE/(R*T(m)));
                       ( 0.071*cos(deg2rad(theta)) - 0.137*sin(deg2rad(theta)))
* (-0.071*sin(deg2rad(theta)) - 0.137*cos(deg2rad(theta)))   +   (
0.071*sin(deg2rad(theta)) + 0.137*cos(deg2rad(theta))) * (
0.071*cos(deg2rad(theta)) - 0.137*sin(deg2rad(theta))) * exp(dE/(R*T(m)));
                       ( 0.137*cos(deg2rad(theta)) - 0.071*sin(deg2rad(theta)))
* (-0.137*sin(deg2rad(theta)) - 0.071*cos(deg2rad(theta)))   +   (
0.137*sin(deg2rad(theta)) + 0.071*cos(deg2rad(theta))) * (
0.137*cos(deg2rad(theta)) - 0.071*sin(deg2rad(theta))) * exp(dE/(R*T(m)));
                       ( 0.137*cos(deg2rad(theta)) + 0.071*sin(deg2rad(theta)))
* (-0.137*sin(deg2rad(theta)) + 0.071*cos(deg2rad(theta)))   +   (
0.137*sin(deg2rad(theta)) - 0.071*cos(deg2rad(theta))) * (
0.137*cos(deg2rad(theta)) + 0.071*sin(deg2rad(theta))) * exp(dE/(R*T(m)))] .* (K
/ (1 + exp(dE/(R*T(m)))));

        ddE = [exp(dE/(R*T(m))) / (R*T(m)*(1+exp(dE/(R*T(m))))) * (K * (-
0.071*sin(deg2rad(theta)) + 0.137*cos(deg2rad(theta)))^2 - Fc(1))
               exp(dE/(R*T(m))) / (R*T(m)*(1+exp(dE/(R*T(m))))) * (K * (
0.071*sin(deg2rad(theta)) + 0.137*cos(deg2rad(theta)))^2 - Fc(2))
               exp(dE/(R*T(m))) / (R*T(m)*(1+exp(dE/(R*T(m))))) * (K * (
0.137*sin(deg2rad(theta)) + 0.071*cos(deg2rad(theta)))^2 - Fc(3))
               exp(dE/(R*T(m))) / (R*T(m)*(1+exp(dE/(R*T(m))))) * (K * (
0.137*sin(deg2rad(theta)) - 0.071*cos(deg2rad(theta)))^2 - Fc(4))];

%         ddE = [(-0.071*sin(deg2rad(theta)) + 0.137*cos(deg2rad(theta)))^2 *
exp(dE/(R*T(m))) * (1/(R*T(m))) * (K / (1 + exp(dE/(R*T(m))))).^2 - Fc(1) * K *
exp(dE/(R*T(m))) * (1/(R*T(m))) / (1 + exp(dE/(R*T(m)))).^2;
%                ( 0.071*sin(deg2rad(theta)) + 0.137*cos(deg2rad(theta)))^2 *
exp(dE/(R*T(m))) * (1/(R*T(m))) * (K / (1 + exp(dE/(R*T(m))))).^2 - Fc(2) * K *
exp(dE/(R*T(m))) * (1/(R*T(m))) / (1 + exp(dE/(R*T(m)))).^2;
%                ( 0.137*sin(deg2rad(theta)) + 0.071*cos(deg2rad(theta)))^2 *
exp(dE/(R*T(m))) * (1/(R*T(m))) * (K / (1 + exp(dE/(R*T(m))))).^2 - Fc(3) * K *
exp(dE/(R*T(m))) * (1/(R*T(m))) / (1 + exp(dE/(R*T(m)))).^2;
%                ( 0.137*sin(deg2rad(theta)) - 0.071*cos(deg2rad(theta)))^2 *
exp(dE/(R*T(m))) * (1/(R*T(m))) * (K / (1 + exp(dE/(R*T(m))))).^2 - Fc(4) * K *
exp(dE/(R*T(m))) * (1/(R*T(m))) / (1 + exp(dE/(R*T(m)))).^2] ./ (K / (1 +
exp(dE/(R*T(m)))));

        if cue == 'y'
            dQcc = Fc ./ (K * 2 * k * T(m) * gama / 10^12 / pi / g / mb);
            dCS = [ddE dtheta dQcc] ./ [bw bw bw];
        elseif isempty(cue) | cue == 'n'
            dCS = [ddE dtheta] ./ [bw bw];
        end


        alpha = alpha + dCS' * dCS;
```

```
Fc = [Fc;Fc];
CS = [cs(:,m), (diaref - Fc)];

figure(size(T,2)+1)
subplot(size(data,2),size(T,2),l)
l = l+1;
plot(CS(:,1),CS(:,2),'.')   % experimental vs theoretical
line([-50 10], [-50 10])
axis([-50 10 -50 10])
axis square
title(['Heme ' num2str(o) '  ' num2str(T(m)) ' K'])
xlabel('ppm')
ylabel('ppm')


calculatedCS(:,m) = CS(:,2);

if dE < 0
    dE = -dE;
    theta = -theta;
end
if beta < 90
    theta = -theta;
end


% -----drawing-----



x = [100 100+abs((diaref(1)-CS(1,1)))*cos(deg2rad(153))
     100 100+abs((diaref(2)-CS(2,1)))*cos(deg2rad(117))
     100 100+abs((diaref(3)-CS(3,1)))*cos(deg2rad(63))
     100 100+abs((diaref(4)-CS(4,1)))*cos(deg2rad(27))
     100 100+abs((diaref(5)-CS(5,1)))*cos(deg2rad(-27))
     100 100+abs((diaref(6)-CS(6,1)))*cos(deg2rad(-63))
     100 100+abs((diaref(7)-CS(7,1)))*cos(deg2rad(-117))
     100 100+abs((diaref(8)-CS(8,1)))*cos(deg2rad(-153))
     230 230+abs(Fc(1))*cos(deg2rad(153))
     230 230+abs(Fc(2))*cos(deg2rad(117))
     230 230+abs(Fc(3))*cos(deg2rad(63))
     230 230+abs(Fc(4))*cos(deg2rad(27))
     230 230+abs(Fc(5))*cos(deg2rad(-27))
     230 230+abs(Fc(6))*cos(deg2rad(-63))
     230 230+abs(Fc(7))*cos(deg2rad(-117))
     230 230+abs(Fc(8))*cos(deg2rad(-153))];

y = [-150*(o-1) -150*(o-1)+abs((diaref(1)-CS(1,1)))*sin(deg2rad(153))
     -150*(o-1) -150*(o-1)+abs((diaref(2)-CS(2,1)))*sin(deg2rad(117))
     -150*(o-1) -150*(o-1)+abs((diaref(3)-CS(3,1)))*sin(deg2rad(63))
     -150*(o-1) -150*(o-1)+abs((diaref(4)-CS(4,1)))*sin(deg2rad(27))
     -150*(o-1) -150*(o-1)+abs((diaref(5)-CS(5,1)))*sin(deg2rad(-27))
     -150*(o-1) -150*(o-1)+abs((diaref(6)-CS(6,1)))*sin(deg2rad(-63))
     -150*(o-1) -150*(o-1)+abs((diaref(7)-CS(7,1)))*sin(deg2rad(-117))
     -150*(o-1) -150*(o-1)+abs((diaref(8)-CS(8,1)))*sin(deg2rad(-153))
     -150*(o-1) -150*(o-1)+abs(Fc(1))*sin(deg2rad(153))
     -150*(o-1) -150*(o-1)+abs(Fc(2))*sin(deg2rad(117))
     -150*(o-1) -150*(o-1)+abs(Fc(3))*sin(deg2rad(63))
     -150*(o-1) -150*(o-1)+abs(Fc(4))*sin(deg2rad(27))
     -150*(o-1) -150*(o-1)+abs(Fc(5))*sin(deg2rad(-27))
     -150*(o-1) -150*(o-1)+abs(Fc(6))*sin(deg2rad(-63))
     -150*(o-1) -150*(o-1)+abs(Fc(7))*sin(deg2rad(-117))
```

```
            -150*(o-1) -150*(o-1)+abs(Fc(8))*sin(deg2rad(-153))];
        figure(m)
        hold all
        line(x', y', 'LineWidth', 2.5, 'Color', 'b') % star diagrams
        text(360, -150*(o-1), ['Heme' num2str(o)])


        x = [-30 -30+20*cos(deg2rad(45+theta-beta/2))
             -30 -30-20*cos(deg2rad(45+theta-beta/2))
             -30 -30+20*cos(deg2rad(45+theta+beta/2))
             -30 -30-20*cos(deg2rad(45+theta+beta/2))];

        y = [-150*(o-1) -150*(o-1)+20*sin(deg2rad(45+theta-beta/2))
             -150*(o-1) -150*(o-1)-20*sin(deg2rad(45+theta-beta/2))
             -150*(o-1) -150*(o-1)+20*sin(deg2rad(45+theta+beta/2))
             -150*(o-1) -150*(o-1)-20*sin(deg2rad(45+theta+beta/2))];


        line(x', y', 'LineWidth', 2.5, 'Color', 'b') %  histidines

        h = 20;

        ang0 = 144;
        ang = 72;
        sides = 5;
        a = 45;

        x = [0;h*cos(deg2rad(ang0))];
        for n = 1:sides-1
            x(:,size(x,2)+1) = [x(2,size(x,2)); x(2,size(x,2))+
h*cos(deg2rad(ang0-ang*n))];
        end


        y = [0;h*sin(deg2rad(ang0))];
        for n = 1:sides-1
            y(:,size(y,2)+1) = [y(2,size(y,2)); y(2,size(y,2))+
h*sin(deg2rad(ang0-ang*n))];
        end

        Rot = [cos(deg2rad(a)) -sin(deg2rad(a))
            sin(deg2rad(a)) cos(deg2rad(a))];

        v = (Rot * [x(:), y(:)]')';

        x=[];
        y=[];
        for n = 1:2:10
            x(:,size(x,2)+1) = v(n:n+1, 1);
        end
        for n = 1:2:10
            y(:,size(y,2)+1) = v(n:n+1, 2);
        end

        x1 = x;
        y1 = y;

        % ------ 2°

        a = -45;

        x = [0;h*cos(deg2rad(ang0))];
        for n = 1:sides-1
            x(:,size(x,2)+1) = [x(2,size(x,2)); x(2,size(x,2))+
h*cos(deg2rad(ang0-ang*n))];
```

```
        end


        y = [0;h*sin(deg2rad(ang0))];
        for n = 1:sides-1
            y(:,size(y,2)+1) = [y(2,size(y,2)); y(2,size(y,2))+
h*sin(deg2rad(ang0-ang*n))];
        end

        Rot = [cos(deg2rad(a)) -sin(deg2rad(a))
            sin(deg2rad(a)) cos(deg2rad(a))];

        v = (Rot * [x(:), y(:)]')';

        x=[];
        y=[];
        for n = 1:2:10
            x(:,size(x,2)+1) = v(n:n+1, 1);
        end
        for n = 1:2:10
            y(:,size(y,2)+1) = v(n:n+1, 2);
        end

        x = x + 2*h* (cos(deg2rad(81)) + cos(deg2rad(27.5))) *ones(size(x));

        x2 = x;
        y2 = y;

        % ------ 3°

        a = -135;

        x = [0;h*cos(deg2rad(ang0))];
        for n = 1:sides-1
            x(:,size(x,2)+1) = [x(2,size(x,2)); x(2,size(x,2))+
h*cos(deg2rad(ang0-ang*n))];
        end


        y = [0;h*sin(deg2rad(ang0))];
        for n = 1:sides-1
            y(:,size(y,2)+1) = [y(2,size(y,2)); y(2,size(y,2))+
h*sin(deg2rad(ang0-ang*n))];
        end

        Rot = [cos(deg2rad(a)) -sin(deg2rad(a))
            sin(deg2rad(a)) cos(deg2rad(a))];

        v = (Rot * [x(:), y(:)]')';

        x=[];
        y=[];
        for n = 1:2:10
            x(:,size(x,2)+1) = v(n:n+1, 1);
        end
        for n = 1:2:10
            y(:,size(y,2)+1) = v(n:n+1, 2);
        end

        x = x + 2*h* (cos(deg2rad(81)) + cos(deg2rad(27.5))) *ones(size(x));
        y = y - 2*h* (cos(deg2rad(81)) + cos(deg2rad(27.5))) *ones(size(x));

        x3 = x;
        y3 = y;
```

```
        % ------ 4°

        a = 135;

        x = [0;h*cos(deg2rad(ang0))];
        for n = 1:sides-1
            x(:,size(x,2)+1) = [x(2,size(x,2)); x(2,size(x,2))+
h*cos(deg2rad(ang0-ang*n))];
        end


        y = [0;h*sin(deg2rad(ang0))];
        for n = 1:sides-1
            y(:,size(y,2)+1) = [y(2,size(y,2)); y(2,size(y,2))+
h*sin(deg2rad(ang0-ang*n))];
        end

        Rot = [cos(deg2rad(a)) -sin(deg2rad(a))
            sin(deg2rad(a)) cos(deg2rad(a))];

        v = (Rot * [x(:), y(:)]')';

        x=[];
        y=[];
        for n = 1:2:10
            x(:,size(x,2)+1) = v(n:n+1, 1);
        end
        for n = 1:2:10
            y(:,size(y,2)+1) = v(n:n+1, 2);
        end

        y = y - 2*h* (cos(deg2rad(81)) + cos(deg2rad(27.5))) *ones(size(x));

        x4 = x;
        y4 = y;



        %---
        x = [x1, x2, x3, x4];
        y = [y1, y2, y3, y4];

        x(:,size(x,2)+1) = [x(2,1); x(2,1) + h*cos(deg2rad(-117.5))];
        x(:,size(x,2)+1) = [x(2,size(x,2)); x(2,size(x,2)) + h*cos(deg2rad(-
62.5))];
        y(:,size(y,2)+1) = [y(2,1); y(2,1) + h*sin(deg2rad(-117.5))];
        y(:,size(y,2)+1) = [y(2,size(y,2)); y(2,size(y,2)) + h*sin(deg2rad(-
62.5))];

        x(:,size(x,2)+1) = [x(2,4); x(2,4) + h*cos(deg2rad(27.5))];
        x(:,size(x,2)+1) = [x(2,size(x,2)); x(2,size(x,2)) +
h*cos(deg2rad(27.5))];
        y(:,size(y,2)+1) = [y(2,4); y(2,4) + h*sin(deg2rad(27.5))];
        y(:,size(y,2)+1) = [y(2,size(y,2)); y(2,size(y,2)) -
h*sin(deg2rad(27.5))];

        x(:,size(x,2)+1) = [x(2,9); x(2,9) + h*cos(deg2rad(-62.5))];
        x(:,size(x,2)+1) = [x(2,size(x,2)); x(2,size(x,2)) + h*cos(deg2rad(-
117.5))];
        y(:,size(y,2)+1) = [y(2,9); y(2,9) + h*sin(deg2rad(-117.5))];
        y(:,size(y,2)+1) = [y(2,size(y,2)); y(2,size(y,2)) + h*sin(deg2rad(-
62.5))];

        x(:,size(x,2)+1) = [x(2,14); x(2,14) + h*cos(deg2rad(152.5))];
```

```
        x(:,size(x,2)+1) = [x(2,size(x,2)); x(2,size(x,2)) +
h*cos(deg2rad(152.5))];
        y(:,size(y,2)+1) = [y(2,14); y(2,14) - h*sin(deg2rad(27.5))];
        y(:,size(y,2)+1) = [y(2,size(y,2)); y(2,size(y,2)) +
h*sin(deg2rad(27.5))];

        x = x + (-30+x(2,22))*ones(size(x));
        y = y + (-150*(o-1)-y(2,21))*ones(size(y));

        line(x,y, 'LineWidth', 2.5, 'Color', 'b')  % heme ring


        theta1 = theta;
        if beta < 90
            theta1 = theta - 90;
        end
        if theta1 < -90
            theta1 = theta1 + 180;
        end

        x = [-30 -30+11.66*dE/1000*cos(deg2rad(45+theta1))
         -30 -30+70*cos(deg2rad(45-theta1))];

        y = [-150*(o-1) -150*(o-1)+11.66*dE/1000*sin(deg2rad(45+theta1))
         -150*(o-1) -150*(o-1)+70*sin(deg2rad(45-theta1))];

        line(x', y', 'LineWidth', 1, 'Color', 'k')  % theta and Chiyy
        if 45-theta1 >= 0 && 45-theta1 <= 90
            text(x(2,2), y(2,2), '\it\chi_{yy}',...
                'HorizontalAlignment', 'left',...
                'VerticalAlignment', 'Bottom',...
                'FontSize', 15)
        elseif 45-theta1 > 90 && 45-theta1 <= 135
            text(x(2,2), y(2,2), '\it\chi_{yy}',...
                'HorizontalAlignment', 'right',...
                'VerticalAlignment', 'Bottom',...
                'FontSize', 15)
        elseif 45-theta1 < 0 && 45-theta1 >= -135
            text(x(2,2), y(2,2), '\it\chi_{yy}',...
                'HorizontalAlignment', 'left',...
                'VerticalAlignment', 'Top',...
                'FontSize', 15)
        end
        if 45+theta1 >= 0 && 45+theta1 <= 90
            text(x(1,2), y(1,2), '\it\theta',...
                'HorizontalAlignment', 'left',...
                'VerticalAlignment', 'Bottom',...
                'FontSize', 15)
        elseif 45+theta1 > 90 && 45+theta1 <= 135
            text(x(1,2), y(1,2), '\it\theta',...
                'HorizontalAlignment', 'right',...
                'VerticalAlignment', 'Bottom',...
                'FontSize', 15)
        elseif 45+theta1 < 0 && 45+theta1 >= -135
            text(x(1,2), y(1,2), '\it\theta',...
                'HorizontalAlignment', 'left',...
                'VerticalAlignment', 'Top',...
                'FontSize', 15)
        end



    end %T

    % standard error determination
```

```
    stderr = (diag(inv(alpha))).^0.5;

    betaerr = (- stderr(1) / ( 1000*(5+cos(4*deg2rad(theta))) * sqrt( 1-
(dE/(1000*(5+cos(4*deg2rad(theta)))))).^2 )).^2 + ...
        (-stderr(2)*4*dE*sin(4*deg2rad(theta)) / ( (5+cos(4*deg2rad(theta))).^2
* sqrt( 1- (dE/(1000*(5+cos(4*deg2rad(theta)))))).^2 )).^2;
    betaerr = sqrt(betaerr);

    dE = dE/1000;
    stderr(1) = stderr(1)/1000;

    if cue == 'y'
        Parameters = [beta betaerr
        theta rad2deg(stderr(2))
        dE stderr(1)
        Qcc stderr(3)];
    elseif isempty(cue) | cue =='n'
        Parameters = [beta betaerr
        theta rad2deg(stderr(2))
        dE stderr(1)];
    end

    if beta < 90
        theta = theta - 90;
        Parameters(2,1) = theta;
    end
    if beta > 90 | beta < -90
        beta = 180 - beta;
        Parameters(1,1) = beta;
    end

    preview = [];
    for n = 1:size(T,2)
        preview = [preview cs(:,n) calculatedCS(:,n)];
    end

    clear a
    a.Methyl2 = preview(1,:);
    a.Tioether3 = preview(2,:);
    a.Methyl7 = preview(3,:);
    a.Tioether8 = preview(4,:);
    a.Methyl12 = preview(5,:);
    a.Propionate13 = preview(6,:);
    a.Propionate17 = preview(7,:);
    a.Methyl18 = preview(8,:);


    Parameters = round(Parameters * 100) /100;


    if cue == 'y'
        a.beta = Parameters(1,:);
        a.theta = Parameters(2,:);
        a.dE = Parameters(3,:);
        a.Qcc = Parameters(4,:);
        a.leastsquares = mq;
    elseif isempty(cue) | cue =='n'
        a.beta = Parameters(1,:);
        a.theta = Parameters(2,:);
        a.dE = Parameters(3,:);
        a.leastsquares = mq;
    end

    param(o) = a;
```

```
end

for n = 1:1:size(T,2)
    figure(n)
    title([num2str(T(n)) ' K'])
    axis equal
    axis off
    print('-dtiff', '-r600', '-painters', [num2str(T(n)), 'K_',
datestr(datenum(date))])
end


clear M1 M3 M5 M8  x0 ans p x R T diaref g gama k mb  alpha ddE dK dtheta bw dCS
betaerr stderr Fc cs x y ang ang0 a...
    sides n v R x1 x2 x3 x4 y1 y2 y3 y4 h options output exitflag CS K
calculatedCS dQcc m par ...
    preview beta cue dE mq theta Qcc
```

File ANGLES13C.m

```
function MQ = ANGLES13C(z, cs, T, R, diaref, cue)

dE = z(1);
theta = z(2);
if cue == 'y'
    Qcc = z(3);
elseif isempty(cue) | cue =='n'
    Qcc = 36;
end

for m = 1:size(T,2)

    k = 1.38*10^-23;
    gama = 6.7282*10^7;
    mb = 9.27*10^-24;
    g = 2;
    K = Qcc / (2 * k * T(m) * gama / 10^12 / pi / g / mb);



    cs1 = diaref - cs(:,m);

    for n = 1:4
        if isnan(cs1(n))
            cs1(n) = cs1(n+4);
        end
        if isnan(cs1(n+4))
            cs1(n+4) = cs1(n);
        end
    end

    Fc = [(- 0.071*cos(deg2rad(theta)) - 0.137*sin(deg2rad(theta)))^2 + (-
0.071*sin(deg2rad(theta)) + 0.137*cos(deg2rad(theta)))^2 * exp(dE/(R*T(m)));
          ( 0.071*cos(deg2rad(theta)) - 0.137*sin(deg2rad(theta)))^2 + (
0.071*sin(deg2rad(theta)) + 0.137*cos(deg2rad(theta)))^2 * exp(dE/(R*T(m)));
          ( 0.137*cos(deg2rad(theta)) - 0.071*sin(deg2rad(theta)))^2 + (
0.137*sin(deg2rad(theta)) + 0.071*cos(deg2rad(theta)))^2 * exp(dE/(R*T(m)));
          ( 0.137*cos(deg2rad(theta)) + 0.071*sin(deg2rad(theta)))^2 + (
0.137*sin(deg2rad(theta)) - 0.071*cos(deg2rad(theta)))^2 * exp(dE/(R*T(m)))] .*
(K / (1 + exp(dE/(R*T(m)))));
```

```
    average = [(cs1(1)+cs1(5))/2;
        (cs1(2)+cs1(6))/2;
        (cs1(3)+cs1(7))/2;
        (cs1(4)+cs1(8))/2];

    mq = (average - Fc).^2;

    mq(mq~=mq)=0;

    MQ(m) = sum(mq);

end %T

MQ = sum(MQ);
```

Matlab routine used to determine the heme axial ligand geometries based on the PDB file. This routine uses the function "ALG" (file ALG.m).

File ALG.m

```
function ANGLES = ALG(pdb, his, chain)

file = pdbread(pdb);

if exist('chain') == 0
    chain = 'A';
end

for o = 1:size(his,2)

    m = 1;
    for n = 1:size(file.Atom,2)       % find coordinates of residue
        if file.Atom(n).resSeq == his(o) & file.Atom(n).chainID == chain
            if  isempty(findstr('HIS', file.Atom(n).resName)) % check is residue
is His
               error('Residue is not an histidine.')
            end
            atom{m,1} = file.Atom(n).AtomName;
            coor(m,1) = file.Atom(n).X;
            coor(m,2) = file.Atom(n).Y;
            coor(m,3) = file.Atom(n).Z;
            m = m + 1;
            %LastAtom = file.Atom(n).AtomSerNo;
            if size(file.Atom(n).AtomName,2) == 3
                if file.Atom(n).AtomName == 'NE2'
                    LastAtom = file.Atom(n).AtomSerNo;
                end
            end
            if m > 17
                break
            end
        end
    end


    % plot3(coor(:,1), coor(:,2), coor(:,3), '.')
    % hold on
```

```
    % line(coor(1:4 ,1), coor(1:4 ,2), coor(1:4 ,3))
    % line(coor([2 5 6 7 9 10 8 6] ,1), coor([2 5 6 7 9 10 8 6] ,2), coor([2 5 6
7 9 10 8 6] ,3))


    for n = 1:size(file.Connectivity,2)  % find connected Fe
        if file.Connectivity(n).AtomSerNo == LastAtom;
            Fe = file.Connectivity(n).BondAtomList;
            break
        end
    end

    for n = 1:size(file.HeterogenAtom,2)   % find correct heme residue number
        if sum(file.HeterogenAtom(n).AtomSerNo == Fe)
            heme = file.HeterogenAtom(n).resSeq;
            break
        end
    end


    m = 1;
    for n = 1:size(file.HeterogenAtom,2)       % find coordinates of heme
        if file.HeterogenAtom(n).resSeq == heme & file.HeterogenAtom(n).chainID
== chain
            heterogenatom{m,1} = file.HeterogenAtom(n).AtomName;
            hcoor(m,1) = file.HeterogenAtom(n).X;
            hcoor(m,2) = file.HeterogenAtom(n).Y;
            hcoor(m,3) = file.HeterogenAtom(n).Z;
            m = m + 1;
        end
    end

    % plot3(hcoor(:,1), hcoor(:,2), hcoor(:,3), '.')

    % a = {[7:10 3 18:21 4 26:29 5 34: 37 2 7]
    %      [7 6 10 18 17 21 26 25 29 34 33 37]
    %      [8 12:15]
    %      [14 16]
    %      [9 11]
    %      [19 22]
    %      [20 23 24]
    %      [27 30]
    %      [28 31 32]
    %      [35 38]
    %      [36 39:42]
    %      [41 43]}; % heme conections
    %
    % for n = 1:size(a,1)  % draw heme
    %     line(hcoor(a{n} ,1), hcoor(a{n} ,2), hcoor(a{n} ,3))
    % end

    % histidine plane

    a = ['CG' 'ND1' 'CE1' 'NE2' 'CD2'];
    atom(1:4) = [];
    m = 1;
    for n = 1:numel(atom)
        if isempty(strfind(a, atom{n}))
            pp(m) = n;
            m = m+1;
        end
    end
    pcoor = coor(5:size(coor,1),:);
    pcoor(pp,:) = [];
```

```
    HisPlane = pcoor \ ones(size(pcoor,1),1);

    % heme plane

    %a = ['FE' 'C1A' 'C2A' 'C3A' 'C4A' 'C1B' 'C2B' 'C3B' 'C4B' 'C1C' 'C2C' 'C3C'
'C4C' 'C1DA' 'C2D' 'C3D' 'CD4' 'NA' 'NB' 'NC' 'ND' 'CHA' 'CHB' 'CHC' 'CHD'];
%     a = ['FE' 'NA' 'NB' 'NC' 'ND' 'N A' 'N B' 'N C' 'N D'];
%     m = 1;
%     for n = 1:numel(heterogenatom)
%         if isempty(strfind(a, heterogenatom{n}))
%             pp(m) = n;
%             m = m+1;
%         end
%     end
%     hpcoor = hcoor;
%     hpcoor(pp,:) = [];

    for n = 1:size(heterogenatom,1)
        if strfind('FE', heterogenatom{n})
            fe = n;
        end
        if strfind('NA', heterogenatom{n})
            na = n;
        end
        if strfind('N A', heterogenatom{n})
            na = n;
        end
        if strfind('NB', heterogenatom{n})
            nb = n;
        end
        if strfind('N B', heterogenatom{n})
            nb = n;
        end
        if strfind('NC', heterogenatom{n})
            nc = n;
        end
        if strfind('N C', heterogenatom{n})
            nc = n;
        end
        if strfind('ND', heterogenatom{n})
            nd = n;
        end
        if strfind('N D', heterogenatom{n})
            nd = n;
        end
    end

    hpcoor(1,:) = hcoor(fe,:);
    hpcoor(2,:) = hcoor(na,:);
    hpcoor(3,:) = hcoor(nb,:);
    hpcoor(4,:) = hcoor(nc,:);
    hpcoor(5,:) = hcoor(nd,:);

    HemePlane = hpcoor \ ones(size(hpcoor,1),1);

    % his heme angle

    ANGLE(1) = rad2deg(    acos(  sum(HisPlane .* HemePlane) /(
sqrt(sum(HisPlane.^2)) * sqrt(sum(HemePlane.^2)) )  )  );


    for n = 1:size(file.Connectivity,2)  %  finding second histidine
        if sum(file.Connectivity(n).AtomSerNo == Fe);
            his2 = file.Connectivity(n).BondAtomList;
```

```
            break
        end
    end
    for n = 1:size(file.Atom,2)
        if file.Atom(n).chainID == chain
            a1 = n;
            break
        end
    end
    for n = a1:size(file.Atom,2)
        if file.Atom(n).chainID ~= chain
            a2 = n-1;
            break
        else
            a2 = size(file.Atom,2);
        end
    end
    his2 = his2(his2 >= a1 & his2 <= a2);
    his2 = his2(his2 ~= LastAtom);


    for n = 1:size(file.Atom,2)   % find correct histidine residue number
        if file.Atom(n).AtomSerNo == his2
            his2 = file.Atom(n).resSeq;
            break
        end
    end

    m = 1;
    for n = 1:size(file.Atom,2)       % find coordinates of second residue
        if file.Atom(n).resSeq == his2 & file.Atom(n).chainID == chain
            if  isempty(findstr('HIS', file.Atom(n).resName)) % check is residue
is His
               error('Second ligand is not an histidine.')
            end
            atom2{m,1} = file.Atom(n).AtomName;
            coor2(m,1) = file.Atom(n).X;
            coor2(m,2) = file.Atom(n).Y;
            coor2(m,3) = file.Atom(n).Z;
            m = m + 1;
            LastAtom = n;
        end
    end


    % plot3(coor2(:,1), coor2(:,2), coor2(:,3), '.')
    % hold on
    % line(coor2(1:4 ,1), coor2(1:4 ,2), coor2(1:4 ,3))
    % line(coor2([2 5 6 7 9 10 8 6] ,1), coor2([2 5 6 7 9 10 8 6] ,2), coor2([2
5 6 7 9 10 8 6] ,3))


    % second histidine plane

    a = ['CG' 'ND1' 'CE1' 'NE2' 'CD2'];
    atom2(1:4) = [];
    clear pp
    m = 1;
    for n = 1:numel(atom2)
        if isempty(strfind(a, atom2{n}))
            pp(m) = n;
            m = m+1;
        end
    end
    pcoor2 = coor2(5:size(coor,1),:);
```

```
    pcoor2(pp,:) = [];


    His2Plane = pcoor2 \ ones(size(pcoor2,1),1);

    % his heme angle

    ANGLE(2) = rad2deg(    acos(  sum(His2Plane .* HemePlane) /(
sqrt(sum(His2Plane.^2)) * sqrt(sum(HemePlane.^2)) )  )  );


    % his his angle

    a = ['CE1' 'NE2' 'CD2'];
    clear pp
    m = 1;
    for n = 1:numel(atom)
        if isempty(strfind(a, atom{n}))
            pp(m) = n;
            m = m+1;
        end
    end
    dcoor = coor(5:size(coor,1),:);  % diedral plan coordinates
    dcoor(pp,:) = [];
    dcoor(size(dcoor,1)+1,:) = hpcoor(1,:);

    HisDPlane = dcoor \ ones(size(dcoor,1),1);

    a = ['CE1' 'NE2' 'CD2'];
    clear pp
    m = 1;
    for n = 1:numel(atom2)
        if isempty(strfind(a, atom2{n}))
            pp(m) = n;
            m = m+1;
        end
    end
    dcoor2 = coor2(5:size(coor2,1),:);  % diedral plan coordinates
    dcoor2(pp,:) = [];
    dcoor2(size(dcoor,1)+1,:) = hpcoor(1,:);

    His2DPlane = dcoor2 \ ones(size(dcoor2,1),1);


    NA = (hpcoor(2,:) - hpcoor(1,:))';
    NB = (hpcoor(3,:) - hpcoor(1,:))';
    NC = (hpcoor(4,:) - hpcoor(1,:))';
    ND = (hpcoor(5,:) - hpcoor(1,:))';


    Proj1 = cross( HemePlane, (cross(HisDPlane, HemePlane))
)/sqrt(sum(HemePlane.^2))^2;
    Proj2 = cross( HemePlane, (cross(His2DPlane, HemePlane))
)/sqrt(sum(HemePlane.^2))^2;


    ang(1,1) = 90 + rad2deg(    acos(  sum(Proj1 .* NA) /( sqrt(sum(Proj1.^2)) *
sqrt(sum(NA.^2)) )  )  );
    ang(2,1) = rad2deg(    acos(  sum(Proj1 .* NB) /( sqrt(sum(Proj1.^2)) *
sqrt(sum(NB.^2)) )  )  );
    ang(3,1) = 90 + rad2deg(    acos(  sum(Proj1 .* NC) /( sqrt(sum(Proj1.^2)) *
sqrt(sum(NC.^2)) )  )  );
    ang(4,1) = 180 + rad2deg(    acos(  sum(Proj1 .* ND) /( sqrt(sum(Proj1.^2))
* sqrt(sum(ND.^2)) )  )  );
```

```
    ang(1,2) = 90 + rad2deg(    acos(  sum(Proj2 .* NA) /( sqrt(sum(Proj2.^2)) *
sqrt(sum(NA.^2)) )  )  );
    ang(2,2) = rad2deg(    acos(  sum(Proj2 .* NB) /( sqrt(sum(Proj2.^2)) *
sqrt(sum(NB.^2)) )  )  );
    ang(3,2) = 90 + rad2deg(    acos(  sum(Proj2 .* NC) /( sqrt(sum(Proj2.^2)) *
sqrt(sum(NC.^2)) )  )  );
    ang(4,2) = 180 + rad2deg(    acos(  sum(Proj2 .* ND) /( sqrt(sum(Proj2.^2))
* sqrt(sum(ND.^2)) )  )  );

    for n = 1:numel(ang)
        while ang(n) > 90
            ang(n) = abs(180 - ang(n));
        end
    end

    beta(1) = sum(abs(ang(:,1) - ang(:,2)))/4;
    beta(2) = sum(abs(ang(:,1) + ang(:,2)))/4;
    if beta(1) > 90
        beta(1) = 180 - beta(1);
    end
    if beta(2) > 90
        beta(2) = 180 - beta(2);
    end

    for n = 1:4
        d(n,1) = sqrt(sum((dcoor(1,:) - hpcoor(n+1,:)).^2));
    end
    for n = 1:4
        d(n,2) = sqrt(sum((dcoor2(1,:) - hpcoor(n+1,:)).^2));
    end

    a = d(:,1); b = d(:,2);
    for n = 1:2
        ord(n,1) = find(a == min(a));
        a(ord(n,1)) = a(ord(n,1)) + max(a);
        ord(n,2) = find(b == min(b));
        b(ord(n,2)) = b(ord(n,1)) + max(b);
    end
    for n = 1:2
        if all(ord(:,n) == [2;1]) | all(ord(:,n) == [1;2]) | all(ord(:,n) ==
[1;4]) | all(ord(:,n) == [4;1])
            ord(:,n) = ord(:,n) + [2;2];
        end
    end
    ord(ord==6) = 2;
    position = sum(ord);
    if position(1) == position(2)
        ANGLE(3) = beta(1);
    else
        ANGLE(3) = beta(2);
    end

    % theta angle

    if position(1) == 5 & position(2) == 5
        ANGLE(4) = (sum(ang(:,1))/4 + sum(ang(:,2))/4) / 2 - 90;
    elseif position(1) == 7 & position(2) == 7
        ANGLE(4) = -(sum(ang(:,1))/4 + sum(ang(:,2))/4) / 2 + 90;
    elseif position(1) == 5
        ANGLE(4) = (sum(ang(:,1))/4 - sum(ang(:,2))/4) / 2;
        if abs(ANGLE(4) - sum(ang(:,1))/4) < 45 & sum(ang(:,1))/4 >
sum(ang(:,2))/4
            ANGLE(4) = ANGLE(4) - 90;
        elseif abs(ANGLE(4) - sum(ang(:,1))/4) < 45 & sum(ang(:,1))/4 <
sum(ang(:,2))/4
```

```
            ANGLE(4) = ANGLE(4) + 90;
        end
    elseif position(1) == 7
        ANGLE(4) = (sum(ang(:,2))/4 - sum(ang(:,1))/4) / 2;
        if abs(ANGLE(4) - sum(ang(:,2))/4) < 45 & sum(ang(:,1))/4 >
sum(ang(:,2))/4
            ANGLE(4) = ANGLE(4) + 90;
        elseif abs(ANGLE(4) - sum(ang(:,2))/4) < 45 & sum(ang(:,1))/4 <
sum(ang(:,2))/4
            ANGLE(4) = ANGLE(4) - 90;
        end
    end

    if ANGLE(1) > 90
        ANGLE(1) = 180 - ANGLE(1);  % angle between his 1 and heme
    end
    if ANGLE(2) > 90
        ANGLE(2) = 180 - ANGLE(2);  % angle between his 2 and heme
    end

    ANGLES.HIS1HEME(o) = ANGLE(1);
    ANGLES.HIS2HEME(o) = ANGLE(2);
    ANGLES.beta(o) = ANGLE(3);
    ANGLES.theta(o) = ANGLE(4);

    if abs(ANGLE(4)) > 45
        a = 90 - abs(ANGLE(4));
    else
        a = ANGLE(4);
    end
        ANGLES.RhombicSplitting(o) =
0.347*(5+cos(4*deg2rad(a)))*cos(deg2rad(ANGLE(3)));

    A = 0.347*(5+cos(4*deg2rad(a)))*cos(deg2rad(ANGLE(3)));
    g0 = [1 2 3];
    g = fsolve(@(g) gvalue(g,A), g0);

    ANGLES.gx(o) = g(1);
    ANGLES.gy(o) = g(2);
    ANGLES.gz(o) = g(3);

    ANGLE = ANGLES;

    % DRAWING-------
    theta = ANGLES.theta(o) + 90;
    beta = ANGLES.beta(o);

    x = [150 150+20*cos(deg2rad(45+theta-beta/2))
         150 150-20*cos(deg2rad(45+theta-beta/2))
         150 150+20*cos(deg2rad(45+theta+beta/2))
         150 150-20*cos(deg2rad(45+theta+beta/2))];

    y = [-150*(o-1) -150*(o-1)+20*sin(deg2rad(45+theta-beta/2))
         -150*(o-1) -150*(o-1)-20*sin(deg2rad(45+theta-beta/2))
         -150*(o-1) -150*(o-1)+20*sin(deg2rad(45+theta+beta/2))
         -150*(o-1) -150*(o-1)-20*sin(deg2rad(45+theta+beta/2))];


    line(x', y', 'LineWidth', 2.5, 'Color', 'k') % histidines

    x = [150 150+70*cos(deg2rad(45-ANGLES.theta(o)))];

    y = [-150*(o-1) -150*(o-1)+70*sin(deg2rad(45-ANGLES.theta(o)))];

    line(x', y', 'LineWidth', 1, 'Color', 'k')  % Chiyy
```

```
%     if 45+ANGLES.theta(o) >= 0 && 45+ANGLES.theta(o) <= 90
%         text(x(2), y(2), '\it\chi_{yy}',...
%             'HorizontalAlignment', 'left',...
%             'VerticalAlignment', 'Bottom',...
%             'FontSize', 15)
%     elseif 45+ANGLES.theta(o) > 90 && 45+ANGLES.theta(o) <= 135
%         text(x(2), y(2), '\it\chi_{yy}',...
%             'HorizontalAlignment', 'right',...
%             'VerticalAlignment', 'Bottom',...
%             'FontSize', 15)
%     elseif 45+ANGLES.theta(o) < 0 && 45+ANGLES.theta(o) >= -135
%         text(x(2), y(2), '\it\chi_{yy}',...
%             'HorizontalAlignment', 'left',...
%             'VerticalAlignment', 'Top',...
%             'FontSize', 15)
%     end

    h = 20;

    ang0 = 144;
    ang = 72;
    sides = 5;
    a = 45;

    x = [0;h*cos(deg2rad(ang0))];
    for n = 1:sides-1
        x(:,size(x,2)+1) = [x(2,size(x,2)); x(2,size(x,2))+ h*cos(deg2rad(ang0-
ang*n))];
    end


    y = [0;h*sin(deg2rad(ang0))];
    for n = 1:sides-1
        y(:,size(y,2)+1) = [y(2,size(y,2)); y(2,size(y,2))+ h*sin(deg2rad(ang0-
ang*n))];
    end

    R = [cos(deg2rad(a)) -sin(deg2rad(a))
        sin(deg2rad(a)) cos(deg2rad(a))];

    v = (R * [x(:), y(:)]')';

    x=[];
    y=[];
    for n = 1:2:10
        x(:,size(x,2)+1) = v(n:n+1, 1);
    end
    for n = 1:2:10
        y(:,size(y,2)+1) = v(n:n+1, 2);
    end

    x1 = x;
    y1 = y;

    % ------ 2°

    a = -45;

    x = [0;h*cos(deg2rad(ang0))];
    for n = 1:sides-1
        x(:,size(x,2)+1) = [x(2,size(x,2)); x(2,size(x,2))+ h*cos(deg2rad(ang0-
ang*n))];
    end
```

```
    y = [0;h*sin(deg2rad(ang0))];
    for n = 1:sides-1
        y(:,size(y,2)+1) = [y(2,size(y,2)); y(2,size(y,2))+ h*sin(deg2rad(ang0-
ang*n))];
    end

    R = [cos(deg2rad(a)) -sin(deg2rad(a))
        sin(deg2rad(a)) cos(deg2rad(a))];

    v = (R * [x(:), y(:)]')';

    x=[];
    y=[];
    for n = 1:2:10
        x(:,size(x,2)+1) = v(n:n+1, 1);
    end
    for n = 1:2:10
        y(:,size(y,2)+1) = v(n:n+1, 2);
    end

    x = x + 2*h* (cos(deg2rad(81)) + cos(deg2rad(27.5))) *ones(size(x));

    x2 = x;
    y2 = y;

    % ------ 3°

    a = -135;

    x = [0;h*cos(deg2rad(ang0))];
    for n = 1:sides-1
        x(:,size(x,2)+1) = [x(2,size(x,2)); x(2,size(x,2))+ h*cos(deg2rad(ang0-
ang*n))];
    end


    y = [0;h*sin(deg2rad(ang0))];
    for n = 1:sides-1
        y(:,size(y,2)+1) = [y(2,size(y,2)); y(2,size(y,2))+ h*sin(deg2rad(ang0-
ang*n))];
    end

    R = [cos(deg2rad(a)) -sin(deg2rad(a))
        sin(deg2rad(a)) cos(deg2rad(a))];

    v = (R * [x(:), y(:)]')';

    x=[];
    y=[];
    for n = 1:2:10
        x(:,size(x,2)+1) = v(n:n+1, 1);
    end
    for n = 1:2:10
        y(:,size(y,2)+1) = v(n:n+1, 2);
    end

    x = x + 2*h* (cos(deg2rad(81)) + cos(deg2rad(27.5))) *ones(size(x));
    y = y - 2*h* (cos(deg2rad(81)) + cos(deg2rad(27.5))) *ones(size(x));

    x3 = x;
    y3 = y;


    % ------ 4°
```

```
    a = 135;

    x = [0;h*cos(deg2rad(ang0))];
    for n = 1:sides-1
        x(:,size(x,2)+1) = [x(2,size(x,2)); x(2,size(x,2))+ h*cos(deg2rad(ang0-
ang*n))];
    end


    y = [0;h*sin(deg2rad(ang0))];
    for n = 1:sides-1
        y(:,size(y,2)+1) = [y(2,size(y,2)); y(2,size(y,2))+ h*sin(deg2rad(ang0-
ang*n))];
    end

    R = [cos(deg2rad(a)) -sin(deg2rad(a))
        sin(deg2rad(a)) cos(deg2rad(a))];

    v = (R * [x(:), y(:)]')';

    x=[];
    y=[];
    for n = 1:2:10
        x(:,size(x,2)+1) = v(n:n+1, 1);
    end
    for n = 1:2:10
        y(:,size(y,2)+1) = v(n:n+1, 2);
    end

    y = y - 2*h* (cos(deg2rad(81)) + cos(deg2rad(27.5))) *ones(size(x));

    x4 = x;
    y4 = y;



    %---
    x = [x1, x2, x3, x4];
    y = [y1, y2, y3, y4];

    x(:,size(x,2)+1) = [x(2,1); x(2,1) + h*cos(deg2rad(-117.5))];
    x(:,size(x,2)+1) = [x(2,size(x,2)); x(2,size(x,2)) + h*cos(deg2rad(-62.5))];
    y(:,size(y,2)+1) = [y(2,1); y(2,1) + h*sin(deg2rad(-117.5))];
    y(:,size(y,2)+1) = [y(2,size(y,2)); y(2,size(y,2)) + h*sin(deg2rad(-62.5))];

    x(:,size(x,2)+1) = [x(2,4); x(2,4) + h*cos(deg2rad(27.5))];
    x(:,size(x,2)+1) = [x(2,size(x,2)); x(2,size(x,2)) + h*cos(deg2rad(27.5))];
    y(:,size(y,2)+1) = [y(2,4); y(2,4) + h*sin(deg2rad(27.5))];
    y(:,size(y,2)+1) = [y(2,size(y,2)); y(2,size(y,2)) - h*sin(deg2rad(27.5))];

    x(:,size(x,2)+1) = [x(2,9); x(2,9) + h*cos(deg2rad(-62.5))];
    x(:,size(x,2)+1) = [x(2,size(x,2)); x(2,size(x,2)) + h*cos(deg2rad(-
117.5))];
    y(:,size(y,2)+1) = [y(2,9); y(2,9) + h*sin(deg2rad(-117.5))];
    y(:,size(y,2)+1) = [y(2,size(y,2)); y(2,size(y,2)) + h*sin(deg2rad(-62.5))];

    x(:,size(x,2)+1) = [x(2,14); x(2,14) + h*cos(deg2rad(152.5))];
    x(:,size(x,2)+1) = [x(2,size(x,2)); x(2,size(x,2)) + h*cos(deg2rad(152.5))];
    y(:,size(y,2)+1) = [y(2,14); y(2,14) - h*sin(deg2rad(27.5))];
    y(:,size(y,2)+1) = [y(2,size(y,2)); y(2,size(y,2)) + h*sin(deg2rad(27.5))];

    x = x + (150+x(2,22))*ones(size(x));
    y = y + (-150*(o-1)-y(2,21))*ones(size(y));
```

```
    line(x,y, 'LineWidth', 2.5, 'Color', 'k') % heme ring
    text(250, -150*(o-1), ['His ' num2str(his(o))])
    axis equal
    axis off

    clear Fe HemePlane HisPlane LastAtom a atom coor hcoor heme heterogenatom
hpcoo m n pcoor pp ANGLE x y...
        x1 x2 x3 x4 y1 y2 y3 y4 beta theta
end % o

print('-dtiff', '-r600', '-painters', [pdb(1:size(pdb,2)-4), '_',
datestr(datenum(date))]
```

APPENDIX F: BIOSYNTHESIS AND SPECIFIC ISOTOPIC LABELING OF THE HEME

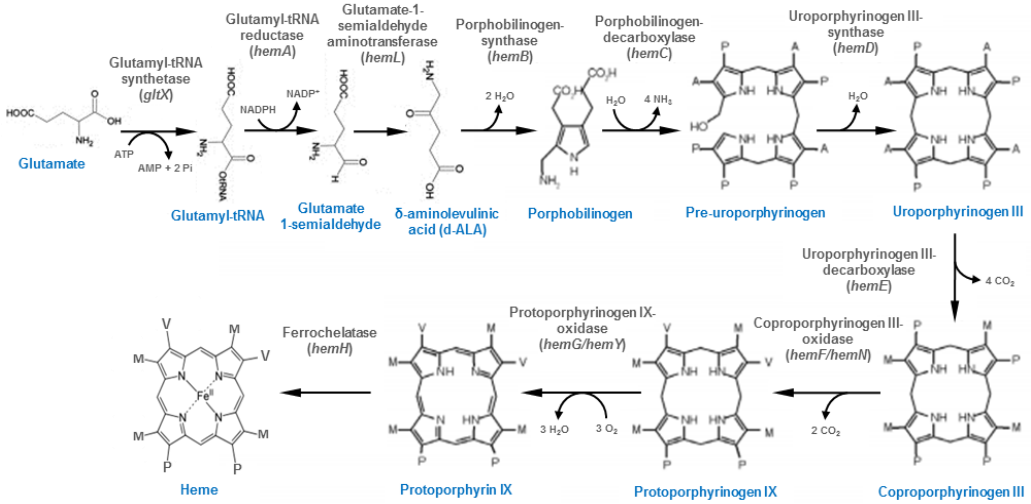

Figure F.1. Heme biosynthesis in *E. coli*. The names of the enzymes and their respective genes are given above the arrows. Synthesis of δ-aminolevulinic acid (dALA) follows the C_5 pathway. A, acetate side chain; P, propionate side chain; M, methyl group; V, vinyl group. Adapted from [15].

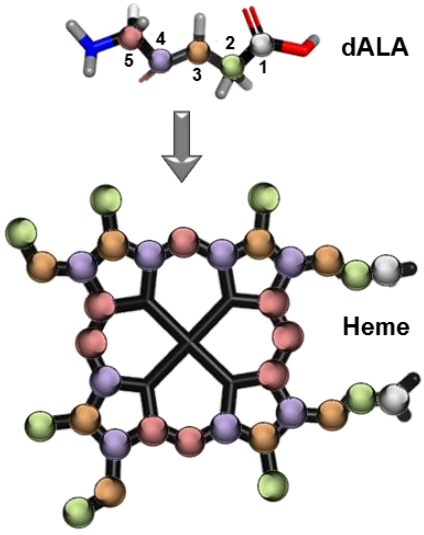

Figure F.2. ^{13}C-Labeling patterns obtained when the heme is biosynthesized using medium supplemented with dALA labeled at different carbon positions. Each sphere represents a different carbon position of labeled ^{13}C. The color shows the position where the labeling will occur in the heme when using dALA labeled at the position containing the same colored labeled carbon. Different labeling combinations of the heme may be obtained by using dALA labeled at various positions.

REFERENCES

[1] Francis, R.T., Jr. and R.R. Becker. 1984. Specific indication of hemoproteins in polyacrylamide gels using a double-staining process. Anal Biochem *136*:509-514.

[2] Santos, H., J.J. Moura, I. Moura, J. LeGall, and A.V. Xavier. 1984. NMR studies of electron transfer mechanisms in a protein with interacting redox centres: *Desulfovibrio gigas* cytochrome c_3. Eur J Biochem *141*:283-296.

[3] Turner, D.L., C.A. Salgueiro, T. Catarino, J. LeGall, and A.V. Xavier. 1994. Homotropic and heterotropic cooperativity in the tetrahaem cytochrome c_3 from *Desulfovibrio vulgaris*. Biochim Biophys Acta *1187*:232-235.

[4] Turner, D.L., C.A. Salgueiro, T. Catarino, J. Legall, and A.V. Xavier. 1996. NMR studies of cooperativity in the tetrahaem cytochrome c_3 from *Desulfovibrio vulgaris*. Eur J Biochem *241*:723-731.

[5] Leys, D., T.E. Meyer, A.S. Tsapin, K.H. Nealson, M.A. Cusanovich, and J.J. Van Beeumen. 2002. Crystal structures at atomic resolution reveal the novel concept of "electron-harvesting" as a role for the small tetraheme cytochrome *c*. J Biol Chem *277*:35703-35711.

[6] Xavier, A.V., D.L. Turner, and H. Santos. 1993. Two-dimensional nuclear magnetic resonance of paramagnetic metalloproteins. Methods Enzymol *227*:1-16.

[7] Turner, D.L. 1993. Evaluation of ^{13}C and ^{1}H Fermi contact shifts in horse cytochrome *c*. The origin of the anti-Curie effect. Eur J Biochem *211*:563-568.

[8] Turner, D.L. 2000. Obtaining ligand geometries from paramagnetic shifts in low-spin haem proteins. J Biol Inorg Chem *5*:328-332.

[9] Turner, D.L., C.A. Salgueiro, J. LeGall, and A.V. Xavier. 1992. Structural studies of *Desulfovibrio vulgaris* ferrocytochrome c_3 by two-dimensional NMR. Eur J Biochem *210*:931-936.

[10] Keller, R.M. and K. Wüthrich. 1978. Assignment of the heme *c* resonances in the 360 MHz H NMR spectra of cytochrome *c*. Biochim Biophys Acta *533*:195-208.

[11] Moss, G.P. 1988. Nomenclature of tetrapyrroles. Recommendations 1986 IUPAC-IUB Joint Commission on Biochemical Nomenclature (JCBN). Eur J Biochem *178*:277-328.

[12] Salgueiro, C.A., D.L. Turner, H. Santos, J. LeGall, and A.V. Xavier. 1992. Assignment of the redox potentials to the four haems in *Desulfovibrio vulgaris* cytochrome c_3 by 2D-NMR. FEBS Lett *314*:155-158.

[13] Louro, R.O., I. Pacheco, D.L. Turner, J. LeGall, and A.V. Xavier. 1996. Structural and functional characterization of cytochrome c_3 from *D. desulfuricans* ATCC 27774 by ^{1}H-NMR. FEBS Lett *390*:59-62.

[14] Dutton, P.L. 1978. Redox potentiometry: determination of midpoint potentials of oxidation-reduction components of biological electron-transfer systems. Methods Enzymol *54*:411-435.

[15] Heinemann, I.U., M. Jahn, and D. Jahn. 2008. The biochemistry of heme biosynthesis. Arch Biochem Biophys *474*:238-251.